جمهورية العراق
وزارة التعليم العالي والبحث العلمي
جامعة بابل / كلية الهندسة
قسم الهندسة الميكانيكية

التصميم الأمثل لقناة ثنائية المجرى مضلعة لتحسين انتقال الحرارة باستخدام الجريان متعدد الطور

أطروحة
مقدمة إلى جامعة بابل / كلية الهندسة وهي جزء من متطلبات نيل شهادة الدكتوراه في الهندسة الميكانيكية (القدرة)

أعدت من قبل
امال حسين عليوي

ماجستير (قدرة)2018

بأشراف

ا.د رياض صباح الطريحي

الخلاصة

دراسة وتحليل تحسين انتقال الحرارة نظريا وعمليا في ممر ثنائي بوجود الاضلاع (الاعاقات) مسخنة لدرجة حرارة ثابته والتي تكون مثبته على قاعدة القاعدة القناة. تم التحقق للتصميم المثالي للقناة ذات الممر الثنائي له مقطع مستطيل وله ثمان اضلاع مثبته وحنية حادة عن طريق فحص العديد من اشكال مختلفة وتم حلها بواسطة المعادلات الحاكمة ثلاثية الابعاد هي حفظ الكتلة وحفظ الزخم وحفظ الطاقة حيث تم حلها ببرنامج ANSYS 2021 R. اما مائع العمل يكون بطورين (ماء-هواء) وبثلاثة اطوار (ماء-هواء-ديزل) وبظروف جوية. واهم المتغيرات التي اخذت بنظر الاعتبار هي نسبة الطول المكافئ الى القطر الهيدروليكي وبمعدل (40 ≤ ل\ق ≤0) ورقم رينولد للجريان الثنائي الطور يتراوح من (72456.5 الى 116031.4) ,بينما للجريان الثلاثي الطور يكون رقم رينولد من 128182الى 223551.6 .ومن اهم النتائج النظرية التي تتمثل باختيار التصميم الأمثل بنسب تحسين انتقال الحرارة لشكل الضلع الكيرف 34.55% اعلى من شكل V . بينما كانت نسبة زيادة بهبوط الضغط في الضلع شكل V 60.01% اعلى من الضلع الكيرف . يعتبر شكل الدائري (3 ملم) افضل شكل للمساحة من ناحية انتقال الحرارة اعلى من المربعة والمثلثة بنسبة تحسين (7.47 % و6.1 %) على التوالي. بينما كانت نسب زيادة هبوط الضغط في المساحة الدائرية اعلى بحوالي (7.48 % ,12.3%) من المثلثة والمربعة على التوالي. تعتبر الدائرة (3 ملم) الأفضل مساحة من ناحية انتقال الحرارة اعلى من الدائرة (6 ملم) و(9ملم) بنسبة تحسين (15.4 % و21.25 %) على التوالي. بينما كانت نسب زيادة هبوط الضغط في (3ملم) اعلى بحوالي (15.1 % ,22.82%) من (6 ملم) و(9ملم). تعتبر الزاوية 45 درجة أفضل زاوية من ناحية انتقال الحرارة اعلى من 30 درجة و60 درجة بنسبة تحسين (19.45 % و7.52%) على التوالي. بينما كانت نسب زيادة هبوط الضغط في 60 درجة اعلى بحوالي (43.98 % ,15.27%) من 30 درجة و60 درجة على التوالي. كانت أهم النتائج العددية هي أن التصميم الأمثل للقناة ذات الممريين للانحناء الحاد ذو اضلاع بشكل كيرف وبحفر ذو شكل دائري بقطر 3ملم) ,وبزاوية حوالي 45 درجة . تم دراسة نوعين من الجريان ثنائي الاطوار وثلاثي الاطوار وبمعدلات جريان مختلفة ودرجات حرارة مختلفة لسطح الضلع . أيضا وجدت نسبة تحسين انتقال الحرارة ((Nu/Nuo تزداد مع زيادة السرع ودرجة حرارة سطح الضلع بينما (f/f_o) تتناقص مع زيادة السرع وتزداد مع زيادة درجات حرارة سطح الضلع . نمط التدفق هو Plug flow) (pattern لنوعين من الجريان لهما تدفق كتلي للطور السائل وطور الغازضمن المدى 300 ≤ 2100) ≥ G_{liquig} و (2 ≥ G_{gas} على التوالي . معامل الأداء الحراري يتناقص مع تزايد السرعة الهواء والماء في حالة الجريان ثنائي الطور وسرعة الهواء والماء والكازاويل في حالة الجريان ثلاثي الطور ولكن تتزايد قيمتة

مع تزايد درجة حرارة سطح الضلع عند ثبوت السرع. الانحراف بين هذه الدراسة والباحث [29] كانت بنسبة 1.8%. كما اجري مقارنة لنتائج مع باحثين [30] , [44] حيث كانت ذات سلوك متشابه للدراستين . وكانت وكان الانحراف بين النتائج العملية والنظري عند جريان ثنائي الطور عند ظروف سرعة الهواء 1.3157 م\ثا الى 3.29 م\ثا عند سرعة ماء 0.01684 م\ثا لكل من معامل انتقال الحرارة (h) و(Nu) و درجة حرارة الخليط وهبوط الضغط ومعامل الاحتكاك (*f*) ونسبة الاحتكاك (f/f_o) 8.75% , 9.5% ,0.2 % ,11.6%, 6.25% و 5.21% على التوالي .وعند الجريان ثلاثي الطور كان نسب الانحراف لكل من معامل انتقال الحرارة (h) و(Nu) و درجة حرارة الخليط وهبوط الضغط ومعامل الاحتكاك (*f*) ونسبة الاحتكاك (f/f_o) حوالي 6.16% , 9.02% ,0.5 % ,12.7%, 5.2% و 6.23% على التوالي .

Republic of Iraq
Ministry of Higher Education
and Scientific Research
University of Babylon
College of Engineering
Department of Mechanical Engineering

Optimization of a Two-Pass Ribbed Channel with Multi-Phase Flow to Enhance Heat Transfer

A Dissertation

Submitted to the

Department of Mechanical Engineering / College of Engineering/ University of Babylon in Partial Fulfillment of the Requirements for the Degree of Doctor of Philosophy in Mechanical Engineering

(Power Engineering)

By

Amal Hussein Oliwie

(M.Sc. 2018)

Supervised by

Prof. Dr. Riyadh S. Al-Turaihi

2023 A.D. ***1444 A.H***

بسم الله الرحمن الرحيم

(قَالُواْ سُبْحَانَكَ لاَ عِلْمَ لَنَا إِلاَّ مَا عَلَّمْتَنَا

إِنَّكَ أَنتَ الْعَلِيمُ الْحَكِيمُ)

صدق الله العلي العظيم

سورة البقرة ﴿32﴾

Supervisor Certification

I certify that this ***dissertation*** *entitled,* ***(Optimization of a Two-Pass Ribbed Channel with Multi-Phase Flow to Enhance Heat Transfer)*** *is being carried out by:* ***Amal Hussain Oliwie*** *under my supervision at the Mechanical Engineering Department College of Engineering /University of Babylon as a partial fulfillment of requirements for the degree of Doctor of Philosophy in Mechanical Engineering (Power Engineering).*

Signature

Prof. Dr. Riyadh Sabah Al-Turaihi
Department of Mechanical Engineering
College of Engineering
University of Babylon/Iraq

/ / 2023

Dedication

To all people who light a candle in their bare hands to make that deep darkness tunnel less lonely, and carry me to the light.

My one and only …

My Father and my mother.

To my husband and my family.

Amal. 2023

Acknowledgments

(In The Name of Allah, The Gracious, The Merciful)

(Thanks to Allah for guidance and help)

I would like to express my sincere thanks and deep gratitude to my supervisor **Prof. Dr. Riyadh Sabah Al-Turaihi** for their invaluable help, advice, and encouragement during the various stages of the present work.

I would like also to submit my thanks to all staff members of the Department of Mechanical Engineering at the University of Babylon.

My deepest thanks, love, and gratitude for all of my family. This study would not have been completed without their love and continuous support.

Amal

/   / 2023

Abstract

Heat transfer enhancement was investigated numerically and experimentally in a two-pass ribbed channel with ribs heated at constant temperature and installed in the base. Optimum design of two-pass channel of rectangular cross-section with eight ribs and sharp bend was investigated with four different configurations depending on the three-dimensional governing equations using ANSYS 2021 R1. The working fluid is classified into two-phase flow, three-phase flow as air-water and air-water-gasoil at ambient condition. Variable parameters of this study could be considered as: the length to hydraulic diameter ratio was with a range of ($0 \leq S/D \leq 40.525$), the Reynold numbers for two phase flow was with a range of (72456.3 to 116031.4) while for the three-phase flow, a Reynolds number was with a range from (128182 to 223551.6). Numerical results of optimum design show that the percentage of enhancing heat transfer of curved ribs is 34.55% higher than that for the V-shaped ribs. While the percentage of increasing pressure drop for V-shaped ribs 60.01% is higher than curved ribs. The circle shape of perforating is enhanced heat transfer more than the square and the triangle perforating shapes for same the area by about 7.47 % and 6.1% respectively. The pressure drop in square area has a maximum value with percentages about (7.48% and 12.3%) for triangle and circle areas, respectively.The area of diameter (3 mm) is enhanced heat transfer more than (6 and 9 mm) by about 15.4% and 21.25% respectively, also, it has the highest pressure drop about (15.1% and 22.82%) in comparison with (6 and 9 mm) respectively. The percentages of heat transfer enhancement for 45° is about 19.45% and 7.52% with respect to 30° and 60° respectively. Whereas the percentages of increasing pressure drop in 60° is about 43.98 % and 15.27 % with respect to 30° and 45°, respectively. The most significant numerical results showed that the optimum design for the two-pass channel of a sharp

bend is with curved ribs of a circular perforating of (3mm) and rib angle of 45° depending on the same conditions. Two types of flow (two-phase flow and three phase flow) with varies flow rates are investigated in an optimum design when the rib temperature varied from 50°C to 70°C.The ratio of the heat transfer enhancement (Nu/Nuo) increases and the friction ratio(f/f_o) decreases both with increasing velocities and rib temperature. The flow pattern is a "Plug pattern" for the two types of the flow that have a mass flux for liquid phase and gas phase of ranges ($2100 \geq G_{liquig} \geq 300$ and $G_{gas} \leq 2$) .The observation shows that the Performance Criteria Evaluation (PCE) decreases with increasing V_{air} and V_{water} for the two-phase flow and increasing V_{air} , V_{water} and V_{gasoil} for the three-phase flow at constant T_{Rib} but it increases with increasing T_{rib} at constant velocities. The deviation percentage between present work and **Dhanasekaran T. S [29]** are calculated about 1.8% .Also , the results were compared with other researchers **Wei Wang [30] and Longfei [44]** where there was good agreement. The deviations between the numerical and experimental results for the two phase flow at conditions V_{air} are varied from 1.3157m/s to 3.29m/s, V_{water}=0.1684m/s and T_{rib}=60°C for heat transfer coefficient (h) ,Nusselt numbers (Nu), temperature of fluid, pressure drop, and friction ratios (f/f_o) are about 8.75% , 9.5 % ,0.2 %,11.6 %,and 5.21 % respectively .In the three phase flow at the same conditions and V_{gasoil}=0.042m/s, the deviations of heat transfer coefficients ,Nu, temperature of fluid, pressure drop, and ratio f/f_o are about 6.16%, 9.02 % ,0.5 %,12.7 %, and 6.23 %, respectively.

Nomenclature

Symbols	Definition	Units
A	Cross-sectional area	m^2
AR	Aspect ratio	….
Cp	Specific heat at constant pressure	J/kg.K
D_h	hydraulic diameter	m
E	Energy	J
e	Rib height	mm
e/D_h	Ratio of rib height to hydraulic diameter	…
e/H	Rib height to channel height	…
f	Friction factor	…
f/f_o	Friction ratio	…
G	Mass flux	…
g	Acceleration of gravity (9.81)	m/s^2
h_x	Heat transfer coefficient	$W/m^2.K$
I	Current	Amper
I	Turbulent intensity	-
k	Thermal conductivity	W/m .K
L	Length	m
$\dot{m}$	Mass flow rate	Kg/s
Nu	Nusselt Number	……
Nu/Nu_o	Enhancement ratio	…
$\overline{Nu}$	Average Nusselt Number	….
P/e	Pitch to rib height ratio	……
P	Pitch	m
P/e	Ratio of pitch to rib height	……
p	Pressure	N/m^2

q	Heat flux	W/m^2
Q	Heat transfer rate	W
$\dot{Q}$	Flow rate	L/min
Re	Reynolds number	…
S	Distance in streamwise direction from inlet of ribbed region, bend, and outlet ribbed region	mm
S/D	Ratio of distance in streamwise direction from inlet of ribbed region, bend, and outlet ribbed region to hydraulic diameter	
t	Time	sec
T	Temperature	K
V	Voltage	Volt
V	Velocity	m/s
ʋ	Mass averaged velocity	m/s
W_{in}/H	Aspect ratio	…
w	Wetted perimeter of the channel	m
y+	Distance from the wall to the first grid cell's center	…

Greek symbols

Symbol	Description	Units
α	Volume fraction	-
ε	Turbulent dissipation rate	m^2/s^3
κ	Turbulent kinetic energy	m^2/s^2
µ	Dynamic viscosity	kg/m. s
ρ	Density	kg/m^3
ΔP	Pressure drops	Pa
ω	Specific rate of dissipation	m^2/s^3

ΔT	Temperature difference	K

Sub scripts

Symbol	Description
air	Air
avg.	Average value
B	Bend
dr	Drift velocity
bulk	Bulk
gasoil	Gasoil
h	Hydraulic
k	Phase
in	Inlet
mixture ,m	Mixture
n	Number of the Phases
o	Smooth
rib	Rib
s	Surface of Rib
t	Turbulent
water	Water

Abbreviations

Abbreviation	Description
ANSYS	Analysis of System
CFD	Computational Fluid Dynamics
CFX	Computational Fluid Xerography
2-D	Two dimensions
3-D	Three dimensions

N	Negative orientation with flow
P	Positive orientation with flow
PN	Positive-Negative orientation.
PCE	Thermal Performance Criteria Evaluation.
ORIR, ORIS, ORRIR,ORRIS, OSRIR, OSIS, OLRIR, OLRIS	Inner (I), Outer (O) bend wall have shapes: Round (R) or Square (S) with two corners (L) left and (R) Right .
RANS	Reynold Averaged Navier Stokes model
SST	Shear Stress Transport Model

Contents

Acknowledgments ………………………………………………………… I

Abstract …………………………………………………………………II

Nomenclature …………………………………………………… ….. IV

1 Chapter One…………….. ……………………………..……1-10

Introduction…………………………………………………1-2

1.1 Passive Heat Transfer Techniques 2

1.1.1 Roughened Surface (Ribs) 2

1.1.2 Curved Geometry (Bend) 3

1.1.3 Surface Area Channels 3

1.2 Rib Geometry 4

1.3 Concept OF Ribbed Surface of Two-Pass Channels 7

1.4 Concept of Bend 7

1.5 Concept of Two-Phase Flow &Three Phase Flow 8

1.6 Industrial Applications 8

1.7 The main objective 9

1.8 Layout of Thesis.. 10

2 Chapter Two: Literature Reviews..11-38

2.1 Introduction.. 11

2.2 Numerical Studies 11

2.3 Experimental Studies 24

2.4 Numerical & Experimental Studies 29

2.5 Summary of Perious Studies.. 32

3 Chapter Three: Numerical Work..33-58

3.1 Introduction 33
3.2 Design consideration 33
3.3 Geometry Model 36
3.3.1 Description of Two-Phase flow in Channel Model 36
3.3.2 Description of Smooth Channel Model 37
3.3.2 Description of Rib shapes Model 38
3.3.3 Physical Models of perforated shape 39
3.3.4 Physical Models perforated area of Ribs 40
3.3.5 Physical Models Ribs Angles 41
3.3.6 Physical Model Optiumum Design 41
3.3.7 Description of Three-Phase Flow in Channel Model 42
3.4 The Geometry 42
3.5 The Mesh 43
3.6 Boundary Condition 44
3.6.1 Boundary Condition of Two-phase Flow 44
3.6.2 Boundary Condition of Three-phase Flow 45
3.6.3 Velocity Inlet Boundary Condition 46
3.7.3 Pressure Outlet Boundary Condition 47
3.7 Simulation Assumptions 47
3.8 Fluent Setup 47
3.8.1 Defining the Material Properties 47
3.9 Computational Flow Dynamic Validation 48
3.9.1 Grid Independence 48

3.9.2 Viscous Models 49

3.9.3 Turbulence Models 50

3.10 Model Of Simulation 54

3.10.1 Two phase Flow 54

3.10.2 Three Phase Flow 55

3.11 Equation Describing fluids in Motion 55

3.12 Turbulence (K- ε)Model 56

3.12.1 Standard K- ε Model 57

3.13 Step of Numerical Solution 58

4 Chapter Four: Experimental Work 59-85

4.1 Introduction…………………………………………………...78

4.2 Description of Test Rig and Experimental Apparatus 59

4.3 Main channel ……………………..…………………….62

4.4 Curved Ribs ………………………………………..….. 62

4.5 Heater……………………………. …………………63

4.6 Converters 64

4.7 Air compressor 65

4.8 Water pump……..…………………………………………64

4.9 Water Tank……………………………………………………65

4.10 Water flow meter……………………………..…………65

4.11 Air Reservoir ……….……….…………………..…………65

4.12 Pressure Regulator ……...………………………………65

4.13 Safety Valve …………………………………………………65

4.14 Air flow meter…………………… ………………………65
4.15 Gasoil pump …..…………………………………..…………..…65
4.16 Gasoil flow meter………..…………..………...…………..…66
4.17 Gasoil Tank …. ……...………..………………………………66
4.15 Gasoil pump …..…………………………………..…………66
4.16 Gasoil flow meter……………….…….…..………...…………66
4.17 Gasoil Tank …. ……...………..………………………………66
4.18 Check &gate valve…. ……...…………….……..…….…………66
4.19 Accumulation Tank …………………..…...………...……..…66
4.20 Mix Region (MR)………… ……...…..…...……… ………67
4.21 Temperature Devises …. ……...……………….…..……………70
4.21.1 Thermcouples Distribution and Fixation....................... 70
4.21.2 Digital Temperature Recorder 71
4.22 Digital Manometer (PM9100)………….……...…..…. ……71
4.23 Capture and Analysis …. ……...……………….…..……………73
4.24 Voltage Variation Device …. ……...…………...….…………73
4.25 Power Measuring Device …. ……...…………………..………74
4.26 Instrument Calibration……. ……...………………..……………74
4.26.1 Digital Temperature Recorder 75
4.26.2 Pressure Calibration 76
4.26.3 Volume Flow rates of Water... 78
4.26.4 Volume Flow rates of Gasoil... 78
4.26.5 Volume Flow rates of Air 79

4.27 Experimental Procedure ……………..……………………………81

4.27 Experimental Calculation……………………………..…………82

5 Chapter Five: Results and Discussion ……………………...83-180

5.1 Introduction……………………………………………………..83

5.2 Comparison of Results ……………………………………………83

5.3 First Part :Results For How design the Optiumum ………85

5.3.1 Shape of Bend & Aspect Ratio 85

5.3.2 Smooth Channel 86

3.3.3 Optimum Ribs Shape 87

5.3.4 Shape of Perforated Area 89

5.3.5 Area of Optiumum Perforated 91

5.3.5 Angles values of ribs 94

5.4 Second Part:two-phase flow and three-phase flow internal optiumum channel ……………………..…………………………...…96

5.4.1 Ditribution of local Nussellt Number 96

5.4.2 Effect of changing velocities of air and water on enhancement ratio Nu/Nuo for different rib surface temperatures T_{rib} ……………………………………………………………………99

5.4.3 Effect of changing velocities of air and water on pressure drop (△P) for different rib surface temperatures T_{rib} 101

5.4.4 Effect of changing velocities of air and water on friction factor ratio (f/f_o) for different rib surface temperatures T_{rib} 102

5.4.5 Effect of changing velocities of air and water on Thermal-Performance Criteria Evaluation (PCE) for different rib surface temperatures T_{rib} 104

5.4.6 Distribution of Air-Water in channel........................... 105

5.4.7 Velocity profile of Two-phase..................................... 107

5.4.8 Pressure Distribution.. 112

5.4.9 Flow Pattern of two-phase behaviour …..………...….116

5.5 Third Part :three phase flow internal optiumum channel ……….121

5.5.1 Distribution of local Nusselt Number………..…………….121

5.5.2 Effect Effect of changing velocities of air and water on average Nusselt number (Nu_{avg}) for different rib surface temperatures T_{rib} ……129

5.5.4 Effect of changing velocities of air and water on enhancement ratio Nu/Nu_o for different rib surface temperatures T_{rib} . ……………... 132

5.5.5 Effect of changing velocities of air and water on friction ratio (f/f_o) for different rib surface temperatures T_{rib} ………………………..138

5.5.6 Effect of changing velocities of air and water on Thermal-Performance Criteria Evaluation (PCE) for different rib surface temperatures T_{rib} ……………………………………………………………...……141

5.5.7 Velocity Distribution of Three-phase flow ……….…144

5.5.8 Pressure distribution of Three phase flow …………….…153

5.5.9 Volume fraction of Three phase flow ……………..…………162

5.5.10 Flow pattern of Three-phase flow behavior……….….……164

5.6.Comparison between Numerical &Experimental Results……..178

Chapter Six: Conclusions and Suggestions…………………………181-182

6.1 Introduction ……………………………………………………...181

6.1 Conclusions ……………………………………………………181

6.2 Suggestions…………………………………………..…………..182

References ……………………………………………………..183-197

APPENDIX A

APPENDIX B

APPENDIX C

APPENDIX D

CHAPTER ONE
Introduction

Chapter One: Introduction

The enhancement of convective heat transfer has a great role in a channel flow which requires more turbulence in the flow. Many modifications have been carried out in the last 10 years on the techniques of enhancing heat transfer. A channel flow is employed in many commercial and variety engineering industries as a power generation, petrochemical, and petroleum depended on the nature of fluids. The technological advancements in thermal energy system required to solve energy problem and determine the cost. On the other hand, the study of enhanced surface heat transfer is of considerable interest in the wide range of industrial and transport applications. In most cases enhanced surfaces are used as the basic element of a devices that deal with concepts of heat exchange [1].

In recent years, the cost /saving of energy and material is increased to produce more efficient heat exchange equipment. For perfect design, as it needs exact analysis of heat transfer rate and pressure drop. The major factor in optimum design is to make the best heat exchange with high heat transfer rate using minimum pumping power [2].

The methods that used to enhance convective of heat transfer is divided into two techniques: passive and active techniques. These techniques are working to enhance heat transfer from one hand and high pressure drop and friction on the other [3]. Techniques of enhancing heat transfer can be classified the mechanisms of enhancing heat transfer as active and passive techniques depending on having or not having extra power [4,5 and 6]. Passive techniques do not require an external power input, except for pump or blower power to move the fluid, and involve the use of roughened surfaces, extended surfaces, displaced promoters, and swirl flow devices. The other kind, active techniques, need extra power such as using an electric or acoustic fields, surface vibration, and mechanical aids merely. One such method, over the past thirty years ribs are used due to their high thermal performance factor [7].

As for the flow within these channels, especially in modern industrial fields, a strong demand focused on analysis of multiphase flow problems [8].

To produce the better understanding of most important mechanisms of heat transfer in a channel flow, numerical simulations may be therefore a helpful tool. Computational Fluent Dynamics (CFD) can be considered as an effective tool for estimating the heat transfer coefficients and the pressure drop to clear the enhancement values. However, the accuracy of the calculation depends on the choice of the most appropriate flow model for (CFD) simulation [9].

1.1 Passive Heat Transfer Techniques

One of the problems is to establish generally-applicable selection criteria for the use of heat transfer techniques. The disadvantages of the passive heat transfer technique are the using of a large number of factors that enter into the decision problem. Many of these are economic factors, such as initial cost, maintenance cost, development cost, etc. and other considerations such as reliability and safety. The essential principle of these techniques is to enhance the convective heat transfer which can be achieved by the following principles [10].

1. Decreasing the thermal boundary layer thickness.
2. Increasing the turbulence in the fluid flow.
3. Increasing the velocity gradient near the heat transfer wall.

The use of this technique causes a swirl in the bulk of the fluids and disturbs the actual boundary layer so as to increase effective surface area. The passive technique involves important techniques, as below: [3,4]

1.1.1 Roughen the Surfaces (Ribs).

It's a common geometric technique to roughen the surface and enhance forced convection by increasing the turbulence effect and increase surface area for heat transfer. Its existence provided more disturbing flow by breaking the boundary layer. Although, the active role of rib that performed, these structures have negatives, as increase friction, the pressure drop leads to high losses [2,7].

1.1.2 Using Curved Geometry (Bend)

Bend is one of the typical components of piping system and any turn (bend) in channel represented as a technique to enhance heat transfer and fluid flow because it generated an additional centrifugal force and grew of secondary flow in the bend region [8,11].

1.1.3 Surface Area of Channels

The increasing surface area of convection represents important factor to enhance heat transfer by using rough walls. The use of walls with shapes such as longitudinal wavy rib along wavy channel or expanded the heat exchange in the channel by increasing the aspect ratio to 2:1instead of 1:1 as shown in Figure (1.1) a, b, [12,13].

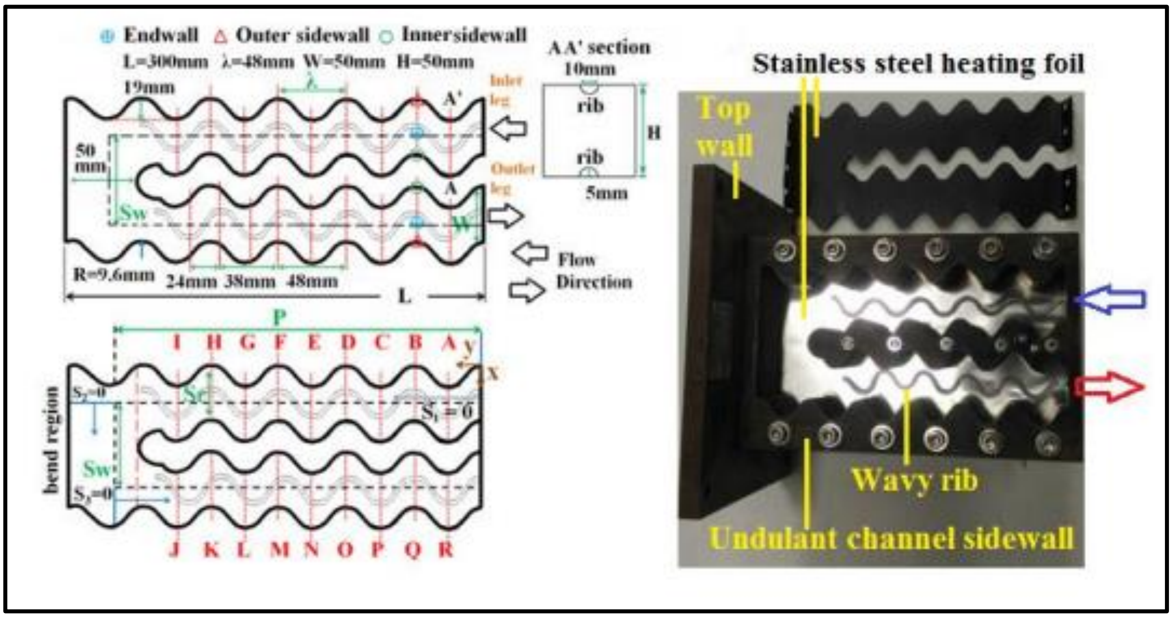

(a) Wavy channel with wavy Rib [12].

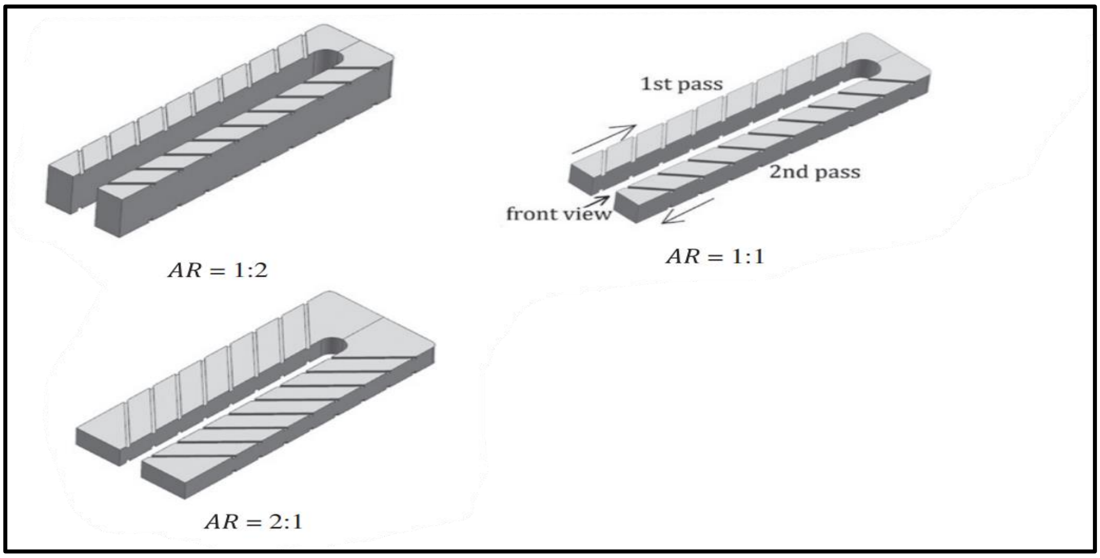

(b) Dimensions and Aspect ratio [13]

Figure (1.1). Increasing the area of heat exchange.

1.2 Rib Geometry

To understand the physics of flow related to the ribs, it should commonly define the features of ribs such as height, configuration, and rib spacing. Figure (1.2) (a) provides the schematic of the flow behavior inside ribbed channel. The significance and principle of ribs is to create a turbulence and break the boundary layer due to the separation and reattachment of flow. From this figure, it can be shown the separated boundary layer is induced by the upstream rib form a separated shear layer and reattaches on wall of channel [14]. Also, the typical behavior of local heat transfer distribution in inter-rib region of the fully developed channel is shown in Figure (1.3). The minimum values of local heat transfer is at a region X8 because of recirculation flow while the local maximum value is in the region X9 because of reattachment in flow. After reattachment, the local heat transfer is decreased until reaching a minimum valve at X10 due to separation. At the corner of the rib in downstream created a small vortex which tapered some flow and produced a maximum local heat transfer in region X11.Enhacment in heat transfer attached an increasing in pressure drop of fluids and pumping power [15].

Many geometries of ribs have been proposed to enhance heat transfer and more of them are still being developed**.** It involved various geometrical parameters as below [14]: -

a. **Shape**: Contribute to turbulence, most of ribs found are rectangular ribs, square ribs, inclined angle ribs, triangular ribs, M-shaped rib, W-shaped rib and V-Shaped rib.
b. **Height**: Available heights of ribs are preferred to achieve turbulence; they effect flow in few numbers of rib.
c. **Space between two ribs:** Distance between ribs effects the reattachment and separation regions.
d. **Width:** Suitable widths of ribs are preferred to increase the surface area for transfer energy.

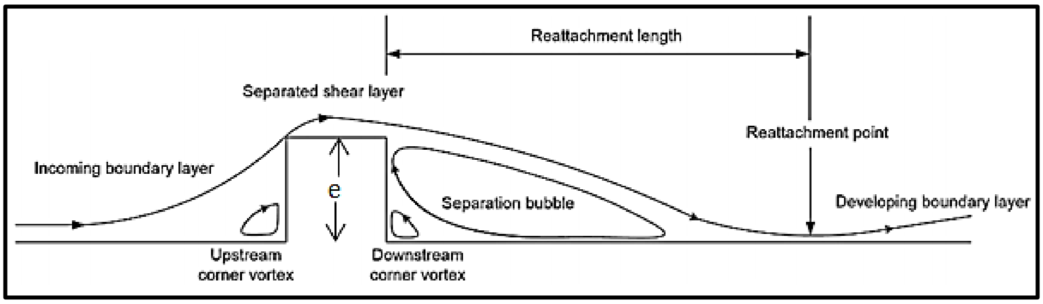

Figure (1.2) Flow structure near the ribbed wall.[14].

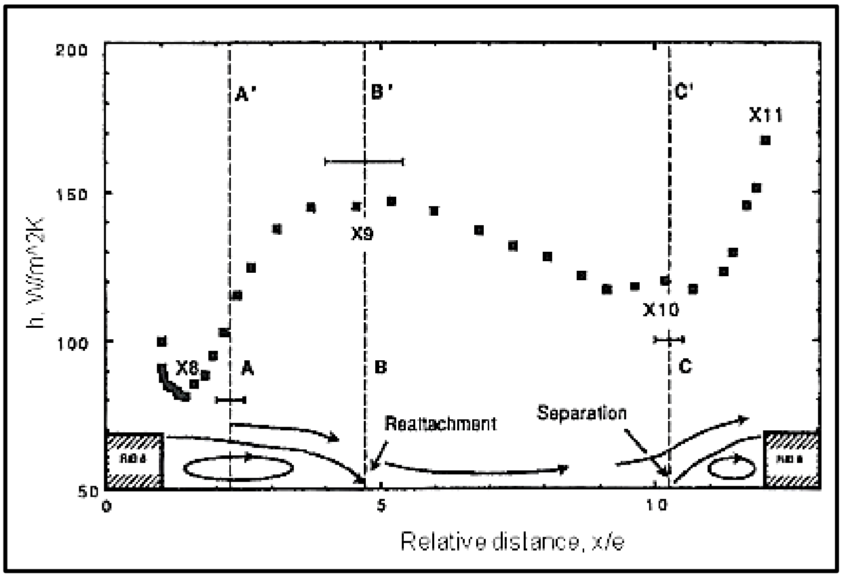

Figure (1.3). Heat transfer distribution behavior with ribs.[16].

e- Ribs Angle and Orientation

The rib angle with respect to the direction of flow represents one of the main factors in creating turbulence and vortices and thus enhancing heat transfer. Using the angle, the efficient area that will be contributed can be determined. Therefore, it is necessary to choose the angle that gives more resistance to more turbulence and more heat transfer as shown in Figure (1.4) a, [17].

Although the term "Rib Orientation" of ribs with respect to the flow direction has a crucial role to enhance the heat transfer within the channel without incurring the penalties of friction and pressure drop that are severe enough to negate the benefits of heat transfer enhancement. The orientations of ribs may be arranged as negative-negative, positive-positive, positive-negative, and negative-positive are measured depending on flow direction in the two pass channels, as shown in Figure (1.4) b, [18].

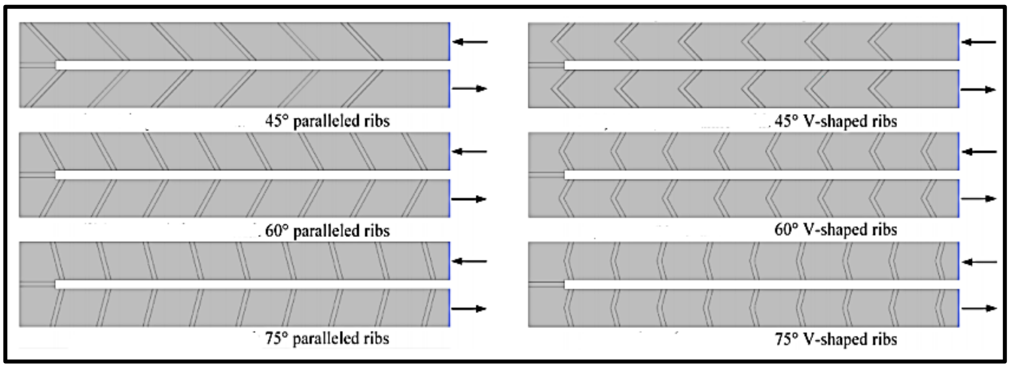

(a) Different Rib angles [17].

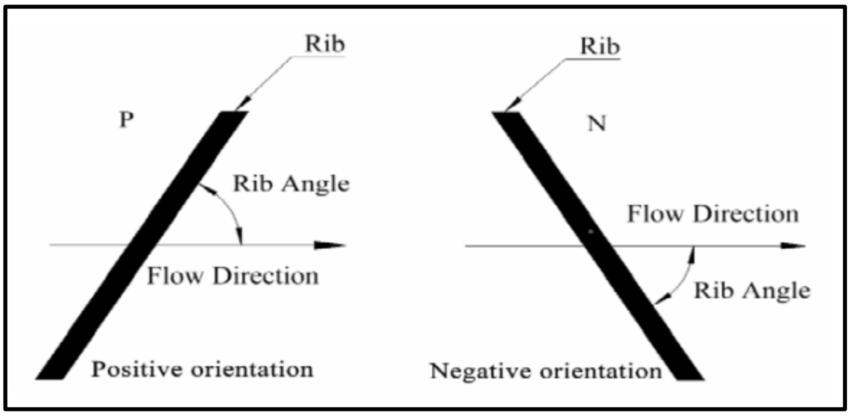

(b) Ribs orientation [18].

Figure (1.4). Ribs angles and orientation arrangement.

1.3 Concept of Ribbed Surface of Two-Pass Channels

The technology development of heat transfer focused mainly on the improvement of ribbed surface to increase the internal area and break down the laminar sublayer to redevelop the boundary layer and help in enhancing heat transfer. When the ribs disturb the incoming boundary layer, it creates a turbulence. Although the complex flow field generated by the ribs provides significant heat transfer enhancement, the presence of these roughness elements results in pressure drop. In the past, numerous experimental and numerical studies have been carried out to assess the thermal performance factor of the roughening features [13-14].

In past, this technique used in gas turbine and heat exchangers when air cooling needs to provide secondary flow for more turbulence. Fluid flow and heat transfer in rectangular channel is most commonly studied due to their wide applications. Therefore, the investigation of heat transfer enhancement in rectangular channel is essential. The rib technique for improving and increasing surface area has been used in heat transfer enhancement to provide efficient mixing and strong secondary flow [4]. Recently, many techniques used to enhance heat transfer are reported, which modify the inclined rib pattern and geometry along the downstream direction to reduce pressure drop. In past several years, most researches had concentrated on ribs and turbulence to provides a better thermal contact between the surface and the fluid create swirl to improve the temperature gradient, which ultimately leads to a high heat transfer coefficient [5].

1.4 Concept of Bend

The bend configuration is almost in transportation systems. It existed necessary in piping system specially oil-water flow application such as petrochemical industries, petroleum production and transportation. The efficient configuration plays a great role to create turbulence when needs to enhance heat transfer. The reasons for using bend with different configuration are related to limit the installation space and change the direction of channel. Besides flexibility, a bend with a specific shape, i.e., a sharp-bend, provides turbulence and pressure drop for the purpose of transferring heat. The bend depends on fluids and purpose of using, it sometime appropriates in transportation fluids from place to another or in heat exchangers, cooling ducts and pneumatic conveying dryer applications [8].

1.5 Concept of Two-Phase Flow and Three Phase Flow

In recent years, the investigation more than one phase flow attracts more interest in many studies. For example, one of the most applications of three-phase flow is in the petrochemical industry in which gas phase usually flows in a combination with oil and water phases in transportation pipelines to enhance heat transfer [8]. Studying flow characteristics such as pressure drop is a necessary for designing this equipment.

Generally, three-phase flows are more complex than gas-liquid two-phase flows because of an additional phase with different physical properties which leads to a wide variety of behavior and properties. The fluids that passed through ribbed region and then in the bend are affected by complex behavior such as secondary flow and turbulence [8,17].

1.6 Industrial Applications

A channel flow that required increasing heat transfer coefficient depends on passing fluids. Rectangular channels with ribs are widely used in compact heat exchangers to enhance the heat transfer, because the ribs increase the turbulent fluid flow near the wall and disrupt the thermal boundary layer [1–3]. However, the traditional methods usually generate great pressure drop and consume more pumps energy. The two-pass channel is used with a wide range when the working fluid as air-water, oil-water, air-steam, and nano fluid–air etc. There are many applications such as piping system, power generation, chemical engineering process, heat exchangers [19-24]. A multi-phase flow used in several industries as petroleum production, transportation and petrochemical industries [8 ,26].

1.7 The main objective

The main objective of this study is to develop and modify a ribbed channel of two-pass flow to obtain an optimum design. The numerical and experimental investigations are used to enhance heat transfer in case of two-phase or three phase flow in a horizontal rectangular Ribbed two-pass channel under turbulent flow with Re ranged for two phase flow and three-phase flow are with a range of (($Re \geq 72456.3$)) and (($Re \geq 128182$)) at constant inlet temperature, respectively. This goal is accomplished through the following main steps:

A. Numerical Part

The aim of the present work is to study and analysis an optimum design of ribbed channel of two-pass using ANSYS Fluent commercial CFD software. There are several modifications are: first, the simple smooth channel is analyzed, then, the comparison between the two shapes of ribs (Curved rib and V-shaped rib) is done to obtain an optimum rib. After that, comparison shapes perforating area are as (circle, triangle, square) at same cross section. Then, investigating the perforating area as circle diameters are (3,6,9) mm. And, comparison rib angles are (30°,45°,60°). Also, the behaviors of two types of flow are two and three phase flow with different ribs temperature and flow velocities.

B. Experimental Part

Experimental test rig of optimum design is built with all necessary apparatuses required to evaluate the heat transfer and pressure drop for two types of flow at varies rib temperature with varies velocities.

1.9 Layout of Dissertation

It consists of six main chapters:

- The introduction and the general overview are introduced in chapter one.
- Chapter two gives a systematic and comprehensive review of the literature on related research problems.
- Chapter three described the work numerical to choose the optimum design after a series of modifications with several experiments with different boundary conditions.
- Chapter four is devoted to describe the experimental construction and measuring instrumentations and show the comparison with the numerical model.
- Results of the study are presented and discussed in chapter five.
- The conclusions and suggestions are summarized in chapter six.

CHAPTER TWO

Literature Review

Chapter Two: Literature Review

2.1. Introduction

This chapter focused on the significant of recent researches that improve the geometric shape of ribbed with two-pass channel or without ribs and its influence on the heat transfer enhancement and flow. The classification of these researches can be done as follows: -

2.2. Numerical Studies

Su et al. [27] studied numerically the effect of high Reynolds numbers on heat transfer coefficients and friction factors in 3-D geometry with three cases of aspect ratios (AR = 1:1; 1:2; 1:4) and same length and bend shape of smooth two-pass channels. Re of air ranged from 10,000 to100,000. Results presented that the AR was strongly affected on vortices also the $Nu\backslash Nu_o$ decreased when Re increased. In addition, the AR=1:2 rectangular channel has the highest $Nu\backslash Nu_o$ at turn region because vortices were stronger than AR=1:1 or 1:4 channels .The heat transfer in bend was high due to turbulence and associated pressure gradient, while the AR=1:2 has higher enhancement in heat transfer than AR=1:4 at same conditions, because vortices generated in bend region would develop to the highest strength and expand to entire second-pass while remaining confined to leading and trailing surface in AR=1:4 of channels. Also, it observed when Re increased that $f//f_o$ decreased for three cases of aspect ratios.

Kamali et al. [28] described numerically the characteristics for the heat transfer and behavior of flow in 2-D channel with many shapes of ribs named as square, triangle and trapezoidal installed in one wall. Re ranged for air flow from 8000 to 20000.The main goal of this study is to provide information about local heat transfer for different ribs of various kinds. The results showed that the heat transfer coefficients were strongly affected by rib shapes. Also, the cases of [trapezoidal rib with decreasing height in flow direction] provided highest enhancement in heat transfer and pressure drop than other cases because of rib feature created more turbulence and losses. In addition, it found that (***f***) in case (the trapezoidal rib with increasing height in flow direction) had lowest value.

Dhanasekaran et al. [29] investigated numerical work the role of ribs and bend on the heat transfer enhancement and Nu distribution of internally air flow through two-pass channel with 45° ribbed with positive–negative arrangement where ribs installed in top and bottom walls. To predict mist cooling enhancement in rectangular ribbed channel with constant heat flux. Re were as 5000,10000,25000 and 40000 and temperature of 300K where assumed the exist pressure to be a constant value of 1 atm. Results showed that the turbulence generated due to bend shape and Nu increased with Re increased through channel. Also, the presented effect of bend on behavior of Nu with the presence of ribs was as a fluctuant curve and it observed that ribbed regions and bend had high Nu values in comparison with smooth channel at Re=25000.

Wei et al. [30] investigated numerically in three-dimensional flow (mist-air) and the heat transfer enhancement in two-pass of square cross section and sharp bend of the channels with 45° angled ribs install on top & base as a heated walls under fixed surface temperature (T_w) with no slip. Re was about 25000 at static pressure 1×10^6. ANSYS CFX 11.0 simulated work and used (k-ε turbulence model). Results indicated that the Nu increased in ribbed regions and bend region. Also, the reasons explained this behavior were that high turbulence in ribbed region led to break boundary layer and created flow pattern was quite complex, but in bend, the turbulence decreased. The curve behavior of Nu at first decreased because of smooth region of low turbulence when in ribbed regions the turbulence increased led to increase Nu with fluctuant behavior.

Siddique et al. [31] analyzed numerically the heat transfer enhancement as three-dimensional geometry in two-pass channels of walls roughened of 45° with aspect ratio equal to (W_{in}/H=1:3) in the inlet pass and (1:1) in outlet pass connected with sharp 180° bend .Also comparison with a reference channel of W/H=1:2 channel .By CFD Fluent simulated and Re equal 100,000 with inlet air temperature 310 K. Results noticed that pressure drop inlet pass W/H=1:3 have lower values in comparison with W/H=1:2 in the entire channel. The less pressure drop was an important advantage in design made W/H=1:3 as aspect ratio was more attractive. In addition, pressure drop decreased with decreasing aspect ratio in ribbed region channel. Also, heat transfer at tip wall and bend decreased for the smaller aspect ratio of inlet pass Win/H=1:3 .Heat transfer enhancement increased with smaller aspect ratio channel.

Shen et al. [32] investigated numerical study of combination two means (dimples and bleed holes) to enhancement heat transfer behavior in two-pass with bend 180° channel. Simulation performed by RANS with different position of hole and angle of installation. Comparison the enhancement of heat transfer of dimples with bleed with other devices of enhancing heat such as ribbed channels. Pressure drop in the two pass was slightly but in the bend was very sharply with Reynolds numbers varied from 12500 to 50000. Results indicated that the rate heat transfer are higher in case of dimples and bleed holes than case of using dimples or holes separately. Results observed that Nu and heat transfer were higher in second–pass than in first pass led to heat transfer more enhancing. The holes of bleed have higher Nu because of boundary layer destruction by different bleed position. In comparison of friction factor increased due to bend than straight channel but the dimple contributed to increased pressure drop was very slightly. Dimpled channels have much lower friction than ribbed channel.

Ramadhan et ,al. [33] presented numerically a two-dimensional of turbulent flow heat transfer through a grooved channel with circle cross section. In this study four geometric shapes such as a (circular, rectangular, trapezoidal and triangular) and aspect ratios of groove-depth to channel diameter (0.1 & 0.2). Re ranged from 10,000 to 20,000 when the boundary conditions were at constant heat flux =1000W/m^2 with inlet velocity ranged from 3.18 and 6.36m/s of air with constant properties at T_{in} equal 300K.Simulation by CFD commercial code FLUENT. Results observed that the best enhancement occurred with the lower depth-groove ratio. Also, it was observed that the grooved provided a considerable increased about 64.4 % in heat transfer than smooth channel. The optimum choice for best enhancing in heat transfer was triangle groove for any depth and in groove of (e/D=0.1) because it has a gained of thermal enhancement factor about 1.52 than other. The groove is the most appropriate choice to enhance the heat transfer based on reason because the (PCE) has 41.1% higher than smooth channel.

Saha et al. [34] studied numerically the effect of bend geometry on heat transfer and pressure drop turbulent flow inside a two-pass channel of AR=1:1with different bend geometries. In this study found geometry that reduced the bend related pressure drop and enhance in heat transfer coefficients. A square channel with a round U-bend is taken as a baseline case and compared with nine different bend geometries named as turning vane geometry, an asymmetrical bulb, three different symmetrical bulbs, two different bow shaped geometries at the end wall, a bend with an array of dimples in the bend region, and a bow and dimples geometry. In CFD simulation used RANS equations and (realizable k-ε turbulence model) depending on computing Nu/Nu_o , f/f_o and PCE .Results found that all bend geometries have significant effect and showing increased in PCE of a two-pass channel. Also, the symmetrical bulb configuration showed reduce in

f/f_o and increased PCE 30% .The highest PCE was 41% over baseline in type symmetrical bulb combined with bow along the outer walls and surface dimples.

Balasubramanian et al. [35] studied numerically the behavior of heat and flow in two-pass channel without ribs .All the wall imposed to constant temperature about 350K when air flow rate with temperature 300K .The turbulence model used realizable k-ε of RANS for two layer $5 < y+ < 30$ as resolution mesh .In simulation used two types of mesh trimmer and tetrahedral for Re around 30000.The results showed that heat transfer coefficient is independent of the grid topology and present key parameter for resolving the heat transfer coefficient at walls depended on the resolution of boundary layer .The strong flow impingement and flow separation at bend and large recirculation bubble in downstream and bifurcation zone due to secondary flow after bend. Also, it showed that high heat transfer in the impingements zone but large recirculation bubble in second pass led to reduce heat transfer coefficient. In addition, the tetrahedral mesh was more sufficient especially in bend region.

Zhu et al.[36]studied numerically the secondary flow and heat transfer enhancement in rectangular two-pass channel with 45° ribs. Re of air flow ranged from 25000 to 40000., Results showed that the main flow secondary flow was thrown to the outer side wall after the bend due to the centrifugal force, and it weakened in second pass and a new main flow secondary flow was generated at same time near the opposite side wall in second pass. In addition, heat transfer strength was dissipated in second–pass cause by interaction between old and new secondary flow. Also, results showed that the increasing of Re led to the reduction of the effect of corner on main flow region in passage 2 ,at Re equal 40000 the secondary flow in main flow region of corner is dissipated before the entrance of pass 2.In addition, the heat transfer strength in the corner was obvious higher than in straight passage due to the additional disturbance generated by secondary flow.

Al-Shamani et al. [37] investigated numerically the affecting of heat transfer due to turbulent forced convective flow of Nano fluids through rib–groove in one pass horizontal channel. Four cases of ribs and groove named different trapezoidal configurations with flow direction and uniform heat flux on up & down walls. The types of nanoparticles SiO_2 ,Al_2O_3, ZnO and CuO. In this study, the results are carried out over a range of Re 10,000–40,000, at constant temperature. Results indicated that the cases trapezoidal with increasing height in the flow direction with rib–trapezoidal groove has the higher heat transfer rate and higher Nu. The type SiO_2 had the highest Nu. Also, Nu increased as the volume fraction increased. In addition, the trapezoidal rib-groove used good candidates for the development of efficient mean for heat exchange.

Andreozzi et al. [38] presented numerically that forced convection enhancement in channels with flow of water/Al_2O_3. Different arrangements of geometric rib used such as trapezoidal, rectangular, triangular shapes heated with constant uniform heat flux. Re ranged from 20,000 to 60,000. Results showed the heat transfer rate increases with increasing Re and nanoparticle volume fraction. The triangular ribs have higher-pressure drop and $\overline{Nu}$ has higher than trapezoidal rib. The $\overline{Nu}$ increases while Re increases in triangular ribs.

Zheng et al. [39] investigated numerically the effects of rib arrangements on the flow pattern and heat transfer in an internally ribbed heat exchanger tube with different rib arrangements. Ribs arranged in two types with parallel type ribs and V shape type ribs. Re of water ranged from 6780 to 20340 with steady flow. The results observed effects of rib arrangement on heat transfer and flow pattern as $\overline{Nu}$ and f in the V-type were about 57-76% and 86-94% higher than those in the P-type ribbed tube, respectively. The (PCE) in V- type varied from 1.32 to 1.74, which were about 27% - 41% higher than that in P-type at same pumping power Also, the longitudinal swirl flow with multiple vortices induced in the V-type ribbed tube was a more effective flow pattern for heat transfer, compared to the longitudinal swirl flow with single vortex generated in the P-type ribbed tube.

Gao et al. [40] investigated and compared numerically conjugated heat transfer through channel with internal flow of stream /air in high aspect ratio in two pass ribbed channel by relationship between flow field and heat transfer under constant heat flux. Re ranged about larger than 30000.The fluid field structure was shown by vortex core technology. The results presented that the generation and separation of secondary flow led to enhance local heat transfer strength. Also, the maximum difference in temperature of inner and outer surface in certain position was lower than 2K.

Kim et al. [41] investigated numerically the effect of the non-uniform inlet velocity profile and heat transfer in ribbed channel. Four inlet air velocity profile named as: fully developed flow, uniform inlet profile, asymmetrical flow of maximum velocity near lower level, asymmetrical flow for upper level when the mass flow rate for all cases was same Re based on mean velocity for all cases. Re varied as 10,000 and 30,000. The rib installation with angle was 60°and ratio of rib-pitch to height ratio (P/e) equal10. Results showed that the local heat transfer and pressure drop affected by the inlet velocity profile in channel. The inlet velocity profile altered the path and strength of the secondary flow. The overall Nu/Nu_o was the highest value for profile of uniform and case (the fully developed inlet profile) resulted in the lowest Nu/Nu_o. The value of *f* was the lowest for case uniform inlet profile, while fully developed inlet profile showed the highest *f*. Also, the PCE had a 20% for fully developed inlet profile higher than uniform inlet profile while other profile showed similar PEC.

Al-Turaihi et al [42] performed a numerical work for two-phase flow (water-air) in ribbed rectangular channel where ribs used with different shapes. Also, this study showed the effect of ribs on coefficient of heat transfer. Three ribs shapes were used rectangular, triangle and trapezoidal. Turbulence model used a k-ε as standard and water-air as primary-secondary respectively. The velocities ranged from (0.12 -0.18) m/s and (0.4-0.8) m/s for air and water respectively. Results presentation as that the heat transfer coefficient increased by adding ribs, it also increased as the velocity of flow increased. Also, heat transfer coefficient has 135.65% for triangle rib and 73.97 % and 99.14 % for rectangular and trapezoidal ribbed duct respectively in comparison with smooth channel. At ribs and the leading edge of the ribs the velocity is increased which increase the heat transfer coefficient, at the trailing edge the velocity is lower which give low heat transfer coefficient.

Pourfattah et al. [43] investigated numerically the effects of (AL_2O_3) and rib angle on enhancement heat transfer when turbulent flow in channel. Several angles of ribs were (30°,60°,90°,120°,150°) where the walls under constant heat flux of 10 kW . The working fluid was water as base flow and nanoparticles of AL_2O_3 with several volume fraction (α=0.02,0.04) when Re ranged from (24000-600000) at constant inlet temperature 300K. The ribs were attached rib and detached rib. The results explained that existence of ribs created a eddy on direction of flow cause better mixture of flow and adding nanoparticles to base flow lead to heat transfer enhancement. To improve heat transfer without considering the applied pressure drop the 90° was best suggested, while the 60° was get the maximum ratio heat transfer enhancement to the applied pressure drop. By increasing Re to 60000, the adding 4% of nanoparticles causes enhancement of heat transfer about 22%.

Wang et al. [44] studied numerically the distribution of heat transfer along ribs surface, end wall surface and all surface during two-pass channel, and effect of Re (10000-40000), ribs (45° and 90°) and aspect ratio on flow behavior and surface heat transfer as local. Results showed that 45°angled ribs increased the area led to enhance heat transfer with 30 % and increased overall heat transfer coefficient about 50 % than smooth channels. The increasing in Re was significant enhancing heat transfer along ribbed channel. In comparison, the wide channel (2:1) has be better enhanced factor than narrow channel (1:2) but narrow channel reduces pressure drop by about 60%. Also, ribs heat transfer quantity increases with an increase of the inlet Re.

Ravi et al. [45] investigated numerically that heat transfer and friction characteristics of air flow in four different rib shape - 45° angled, V-shaped, W-shaped and M-shaped ribs in a two-pass channel with aspect ratio 1:1 . Re varied 20,000 to70,000. Simulation performed by RANS with commercial software ANSYS used k-ε (realizable). The results showed that the heat transfer enhancement performed by V-shaped ribs was 7% higher than 45 ribs, 28% higher than W-shaped ribs and 35% higher than M-shaped ribs. However, the pressure penalty for V-shaped ribs was 19% higher than 45 ribs, 24% higher than W-shaped ribs and 28% higher than M-shaped ribs.

Xie et al. [46] studied numerically the fluid flow and heat transfer characteristics in a cooling channel with various crescent ribs mounted on one wall. Kinds of ribs named as straight, crescent rib concave to the stream-wise direction, the crescent rib convex to the stream-wise direction. Re ranged from 8000 to 24,000 for air flow. Results showed that the cases with crescent ribs significantly outperform the case with straight ribs with respect to heat transfer performance. Also, the crescent ribbed channels provide a 21–41% higher normalized average Nu relative the straight ribbed channel, while inevitably lead to a 15–80% higher pressure drop. Enhancing by ribs met a induce high pressure.

Rasool et al. [47] indicated numerically effect of ribs shape on heat transfer and friction factor for air turbulent flow in a two-pass channel. Different shape of ribs was square, boot, trapezoidal and house rib with surface temperature about 100 °C. Re for turbulent flow ranged of 5000-52000. The results presented that shaped rib design significantly influenced on characteristic transfer distribution and fluid flow. The boot shaped rib design had better heat transfer and friction factor than other shapes. Boot shaped rib had a best heat transfer enhancement and pressure drop lower than square rib but best pressure loss performance had by house shaped rib. Generally improving heat transfer coefficient was by increasing Reynolds number.

Rasool et al. [48] studied numerically the perforated ribs in two-pass channel to heat transfer enhancement and pressure drop. Cases named as solid rib, cylindrical hole at bottom, square hole at bottom, cylindrical hole inclined at 30° and tilted cylindrical holes and heated to 100C°. Air was working fluid at Re about 10000-50000. Results showed that the perforation in the ribs enhanced heat transfer coefficient about 1.4 -5.7 % than conventional solid ribs. Also, the inclined perforations in rib had better heat transfer coefficients by increment about 18.3 -25.4% and higher friction factors compared with conventional solid ribs. Pressure drop increment was up to 0.89 -6.3 % higher than solid ribs under similar flow conditions, square hole at bottom had higher Nu than other cases.

Gao et al. [49] investigated numerically the generation and distribution of secondary flow and influence of rib angle and rib orientation during two-pass ribbed channel .Re ranged of air flow 30000.The turbulent model of

ANSYS CFX 14 was SST-k-ω with boundary conditions as 1 atm of static pressure and inlet temperature 298K with turbulent intensity 5%.Results observed more secondary transport lead to enhance heat transfer .In first pass the local heat transfer limited by rib angle but in second –pass limited by rib angle , orientation, and bend region .The percentage of average heat enhancement in 30°,45°,60°,75° as rib angle through first pass was 93.97%,121.65%,127%,81.97% but about 60.33% in second pass of channel with 60°PN. The lowest average heat transfer enhancing in 75NP was 11.23%.

Jiang et al.[50] studied numerically the characteristics of heat and flow in a two-pass ribbed channel .The ribs was about different rib angles of 45°,60°,75° with constant heat flux .Various shapes of ribs were 45°paralleled ,60° paralleled ,75° paralleled ,45°V-shaped ribs,60°V-shaped .Re varied in flow of air about . Numerical simulation perforated by k-ε standard model ,RNG model ,SST model to select the k-ε standard as optimum model .Results observed that ribs of V-shaped secondary flow in first pass in center area while paralleled-shaped was more closed to outer wall of passage .Also due to increase mist/steam ratio was increased heat transfer gradually .Two-pass channel with 45-paralleled ribs or V-shaped ribs had higher heat transfer while channel with 75 paralleled ribs or V-shaped ribs had lower heat transfer .Nu in 45° V-shaped was about 20.78% higher than 75° V-shaped .Also ,Nu in 45° paralleled ribs was about 10.86% higher than 75° paralleled ribs .

Göhring et al. [51] investigated numerically stationary smooth and ribbed two-pass cooling channels. As a goal of studying, the results of numerical simulation validated with experimental data of another studying. The configuration of rib with flow direction inclined by angle 45°. The Reynolds number was 25,000 with wall temperature about 71.11°C. A model of turbulence SST with combined Reynolds stress model performed with reattachment modification. The results showed that this model was capable to predict the experimental reference data of heat transfer results within an overall deviation of 19%. The deviation of Nu/Nu_o ratios about 23% and 13% for smooth and ribbed respectively.

Jiang et al. [52] studied numerically the effect of two-phase flow (mist/steam) on heat transfer internally in in ribbed channel with two-pass of two array of rib , top and bottom walls with angle about 60°.Also ,this study analyzed the effect of 60° angled ribs on generation of secondary flow .The turbulence model utilized standard K-ε and dispersed phase model for water mist in simulation work ,under conditions was no-slip with constant heat flux about 10000 W/m^2 ,with Re greater than of 200.The results showed that the influence of ribs as a vortex regions in main stream .The locations of this vortex were outer side wall and inner side wall for first pass and second pass respectively. But, in turning region and near ribs appeared the strongest vortex strength.

Mondol et al. [53] studied numerically the behavior of flow in 180° bend and characteristic the profile and distribution of velocity and pressure in 2-D channel. Reynolds numbers values ranged 827 to 1654 inlet velocity 10,15,20 m/s, water as working fluid. Boundary conditions were as outlet pressure and no slip. The results presented that the behavior of pressure in lower and upper portion of the bend, when its increased and then decreased after passing through bend. While for velocity distribution increased with Re but maximum velocity occurred in bend because of flow separation. In addition, for different Reynolds number, it showed a changed in pressure and velocity distributions. The velocity was increased when Reynolds numbers was increased, and pressure drop increased in centerline of channel.

Gao et al.[54] investigated numerically influence of heat transfer and friction loss with configuration rib in two-pass ribbed channels. Four rib orientation (PP, NN, PN, NP), two ribs angles of 45°and 60° and eight different bend shapes (ORIR, ORIS, ORRIR, ORRIS, OSRIR, OSIS, OLRIR, OLRIS). Re varied as 30000.The results showed that rib orientation determined the position secondary flow while the shape of bend determined the local secondary flow generation. The sharp edge outer has a significant enhancement of heat transfer at entrance of the second pass. The case of ORIR have a least pressure drop and NP leaded a higher heat transfer. Angle of 45° leaded to similar but weaker secondary flow corresponding angle with 60° ribs. The Nu increased about 2.0% in case of 60 NP ORRIS.

Luan et al. [55] investigated numerically a method of connecting holes between legs of a two-pass channel with and without ribs. Re ranged 10,000, 30,000 and 50,000. Different rib configurations and holes positions were designed. The result showed that positive effect of the holes on the enhancement especially in ribbed channels. Connecting holes largely reduced pressure drop across the channel but heat transfer decreased. For the smooth channel, pressure loss reduced by 14.66% at the heat transfer loss of 1.68%, for the ribbed channel pressure loss reduced by 47.99% with merely 8.24% decreased in heat transfer with ribs when connecting holes.

He et al. [56] investigated numerically optimization ribbed U-bend cooling channel to enhance heat transfer in internal cooling designs use complex geometries consisting of ribbed serpentine channels. Comparison the optimization results to get optimum design and arrangement that lead to lower pressure loss while enhancing heat transfer. Boundary conditions were of Re about 42000, inlet temperature of air was 293.15K when the wall temperature about 303.1K. Several variables the rib design depended upon shape, height, pitch, and angle. The results showed that the optimizing the U-bend shape was more effective for improving overall heat transfer than optimizing the rib arrangement. Also, the optimizing ribs was more effective for improving local heat transfer.

Yan et al. [57] studied numerically the effect of inclination divider on heat transfer and flow characteristics in a ribbed two-pass channel for Re varied from 10,000 to 50,000. The inclination angles of divider were − 3◦, − 2◦, − 1◦ ,0◦, + 1◦, +2◦ and + 3◦and ribs with angle of 45◦. Results showed that channels with wall divider inclined produced friction factors is higher cause by pressure drop than a channel with straight divider wall. Also, channel have larger negatively inclined of wall divider showed best enhancement in heat transfer in the second passage while worse heat transfer in the first pass and bend region.

2.3- Experimental Studies

Al-Hadhrami et al. [58] investigated experimentally the effect of various 45°angled rib turbulator arrangements on the heat transfer enhancement, two-pass square channel with copper plates were heated to provide a uniform heat flux. Experiments carried out for Reynolds numbers from 5000 ,10000 to 25000. Arrangements of rib turbulators are arranged in angle of (+45° &-45°) in the flow direction, and heated surface around 65°C. The results showed that the 45° parallel rib arrangement provided higher heat transfer enhancement were compared to 45° crossed rib.

Liu et al. [59] investigated experimentally the effect of rib spacing on the heat transfer enhancement and pressure penalty in stationary rectangular, cooling channels. Re ranged from 5000 to 40000 for air as a working fluid. In this studying, it investigated which ribs spacing have highest enhancements. In the 1:2 rectangular channels, 45° angled ribs of square placed on the leading and trailing surfaces with rib spacing (P/e) as

3, 5, 7.5 and 10. The result observed that the case of very close rib spacing of P/e = 3 have greatest heat transfer enhancement, while the P/e = 5 spacing has the greatest pressure penalty.

Salameh et al. [60]studied experimentally that pressure drop and heat transfer for turbulent flow inside a U-channel for outer wall rib bends and smooth. Re number was varied from 8000 to 20000 with uniform heat flux. The results showed that friction factor ratio and the heat transfer enhancement ratio in ribbed bend at a Reynolds number of 20000 were 48.75 and 2.66, respectively. Also, it found that the presence of the rib increased the heat transfer coefficient on outer wall of bend. In addition, uncertainties were 3% and 6% for the Nusselt number and friction factor, respectively.

Elfert et al. [61] investigated experimentally the flow characteristic in two-pass channel by using a technique "nonintrusive particle image velocity (PIV).The ribs were on two opposite walls in a symmetric orientation inclined with angle 45°with square cross section to turbulent flow direction. Dimensions were length equal $10d_h$ when d=25mm, p/e=10 , e/D=0.1,0.06. Re values were 50000, while air as working fluid of test model. The results also showed the effect of the presence of the ribs on the flow, which would cause a change in the fluid movement as desired by created advanced vortices in both passes and bend created vortices notice in second pass beginning.

Wang et al. [62] investigated and presented experimentally the end wall heat transfer characteristics at bend the effects of periodic ribs on end wall heat transfer in channel of two–pass in square cross section 50×50 mm^2.Air was a liquid as working fluid. Reynolds numbers ranged 11000 to 26000. Plexiglass were fitted onto the end wall e/D_h =0.06, P/e varied from 6 to15.The rib with square cross section is fixed on the end wall vertically on base of bend and provided with heat flux. Results showed that domination of heat transfer at the bend in case of ribs absence due to flow impingement. Also, heat transfer distributions in the end wall were changed. Turbulence levels lead to change in heat transfer were very significantly. Heat transfer enhancement had best value in rib pitch ratio equal to 12.

Pietrzak et al. [63] presented an experimental method for how to measure the pressure drops of gas-liquid and liquid-liquid-gas during horizontal pipe with 180° bend of channel. Results shows the void fraction increases along with increased air velocity and it presented a method and ensure high precision and could be calculated all parameters during two-phase flow and three-phase flow with various shape geometry of bend. Also, in this study calculated the pressure drop in horizontal pipe for two-phase flow.

Oliveira et al. [64] studied experimentally the pressure gradient and gas holdup in two–phase flow (air-water) during vertical channel with 180° bend and two horizontal passes. Boundary condition named with superficial velocities of water and air were 0.2m/s and 0.4 ,4 ,20 m/s, respectively. It was noted that the variation pressure gradients were more sharply occurred in downstream of bend from negative to positive. The limited change in the pressure was about of 40~60 diameter channel for upstream and downstream of the bend, respectively. The results showed that the maximum pressure drop occurred in bend region in compared with other. The bend finding led to destroy the waves of flow.

Liou et al. [65] presented experimentally the effects of rib angle ,rib orientation on air flow field in two–pass parallelogram channel with 180°bend by description flow pattern and turbulence .This study included secondary flow mean velocity vector ,turbulent intensity ,Reynolds stress and turbulent kinetic energy in various orientation (45°,-45°,90°) in ribbed channel .Air as working fluid at Reynolds number about 10000.The results presented a difference in flow characteristics near top &bottom of ribbed channel for three angle but heat transfer distributions were same for ±45° same Nu/Nu_o distributions on top and bottom walls of square channels whereas difference in flow characteristic near top and bottom wall in parallelogram channel.

Singh et al. [66]investigated experimentally the characteristic of heat transfer in combination V-shaped rib and cylindrical dimples in two-pass channel .Different configuration named as : dimples alone ,ribs alone , and combining of both rib-dimples. In, this studying to know the enhancement of heat transfer normalized depending to smooth case, pressure drop depended on smooth channel as reference and correlation turbulence model by Blasius correlation. Reynolds numbers ranged from 19500 -69000, pressure drop calculated by pressure across two-pass. Results showed that the combination of ribs and dimples observed higher heat transfer enhancement led to higher thermal hydraulic performance as compared with ribs or dimples as alone.

Liou et al. [67] presented experimentally that the Nusselt number (Nu) distributions and flow fields in the two-pass parallelogram channels. The ribs of square shape on two opposite channels. The ribs along wall channel with configuration as attached or detached. In this studying, its investigation about Nusselt Number and friction factor for Reynolds number ranged for air flow from 5000 to 20,000. The results noticed that the heat transfer enhancement in detached ribs have higher values than attached ribs. The ratios of $\overline{Nu}/Nu_o$ of inlet leg, turning region, outlet leg, and entire end wall for the attached rib case varied 2.53–2.46 ,3.77–2.89, 3.03–2.75 and 3.11–2.7 for Re range, and for detached ribs about 2.9–2.75, 3.78–2.94, 3.29–2.94 and (3.32–2.87) for Re ranges. The ratios of f/fo ratios for two types ranged from 4.1–6.7 and 4.5–8.1 for 5000 Re 20,000.

The friction factor in detached ribs have higher value in comparison with attached ribs for this range of Re.

Yang et al. **[68]**studied experimentally the effect of heat transfer and characteristics of pressure drop on a square channel with two opposite surfaces roughened by high blockage ratio ribs (with large blockage ratio (0.2,0.33) and P/e ranged from (5 to 15). Re ranged from 1400 to 9000. Results showed that heat transfer enhancement increased with the increased of Reynolds number at higher pressure drops. Also, the best P/e was 10 for highest heat transfer enhancement in comparison with 5, 15. In addition, the heat transfer when used symmetric arrangement ribs was higher than staggered arrangement ribs while pressure drop in the symmetric arrangement ribs was larger than the staggered arrangement ribs. And, the two-side enhancing heat transfer higher than one-side ribbed channel.

Qayoum et al.[69] presented experimentally enhancement heat transfer during internal flow through the permeable repeating ribs installed on base of two-pass channel and ribs configuration investigated friction characteristics when enhancing heat transfer with named as smooth, slit-ribbed ,solid-ribbed, and slit- split ribbed. Re varied 5500- 16400 and air as a working fluid. The results showed that the array as slit rib did not provide sizeable heat transfer advantage but split silt has effective on heat transfer compared to the solid rib, however, there is drop in pressure penalty for the slit rib. A slit-ribbed and split-slit-ribbed have percentages in the heat transfer enhancement to solid ribs was observed as 4–5% ,14–21%.

Chang et al. **[70]** investigated experimentally the wavy ribs in longitudinal alongside walls of two-square channel with V or W a ribs at uniform heat flux. Reynolds Numbers were 5000 to 30000. . Averaged Nu ranged along 1-pass, bend and 2-pass of 5.8-5.5,6.07-5.52,5.81-4.94, and 5.7-5.12 times Dittus Bolter equation but friction factors *f* ranged of 43.67-21.43 times Blasius correlation to pressure drop across two-tap. The results showed that the Nu/Nu $_s$ ratios in inlet, outer pass, and bend increased as Re increased from 5000 to 30000.

Hayashi et al. [71] investigated experimentally the characteristics of two-phase flow(air–water) and pressure drops in two-pass channel. Test channel was smooth with circular cross section with liquid velocity were between (0.1- 2.4) m/s, and gas volumetric flux were between (0.02-11) m/s. The Re ranged less than 33000.The results showed that the pressure linearly decreased toward the bend in the upstream of bend, the effect of bend was small on pressure drop in the upstream channel. Also, the bend caused a large pressure drops ΔP_B ,and the flow disturbed in the bend was redeveloping in downstream channel. In addition, the effect of ratio D_B^* (diameter of curvature to hydraulic diameters) changed from 3 to 6 on ΔP_B at same mixture velocity was smaller than effect of mixture on ΔP_B.

Kore et al. [72] investigated experimentally different shapes of ribs on heat transfer and fluid flow characteristics through one –pass channel with square, house, boot shaped rib. Air was the working fluid at constant heat Flux. Re ranged 6000 to 30000. The results showed that type house had higher heat transfer enhancement among all ribs due to mixing of primary and secondary flow lead to turbulent mixing. Boot shaped of 20mm pitch had a higher thermal performance. House shape ribs showed lowest pressure drop but boot and square ribs showed similar results of pressure drop.

2.4- Numerical &Experimental Studies

Sriromreun et al. [73] investigated experimentally and numerically the influence of baffle turbulators on heat transfer augmentation in a rectangular channel with a zigzag shape (Z-shaped baffle) with inclined with 45° were optimum and Re varied 4400 to 20,400 for air flow. A [Z-baffles inclined to 45° with respected to the main flow direction are characterized at three baffle- to channel-height ratios (e/H=0.1, 0.2 and 0.3) and baffle pitch ratios (P/H=1.5, 2 and 3). The results showed a significant effect of the presence of the Z-baffle on the heat transfer rate and friction loss over the smooth channel with no baffle. Also, the results found 45° Z-baffle with larger of e/H=0.3 provided higher heat transfer and friction loss than the one with smaller of e/H=0.1].

Li et al. [74] studied experimentally and numerically heat transfer characteristic and also flow in rectangular cross-section ribbed channels. The working fluid was air at ambient temperature, flow internally in channels with five ribs regularly placed on bottom wall with rib pitch–to-height ratios ranged from (10 to 30) with uniform heat flux. The Re ranged from 57000 to 127000. Numerical simulation performed by realizable k-ε as turbulence model. The results showed in case of p\e =10 local maximum heat transfer occurred between first and second ribs located about distance (9e) from upstream. Averaged Nu was higher for P/e = 20 and 30 than P/e=10.Although, pressure drop in P/e=20 higher value but P/e=30 lesser value constant Re because it has large distance between reattachment and next of rib.

Erelli et al. [75] studied and analyzed experimentally& numerically the turbulence flow and heat transfer in a two–pass smooth square channel with different divider and outer turn at uniform heat flux . Reynolds Numbers namely 25000,35000, and 45000.The results show that the higher heat transfer obtained in the turn region and its increase with increasing strength of the secondary flow.

Singh et al. [76] studied numerically and experimentally of flow and heat transfer in two-pass ribbed channel and rib geometries. Different Ribs of 45°. Angled analyzed such as V, W, M shaped, uniform heat flux. The working fluid was air and Reynolds Numbers 19500-69000.The results observed that V-shaped with 45° ribs had slightly higher heat transfer enhancement and friction factors than M and W shaped ribs. In bend region heat transfer enhancement decreased with increased Reynolds Number and V-shaped has higher values. Also, normalization for smooth surface Nu/Nu_s levels ranged in lower than for correlation of Dittus Boelter Nu/Nu_o.

Kaewchoothong et al. [77] studied experimentally and numerically the effect of rib arrangement on the distributions of the local heat transfer coefficient in a ribbed single channel with eight differences of rib with angles of inclined about of 30◦, 45◦, 60◦, 90◦, 45◦ and 60◦ V-shaped, and inverted V-shaped ribs exerting a uniform heat flux and Re about 30000. The results showed that the Nu improved in ribs angle about 45° ,60°, and 60° V-shaped ribs with percentage about 25%, 20% and 30% higher than 90° and 60°V-shaped ribs have highest Nu. Enhancement in convective coefficient distributed higher value in 60° V-shaped and then, 60° and 45°inclined ribs compared with 90° was about 32.6%,19.3% and 23.5% respectively.

Al-Jibory et al. [78][studied numerically and experimentally the effects of triangular ribs inside a rectangular channel on the heat transfer and flow behavior. Reynolds numbers varied from 8082, 9698 and 11778.The results showed that the temperature distribution for the inner wall surface of the ribbed channel was lower than smooth one by (8.9 %) for the triangular ribs with angle of 90° and (Re=11778) due to the fact that the ribs create turbulent conditions and increasing thermal surface area, and thus increasing heat transfer coefficient than the smooth channel. Also, the triangular ribs with angle of 90 was the best as compared to the other two cases for cooling the rectangular channel. In addition, after modification and analysis have been done, Nusselt Number enhanced by (36%]).

Al-Kumait et al. [79] presented experimentally and numerically the ability to get high enhancement in heat transfer and low friction factor by combined ribs configuration and flow of TiO_2 Nano-fluid flow ,turbulent with Reynolds numbers of 5000-40 000 under uniform heat flux along channel .The results observed that helical ribbed channel ,circumferentially ribbed and longitudinal ribbed channel gave a enhanced about 2.0%, 1.9% and1.88% respectively. The helical ribbed channel has higher turbulent kinetic energy and a higher Nu with uniform distribution because of a stronger swirl intensity led to a thinner thermal boundary layer. In addition, the deviation of Nu and *f* deviated with values ±2% and ±3%, respectively.

Abed et al. [80] investigated numerically and experimentally the effect of many superficial velocity of air and water with constant heat flux on the coefficient of force convection, temperature distribution and compare both results experimentally and numerically which they get it for ribbed channel, triangle ,trapezoidal ,semi-trapezoidal and rib groove with smooth channel .The range of the inlet velocity of water and air between 0.105-0.310 m/s and 0.263-1.320 m/s respectively .When the Re increased the turbulent with increase and the heat transfer with enhance .The best efficiency with triangle rib and also it had the lowest temperature distribution. The deviation between the experimental results and numerical result was about 4.0% -7.5%. Also, the highest heat transfer with the triangle ribs. It was higher than trapezoidal and semi-trapezoidal around 56% and 44% respectively.

2.5- Summary of Previous Studies

As focused on the literature review, several researchers have studied the effect of several factors such as: rib angles and orientation, shape of rib, and flow type when walls with constant heat flux or constant temperature is employed. There were a few researchers who studied the two-phase flow of air-water only using a horizontal one pass channel as shown in table (2.1). The detailed scope of the present work is to investigate numerically the optimum design and two types of flow (two and three phase flow) are investigated numerically and experimentally. The thermal performance criteria evaluation (PCE), enhancement ratio and losses ratio are then taken into account.

Table (2.1): Summery of important investigation of 180° bend of two-pass channels.

Authors	Working Fluid	Configuration of 180° bend channel	Type of investigation	Observation
Dhanasekaran et al. [29]	Air+Mist Re= 5000,10000,25000 ,40000	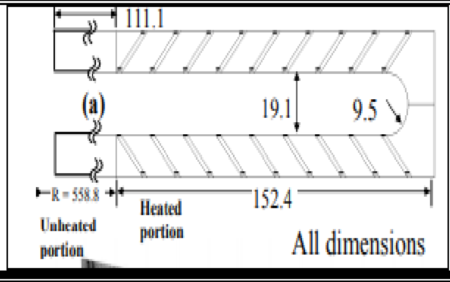	Numerical of Two-Pass ribbed 45° as angled ribs in channel.	• Enhancement about 30% at second pass and 20% at first pass at 2% mist injection.
Wei et al. [30]	Mist and Air Re =25000	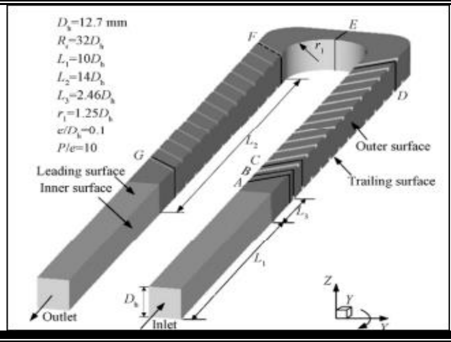	Numerical two-pass Channel two-pass channels with 45° ribbed.	• Secondary flow pattern was quite complex due to combination effect of ribs and 180° sharp turn results heat transfer enhancement.
Shen et al[32]	Air Re=12000,25000 ,50000	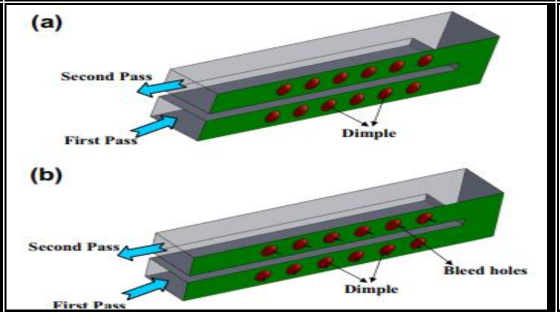	Numerical SST, k-ε turbulence model with dimple with bleed on bottom wall.	• Heat transfer rates are higher in dimples with bleed holes than other cases.

Zhu et al.[36]	Air 25000 ≤ Re ≤ 40000	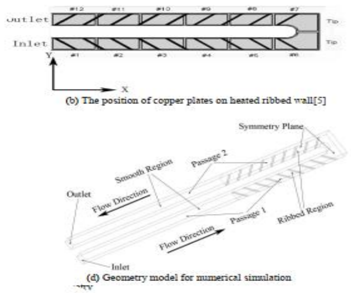	Numerical work in rectangular two-pass channel with 45° ribs	• When Re increased lead to effect reduction in corner on main flow in passage 1and 2 . • Heat transfer strength was higher than in straight passage due to interaction original main flow with new flow in corner.
Wang et al.[44]	Air (10000≤ Re ≤ 40000),	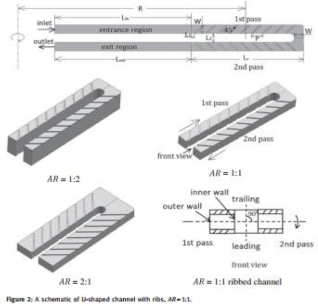	Numerical work of ribbed two-pass channel with different aspect ratio.	• The increasing in Reynolds number was significant enhancing heat transfer along ribbed channel. • Better augmented and value in friction factor through a channel with aspect ratio 2:1 in compared with channel 1:2.
Ravi et al. [45]	Air 20,000≤ Re ≤ 70,000	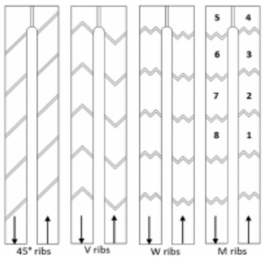	Numerical work of ribbed two-pass channel with different shapes of ribs.	• Heat transfer enhancement of V-shaped ribs was 7% higher than 45° ribs, 28% higher than W-shaped ribs and 35% higher than M-shaped ribs.
Rasool et al. [47]	Air 5000≤ Re ≤ 52000.	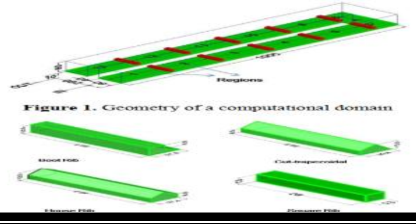	Numerical in two pass ribbed channel	• Shaped rib design effected on characteristic transfer distribution and fluid flow in between the rib.

Rasool et al [48]	Air 10000≤ Re ≤ 50000.	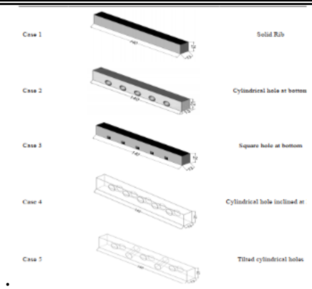	Numerical in two-pass square channel with ribs of different perforated areas	• Perforation ribs enhanced heat transfer coefficient 1.4-5.7% than convention solid ribs.
Gao et al. [49]	Air flow Re =30000	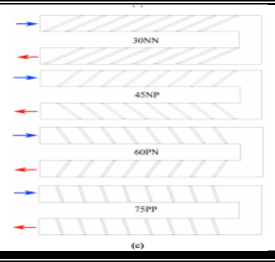	Numerically two-pass channel	• Flow in first pass affected only rib angle while in the second pass the flow is affected by the angle and orientation of the rib.
Jiang et al.[50]	Water Mist–Steam Re >200	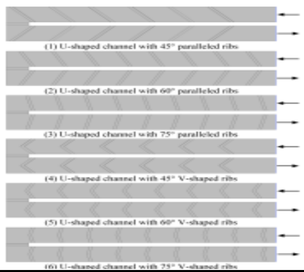	Numerical work of in two-pass channel with various shapes ribs	• V-shaped secondary flow in first pass in center while paralleled-shaped was more closed to outer wall.
Jiang et al. [52]	Water Mist–Steam Re> 200	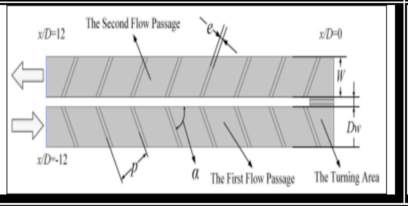	Numerical Rib in top and bottom walls Rib angle 60°.	• Strongest vortex strength located in Turing region and in regions near ribs.

Mondol et al. [53]	Water Re=827-1654	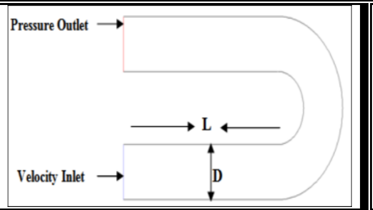	Numerical in two-pass channel	• Investigated the behavior of pressure and the velocity distributions in 180 ° bend.
Yan et al. [57]	Air $10{,}000 \leq Re \leq 50{,}000$	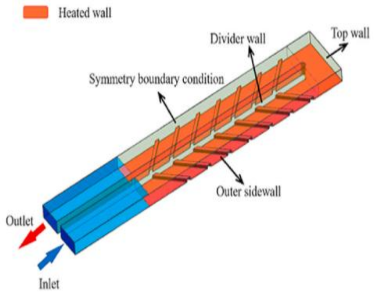	Numerical work to investigate inclination divider angle	• A channel with larger negatively inclined divider showed better enhancement in heat transfer in the second passage while worse heat transfer in the first pass and bend region.
Liou et al. [65]	Air Re=10000	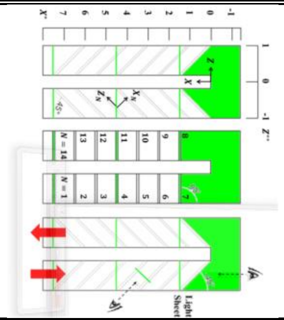	Experiments two–pass parallelogram channel.	• Heat transfer distributions were same for ±45° same Nu/Nu_o distributions on top and bottom walls. •
Qayoum et al [69]	Air Re=5500, 12800 and 16400	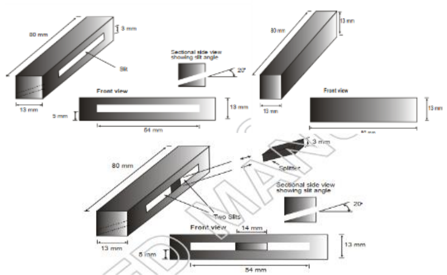	Numerical study of solid, slit-rib and split-slit-rib in two-pass square channel	• Split silt improvements in heat transfer. • Pressure drop penalty for slit rib.

Singh et al [76]	Air 19500≤Re≤69000	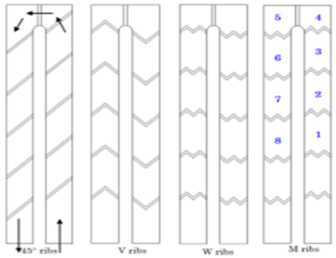	Numerical and Experimental work with ribs on bottom wall in two passes .	• Combination of ribs and dimple observes higher heat transfer enhancement. . •
Present study	Air-Water Re ≥ 72456.3 Air-Water-Gasoil Re ≥ 128182))	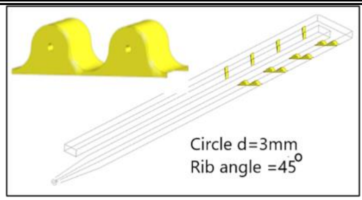 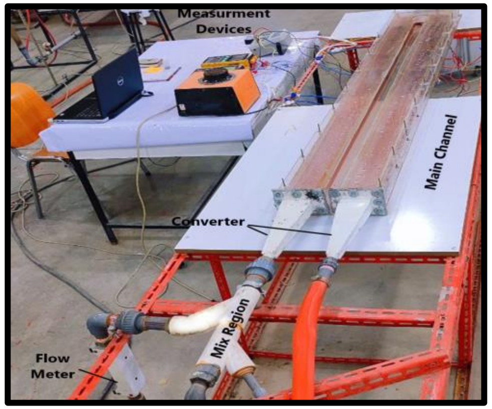	Study optimum design of ribs two-pass ribbed channel and investigation numerically and experimentally.	• Enhancement in heat transfer. • Pressure behavior. • Pressure drop & friction factor and Performance Criteria Evaluation (PCE).

CHAPTER THREE

Numerical Work

Chapter Three: Numerical Work

3.1. Introduction

This chapter presents the optimum design of physical model after a series of modifications or improvements in a ribbed two-pass channel to achieve the maximum enhancement of heat transfer using a computational fluid dynamics (CFD) software package of commercial code **ANSYS FLUENT 2021 R1**.

3.2. Design Consideration

The numerical computation is carried out to solve the governing conservation equations using finite volume method. There are many models in this study such as mixture, Volume of Fluid model and Eulerian model. Also, there are many turbulent such as Standard k-ε turbulence model, k-ε as Realizable, RNG, and standard k-ω. after comparison between other turbulence models of k-ε as Realizable, RNG, standard k-ω and previous studies. Table (3.1) shows all consideration and the results of the previous studies.

The improvements and the choosing of the optimum design are depended on the enhancement heat transfer and these divided into three categories as follow: First is concerned with a smooth channel of eight hot areas in along the base wall.

The second category is related to ribs and modifications with four stages: first choose the optimum design of rib depending on the configuration (V-shaped and Curved-ribs). Second stage includes the chosen of the perforating shapes (square, circle, triangle) with the same cross-sectional area for optimum rib. In the third stage the optimum perforating area with a circular shape of three diameters 3, 6 and 9 is chosen.

In the fourth stage the optimum angle with three values 30°,45° and 60° (see table (3.2)) is chosen. All experiments are performed at the same boundary conditions.

Third category of improvements is related to the type of flow and rib temperatures after design the optimum channel, and made the flow as two-phase and three phase flow. For the two-phase flow of air- water the flow rates of air and water are (10-25) L/min and (4-12) L/min, respectively. While for the three-phase air-water-gasoil, the flow rates for air (10-25) L/min, gasoil (2 - 4) L/min, and water (4-12) L/min.

In addition, the rib temperatures are varied as 50°C, 60°C and 70°C.The most important outputs of this simulation are displayed as contour and values of heat transfer coefficients, Nusselt numbers, pressures, temperatures, velocity distribution, and volume fraction for all phases separately.

Table (3.1). References of geometry characteristic.

Parameters	**Equations**	**Researchers**	**Reasons**
Aspect ratio	AR=2:1	[44]	High enhancement in heat transfer.
Height of the channel	H=0.5 W	[44]	High enhancement in heat transfer.
Entrance and exit regions	L_{in}=15~20D_h	[44,74]	Sufficiently far from the channel inlet.
Sharp bend	Sharp edges is bent with 180°	[30,31,75]	High enhancement in heat transfer.
Length of pass	L_{pass}=30~36 D_h	[44,47,48]	High enhancement in heat transfer.
Pitch-to-rib height//ratio (P/e)	P/e≈8 to 10	[44]	High enhancement in heat transfer.
Shape of Perforating	Circular inclined perforating on rib	[47,48]	High heat transfer

Table (3.2). Configuration of Ribs

Tests	Ribs Configuration		
1	Choose Rib Shape		
	Curved- shaped rib	V-shaped rib	(Without rib)
	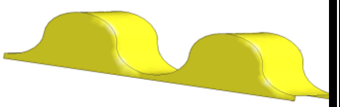	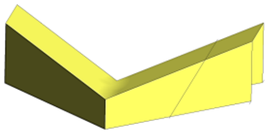	
2	Choose shape of perforating same area		
	Circle Perforating	Square Perforating	Triangle Perforating
	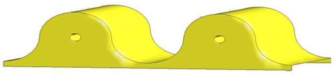		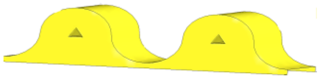
3	Choose area of perforating		
	Curved- rib with 3mm	Curved- rib with 6mm	Curved-rib with 9mm
	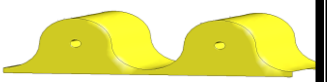	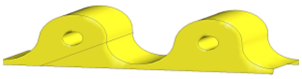	
4	Choose rib angle		
	Rib with angle of 30°	Rib with angle of 45°	Rib with angle of 60°
			
5	Rib of Optimum Design		
	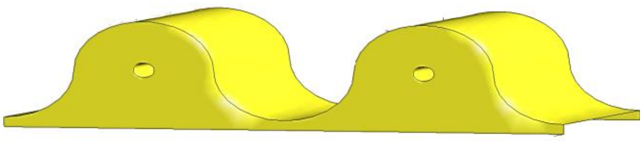		

3.3 Geometric Model

The 3-D geometric model consists of a two-pass ribbed channel with several improvements. The working fluids flow as Two-phase and Three phase.

3.3.1 Description of the Two-Phase Flow Channel Model

The description of the two-pass channel can be seen in Figure (3.1). The two sides of the design are set to be with zero velocity whereas the one pass is set to be with an inlet fluid velocity. The second pass is set to be with outlet pressure of a gage pressure about zero pascal, which is selected as constant for each experiment. Also, all dimensions choose to design channel in Table (3.3).

Table (3.3). Dimensions of channel in (mm).

Parameter	Value	Parameter	Value
D_h	**53.3**	**Bend length L_B**	**240**
Ribbed region L_{out}	**960**	**W×H**	**80×40**
Outlet length L_E	**960**	**Clearance of bend (Tip to end wall).**	**80**
Converter length L_C	**300**	**Distance between passes**	**80**

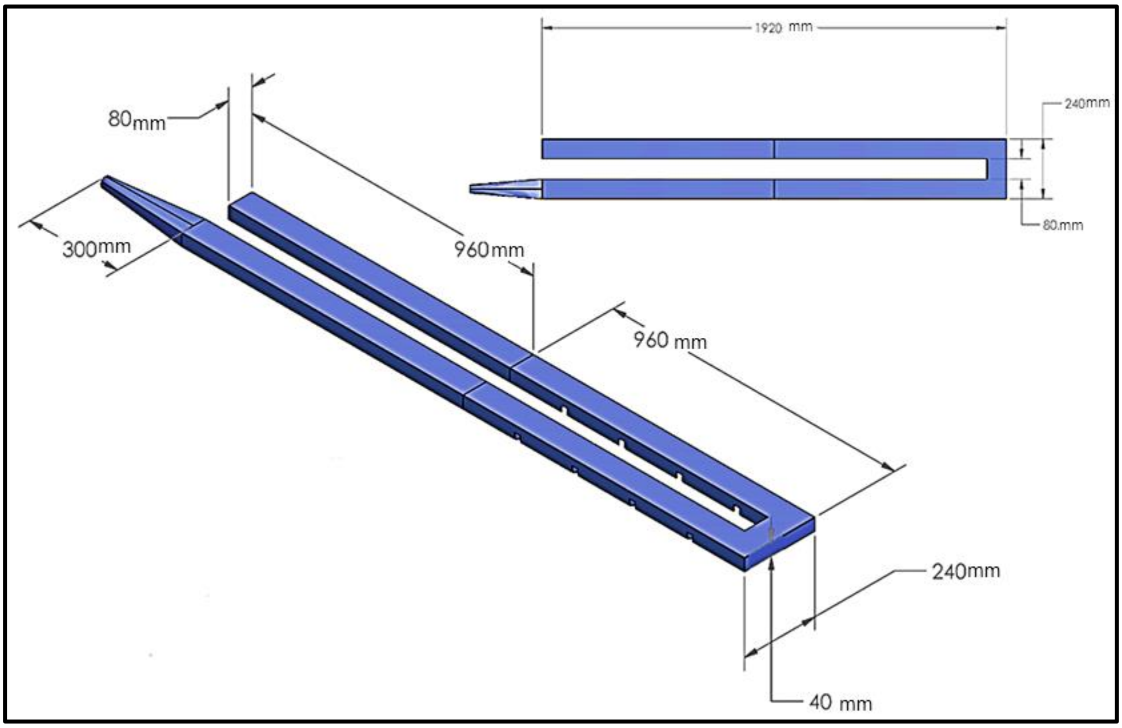

Figure (3.1). Physical geometry of Ribbed Two-Pass Channel.

3.3.2 Description of Smooth Channel Model

Numerical model is described as a two pass channels as shown in Figure (3.2). It has eight hot areas inclined with angle 45° in base, these areas have width of 20mm and temperature of 60°C.

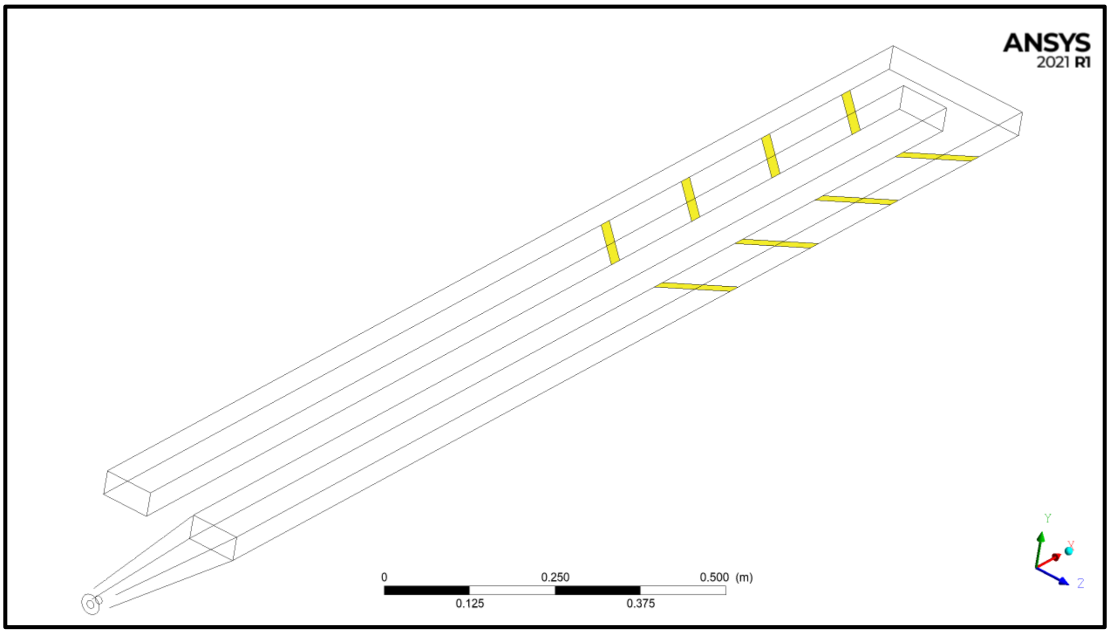

Figure (3.2). Smooth Channel

3.3.3 Description of Rib shapes Model

A schematic diagram of ribs inside a channel is shown in figure (3.3). The rib is geometrically defined by a ratio of a spacing pitch to the height of the rib (e) as (P/e) which is about 9. The number of ribs is 8 at the surface of constant temperature. The cross-section area of the rib is (20 ×22) mm^2**,** as shown in table (3.4).

Two types of ribs are taken in account which are: curved shape, and V-shaped with same cross section area. A comparison between two types of ribs is done to study and choose the optimum rib design, as shown in Figure (3.4).

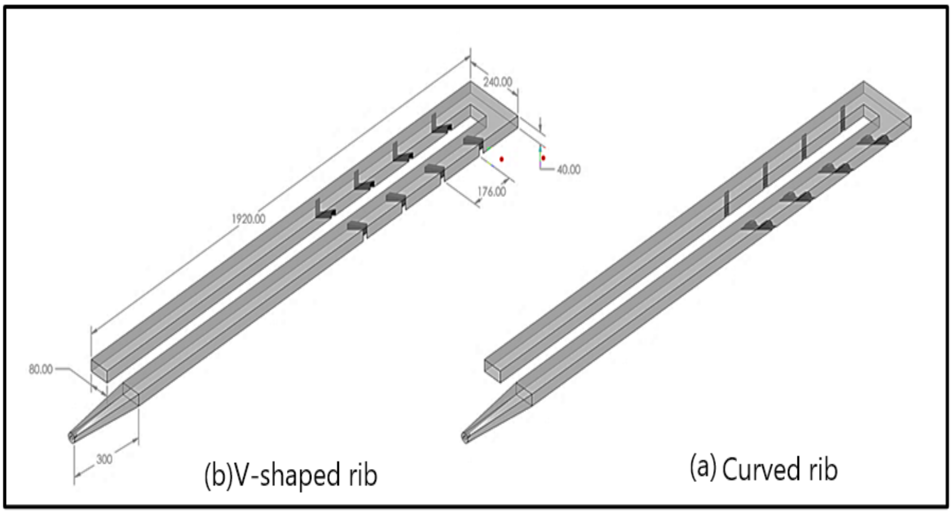

Figure (3.3). 3-D Model of channel with Curved-rib and V-shaped rib.

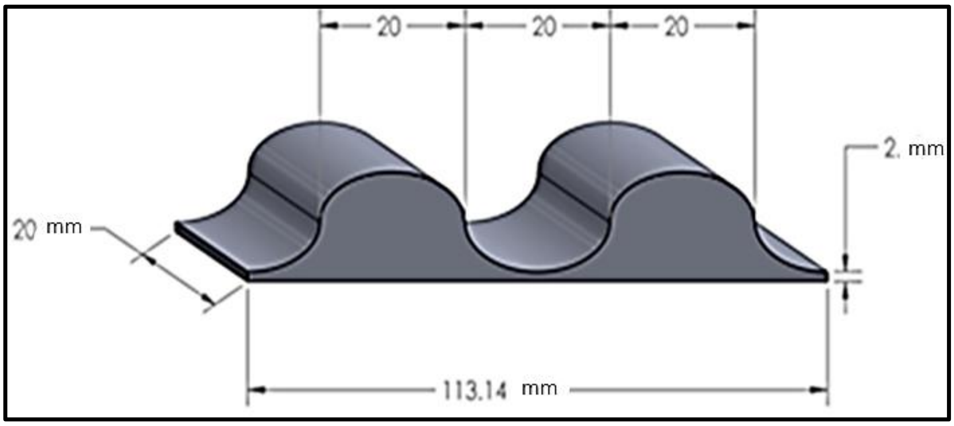

(a) Curved Rib

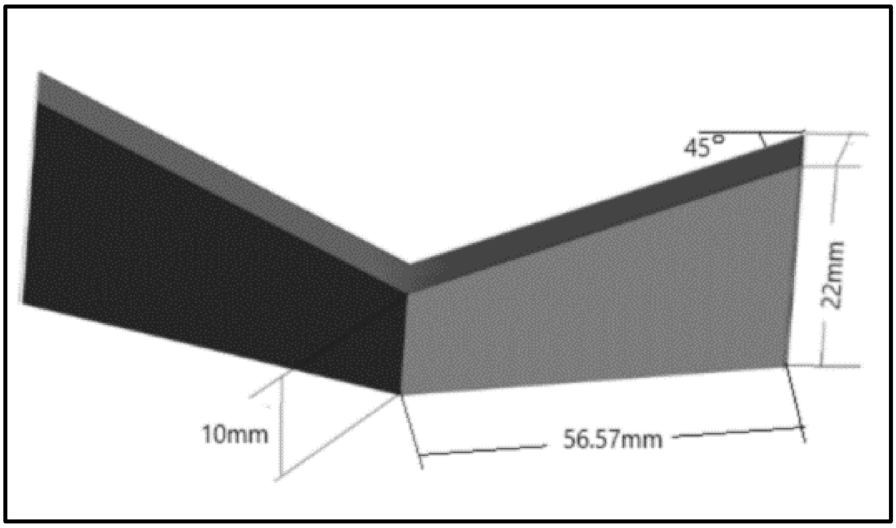

(b) V-shaped Rib

Figure (3.4). Two types of Ribs

Table (3.4). Dimensions of rib (in millimeter)

Rib Type	Cross Section	Height (e)	Pitch (P)	e/D_h	P/e
Curve	**22×20**	**20**	**196**	**0.41**	**9**
V-shaped	**22×20**	**20**	**196**	**0.41**	**9**

3.3.4 Physical Models perforated shape

Three numerical l models are designed with different perforating shapes (triangle, square and circle) and compared with solid case the same cross section area for perforating from the previous stage as shown in figure (3.5). In the centers of convexity are perforated shapes of areas as circular, square and triangle cross section area.

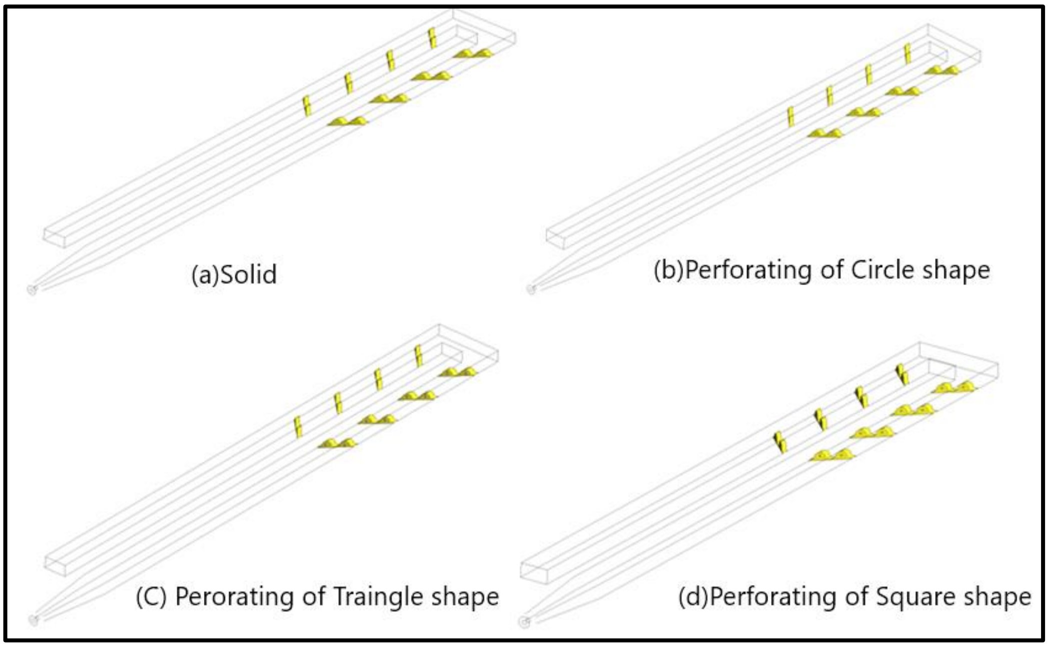

Figure (3.5). Models of perforated shape area.

3.3.5 Physical Models for the perforated area of Ribs

Three numerical models are designed to study the perforating area with different diameters (3, 6 and 9) mm in the curved rib, as shown in Figure (3.6). Two perforations are done in each rib, which are concentrated in the convexity centers.

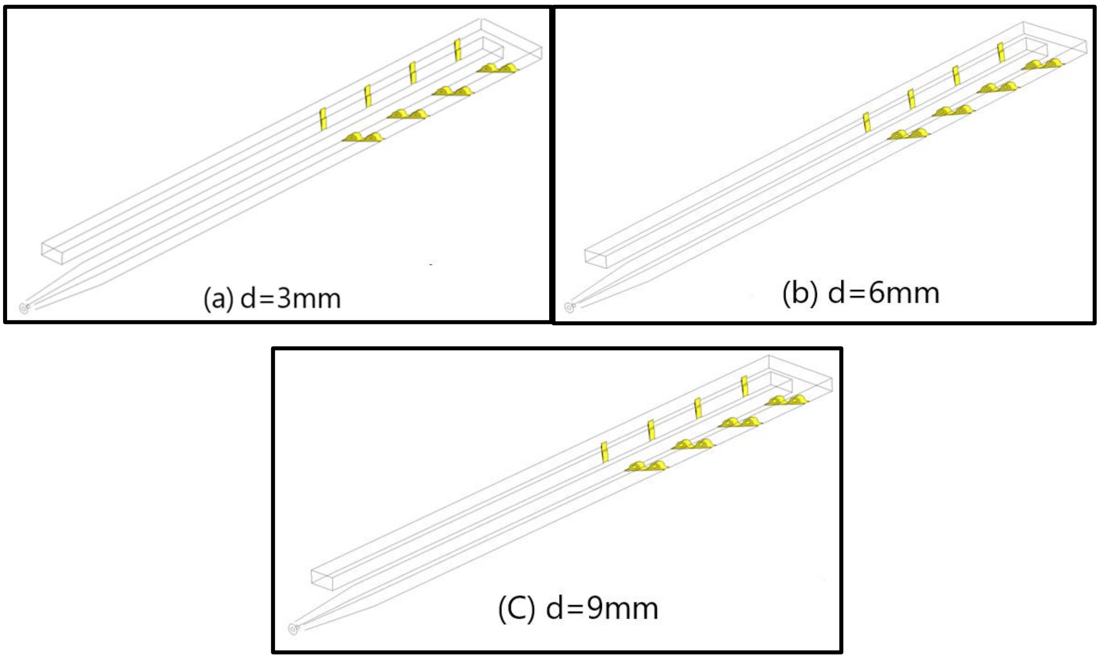

Figure (3.6). Models of perforated circle.

3.3.6 Physical Models for Ribs angles

Rib angle is the angle of flow direction with ribs. Three models of curved rib of circular perforating area are inclined with angles of 30°, 45° and 60°. To study the rib angle according to high heat transfer enhancement the position of the rib inside the channel, as shown in figure (3.7).

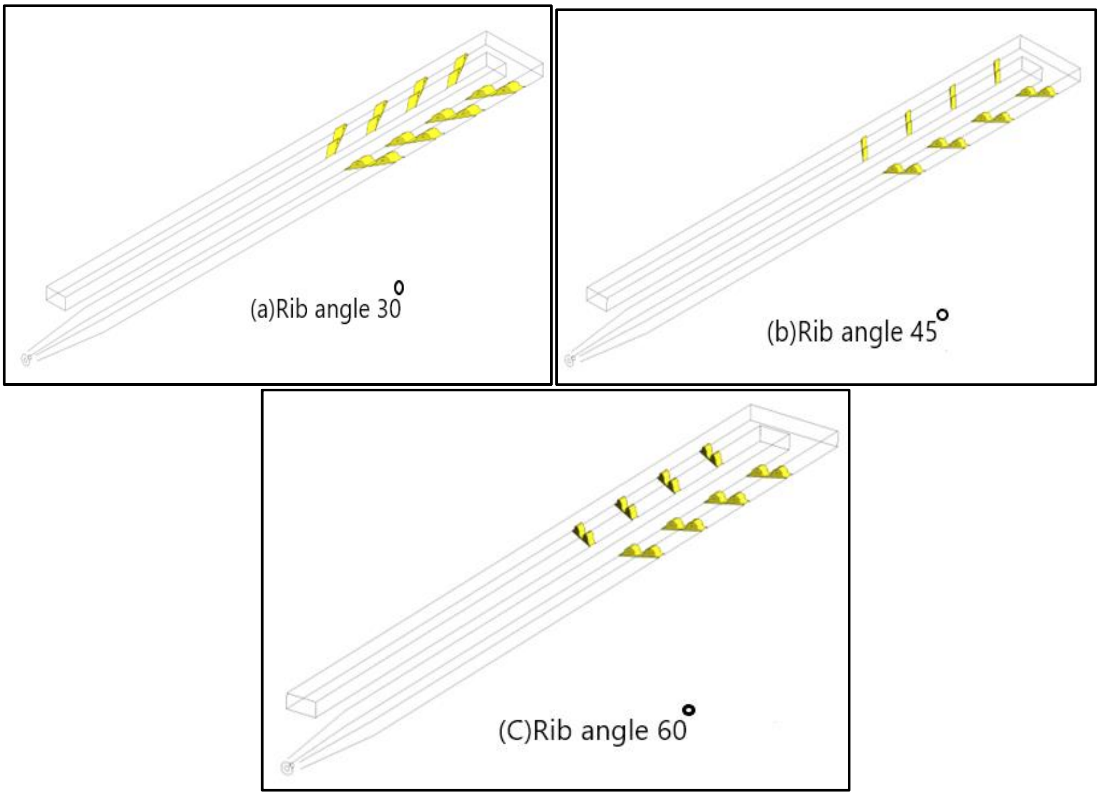

Figure (3.7). Models of Ribs angles.

3.3.7 Physical Models of Optimum Design

An optimum channel is designed according previous cases of the previous stages, the ribs and its accessories according to the previous stages.

A curved rib with circular perforating area of diameter 3mm and rib angle about 45° is represented as an optimum design according this study (see figure (3.8)).

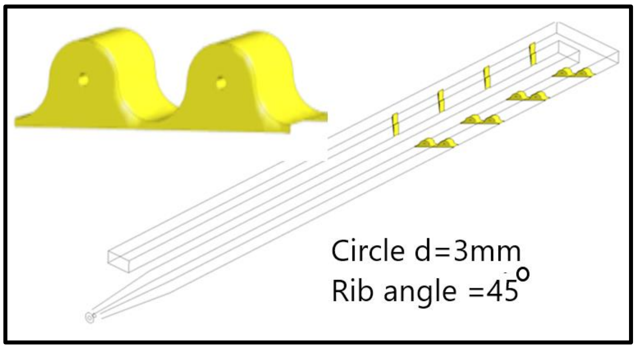

Figure (3.8). Optimum Model

3.3.8 Description of Three-Phases Flow in a Channel Model

The optimum channel model is obtained from above improvement utilizing of the three phases flow. The first-pass of the structure is set to be two inlets together: first inlet is air with velocity and second inlet is for the water-gasoil velocities is entered the channel. While the second pass is set to be outlet pressure with the mixture of three–phases. The rib temperatures were set to be constant during flow of one experiment.

3.4 The Geometry

The geometries for all improvements of the problem are modeled and simulated as a 3-D design channel structure using solid 2021 combined with ANSYS Workbench 2021 R1. There are a group of models designed in table (3.5). The geometry was set to be fluid.

Table (3.5): All simulation Models

Improvements	Number of Models
smooth channel	1
shape of ribs	2
shape of area perforating	3
area of perforating	3
angle of rib	3
optimum design for two-phase flow	1
optimum design for three-phase flow	1

3.5 The Mesh

In the present work, fluent unstructured solver is used to assign the order of the cells, faces, and grid points in a mesh and to maintain a contact between adjacent cells in order to get the best grid topology for complex geometry. Fluent code uses different element types for mesh topology [81].

In this study tetrahedron element type is used for three-dimensional geometry due to its priority use in the sophisticated and complex geometries [81]. The geometry is divided into small elements using the Meshing with ANSYS Workbench 2021 R1. The model mesh details are shown in table (3.6). All geometries meshed a fine relevance with elements sizes and maximum layer, 5 mm ,5 respectively, as indicated by table (3.6). That is why it was decided to use a fine mesh in the region near to the surfaces and use coarse meshes as the distance from the surface grows. Figure (3.9) show the layer inflation that is used to get more resolution with a number of rows of 5 and a growth factor about 1.2. The governing equations would be solved at each element of the model geometry [82].

Table (3.6) Mesh Information

Improvements	Number	
	Node	Element
smooth channel	501522	1116994
Shape of ribs (V-shaped, curved rib)	(489710) ,(538399)	(1090503),(1222735)
shape of area perforating (circular, square, triangle)	(879312), (648061), (639976)	(2083447),(1486814), (1466322)
circular area of perforating (Diameter of 3,6,9) mm	(879312), (729529), (665240)	(2083447),(1711548), (1549927)
rib angles (30°,45°,60°)	(1202041), (879312), (887567)	(2875688), (2083447), (2084908)
optimum design	(879312)	(2083447)

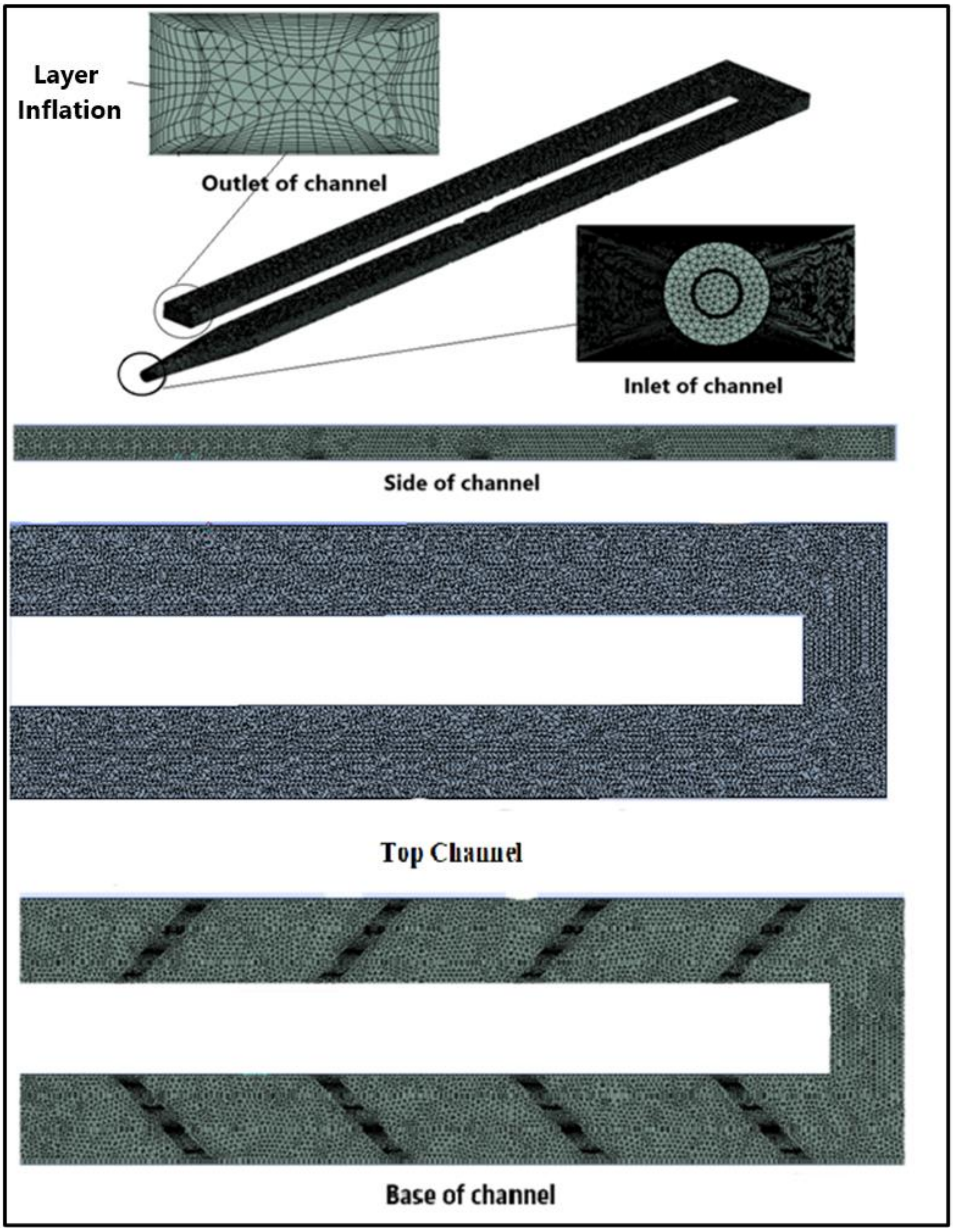

Figure (3.9) Mesh of the geometry.

3.6 Boundary Condition (B.C)

3.6.1 Two-Phase Boundary Condition

B.C are defined for every zone of domain the computational domain. Two inlets of the geometry were named: inlet air and inlet water which are the inlets of the channel as shown in Figure (3.10). The velocities of primary phase (air) and secondary phase (water) are setting in inlets. Rib surface temperature is set in experiments for three cases (50,60,70) °C. The outlet of the channel, which is the end edge of the geometry, was set to be outlet pressure equal zero. The relaxation of the pressure, momentum, and volume fraction of two-phases in ribbed channel with two-pass are shown in table (3.7).

3.6.2 Boundary Conditions of Three-phase flow

The primary phase was set (air phase) and secondary phase was set as mixture of water-gasoil as shown in Figure (3.10). The inlets of the geometry were divided into two inlets: first inlet is for air only while the other inlet is for water &gasoil with different velocities. Properties of water and gasoil can be defined as input in materials tab in Fluent. However, the internal domain ribs have the same conditions in two-phase case. The outlet of the channel, which is the end edge of the geometry, was set to be outlet pressure, The relaxation of the pressure, momentum, and volume fraction are shown in table (3.7).

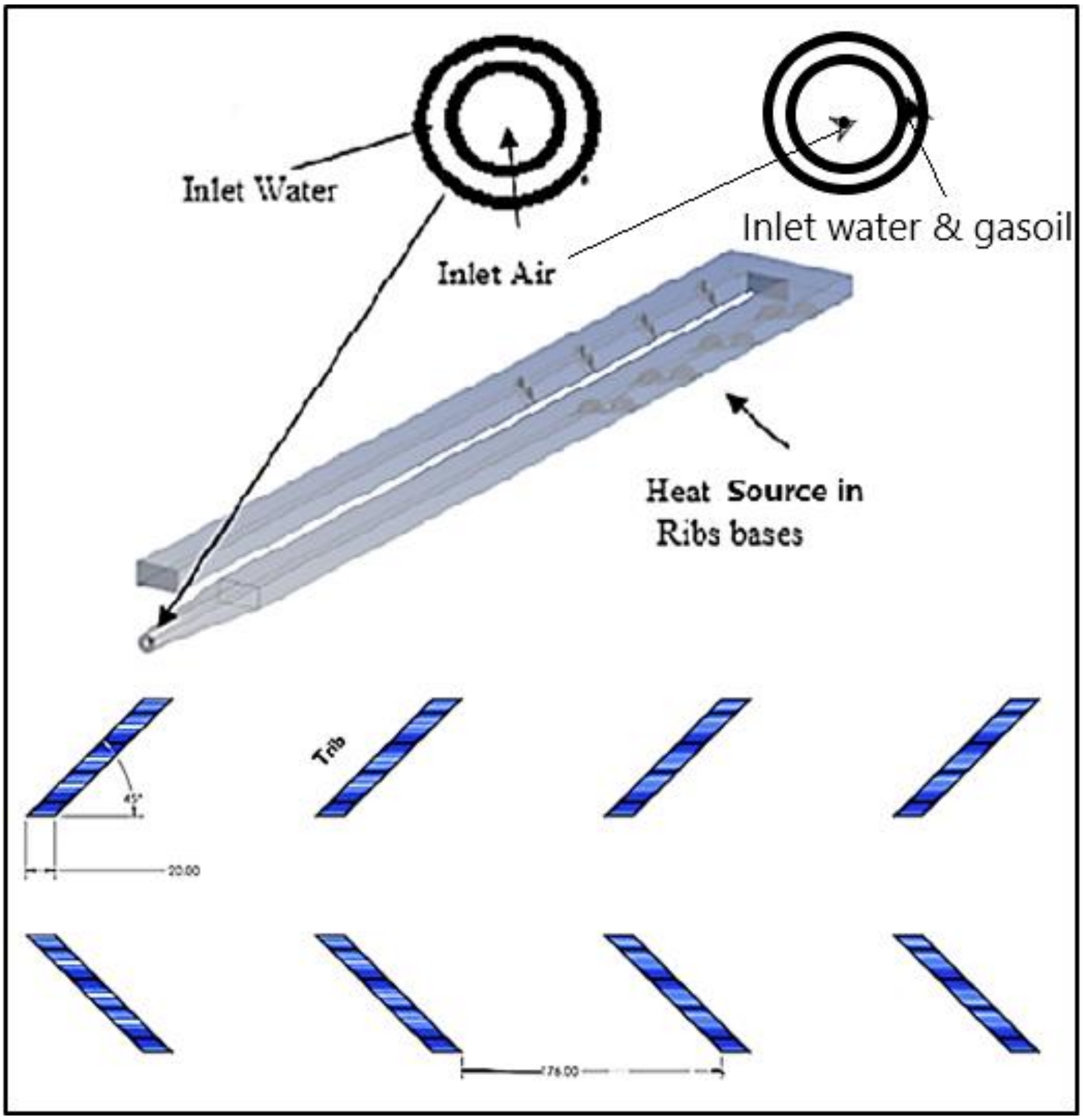

Figure (3.10). Boundary condition of the computational domain.

Table (3.7) Relaxation Factors [83]

Relaxation	Factor Value	
	Two-phase flow	Three-phase flow
Volume fraction	0.8	0.3
Pressure	0.1	0.1
Momentum	0.1	0.1
Another factor	0.8	1

3.6.3 Velocity Inlet Boundary Condition

Inlet velocity is defined in this study depending on the flow rate of the working fluid (water). The flowrate of the working fluid is shown in tables (3.8) and (3.9) for two and three phase turbulent flow, respectively. Also, the inlet temperature is set be to be (27°C) for all fluids.

Table (3.8) Flow rate values (Two-Phase Flow)

Q_{air} (L/min)	10	16.67	25
Q_{water} (L/min)	4	8	12

Table (3.9) Flow rate values (Three Phase Flow).

Q_{air} (L/min)	10	16.67	25
Q_{Gasoil} (L/min)	2	3	4
Q_{water} (L/min)	4	8	12

3.6.4 Pressure Outlet Boundary Conditions

A pressure outlet is specified at the outlet domain where the pressure is assumed to be zero.

3.7 Simulation Assumptions

The following assumptions are used in the model:

1. Three-Dimensional, steady state and turbulent flow.
2. Non-Homogenous model.
3. Gravity is $9.81 m/s^2$.
4. Incompressible and Newtonian fluids
5. Constant inlet temperature.
6. No heat generation along channel.
7. Constant physical properties.
8. The primary phase is air while, water is a secondary phase in the case of two-phase flow and the of mixture water-gasoil is secondary phases in case of three phase.

3.8 Fluent Setup

3.8.1 Defining the Material Properties

In this section the input contains the options for the materials is chosen. For air-water case is under material tab in Fluent at 27°C input temperature condition and velocity in first and second inlets respectively. But in three-phase flow, the properties of air inlet that separated from the inlets of mixture (water-gasoil) is defined as input in materials tab in Fluent. The water-gasoil velocities are taken as zero in air inlet while air velocity was zero in the second inlet in channel wall with material considered for analysis is aluminum. The properties of water, air, gasoil liquid and a mixture of (water-gasoil) are taken as follows (see table (3.10)):

Table (3.10) Properties of fluids at 27 °C [83].

air	**Primary phase**	**ρ**	**1.1774 kg/m³**
		μ	**1.8462×10^{-5}**
		Cp	**1.005 J/kg.K**
		k	**0.02624 W/m.K**
water	**Secondary phase**	**ρ**	**995.8 kg/m³**
		μ	**8.6×10^{-4} kg/m.s**
		Cp	**4.179kJ/kg.K**
		k	**0.62 W/m.K**
gasoil	**Secondary phase**	**ρ**	**830 kg/m3**
		μ	**2.778×10^{-3} kg/ms**
		Cp	**2.2J/kg.K**
		k	**0.145W/m.k**

3.9 Computational Flow dynamics Validation

3.9.1 Grid Independence.

Figure (3.11) and (3.12) show the average Nusselt number and pressure for inlet flow conditions in grid independence study. This study is carried out with mesh sizes of 0.5 ,1.8, and 2 million. The predicted results show a small variation from (0.5 and 1.8) million different mesh numbers and specially for (0.5 and 1.8) million meshes until it reaches 1.8 million, the results are stabled. Therefore the rest of computational analysis is conducted with 2 million meshes because of the curve of Grid independency stability after 1.8 million meshes and the required precision .Also, due to the difficulty of interpretation it is very necessary to know how to simulate and know how to deal with its parameters and boundary conditions so that the consultation chooses his closest case study and simulates to get enough experience to simulate the present work .Simulation of case study of literature survey [29] and getting a deviation percentage about 1.8% in comparison with present work depending on velocity and temperature contours as shown in Figure (3.13) & (3.14) .Because of the computational is carried out using the commercial CFD software FLUENT (version 6.2.16) from ANSYS at different dimensions various flow rates of air working fluid of 300K and constant heat flux.

3.9.2 Viscous Models

The selection of study model is achieved by the exceptional perception of the phenomena. Three model are investigated in the validation of a viscous model called: Volume of Fluid (VOF), Eulerian and Mixture models. Figure (3.15) shows the simulation of behavior of the heat coefficient of convective in three models along channel. The red line represented the heat transfer coefficient in the Eulerian model which is straight because this model cannot model heat transfer and heat transfer coefficient if it’s a constant [83].

Also, another two lines have the same behavior of heat transfer coefficient of VOF and Mixture models, but the black line has a higher value are not within the range work because this model simulated heat and mass transfer phenomena itself of immersible fluids and it is designed for two or more immiscible fluids where the position of the interface between the fluids is of interest. The Mixture model which is appeared with green line in figure (3.15) has accepted values. The mixture model is more realistic in this phenomenon because it can be used to model multiphase flows where the phases move at different velocities, only phase and fluid move in slip ratio. Also, a multiphase model may not feasible when there is a wide distribution of the particulate phase or when the interphase laws are unknown and not important between phases.

3.9.3 Turbulence Models

To improve the accuracy of a simulation for a model apart from the (standard k-ε turbulence model) and compared with three turbulence model as (Realizable k-ε, RNG k-ε and standard k-ω). Figure (3.16) shows the behavior of average Nusselt number when used above turbulence model and compared with results of equations for the entire Re range along channel. It observed that the standard k-ε turbulence model have a good variation value, also this model is used in many research [23,24],[29] in the study of an internal flow with heat transfer with walls in two-pass ribbed channel.

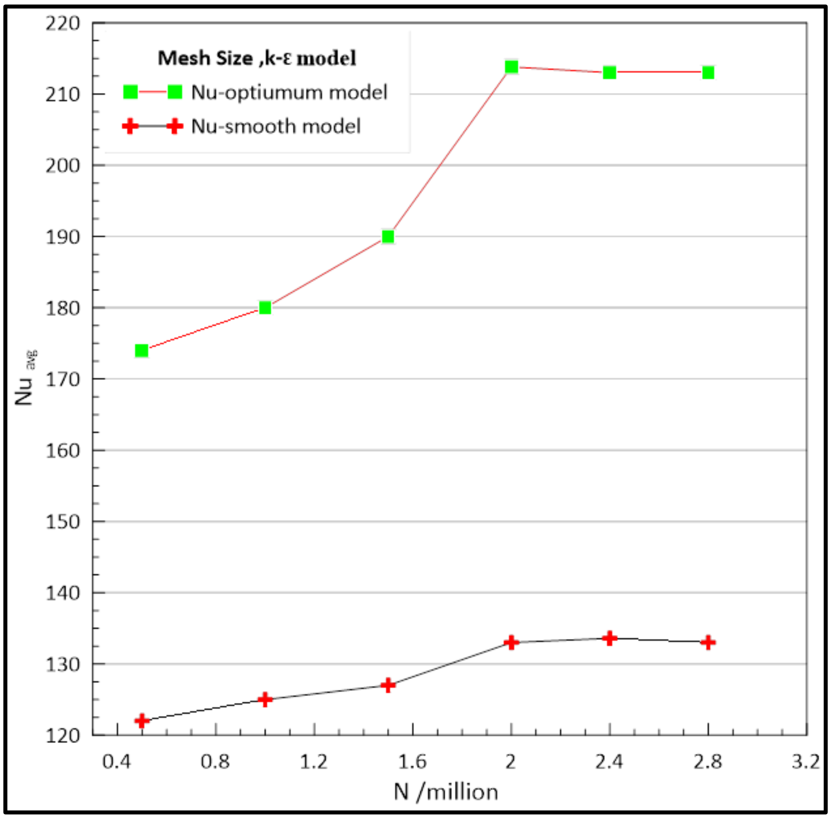

Figure (3.11). Nu $_{avg}$ for Grid independency test 1.

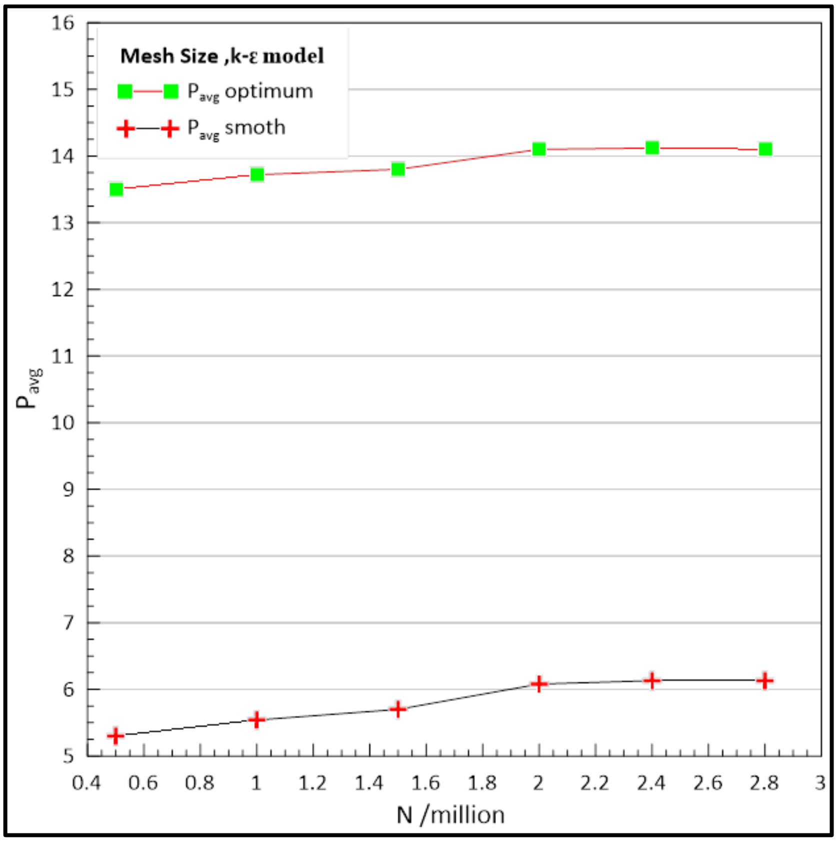

Figure (3.12).P_{avg} for Grid independency test

Present Work **Dhanasekaran [29]**

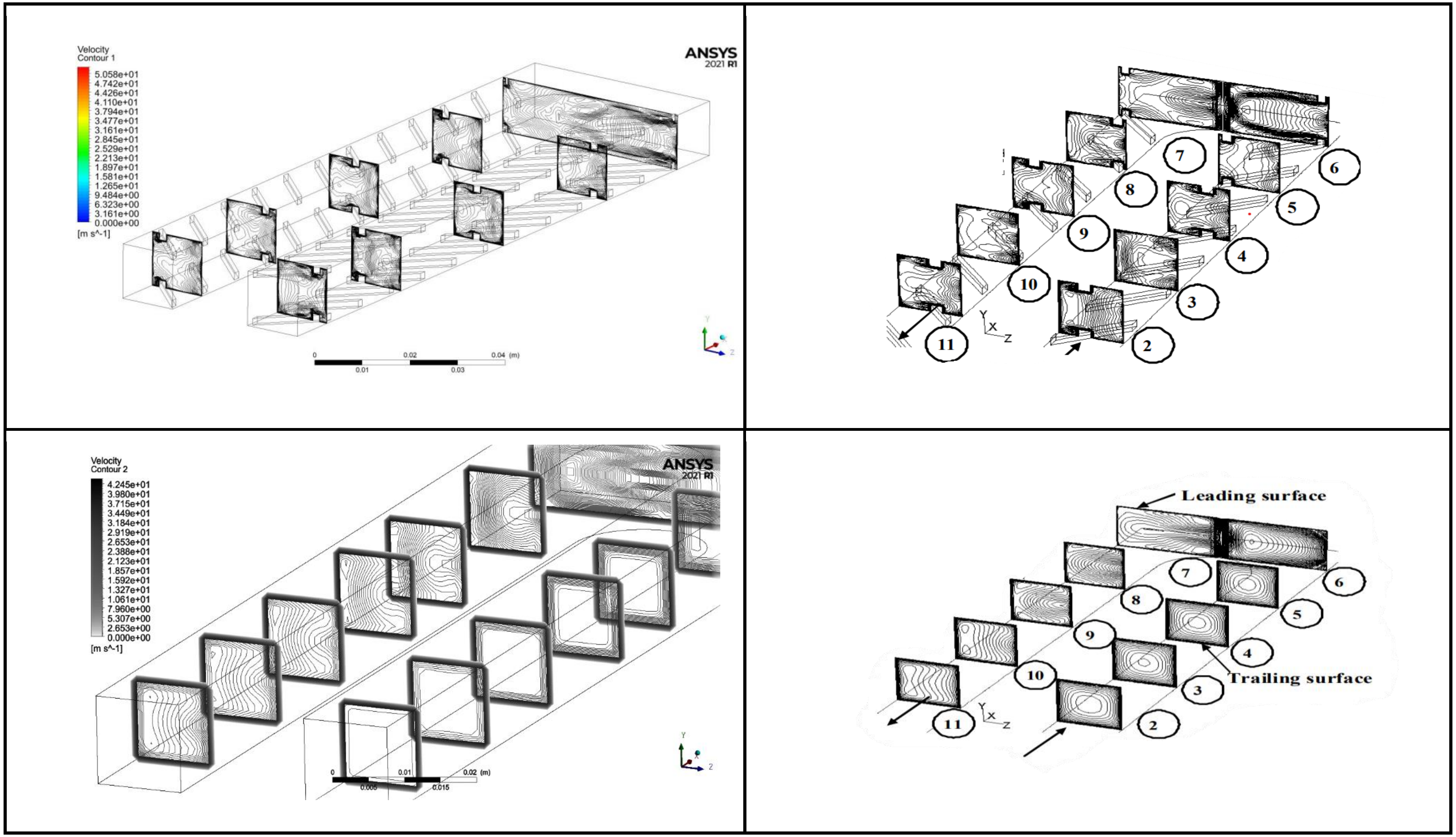

Figure (3.13). The CFD comparison of velocity contour

Present Work **Dhanasekaran [29]**

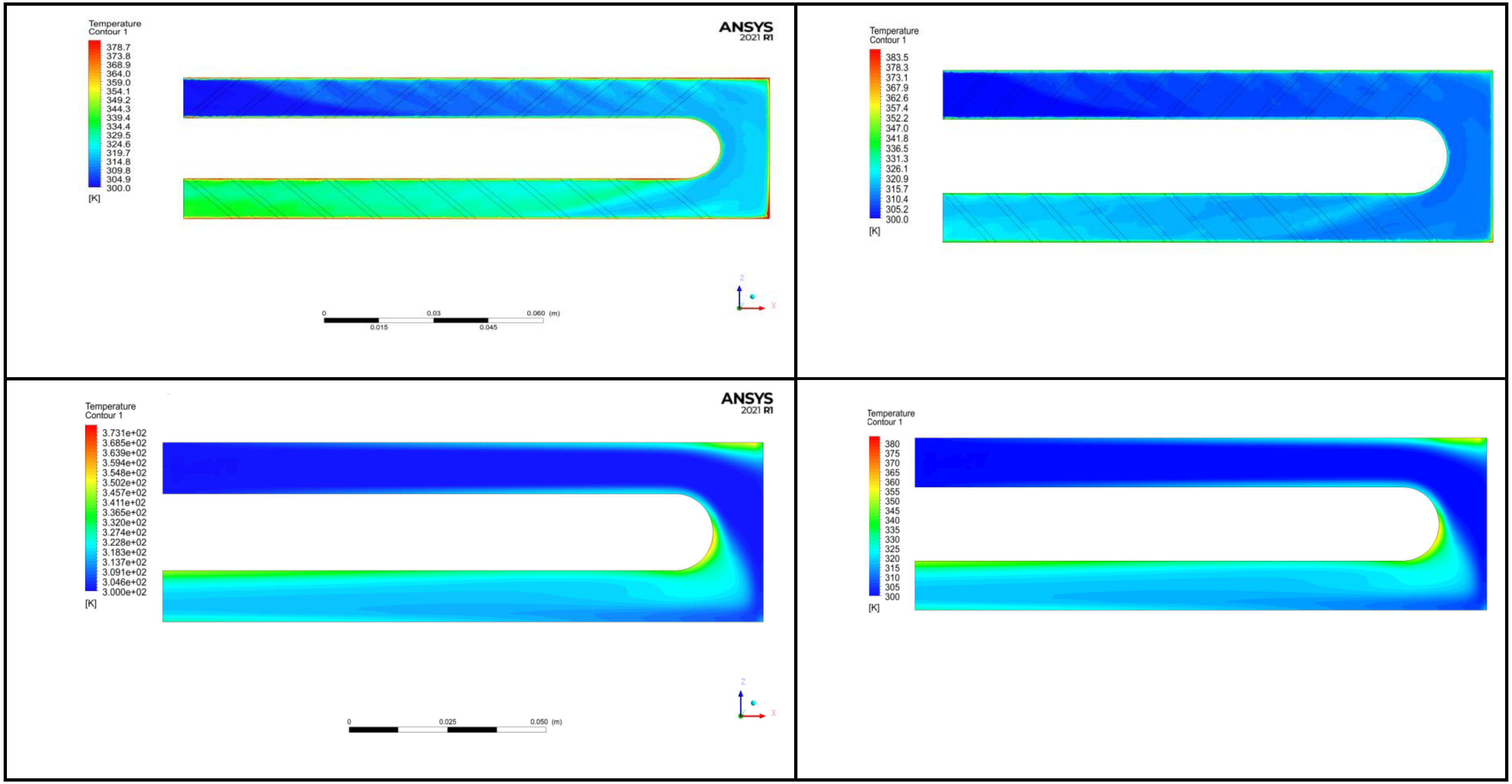

Figure (3.14). The CFD comparison of Temperature contour.

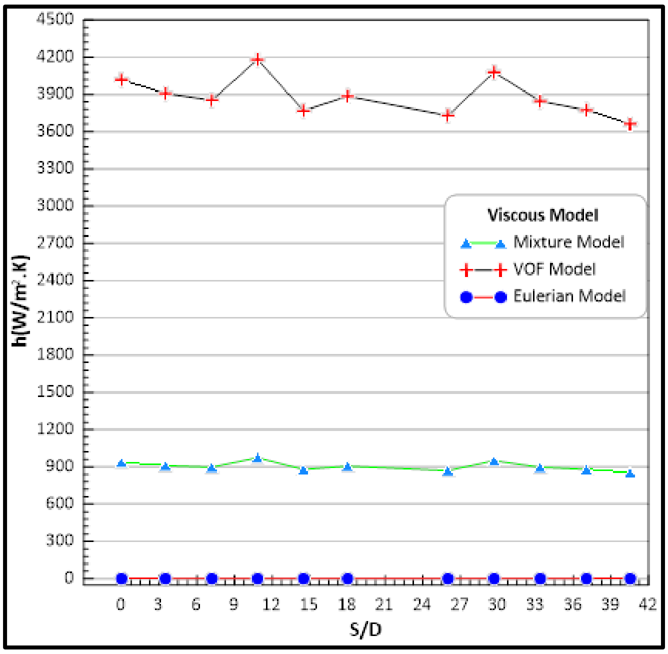

Figure (3.15). Viscous Models Behavior.

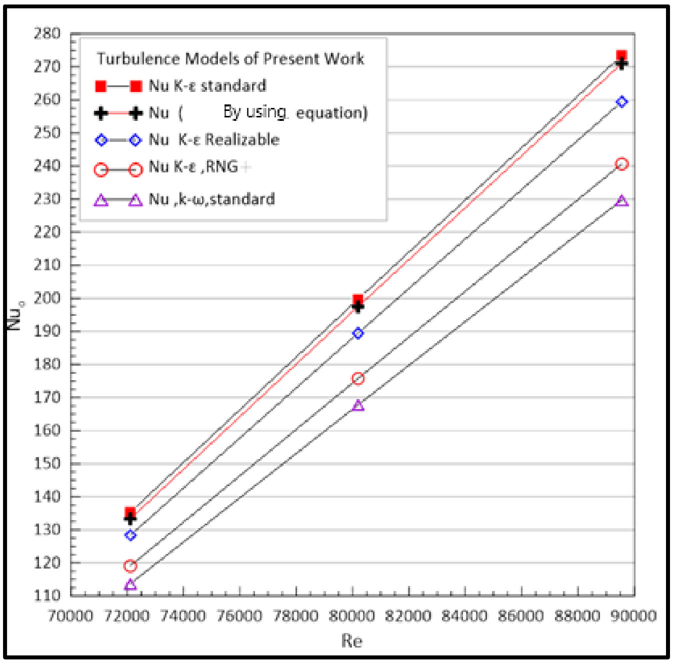

Figure (3.16). Effect of four turbulence models on Nu distribution

3.10 Model of Simulation

3.10.1 Two Phases Flow

Mixture model multiphase model are chosen to simulate the two phases flow. The air phase was set to be the primary phase whereas the water is set to be secondary phase, it used to simplify the complex flow as two-phase flow. The solver is pressure based and turbulent intensity about 5%.

3.10.2. Three Phases Flow

Mixture multiphase model is used to simulate the three phases in the channel. In this model, it is assumed to be a balance in a special length in which the phases flow and moving in different velocities. Also, in these cases used pressure-based solver and turbulent intensity about 3% are used.

3.11 Equations Describing Fluids during Motion

1- Continuity Equation (Conservation of Mass)

The continuity equation for mixture is [84]:

$$\nabla.(\rho.\overrightarrow{v_\iota}) = 0 \qquad \dots (3.1)$$

where $\overrightarrow{v_m}$ *is the* mass-averaged velocity: mixture density ρ_m is constant, the volume fraction of phase.

$$\overrightarrow{v_m} = \frac{\sum_{k=1}^{n} \alpha_k \rho_k \vec{v}_k}{\rho_m} \qquad \dots (3.2)$$

And ρ_m is calculated as:

$$\rho_m = \sum_{k=1}^{n} \alpha_k \rho_k \qquad \dots (3.3)$$

α_k is volume fraction of phase k.

2- Momentum equation

The general expression for phases:

$$\nabla.(\rho_m \overrightarrow{v_m}.\overrightarrow{v_m}) = -\nabla \cdot p + \nabla \cdot \left[\mu_m \left[\nabla\ \overrightarrow{v_m} + \nabla\ \overrightarrow{v_m}^T\right]\right] + \rho_m \vec{g} + \vec{F} -$$

$$\nabla.\left[\sum_{k=1}^{n} \alpha_k \rho_k \overrightarrow{v_{dr,k}}\ \overrightarrow{v_{dr,k}}\right] \qquad \dots (3.4)$$

where n is the number of phases, $\vec{F}$ is a body force and $\mu_m$is the viscosity of mixture:

$$\mu_m = \sum_{k=1}^{n} \alpha_k \mu_k \qquad \dots (3.5)$$

$\overrightarrow{\mathbf{v}_{\mathbf{dr},\mathbf{k}}}$: is the drift velocity for secondary phase k.

$$\overrightarrow{\mathbf{v}_{\mathbf{dr},\mathbf{k}}} = \vec{v}_k - \vec{v}_m \qquad \dots (3.6)$$

3- Energy equation

The expression of energy equation for all phases mixture can be getting by sum individual energy equations for phases:

$$\nabla . \sum_{k=1}^{n} [\alpha_k \vec{v}_k \, (\rho_k \, E_k + p)] = \nabla \cdot \left[k_{eff} \nabla T\right] + S_E \qquad .. (3.7)$$

Where $\boldsymbol{k_{eff}}$ is the effective conductivity calculated as: -

$$\mathrm{k_{eff}} = \sum \alpha_\mathrm{k} [\mathrm{k_k} + \mathrm{k_t}] \qquad \ldots (3.8)$$

$\boldsymbol{k_t}$ is the turbulent thermal conductivity. The first three terms on the right-hand side of Equation (3.8) represent energy transfer due to conduction. $\boldsymbol{S_E}$includes any other volumetric heat sources.

$$\mathrm{E_k} = \mathrm{h_k} - \frac{\mathrm{P}}{\rho_k} + \frac{v_k^2}{2} \qquad \ldots (3.9)$$

For a compressible phase, and $\boldsymbol{E_k = h_k}$ for an incompressible phase, where $\boldsymbol{h_k}$ is the sensible enthalpy for phase k.

4- Volume Fraction of Secondary Phase

The continuity equation for secondary phase k, the volume fraction equation for secondary phase k can be obtained: -

$$\frac{\partial}{\partial \mathrm{t}} (\alpha_\mathrm{k} \rho_\mathrm{k}) + \nabla . (\alpha_\mathrm{k} \rho_\mathrm{k} \, \overrightarrow{\mathrm{v_m}}) = -\nabla . \left[\alpha_\mathrm{k} \rho_\mathrm{k} \, \overrightarrow{\mathrm{v_{dr,k}}}\right] + \sum_{\mathrm{q}=1}^{\mathrm{n}} \left[\dot{\mathrm{m}}_{\mathrm{qk}} - \dot{\mathrm{m}}_{\mathrm{kq}}\right] \ldots (3.10)$$

3.12 Turbulence (k-ε Model)

The simplest complete models of turbulence are the two-equation models in which the solution of two separate transport equations allows the turbulent velocity and length scales to be independently determined. The standard k-ε model in ANSYS-Fluent falls within this class of models and has become the workhorse of practical engineering flow calculations. Robustness, economy, and reasonable accuracy for a wide range of turbulent flows explain its popularity in industrial flow and heat transfer simulations. It is a semi-empirical model, and the derivation of the model equations relies on phenomenological considerations and empiricism. As the strengths and weaknesses of the standard k-ε model have become known, improvements have been made to the model to improve its performance. Two of these variants are available in ANSYS Fluent: the RNG k-ε model and the realizable k-ε model. The distribution of eddy viscosity throughout the flow domain must be established in order to calculate the momentum and heat diffusion coefficients for turbulent equations. The model used in the present work was standard k-ε model, which provides superior performance for flows, boundary layers under strong adverse pressure gradients, separation, and recirculation, suitable for complex flows involving severe pressure gradient, strong streamline curvature [84].

3.12.1 Standard k-ε model

The turbulence kinetic energy (k), and its rate of dissipation (ε) respectively, are written as [83]:-

$$\frac{\partial}{\partial t}(\rho_m k) + \nabla.(\rho_m \overrightarrow{v_m}\, k) = \nabla \cdot \left[\frac{\mu_{t,m}}{\sigma_k}\nabla k\right] + G_{k,m} - \rho_m \varepsilon \qquad \dots (3.11)$$

$$\frac{\partial}{\partial t}(\rho_m \varepsilon) + \nabla.(\rho_m \overrightarrow{v_m}\, \varepsilon) = \nabla \cdot \left[\frac{\mu_{t,m}}{\sigma_\varepsilon}\nabla \varepsilon\right] + \frac{\varepsilon}{k}C_{1\varepsilon}G_{k,m} - C_{2\varepsilon}\rho_m \varepsilon \qquad \dots (3.12)$$

The rate of turbulence dissipation, σ_ε , σ_k turbulent Prandtl number for ε ,k and $G_{k,m}$ is the rate of generation of the turbulent kinetic energy. $\rho_m\varepsilon$ is its destruction rate. $\mu_{t,m}$ turbulence viscosity can be calculated using the equations:

$$\rho_{t,m} = \sum \alpha_i \rho_i \qquad \dots (3.13)$$

$$\mu_{t,m} = \rho_m C_\mu \frac{K^2}{\varepsilon} \qquad \dots (3.14)$$

$$G_{k,m} = \mu_{t,m}\left[\nabla\overrightarrow{v_m} + \nabla\overrightarrow{v_m}^{T}\right] : \nabla\overrightarrow{v_m} + \frac{2}{3}\rho\, k\, \nabla\overrightarrow{v_m} \qquad \dots (3.15)$$

The boundary values for turbulent quantities near the wall are specified with the enhanced wall treatment method as shown in Table (3.11).

Table (3.11): Model Constant

Constant	**Values**

C_μ	0.09
$C_{1\varepsilon}$	1.44
$C_{2\varepsilon}$	1.92
σ_k	1.0
σ_ε	1.3
Pr_t	0.75

3.13 Step of Numerical Solution

Simulation performed the channel model of computational fluid dynamic with steps strategy

1. **SOLIDWORK 2021** used to configuration the geometry.
2. **ANSYS Workbench 2021** used to generation mesh.
3. The model was Mixture.
4. The materials depend on whether it is two or three phases field.
5. Choosing phases and boundary conditions were set.
6. The solution initialization.
7. The solution was run with steady and a maximum iteration **(1000)**. The residual of the solution is shown in figures (3.17).
8. The results of simulation were extracted as data and contours.

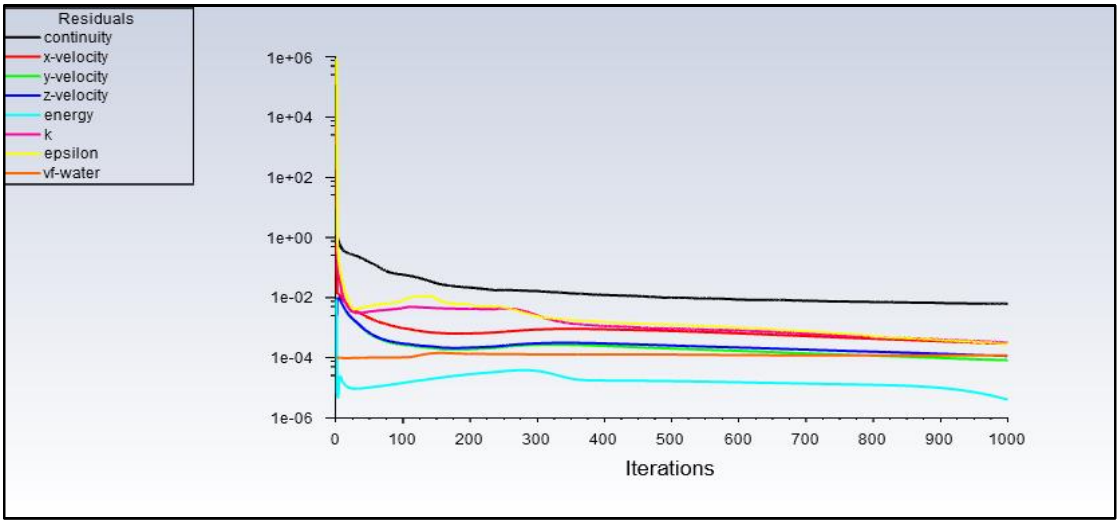

Figure (3.17): process of residuals plot.

CHAPTER FOUR

Experimental Work

Chapter Four: Experimental Work

4.1 Introduction

This chapter describes all the steps of designing and building the experimental test rig. It presents a detailed description of apparatus used in the laboratory experiments and the experimental investigation of heat transfer enhancement and flow of two-phase and three phase in a horizontal rectangular ribbed two-pass channel at different Reynolds number. It can be classified into three main categories: The first concerns with building experimentally the optimum model resulting from the numerical part within the fluid laboratories of the Mechanical Engineering Department at University of Babylon. The second deals with two-phase flow (air–water) and three phase flow (air-water-gasoil) at different flow rates and with different ribs surface temperature. The third category is concerned with studying the heat transfer enhancement and the pressure drop. All the experiments have been done at in a laboratory condition (27 ºC and 1 atm).

4.2 Description of Test Rig and Experimental Apparatus

To achieve the best experimental investigation, the test rig is designed and manufactured to deal with all measurement's cases especially two and three phase flow requirements and care has been taken to build parts of the test rig. Figures (4.1) and (4.2) show the schematic diagram and photo of the experimental apparatus. These parts have been fixed on the frame structure which is designed to ensure both easy operation and maintenance through the experiments.

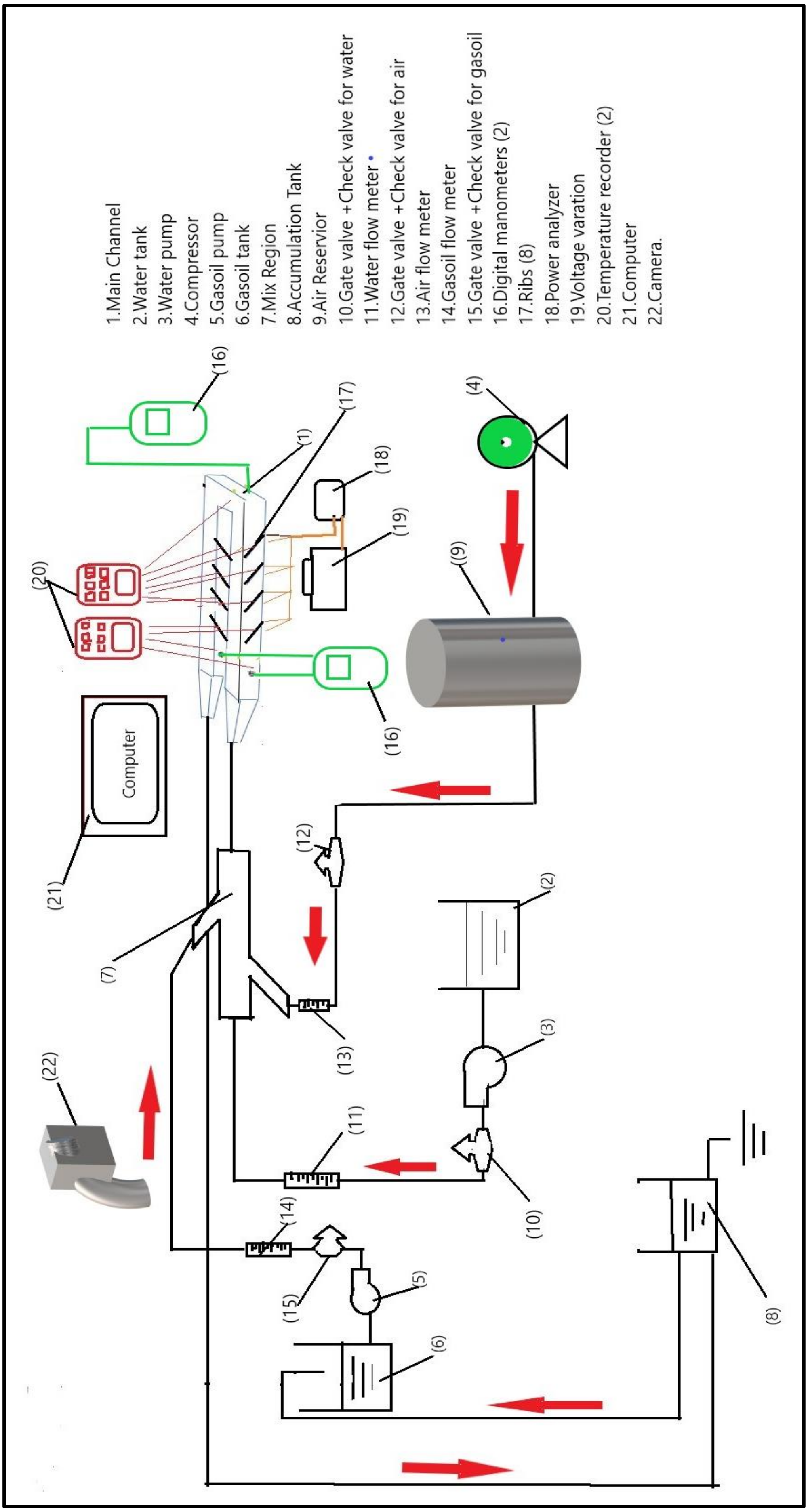

Figure (4.1): Schematic diagram of the experimental Rig.

Figure (4.2): Experimental Rig.

4.3 Main channel

A channel of two-pass used in the experiment has a pass length of (4080) mm and a rectangular internal cross section of (80mm by 40mm) (W×H). The hydraulic diameter of the channel is 53.3mm. It consists of three sections, i.e., the inlet section 960mm, test section (ribbed regions and bend) (1920+240) mm and outlet section (960) mm. The channel is manufactured by using 10 mm thickness transparent Plexiglas Plates (Acrylic) for the optical access to flow. Two-phase flow & three phase flow from laboratory room is drawn through the inlet contraction and entered the channel as shown in Figure (4.3).

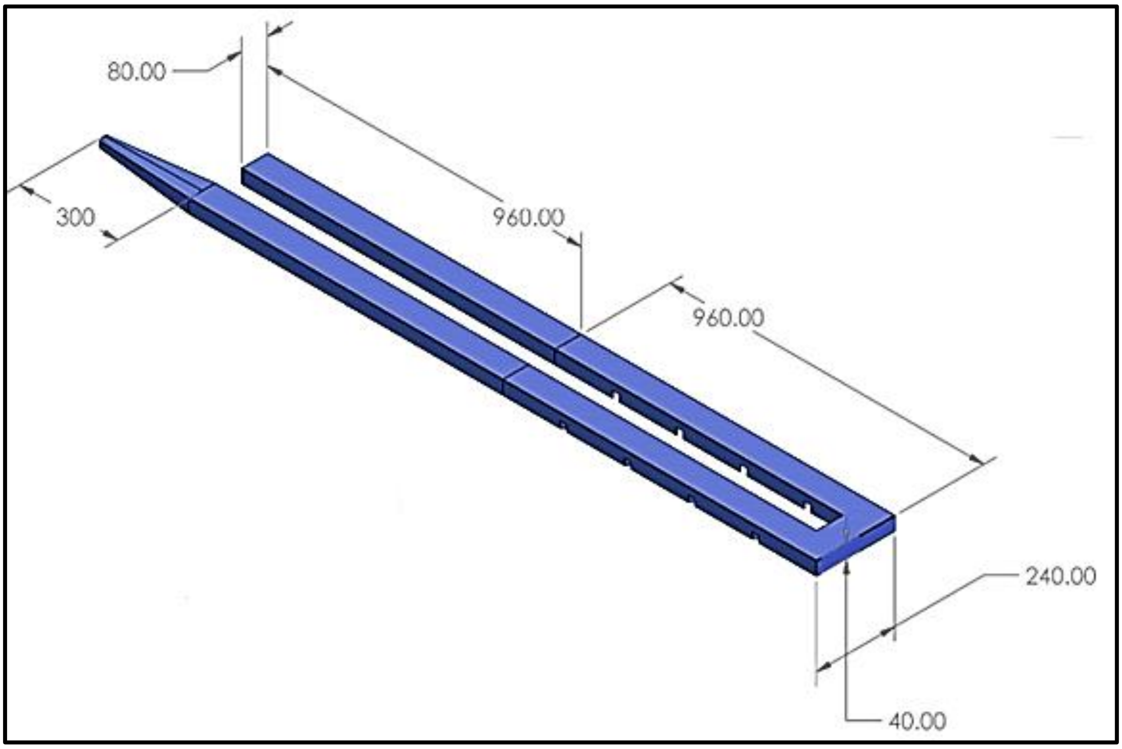

Figure (4.3). Main Channel (all dimension in mm).

4.4 Curved Ribs

The Curved Ribs are manufactured from an aluminum metal of angle 45° with constant temperature and installed after entrance length. The ribs are of length (80 mm) and cross section (22×20) mm in a Positive-Negative

(PN) arrangement and two perforating circle area with 3mm as diameter. There is a heat source installed at the base of the rib to maintain the required temperature for rib surface. Eight ribs are manufactured from aluminum metal, 4 ribs in each pass of channel. They are formed by CNC lathe machine to form ribs with (22mm) height and (20 mm) thickness as shown in figure (4.4).

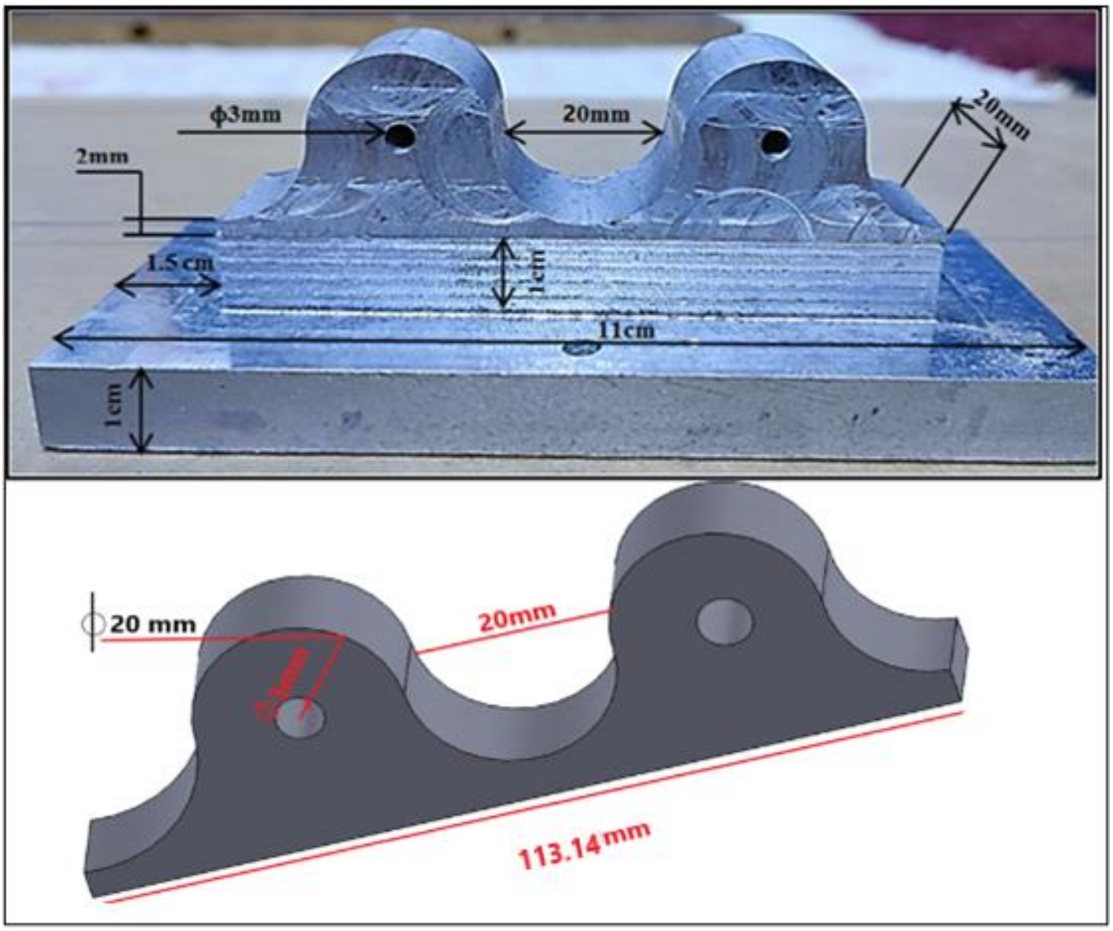

Figure (4.4). Rib Configuration

4.5 Heaters

Heat is supplied to the ribs using a finger heater with (6mm ×80mm) as shown in Figure (4.5). It made of stainless steel with specifications 220Volt, Current (3~4) Amp and 700 Watt. Eight heaters are installed to supply heat flux on the external base of ribs. All heaters are connected to a volt regulator with a known voltage and a Digital Power Analyzer to read the wattage value.

4.6 Converters

A Converter has been connected to the channel to supply mixture of two and three phase flow to the channel and connect channel with another parts of rig. Two-Converters, one at the inlet and the second at the outlet region are used. They are is made from galvanized material and with a circular cross-sectional area at the fluid entry side and a rectangular sectional area at the channel side. The beginning of the Converter opens the air tube with a diameter (0.5 in) which is intertwined with a large tube with a diameter (1.25 in), as shown in Figure (4.6).

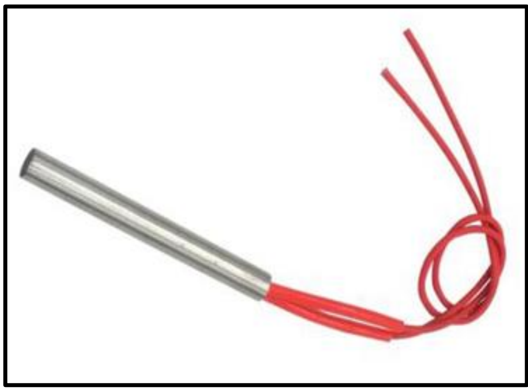

Figure (4.5). Finger Heater

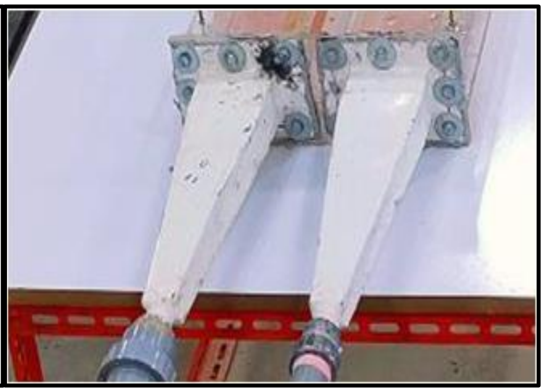

Figure (4.6). Converters

4.7 Air compressor

Figure (4.7) shows a compressor designed by Ingersoll-Rand company type (WELDED AIR RECIVER–BS 5169 IIIE), which works as positive displacement machine. It consists of piston driven by a crankshaft to deliver gases at high pressure with a connecting rod.

4.8 Water Pump.

To provide water to the system, specifications as a centrifugal type, model NO. SHFM5AM, quantities (5 to 480) Lpm, head (5 to 20) m, power (1.5

KW) and work at constant voltage (220 V) are taken into account, as shown in figure (4.8).

4.9 Water Tank.

It has a capacity of (500) liter with a cylindrical shape. The water used in experiments is at a laboratory temperature.

4.10 Water flow meter

It is a variable area flow meter (Rotameter), which consists of a vertical conical measuring tube and mobile float based on the weight force that equals to the bouncy force as shown in figure (4.9). It is used to control and measure in Litters /minute the water quantity with a range of (10 to 70) LPM.

4.11 Air Reservoir

To collect the air coming from compressor under a pressure in order to provide a pure air flow rate with high stability. Gas reservoir of cylindrical shape has a capacity of (1000 Liter) with (6 bar) and a laboratory temperature is used (see Figure (4.10)).

4.12 Pressure Regulator

There are two pressure regulators gages are used, the first gage is ranged from 0 to 6 bar to know the pressure inside the reservoir range as shown in Figure (4.11).

4.13 Safety Valve.

A safety valve is used to control the air pressure and air flow coming from air reservoir. It has a pressure regulator with a range of (0 to 12) bar, as shown in Figure (4.12).

4.14 Air flow meter.

Figure (4.13) shows a flow rate range from (350 to 3500) l/hr. It is used to manage and control the gas flow rate that enters the Converter. It consists of a tube made of a clear material with a float that is exerted a drag force of the flow and gravity.

4.15 Gasoil pump.

Centrifugal pump is used to supply the gasoil into the test channel from tank. It is **(2×2)** inch size with a maximum discharge of **30 Lpm,** a power supply of **370 Watt,** and a maximum head of **(30 m)** as shown in Figure (4.14).

4.16 Gasoil flow meter

The purpose of using the flow meter is to control and measure the gasoil flow rate that enters the mixing pipe, with a range of (1 to 22) Lpm as shown in Figure (4.15).

4.17 Gasoil tank

It used in experiments is stored in a cylindrical tank capacity (500 liter).

4.18 Check & gate valve

Check valve is used to prevent the backflow of water and air. It positions between the flow meter and gate valve. The gate valve utilized to control the flow rate that enter to the flow meter.

4.19 Accumulation tank

The mixture of water and gasoil coming out of the channel are collected through a downward pipe into a tank and left there for a day or until the oil and water are separated from each other due to the difference in density. The gas is discharged to the atmosphere and oil is then returned into the oil tank from the separation tank to be reused while water is draw out to the drain. The separation tank is made of plastic material with a capacity of (500 litter), (see Figure (4.16)).

4.20 Mix Region (MR)

It’s a part of the piping system consists of two entrances in case of two-phase flow and three entrances in three-phase flow, as shown in Figure (4.17). Water entrance is as a straight line with the (MR) while air entrance has pipe of 1.27cm open in beginning Converter to avoid chocking flow due to high pressure of air. In three-phase flow, the gasoil entre (MR) in acute angle and mixing with water. The acute of entrances is for reduction losses during flow. The opposite side, mixture of Water-Gasoil is leaving.

Figure (4.7). Compressor

Figure (4.8). Water Pump Figure (4.9). water flow meter

Figure (4.10). Air Reservoir Figure (4.11). Pressure Regulator

Figure (4.12). Safety Valve Figure (4.13). Air Flow Meter

Figure (4.14): Gasoil Pump

Figure (4.15). Gasoil Flow-meter

Figure (4.16). Accumulation Tank

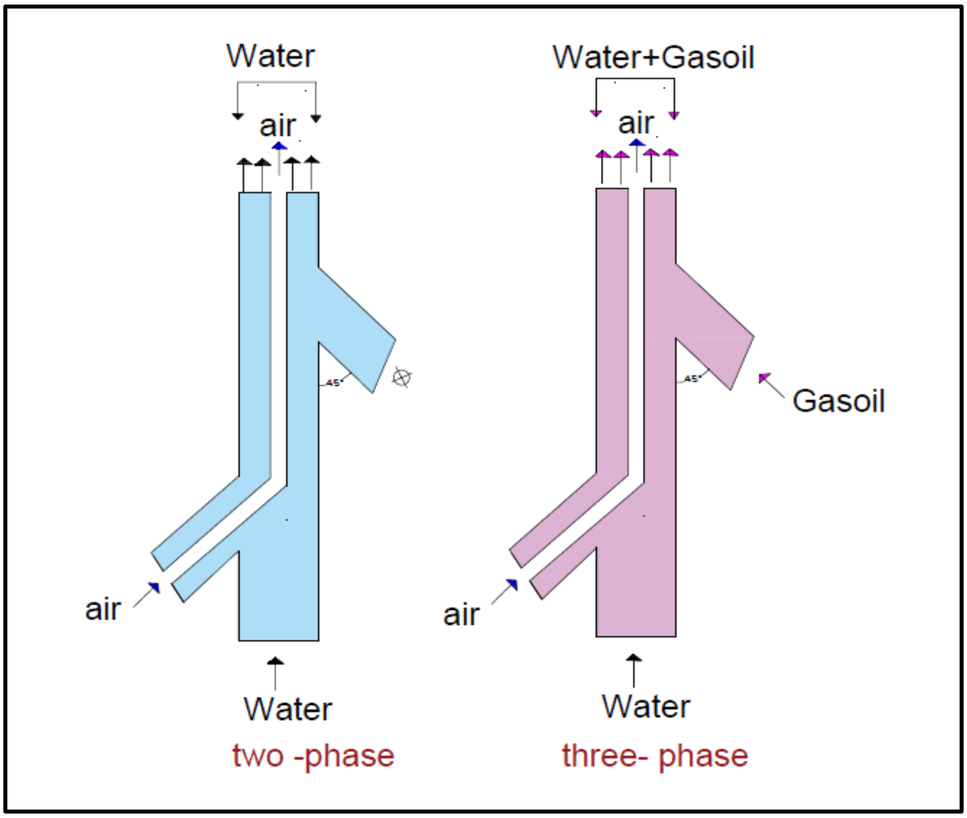

Figure (4.17). Mix Region

4.21 Temperature Devises

4.21.1 Thermocouples Distribution and Fixation

Thermocouples are used to convert a signal of thermocouples to a digital reading at same time, with specification according to table (4.1). Eleven thermocouples (K–types, TP–01) are installed along channel. All thermocouples are attached to by drilling to the channel in a specific place with a suitable adhesion epoxy. Three thermocouples (k-type) are located in inlet ribbed region in first pass, bend, and outlet ribbed region in second pass at 0mm, 1040mm, and 2080mm from the entrance of the ribbed section to measure the temperature of the mixture. The eight thermocouples are located in the center of each rib from the outside of channel. Thermocouples produce a voltage as a result of the heat effect, and this voltage can be used to measure rib temperature.

Table (4.1). Thermocouples Specification [89].

Sensor type	Resolution	Range	Accuracy
Type K Chromium–aluminum)	0.1°C	(-50.1°C to -100°C)	+(0.4 % +1°C)
		(-50.0°C to 999.9°C)	+(0.4 % +0.5°C)
	1°C	(1000°C to -1300°C)	+(0.4 % +1°C)

4.21.2 Digital Temperature Recorder

Thirteen channel portable temperature recorder model (BTM-4208SD) has been used to measure the temperature and to save the measuring data at a certain time into SD memory card. The measured temperatures are showed via Microsoft Excel for each second. Figure (4.18) shows the temperature recorder and the thermocouple.

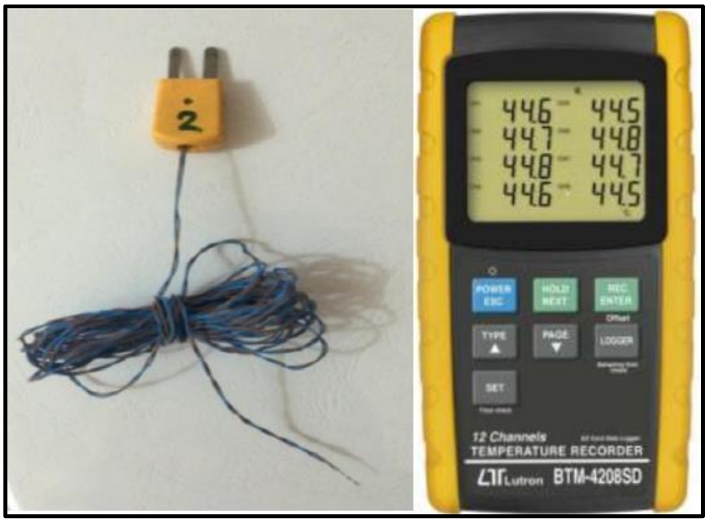

Figure (4.18). Temperature recorder device and thermocouple.

4.22 Digital Manometer (PM 9100)

Two Digital Manometer device are used to measure the change in the pressure across a small channel inside the ribbed channel as shown in

Figure (4.19). They work on principle of piezoelectricity (where electricity is generated if mechanical stress is applied to the thin membrane with accuracy of (0.1 %) as shown in table (4.2). The recorded data show the maximum and minimum of readings. Channels are located at different distances (S) from a reference point (inlet point): inlet channel, bend channel and outlet channel at distances (0 ,1040, 2120) mm from inlet point to ribbed section, respectively. The small channels are located at the channel base of ribbed region with three holes, first is inlet and outlet ribbed region channel as shown in Figure (4.20).

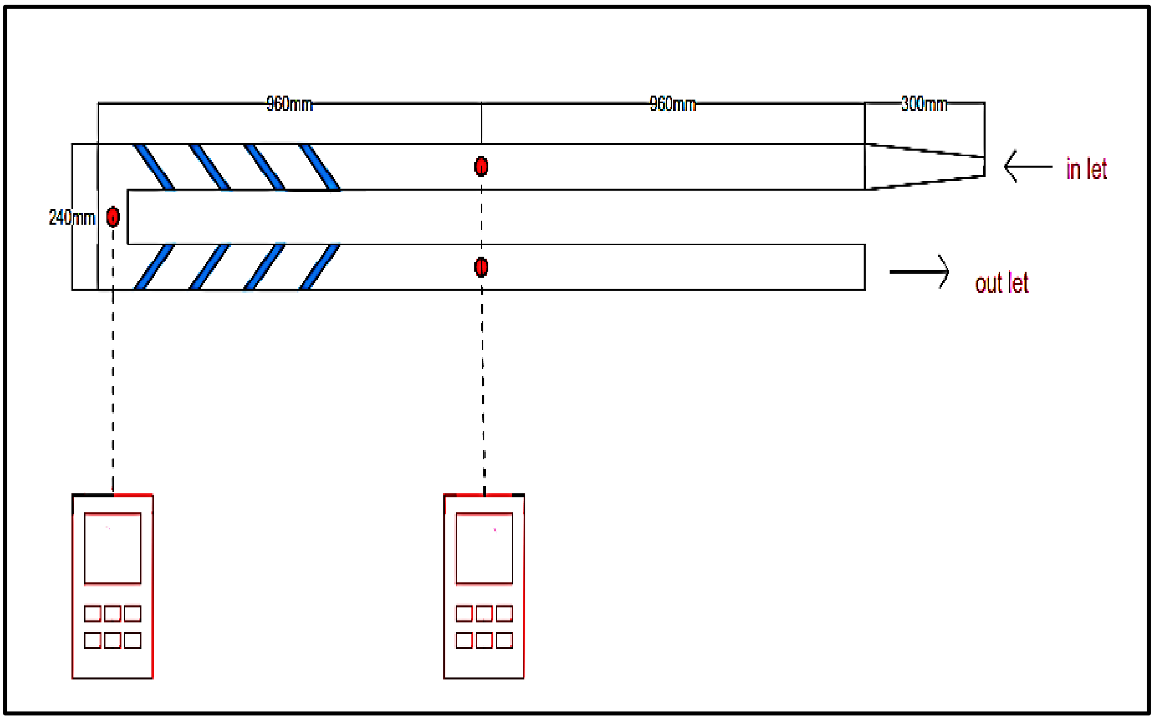

Figure (4.19). Position of channel manometers.

Figure (4.20). Digital Manometers.

Table (4.2): Manometer Specification [87]

Sensor type	Accuracy	Range	Dimension (mm)	Display Units
Piezoelectric	±2% Full Scale	Temperature (0°C to 50°C) Humidity Less than 80%	180×72×32	Mbar, Psi Kg/cm^2 , mmHg Atmospheric

4.23 Capture and Analysis

A camera is used to monitor a flow with slow motion after added a potassium Permanganate into water in the ribbed channel.

4.24 Voltage Variation Device

A variable voltage device, as shown in figure (4.21), was used to supply the required voltage with a range of (0-260) V, and supply the required power for heater. In addition, there is an internal resistance to control the variations of voltage till reach the demanded value is used.

4.25 Power Measuring Device

The power analyzer model (DW-6091) as presented in figure (4.22) is utilized to measure the supplied electric power values that feed the heaters with specification as indicated by table (4.3). The input heat is given as:

$$Q_{in} = I * V \cos\theta \quad \ldots (4.1)$$

The uncertainty of Q_{in} equal 1.4%.

Table (4.3) Information of power measurement device. [90]

Quantity	Range	Resolution
Power (Watts)	1-6000	150-200 Watts
Voltage (Volts)	0.1-299.9	196.9-228.2 Volt
Current (Amp.)	0.1-200	0.74-0.86 Amp.

Figure (4.21) variable voltage device. Figure (4.22) power device

4.26 Instrument Calibration

To increase the accuracy of measurements devices, it performed a calibrate each of the flow meters, manometers, and the recorder device.

4.26.1 Digital Temperature Recorder

To calibrate the temperature recorder, a thermocouple is used as shown in Figure (4.23). In this way, the deviation values for all channel temperatures recorded. The method carried out by input a value to a calibrator and compared the deviation between two devices as shown in table (4.4). Figure (4.24) presents the calibrated data.

Figure (4.23). Calibration method temperature recorder.

Table (4.4): Calibration Results of Thermocouple

Reference value	Indicated value Device 1 °C	Indicated value Device 2 °C	Correlation value °C	
			Device1	Device 2
25	24.6	24.54	-0.4	-0.723
30	29.8	29.199	-0.2,	-0.801
35	34.5	34.35	-0.5	-0.65
40	39.8	38.78	-0.2	-1.22

50	49.6	48.67	-0.4	-1.33
60	59.8	59.1	-0.2,	-0.9

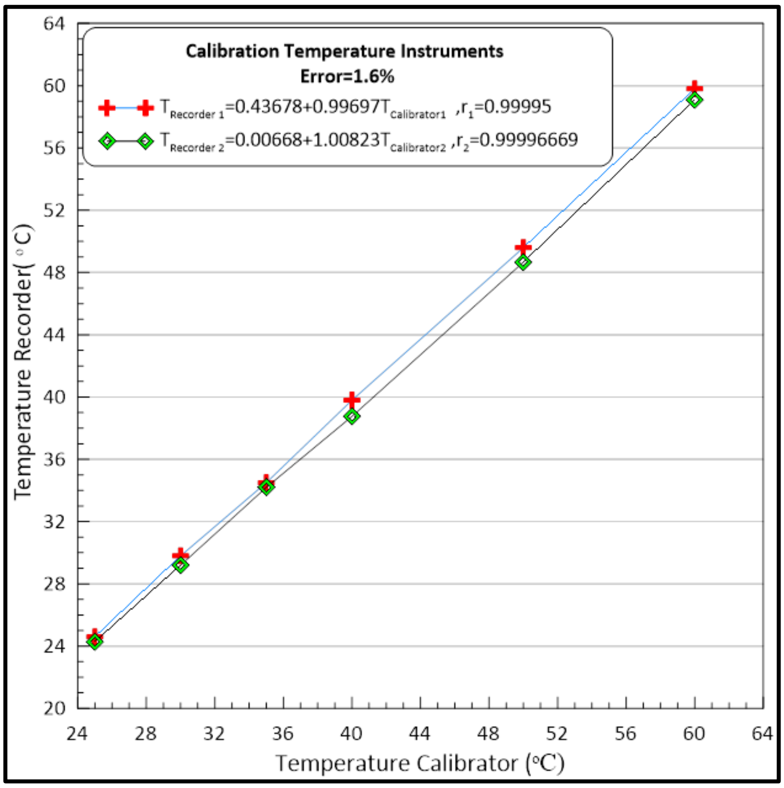

Figure (4.24). Calibration Curves of temperature.

4.26.2 Pressure Calibration

To calibrate the digital manometer is done by using a U-tube manometer. The difference of pressure is the different between the high of the water in the tube where is close of the channel and the high of the water in the opened tube to the atmospheric. The difference between the pressure value of the two manometers readings at same time and for the same values of flow rate. The measured reading of the pressure difference (pressure drop) and the standard reading of the pressure difference are drew as shown in figure (4.25).

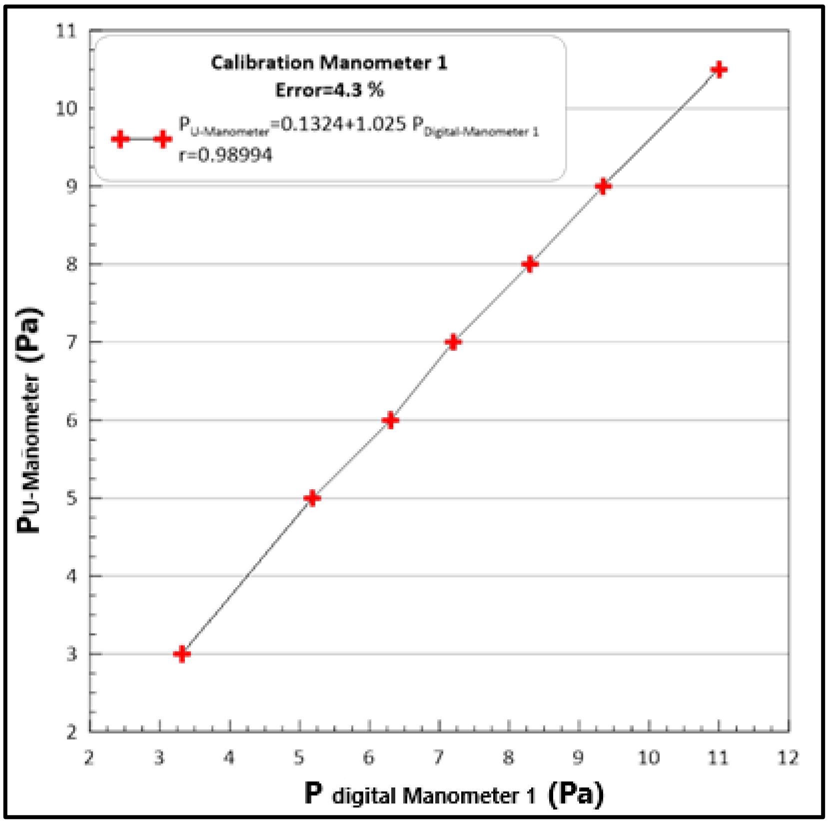

(a) Digital Manometer device no. (1).

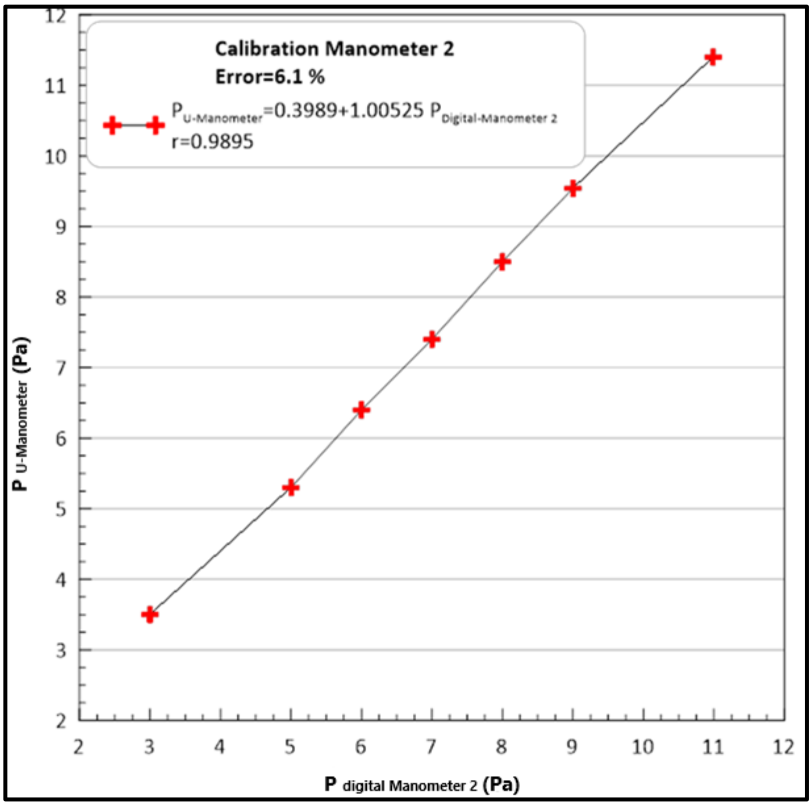

(b) Digital Manometer device no. (2)

Figure (4.25). Calibration Curves of Digital Manometers.

4.26.3 Volumetric Flow rate of water

The flow meter used to measure the water flow rate is calibrated by using a scaled container filled with the water coming out of the channel at a specific flow rate, the time for the water to reach a specific point on the container is recorded. This process was repeated for five times and the values are represented in curve with the flow meter values as shown in figure (4.26).

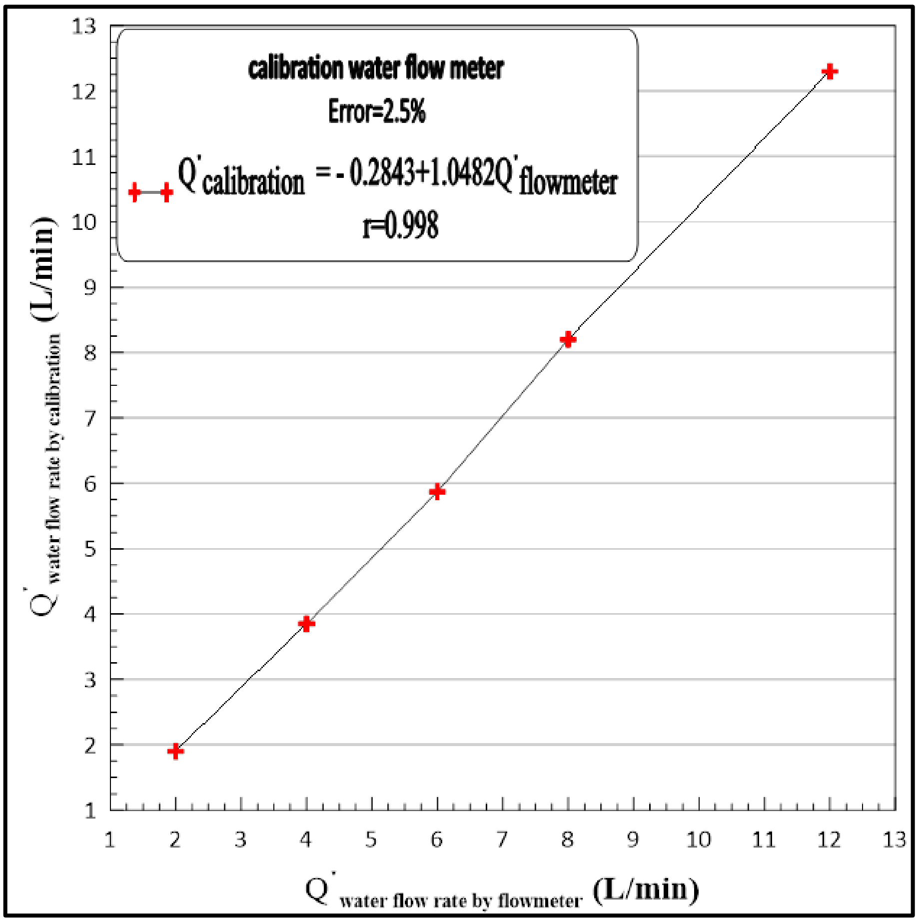

Figure (4.26). Calibration Curves of Waterflow meter.

4.26.4 Volumetric Flow rates of Gasoil

The flow meter used to measure the gasoline flow rate is calibrated by using a scaled container in the same way as water flow meter where it filled with the gasoil that is coming out of the channel at a specific flow rate. The time is recorded for the gasoil to reach a specific point in the container. This process was repeated for five times and the values are represented in curve with the flow meter values as shown in figure (4.27).

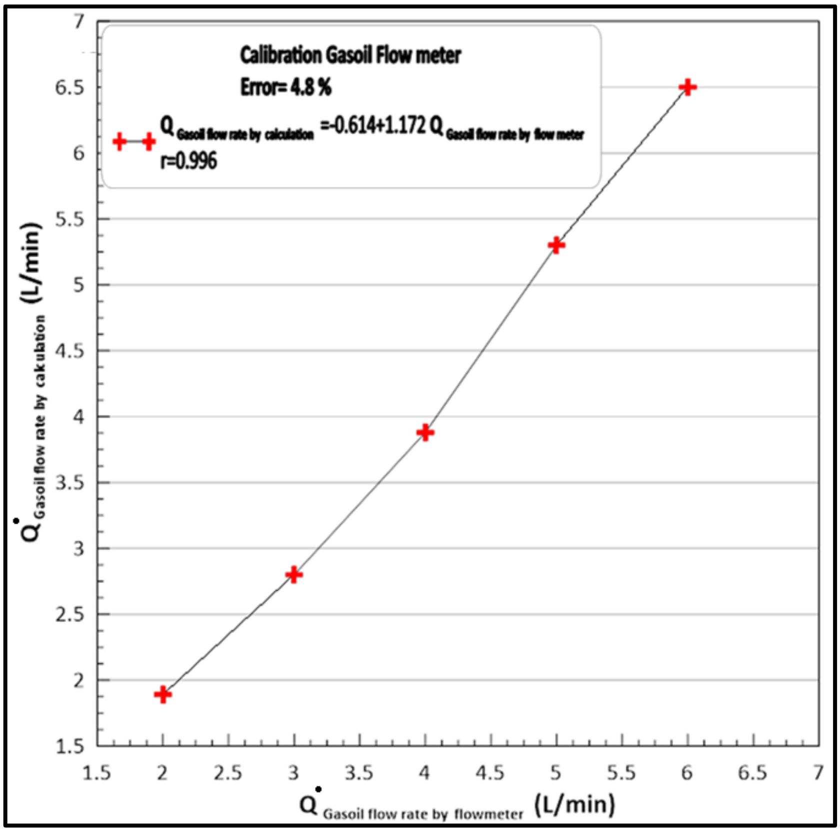

Figure (4.27). Calibration Curves of gasoil flow meter.

4.26.5 Volumetric Flow rates of Air

The air flow meter is calibrated by measuring the pressure difference through orifice meter, which has a restriction to create a pressure drop. The pressure difference is measured using a **U**-tube water manometer as shown in Figure (4.28). It consists of a straight length pipe of 50 cm; with a central orifice of (32) mm outlet diameter and 25.4 mm inlet diameter. The theoretical discharge (Q_{theory}) is calculated by assuming the air is as incompressible fluid and using a Bernoulli's equation for two points (before and after orifice). Neglecting the pressure drop is resulted from friction losses. The linear relation of calibration is shown in Figure (4.29). The theoretical volumetric flow rate can be calculated as [91]:

$$Q_{theoritical} = \frac{A_2}{\sqrt{1-\left[\frac{A_2}{A_1}\right]^2}}\sqrt{\frac{2(\Delta P)_{air}}{\rho_{air}}} \qquad \dots (4.2)$$

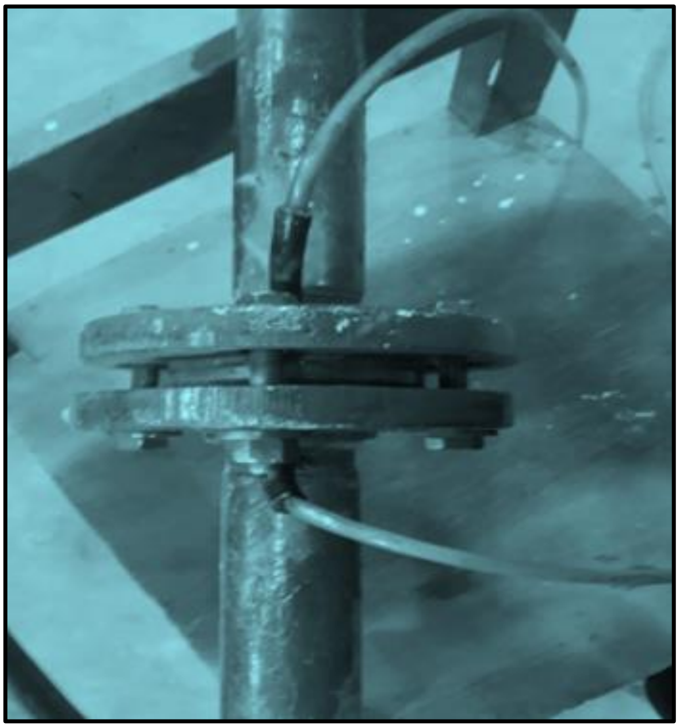

Figure (4.28). Orifice meter and U-manometer.

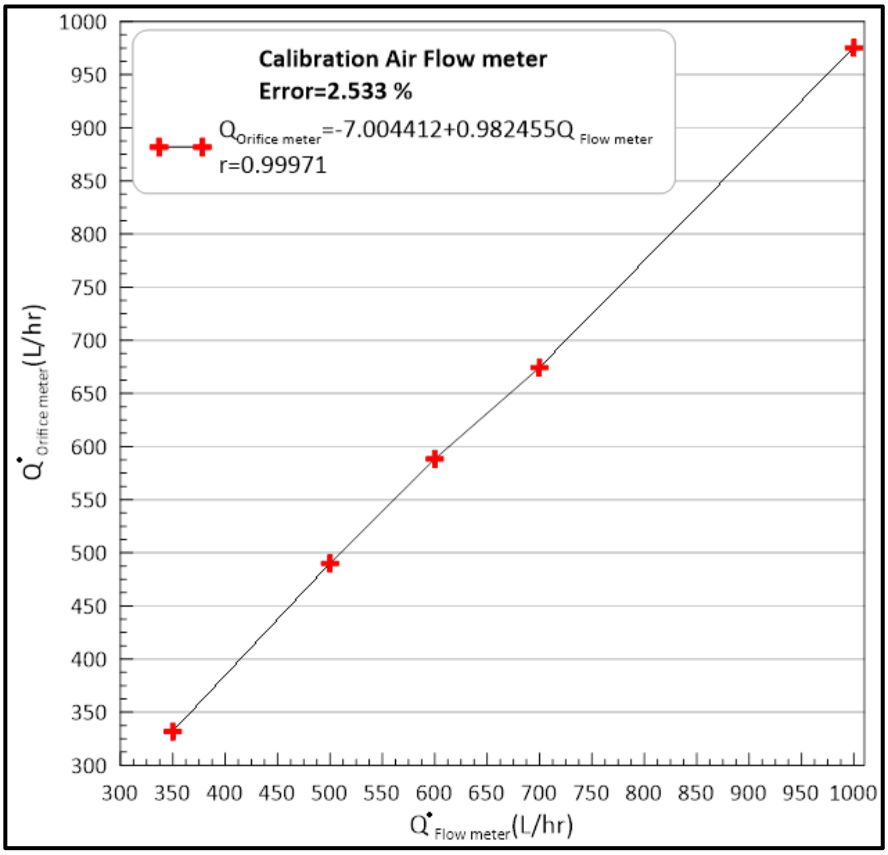

Figure (4.29). Calibration Curves of air flow meter.

4.27 Experimental Procedure

The following procedure has been applied for the purpose of investigating and analyzing the ribbed channel enhancement in heat transfer, pressure behavior, and temperature distribution. The producer of running experiments is: -

A. First set of experiments (Water-Air) Twenty-seven of them are with a two-phases flow:

1. The electrical heater is operated and adjusted to get the first constant rib temperature (50°C) using a regulating device (220 volt).
2. The compressor is run to get the air amount in the gas receiver.
3. The air loop is opened with a first value of flow rate.
4. The water loop is opened with first value of flow rate.
5. The pressure is measured by three channels of the Digital manometer for the first run 5-minutes data recording for stability in measuring. And images for the experiment were taken.
6. The procedure from the 5 previous steps is repeated for other experiments rib surface and flow rates as Table (4.3).

B. Second sets of experiments (Water–Air-Gasoil) eighty-one of them are with a three-phases flow:

1. The electrical heater is operated and adjusted to get the first constant rib temperature (50°C) by the regulating device (220 volt).
2. The compressor is run to get the air amount in the gas receiver.
3. The air loop is opened with first value of flow rate.
4. The water loop is opened with first value of flow rate.
5. The gasoil loop is opened with first value of flow rate.
6. The pressure is measured by three channels of the digital manometer for the first run 5-minute data recording for stability in measuring. And images for the experiment were taken.

7. The procedure from the 5 previous steps is repeated for other experiments rib surfaces and flow rates as table (4.4).

Table (4.3). The variables of experiments (Two-Phase Flow)

Q_{air} (L/min)	10	16.67	25
Q_{water} (L/min)	4	8	12
T_{Rib} (°C)	50	60	70

Table (4.4). The variables of experiments (Three-Phase Flow).

Q_{air} (L/min)	10	16.67	25
Q_{Gasoil} (L/min)	2	3	4
Q_{water} (L/min)	4	8	12
T_{Rib} (°C)	50	60	70

4.28 Experimental Calculations

1. Calculation effective properties (Air-Water).

To calculate the effective properties for mixture of (air-water) as two-phase flow with the help of certain mixing rules and definitions [85,88]. Assuming the air is a controlled phase while water is secondary phase of flow.

a) Void Fraction (α)

It is Dimensionless quantity represented the volume of gas phase to total volume of all phases in channel [85]:

$$\alpha = \frac{\text{Volume of gas phase}}{\text{Total volume}} \quad \dots (4.3)$$

$$1 - \alpha = \frac{\text{Volume of liquid phase}}{\text{Total volume}} \quad \dots (4.4)$$

b) Velocity of Mixture

The mixture velocity as a relative velocity for two-phase flow of mixture (m/s) as follow [85]:

$$\boldsymbol{V_{mixture}} = \boldsymbol{V_{air}} + \boldsymbol{V_{water}} \quad \dots (4.5)$$

c) Dynamic Viscosity of Mixture

To calculate viscosity of mixture by equation,[85]:

$$\boldsymbol{\mu_{mixture}} = \alpha * \boldsymbol{\mu_{air}} + (1 - \alpha)\, \boldsymbol{\mu_{water}} \quad \dots (4.6)$$

d) Specific heat at constant pressure (Cp).

The value of **Cp** for mixture can be calculated depended on the void fraction and **Cp** for phase as according to equation below [85]:

$$\boldsymbol{Cp_{mixture}} = \alpha * \boldsymbol{Cp_{air}} + (1 - \alpha)\, \boldsymbol{Cp_{water}} \quad \dots (4.7)$$

2. Calculation effective properties (Air-Water-Gasoil).

To calculate the effective properties for mixture of (air-water-Gasoil) as equations [85] and [88]. Assuming the air is the controller phase and water is secondary phase in flow.

a) Void Fraction (α)

It is dimensionless quantity represented as [85].

$$\alpha_{air} = \frac{\text{Volume of gas phase}}{\text{Total volume}} \quad \dots (4.8)$$

$$\alpha_{water} = \frac{\text{Volume of water phase}}{\text{Total volume}} \quad \dots (4.9)$$

$$\alpha_{\text{gasoil}} = \frac{\text{Volume of gasoil phase}}{\text{Total volume}} \quad \dots (4.10)$$

b) Mixture Velocity

The mixture velocity is a relative velocity for a two-phase flow of mixture (m/s) as follows [85]:

$$\boldsymbol{V_{mixture}} = \boldsymbol{V_{air}} + \boldsymbol{V_{water}} + \boldsymbol{V_{gasoil}} \quad \dots (4.11)$$

c) Dynamic Viscosity of Mixture

To calculate viscosity of the mixture use:

$$\boldsymbol{\mu_{mixture}} = \alpha_{air} * \boldsymbol{\mu_{air}} + \alpha_{water} \cdot \boldsymbol{\mu_{water}} + \alpha_{\text{gasoil}} \cdot \mu_{\text{gasoil}} \quad \dots (4.12)$$

d) Specific heat at a constant pressure (**Cp**)

The value of **Cp** for mixture can be calculated depending on the void fraction and **Cp** for phase as [85] :

$$\boldsymbol{Cp_{mixture}} = \alpha_{air} * \boldsymbol{Cp_{air}} + \alpha_{water}.\boldsymbol{Cp_{water}} + \alpha_{gasoil}.\boldsymbol{Cp_{gasoil}} \quad \ldots(4.13)$$

e) Density ($\boldsymbol{\rho_{mixture}}$) [85].

$$\boldsymbol{\rho_{mixture}} = \boldsymbol{\rho_{gasoil}} * \boldsymbol{\alpha_{gasoil}} + \boldsymbol{\rho_w} * \boldsymbol{\alpha_w} + \boldsymbol{\rho_{air}} * \boldsymbol{\alpha_{air}} \quad \ldots(4.14)$$

3. Reynold Numbers [86]

The ranges of Re for two types of flow are calculated in APPENDIX E.

$$\mathrm{Re} = \frac{\rho_m U_m d}{\mu_m} \quad \ldots(4.15)$$

4. Friction Factor (f) [44]

$$\boldsymbol{f} = \frac{\Delta \boldsymbol{P}}{\frac{1}{2}\boldsymbol{S}.\boldsymbol{u}^2_{\boldsymbol{mixture}}\,\boldsymbol{\rho_{mixture}}} \quad \ldots(4.16)$$

$\Delta\boldsymbol{P}$: Pressure drop (pa).

S: distance from the inlet to the outlet of ribbed region and bend (m).

For smooth channel can be calculated as [45]:

$$f_o = 2(2.236 \ln Re - 4.639)^{-2} \quad \ldots(4.17)$$

5. Heat Transfer Coefficient

The heat transfer coefficient over the ribbed surface is [86]:

$$\boldsymbol{h} = \frac{\mathbf{q}''}{\mathbf{T_{wall}} - \mathbf{T_{bulk}}} \quad \ldots(4.18)$$

$\mathbf{q}''$ equal to Q_{in} by surface area of heat transfer the heat flux from the heated surface to the surrounding bulk fluid. T_{wall}, was read from thermocouples fixed on ribs surface. The bulk temperature T_{bulk} at position X along the direction of flow and is measured on the assumption that the temperature of linear working fluid flows along the channel, and can be calculated as [92]:

$$T_{bulk} = T_{in} + (T_{out} - T_{in})\frac{X}{L} \quad \dots (4.19)$$

6. Thermal-Performance Criteria Evaluation (PCE) [45].

$$\mathbf{PEC} = \frac{\frac{\mathbf{Nu}}{\mathbf{Nu_o}}}{(\frac{\mathbf{f}}{\mathbf{f_o}})^{\frac{1}{3}}} \quad \dots (4.20)$$

For smooth channel Nu (Dittus-Boelter) can be calculated as [45]:

$$\mathbf{Nu_o} = \mathbf{0.023Re^{0.8}Pr^{0.4}} \quad \dots (4.21)$$

For ribbed channel Nu can be calculated as [44]:

$$\mathbf{Nu} = \frac{\mathbf{hL}}{\boldsymbol{K}} \quad \dots (4.22)$$

8. Error Analysis

The relation between temperature recorders and thermocouple calibrator are linear formula for device 1and 2 as in equations:

$$\mathrm{T_{calibrator}} = 0.43678 + 0.99697\mathrm{T_{temperature\ recorder1}} \quad \dots (4.23)$$

$$\mathrm{T_{calibrator}} = 0.00668 + 1.000823\mathrm{T_{temperature\ recorder2}} \quad \dots (4.24)$$

The calibration for digital manometers is done with an accurate U-tube manometer and the relation is linear formulas for 1 and 2 as given in equations (4.25) and (4.26).

$$\mathrm{P_{U-tube\ Manometer}} = 0.1324 + 1.025\mathrm{T_{digital\ manomwter\ 1}} \quad \dots (4.25)$$

$$\mathrm{P_{U-tube\ Manometer}} = 0.3989 + 1.00525\mathrm{T_{digital\ manomwter\ 2}} \quad \dots (4.26)$$

The calibration for water, gasoil & air flowmeters are done with an accurate scaled tube and the relation is linear formulas as given in equations (4.27) to (4.29).

$$\mathrm{Q_{water\ calculation}} = -0.2843 + 1.0482\ \mathrm{Q_{water\ flowmeter}} \quad \dots (4.27)$$

$$\mathrm{Q_{gasoil\ calculation}} = -0.614 + 1.172\mathrm{Q_{gasoil\ flowmeter}} \quad \dots (4.28)$$

$$\mathrm{Q_{Orifice\ meter}} = -7.004412 + 0.982455\mathrm{Q_{Air\ flowmeter}} \quad \dots (4.29)$$

CHAPTER FIVE

Results and Discussion

Chapter Five: Results and Discussion

5.1 Introduction

In this study, the results are discussed in two parts, the first is related to the steps of design the optimum channel to enhance heat transfer and pressure drop. The second part is related to two types of the flow are air and water and air, water, and gasoil for two and three phases flow respectively. Also, comparisons between computational fluid dynamics results and experimental results are investigated the flow. All results are calculated in the inlet pass, outlet pass of ribbed region and bend.

5.2 Comparison of Numerical Results

The current numerical analyses of the flow and heat transfer values along two-pass channels have been performed in order to demonstrate the validity and correctness of the numerical process for this study. These analyses have been compared to the numerical results produced by prior researchers for studies [29,30,44]. The current study is performed in a 45° angled AR=2:1 channel with two-phase flow Re 72456.3 at T_{rib}=60°C along two passes of curved rib with circular perforating area (3mm).

Figure (5.1) shows the flow behavior of smooth channels for research [29] in the air conditions of Re equal to 25000 and 36 ribs of are attached in top and bottom with heat flux equal 4800W/m^2 channel and exist P_{static} =1*10^6 in a different dimension two-pass with AR=1:1).

Figure (5.2) shows the effect of rib on the behavior of Nu at different conditions. The research [30] is used (air in Re=25000, P_{static} =1*10^6, all heated walls at fixed temperature (T_w) in a different dimension two-pass with AR=1:1 where ribs (52) are attached in top and bottom channel. It is seen very clear from comparison between [29,30] and this current work, the two curves have same trend, that is good agreement. The high deviation between curves so as to difference in boundary conditions as well as the channels have a different dimensions and obstruction have shapes and modifications in current ribs. The working fluids, the researchers used as one phase while the current study used two-phase flow.

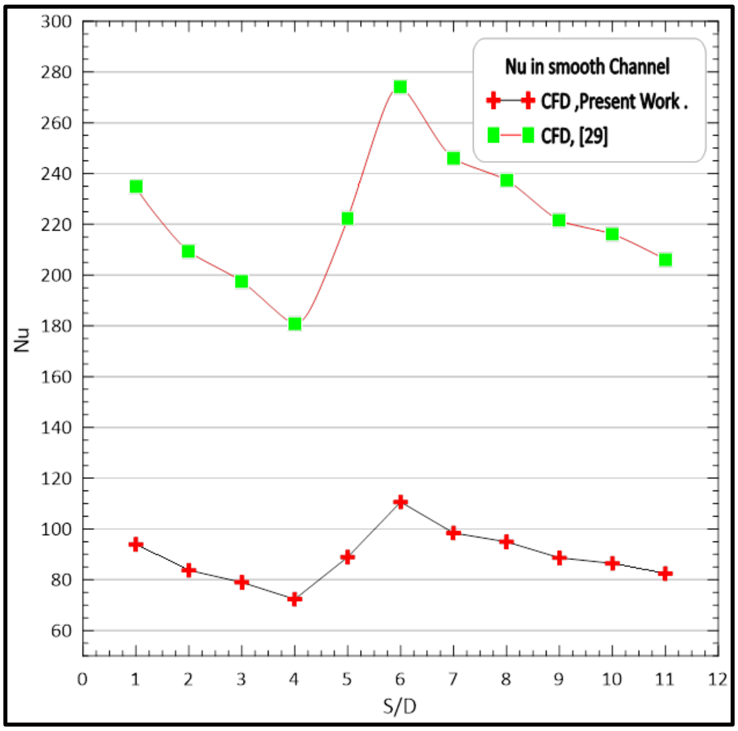

Figure (5.1). Nu behavior in smooth channels.

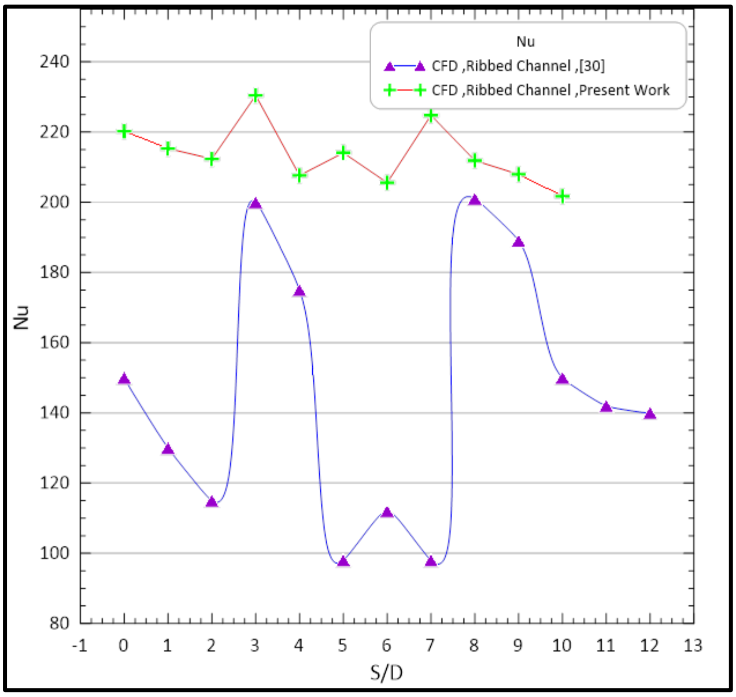

Figure (5.2). Nu behavior in ribbed channel.

5.3 First Part: Results for Choosing the Optimum Design.

5.3.1 The Shape of Channel the Bend, and an Aspect Ratio

For the purpose of improving channel heat transfer, the bend and channel shape choices have been extensively studied and determined in relation to the amount of turbulence produced. In compared to alternative arrangements, the acute bend is made possible by a significant improvement in heat transfer. According to sciences, increased turbulence and mixing caused by sharp edges also boosted Re and improved heat transfer. On another side, the sharp edges produced additional pressure drop due to increased friction and losses.

Additionally, the aspect ratio must take into account the height of the ribs and have a good streamline flow. An acceptable aspect ratio was around (2:1). These results have a good agreement with previous study [44] because the streamline flow caused turbulence, which in turn led to high heat transfer for reasonable values of velocity and friction, as well as because increasing channel width (which indicates an increase in the length of ribs) led to larger area and increasing rate of heat cause more enhancing in heat transfer. Figure (5.3) shows the channel's optimum design for this study.

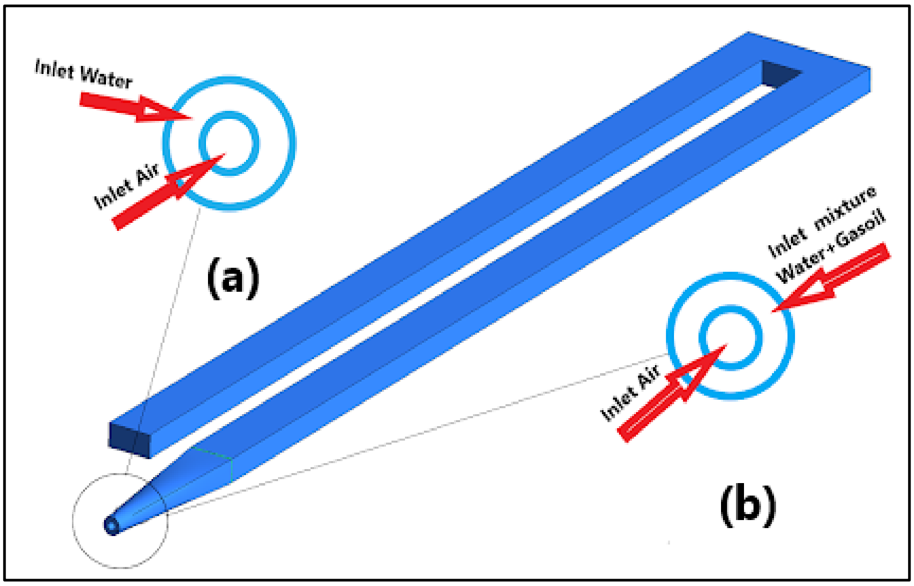

Figure (5.3). Physical Model of Channel

5.3.2 Smooth Channel

To be able to gain design ideas about the configuration of ribs that achieved the necessary amount of enhancement in heat transfer, as well as to compare with rib cases and understand the behavior of pressure drop, it is first necessary to study a simplified case for a channel without ribs and with a hot area (same area of base of rib) at 60°C and inclined with 45° at the same level of channel base.

Figure (5.4) (a) explains the effect of hot area and bend on velocity of mixture at air and water velocities about 1.3157 m/s and 0.1684 m/s respectively. It observed that the velocity started to increase gradually in first pass and reached maximum in the bend region, gradually increase in velocity of mixture at first-pass. Because the increase temperature due to hot areas lead to expanding air phase with flow direction and increasing velocity of mixture. The maximum values of velocity in bend because the area of flow decrease at constant flowrate, also the increasing turbulence of mixture so to sharp edges was led to increase friction, more losses and turbulence.

Figure (5.4) (b) shows the effect of hot areas and sharp bend on pressure at same above conditions. It observed that the pressure decreased gradually toward the bend and minimum pressure in bend because of gradually increasing in velocity and maximum velocity in bend. Also, the red regions in the sharp edges caused by high friction in these regions.

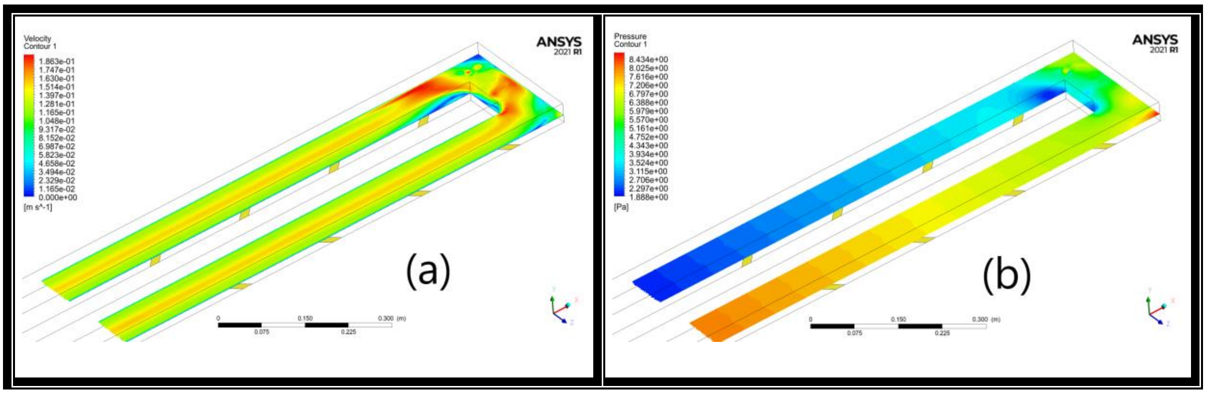

Figure (5.4). Distribution of :(a) Velocity, (b)Pressure

5.3.3 Optimum Ribs Shape

Choosing an appropriate shape and design is required to achieve a large area and turbulent flow, therefore; two designs, Curved and V-shaped ribs are used to enhance the heat transfer and pressure drop. A V-shaped ribs have sharp edges great more turbulence, few covering in previous studies. While curved-rib have smooth edges with wavy surface contact area.

Figure (5.5) shows the effect of curved ribs on heat transfer coefficients at the same conditions of the previous stage. It observed that the heat transfer coefficients are increased in two-types of ribs but curved rib has high enhancing in heat transfer and more efficient. The percentages of enhancing of curved ribs has 34.55% higher than V-shaped ribs and enhancing with 147.85% and 40.8% with respect to smooth case, respectively. Because the Curved ribs have smoothing flow where mixture passes and exchanges heat with ribs better than V-shaped ribs. Also, Curved ribs have higher heat transfer coefficients because of higher heat rate, in spite of these have surface area equal $5.3086 \times 10^{-3} m^2$, while V-shaped ribs equal $6.7632 \times 10^{-3} m^2$. Figure (5.6) shows the effect of two rib shapes on pressure along the ribbed and bend region. It observed that pressure decreased from inlet to outlet with high dropping in the bend region. The percentages of increasing pressure of V-shaped has 10.1 % higher than curved ribs and enhancing with 40. 5% and 72.5 % with respect to smooth case, respectively. The pressure in V-shaped ribs have maximum value because the shape of rib makes high obstruction opposite flow lead to minimize velocity, high friction losses and increased pressure. The Curved ribs have obstruction lower than V-shaped ribs because the curved ribs configuration has wavy surfaces less friction, also low friction and low pressure. While the percentages of increasing pressure drop, it observed that V-shaped rib higher than curved ribs about 60.01% also, in comparison with smooth case, the percentage of increasing pressure about 150% and

56.2% for V-shaped and curved ribs respectively, because V-shaped have a sharp edge with high friction. Figure (5.7) (a) and (b) show the behavior of pressure as contour and effect of the shape of the ribbed and bend region of the channel. The red region in V-shaped is large especially inlet region because of large resistance to flow generated so to feature than curved rib that has orange inlet region because the flow impact with sharp corners lead to increase pressure more than in curved rib of smooth configuration. Figure (5.8) (a) and (b) show the behavior of velocity as contour and effect of the shape of the ribbed and bend region of the channel. In bend the velocity has maximum values due to decrease in pressure so to high turbulence. But in the passes the velocity gradually increased so to decrease in cross section area and decreased in pressure. The blue and green region concentrated in bend corners have a lower velocity so to high friction losses. It considered that curved ribs optimum design according above reasons.

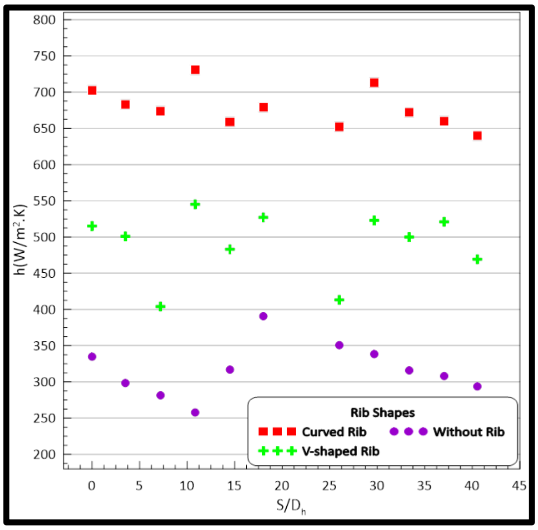

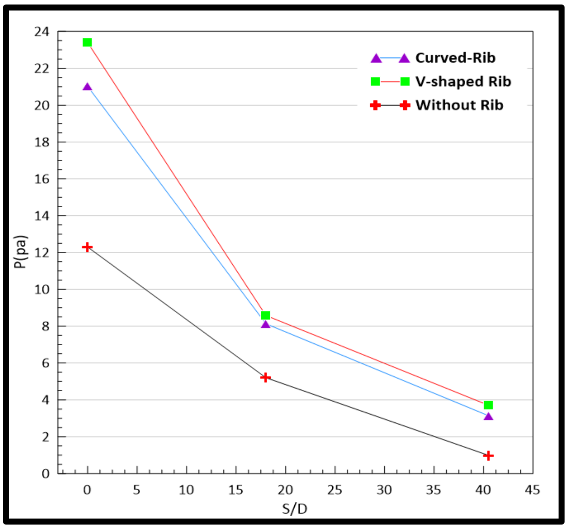

Figure (5.5). Heat convective coefficients. **Figure (5.6).** Pressure behavior.

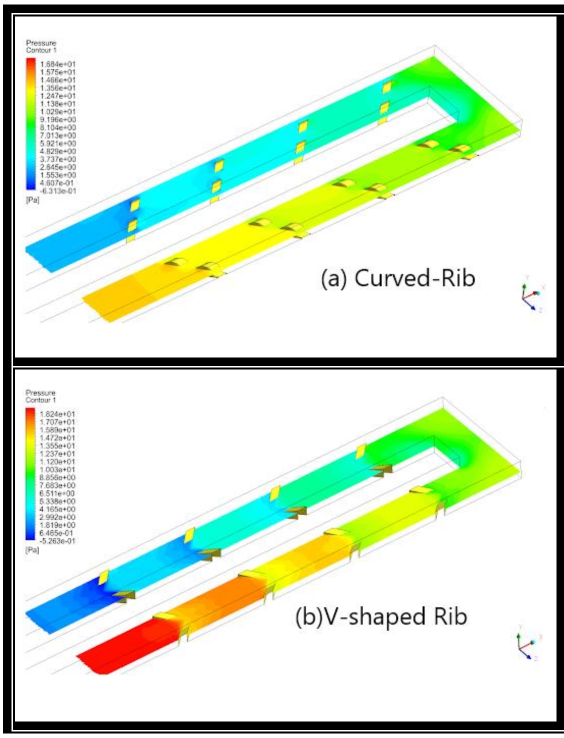

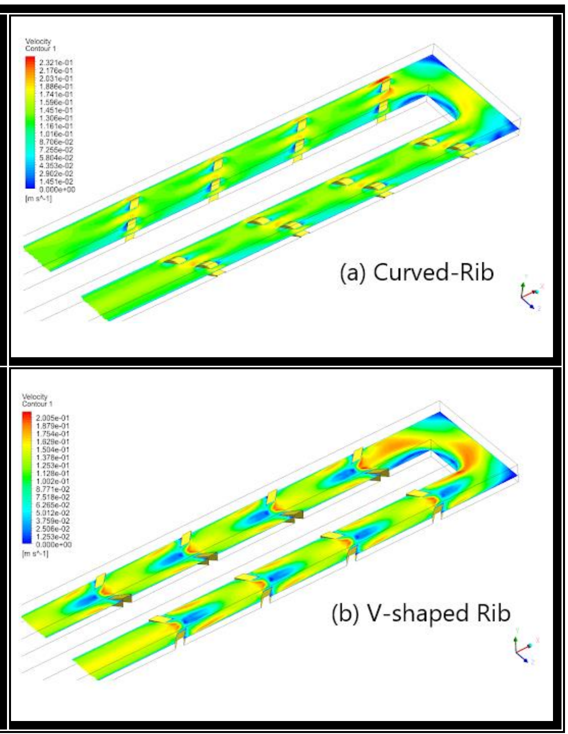

Figure (5.7). Pressure distribution. **Figure (5.8).** Velocity-distribution.

5.3.4 Shape of Perforated Area

After choosing the optimum area will choose the shapes according to heat transfer enhancement. Square, circle and triangle have the same cross section area of perforated that were examined to obtain the optimal perforating shape. Figure (5.9) shows the effect of shape of perforating area on heat transfer enhancement. It observed that the circle has a high-enhancing in-heat transfer, according the percentages of enhancement are about 7.47 % and 6.1% for square and triangle perforating area, respectively. Because the circle area has a largest heat transfer area with smoothly in flow when square and triangle area have small heat transfer area due to generate eddies consider as insulator prevents heat transfer in sharp edges. When comparison heat transfer in square has higher than triangle areas because square area higher than triangle areas.

Figure (5.10) shows the effect of the shape area on pressure at the same condition of previous stages. It observed that the square area perforating has high pressure comparison with triangle and circle area, because it has sharp edges in which generating eddies that lead to increase pressure of flow. Also, pressure drops in square area has maximum value, the percentages of increasing for square about for three cases along the ribbed region and bend were about (7.48% and 12.3%) with respect to triangle and circle areas, respectively. Because the friction losses in sharp edges of square area and triangle were higher than in circle area.

Figure (5.11) shows the behavior of pressure as contour in presence of a different shape of perforating at same conditions, it observed that pressure decreased gradually toward the outlet, in bend it decreased sharply because of more friction. In addition, it is observed that the circle shape has high pressure (high red region) at inlet because it has low contact area at same area of cross-section in comparison with triangle and square shapes.

Figure (5.12) shows the behavior velocity in same above cases, it is observed that the circle shape has high velocity in comparison with triangle and square shapes more turbulence because it has high contact area with small surface area when square has high surface area.

Finally, it observed that the circle perforating is the optimum shape area with high enhancement.

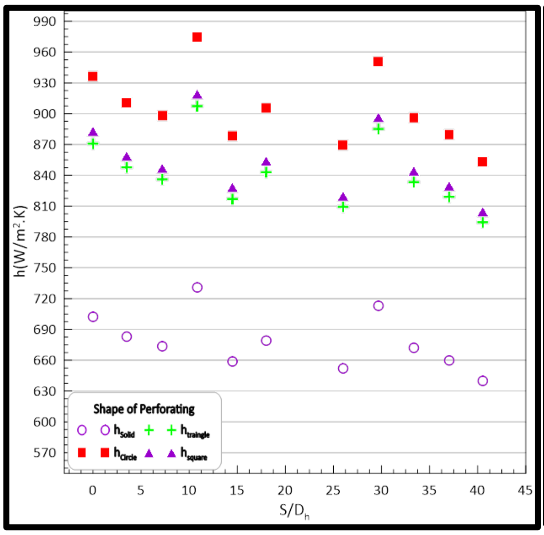

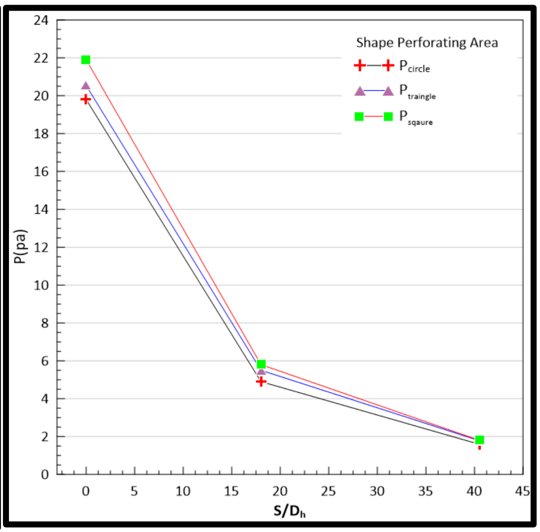

Figure (5.9): Heat transfer behavior. **Figure (5.10):** Pressure behavior.

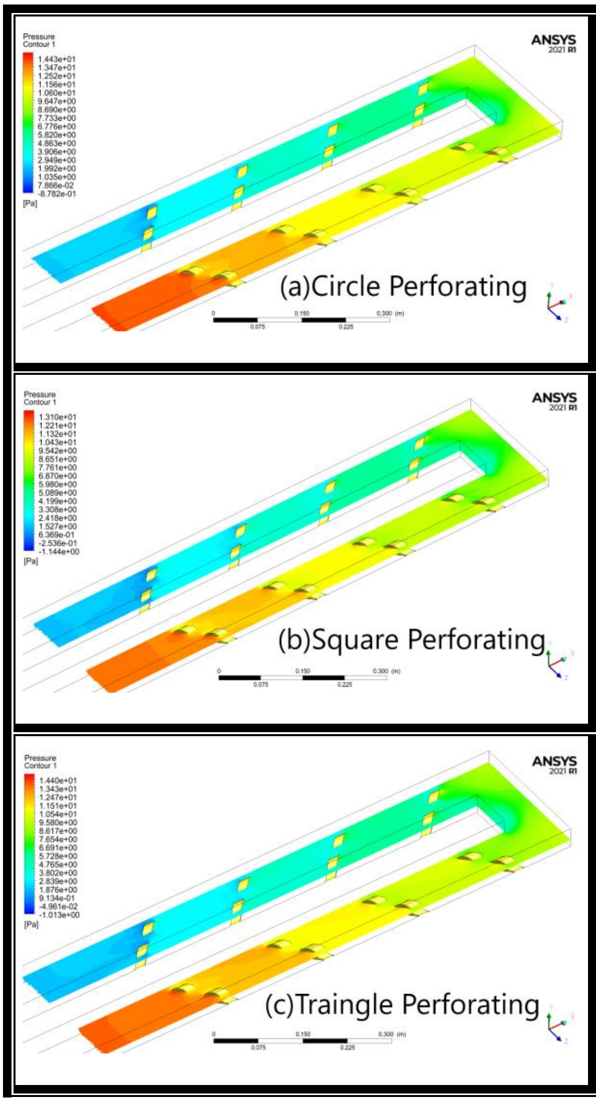

Figure (5.11). Pressure-distribution

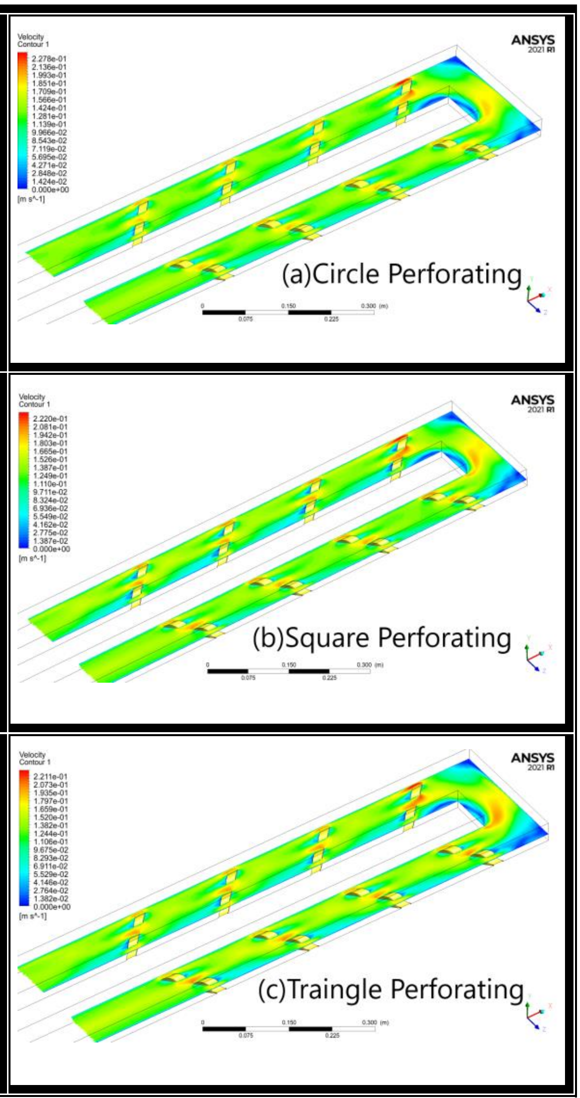

Figure (5.12): Velocity-distribution

5.3.5 Area of Optimum Perforated

The idea of creating a perforate inside the rib is to increase the area of heat transfer and turbulence in ribbed region. Three cases of circle perforating as (3,6 and 9) mm diameters inside ribs were used and it was chosen the optimum diameter for that more enhancement in heat transfer. Figure (5.13) shows the behavior of heat transfer coefficients for three circles perforated at same conditions of previous stage along the channel. It observed that coefficients (h) increased with decreased diameters from inlet to outlet with high dropping in bend. From observation, the percentages of enhancement in 3mm are about 15.4 % with respect to 6mm, 21.25% with respect to 9mm, when comparison with solid rib is enhanced about 33.425% ,16.13% and 10.07% for (3,6 and 9) mm, respectively. Because the circle gives more smoothly in flow with low losses, also the 3mm circle allows the largest velocity depending on continuity equation and relation of velocity with area, that getting to more turbulence than (6 and 9) mm leads to more enhancement in heat transfer.

The solid rib has a minimum heat transfer coefficient because the surface area of heat transfer and turbulence are low.

Figure (5.14) presents the effect of three diameters on behavior of pressure at same conditions. It observed that pressure decreases with increased circle diameters so to the circle of 3mm diameter has a maximum pressure while the circle of 9mm diameter has a minimum pressure. Because when the flow passed with hardly through small perforating area led to increase pressure, this mean that 3mm has maximum pressure in comparison with (6 and 9) mm at same conditions. Also, the increasing percentages of pressure drop for (3 mm) were about (15.1% and 22.82%) with respect to (6 and 9 mm), respectively along the ribbed region and bend. The reasons that become the area of 3mm have maximum pressure drop and percentage are the maximum velocity in 3mm in comparison with other areas.

Figure (5.15) (a), (b) and (C) show the behavior of pressure as contour in cases of perforating diameters at same conditions. It observed that the pressure decreased gradually toward outlet. The red region in 3mm is large because of higher pressure than other cases. Because the flow passed with hardly through small perforating area led to increase pressure.

Figure (5.16) (a), (b) and (c) show the behavior of velocity as contour and effect of the perforating diameters in the ribbed and bend region of the channel. The inlet region in area of 3mm was light colored that mean the velocity of lower than other because of according to Bernoulli's equation. The inlet region in areas (6) mm was dark color, while area 9mm was more dark color that mean the velocity in 9mm have maximum value than other because of this area has lower pressure and according to Bernoulli's equation. The edges have lower velocity because of friction where higher velocity in bend because of more turbulent. In outlet region in 3mm has greenish yellow because of low velocity where increase in (6and 9) mm higher than 3mm.

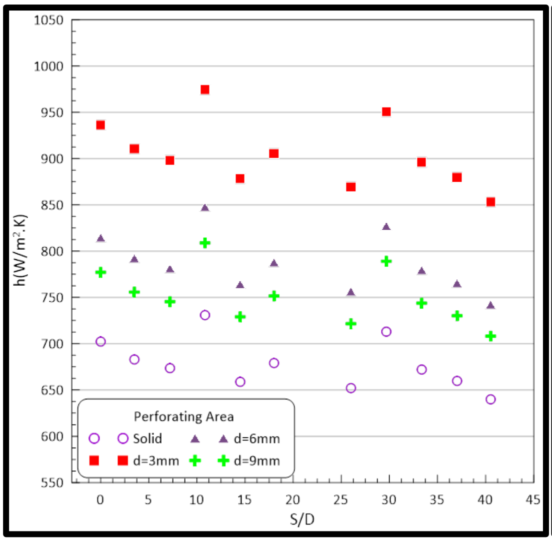

Figure (5.13). Heat transfer behavior.

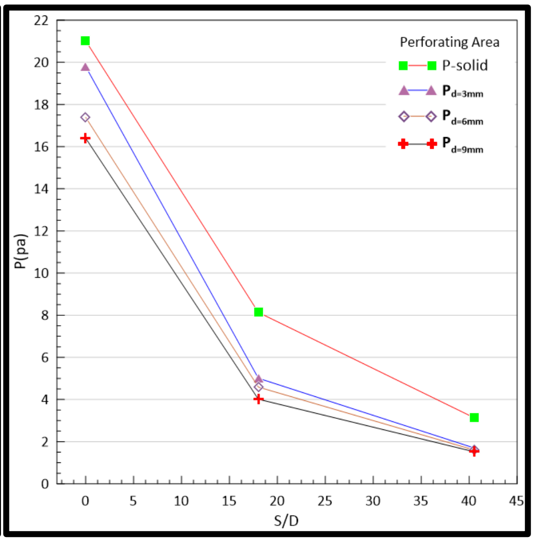

Figure (5.14): Pressure distribution

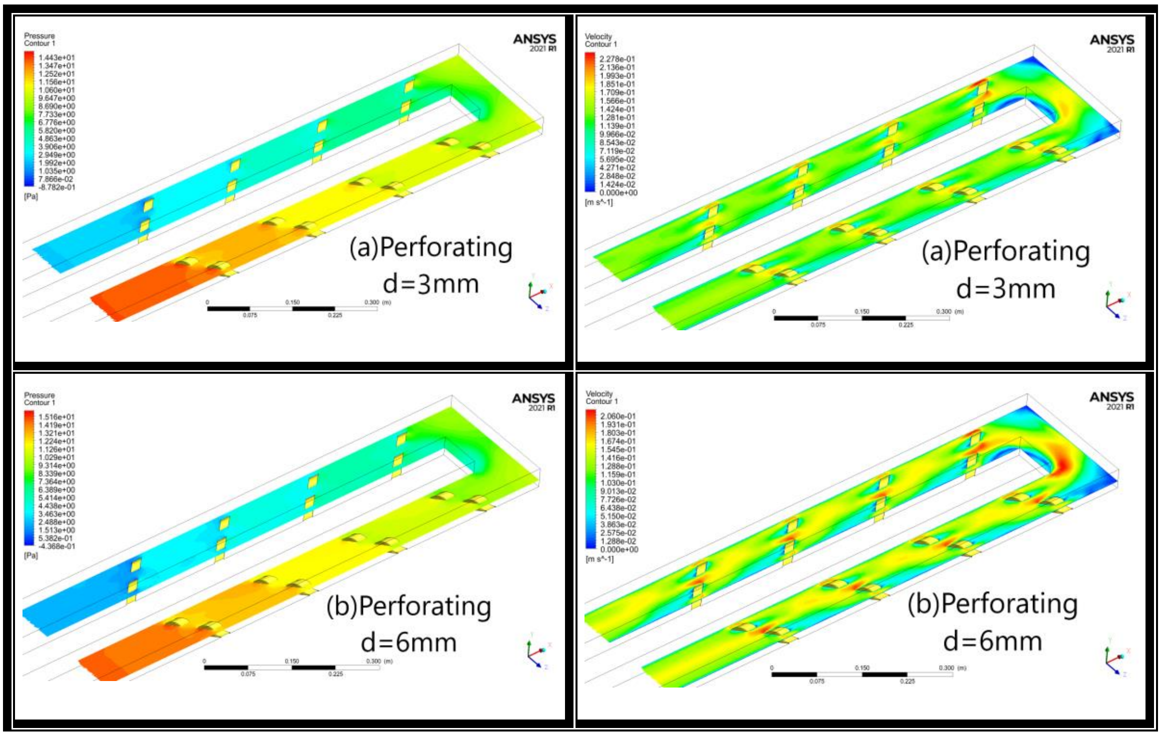

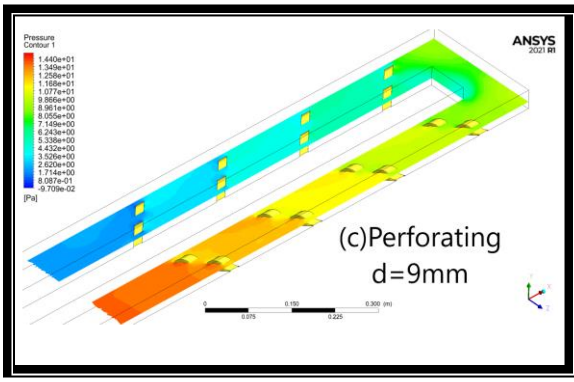

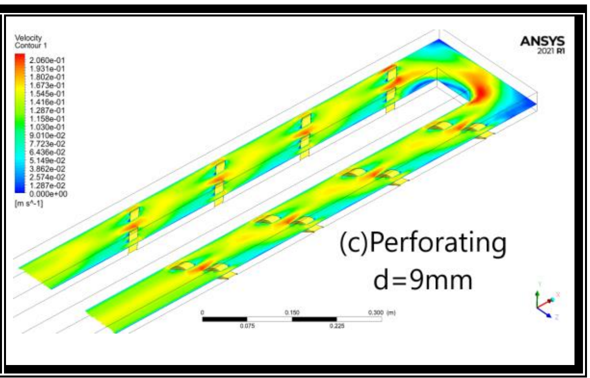

Figure (5.15). Pressure distribution **Figure (5.16).** Velocity distribution.

5.3.6 Angles values of ribs

To provide the high turbulence and large surface area of heat transfer to achieved the maximum enhancement in heat transfer. Three ribs angles are tested to find optimum angle :30°,45°and 60° at same conditions of previous stages. Figure (5.17) shows the effect of rib angles on heat transfer enhancement. It observed that 30° has the lowest heat transfer coefficients due to low turbulence while angle 60° is higher than 30° in compared with other angles. Because the angle 30° has less obstruction area lead to low resistance and low heat transfer from other cases. Also, it observed that 45° has a maximum heat transfer coefficient. Because area of heat transfer was higher lead to high rate of heat transfer and more turbulence. In addition, angle 60° has higher area of heat transfer lead to low-rate heat transfer. The percentages of heat transfer enhancement for 45° are about 19.45% and 7.52% with respect to 30° and 60° respectively. The results show that 30° low flow resistance because ribs are low confrontation area with flow wherefore low turbulence in comparison with other angles.

Figure (5.18) shows the effect of angles on pressure at same conditions of previous stages. It observed that the pressure in 60° has high values because of more resistance and abstraction for flow. The percentages of increasing pressure drop in 60° was about 43.98 % and 15.27 % with respect to 30° and 45° respectively. Because pressure drop increased with increasing confrontation area for flow when 60° has maximum confrontation area.

Figure (5.19) shows the behavior of pressure in presence of a different shape of perforating, it is observed that the 30° has low pressure in comparison with 45° and 60° because of low obstructions for flow. Figure (5.20) shows the behavior velocity in presence of a different angles for ribs, it is observed that the 30° has high velocity in comparison with 45° and 60° these have low velocities because of low obstruction to flow. Finally, it observed that 45° is the optimum shape area with high enhancement.

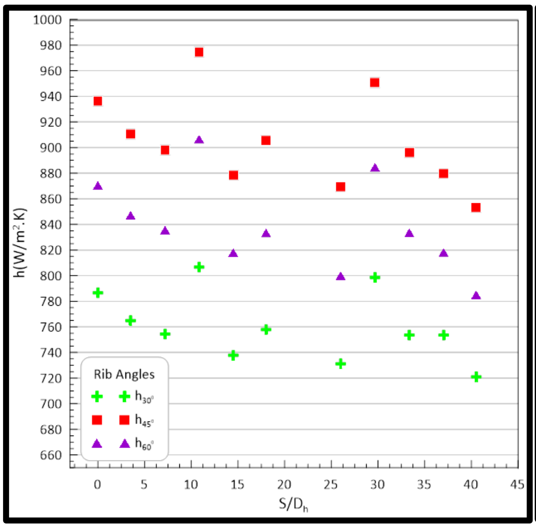

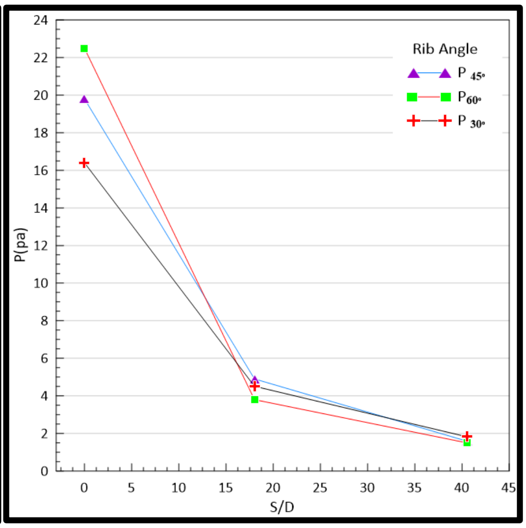

Figure (5.17). Heat transfer behavior **Figure (5.18). Pressure** behavior

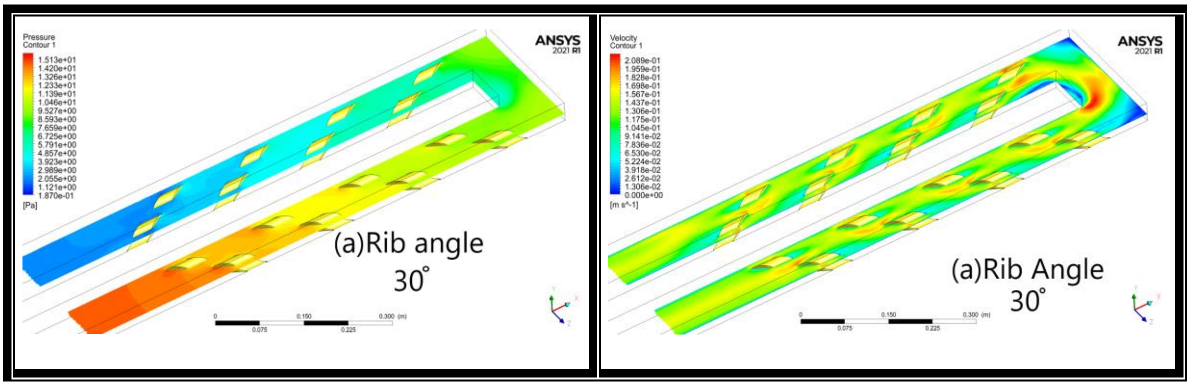

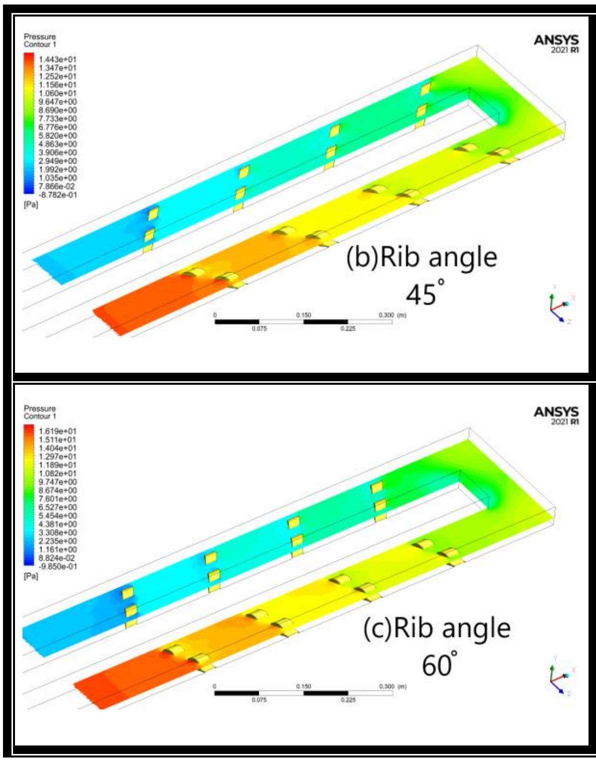

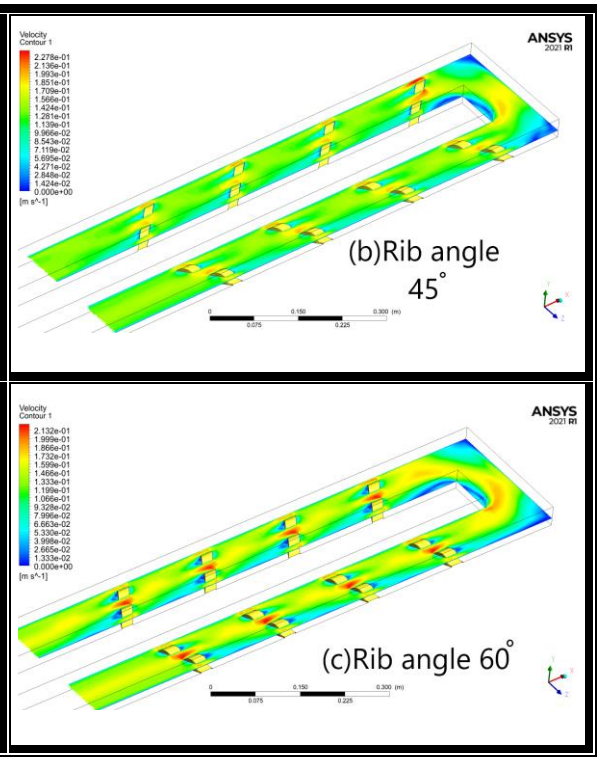

Figure (5.19). Pressure distribution **Figure (5.20).** Velocity distribution

5.4 Second Part: Two-phase flow internal Optimum channel

5.4.1 Distribution of local Nusselt Number (Nu).

Figure (5.21) displays the behavior of Nu across the ribbed and bend regions for experimental and numerical work. The Nu behavior shows multi peaks across the channel due to the increase of turbulent flow. A maximum an increase in the Nu is indicated at S/D=10.84 and 29.68. The curves have several regions: the first region (from inlet to first ribs) shows decrease in Nu because of decreasing velocity due to friction. Second region (first rib to fourth rib) shows increase in Nu because of turbulence that leads to increased molecules contiguity between them and transferred heat, this region has fluctuation behavior until maximum peak in point S equal 10.84 times hydraulic diameter because the flow is made the eddies and turbulence from inlet to ribbed region until is reached maximum turbulence in S/D=10.84. After the third rib, Nu is decreased because the impact of sharp corners and friction. Third region (fourth rib to bend start) shows decrease in Nu because of low turbulence. Fourth region (bend) shows increase in Nu because turbulence increases. Fifth region (bend end to first rib after bend) shows decrease in Nu because the flow has maximum velocity and smoother in this region than flow in ribbed region, the configuration of surface, and centrifugal force is accelerated the flow and low turbulence. After the flow leaved bend region with high velocity and entered the sixth region (first rib after bend to fourth rib after rib) shows increase in Nu because of presence ribs led to high turbulence. This region has fluctuation behavior until reach maximum peak in point S equal 29.68 times hydraulic diameter in second pass because the flow is created eddies due to impact with the rib. After the point S/D= 29.68 the eddies are disappeared due to decrease in mixture velocity led to low turbulence.

Seventh region (fourth rib after bend to outlet) shows decrease in Nu because low velocity and low turbulence. Also, the observations show same behavior at different velocities, Nu increases with increasing mixture velocities because the turbulence in flow increase heat transfer. In addition, the increase T_{rib} from 50˚C to 70˚C works to increase Nu because it increases the kinetic energy of the flow and enhance heat transfer. Also, the numerical and experimental curves have same behavior and same location of maximum peaks. Figure (5.22) shows the effect of changing rib surface temperature (T_{rib}) on Nu at different air velocities at maximum peak in point S equal 10.84 times hydraulic diameter in constant water velocity 0.1684m/s. It observed that the Nu increases with increasing rib surface temperature (T_{rib}) because the increase rib surface temperature (T_{rib}) leads to increase kinetic energy of mixture. Also, the increase air velocities are enhanced Nu because turbulence is increased with increasing velocities.

Figure (5.23) shows the effect of changing rib surface temperature (T_{rib}) on Nu when water velocities vary from 0.0842 to 0.2526m/s at maximum peak in point S equal 10.84 times hydraulic diameter in constant air velocity 1.3157m/s. It observed that the Nu increases with increasing rib surface temperature (T_{rib}) because the increase rib surface temperature (T_{rib}) leads to increase kinetic energy of mixture, and the increase water velocities is enhanced Nu because turbulence is increased with increasing velocities. The enhancement in case of constant air velocity and case of constant water velocity are compared. The case of varies water velocities are the highest enhancement in heat transfer because the water has more heat capacity than air.

In addition, when the water and air velocities and rib surface temperature 50 ºC to 70 ºC are varied three times, all the numerical and experimental results have the same behavior with percentages according Appendix B.

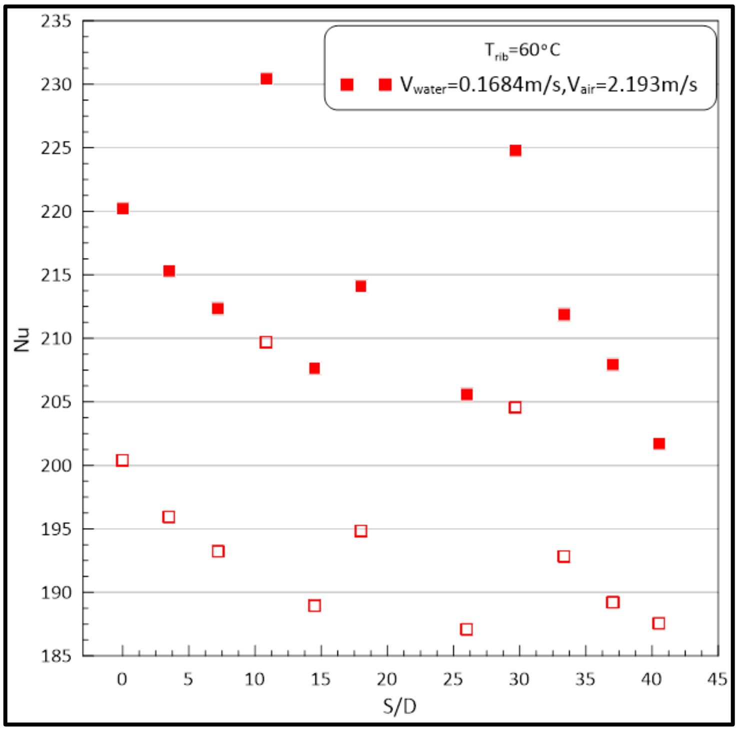

Figure (5.21): Nu-distribution along ribbed and bend region of the channel.

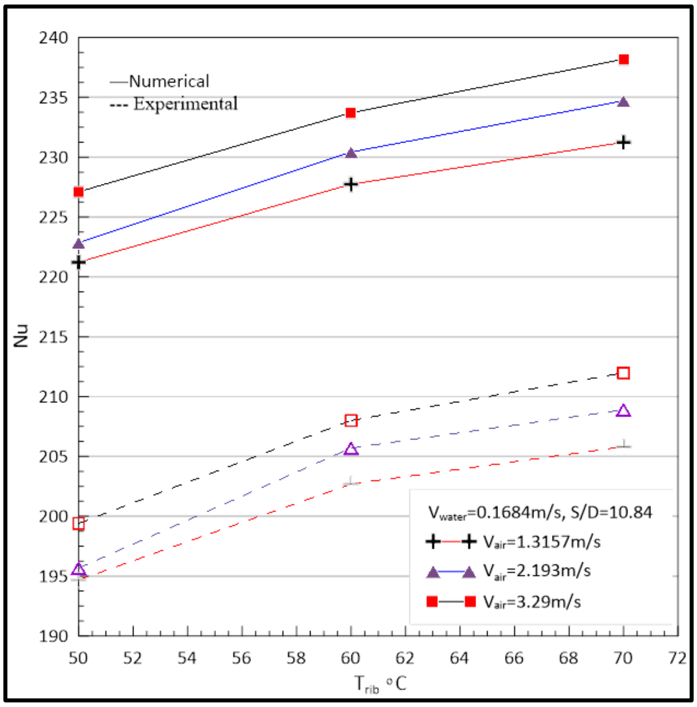

Figure (5.22): Variation Nu for different T_{rib} in S/D=10.84 at constant V_{water}

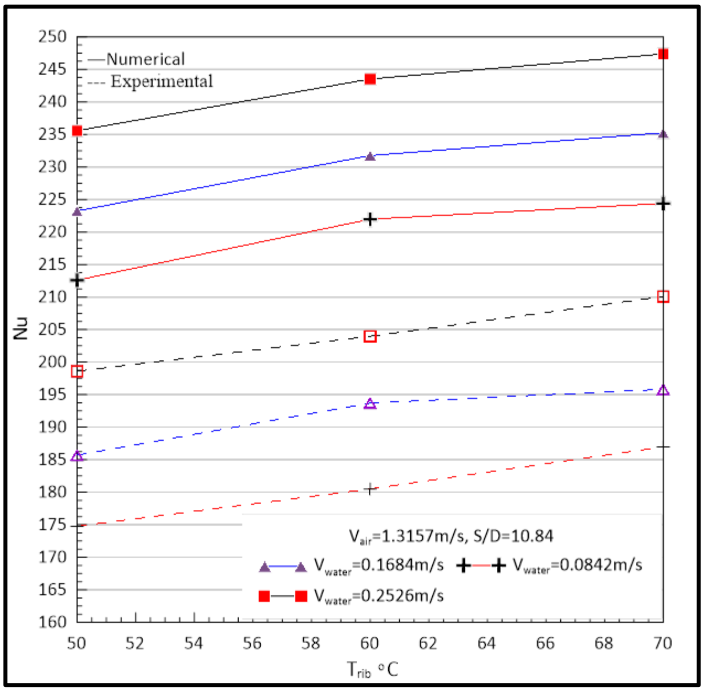

Figure (5.23): Variation Nu for different T_{rib} in S/D=10.84 at constant V_{air}

5.4.2 Effect of changing velocities of air and water on enhancement ratio Nu/Nu_o for different rib surface temperatures T_{rib} .

To investigate the heat transfer enhancement due to various velocities and different T_{rib} the Nusselt number ratio or enhancement ratio (Nu/Nu_o)

is calculated. Figure (5.24) shows the effect of rib surface temperature T_{rib} on ratio Nu/Nu_o when the V_{air} is varied from 1.3157m/s to 3.29m/s at constant V_{water} . It observed that the Nu/Nu_o is increased with increasing T_{rib} because the increase T_{rib} is led to enhance heat transfer by increasing the turbulence and kinetic energy. In addition, it observed the increasing V_{air} ,it is increased enhancement ratio Nu/Nu_o because the increase V_{air} is led to increase heat transfer between mixture and hot ribs .Figure (5.25) presents the behavior of Nu/Nu_o due to increase V_{water} ,it is enhanced higher than V_{air} case when rib temperature varied from 50˚C to 70˚C because the water able to absorb more heat than air so as to it has high heat capacity than air. The increasing percentages of enhancement ratio at different T_{rib} , V_{air} and V_{water} is calculated in APPENDIX B.

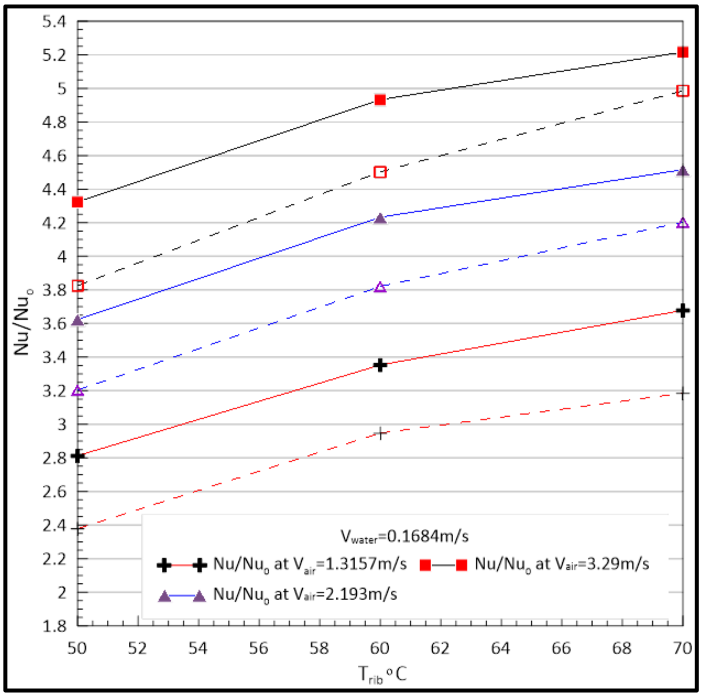

Figure (5.24): Variation Nu/Nu_o with rib surface temperature T_{rib}.

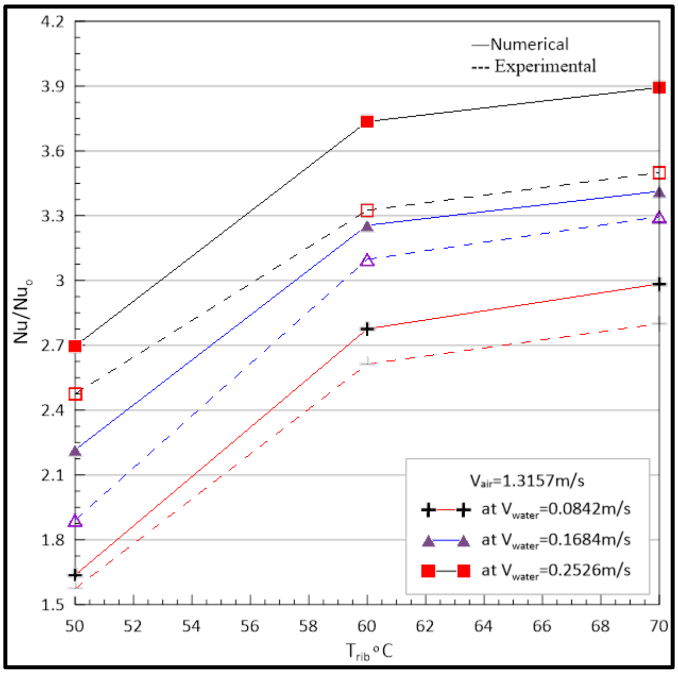

Figure (5.25): Variation Nu/Nu_o with T_{rib} at V_{air} constant.

5.4.3 Effect of changing velocities of air and water on pressure drop (△P) for different rib surface temperatures T_{rib} .

Figure (5.26) shows the effect of increasing rib surface temperature from 50 °C to 70 °C on the pressure drop when the V_{air} is varied from 1.3157 to 3.29 m/s at constant V_{water}. It presented that the pressure drop increased with increasing T_{rib} because the increase T_{rib} is heated the mixture and more created more turbulence so as to kinetic energy. Figure (5.27) shows the effect of increasing rib surface temperature from 50 °C to 70 °C on the pressure drop when the V_{water} is varied from 0.0842m/s to 0.2526m/s at constant V_{air}. When increase T_{rib} from 50 °C to 70 °C, the increasing percentages are varied 25.3% to 31.4%. Also, it observed that the pressure drop increased with increasing V_{water} and V_{air} at constant T_{rib} with percentages for 50 °C about (29.53% ~30. 5%) and (43.8%~45.39%) respectively, for 60°C (29.53%~30.5%) and (43.8%~45.39%) respectively, and 60 °C about (31.83% ~33. 5%) and (45.02%~46.79%) respectively. Because the friction increased with increase velocities and kinetic energy lead to increase losses. In addition, it observed that the increasing percentages in air case is higher than water case.

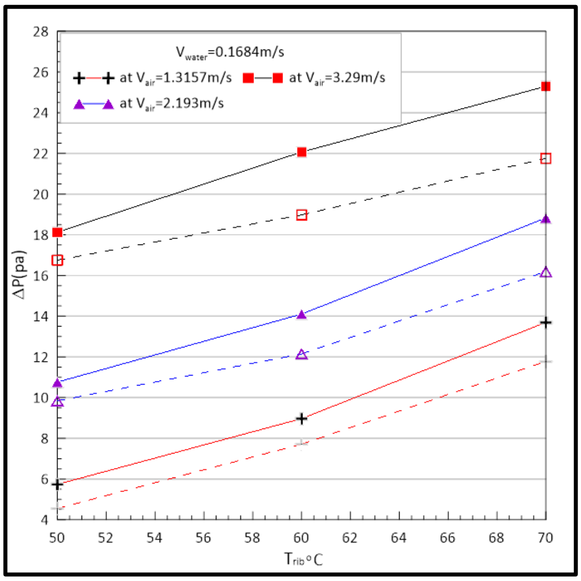

Figure (5.26): Variation **ΔP** with different V_{air}

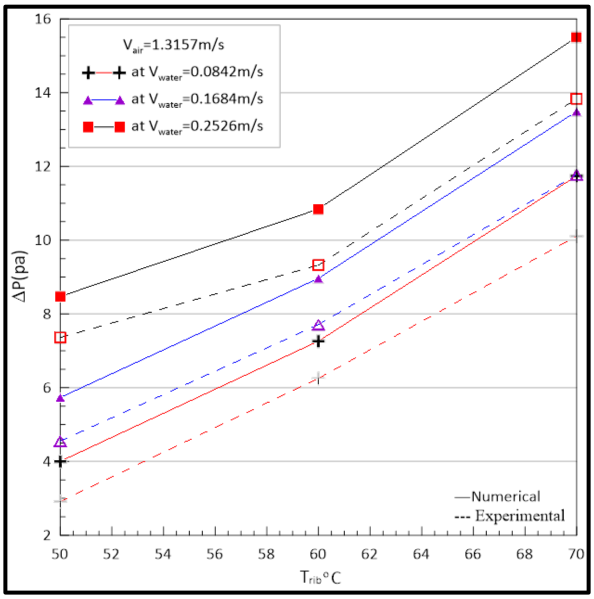

Figure (5.27): Variation **ΔP** with different V_{water}.

5.4.4 Effect of changing velocities of air and water on friction factor ratio (f/f_o) for different rib surface temperatures T_{rib} .

To investigate the friction factor ratio (f/f_o) due to various velocities and different T_{Rib} ,related to friction factor in without ribs cases is calculated. Figure (5.28) shows the effect of increasing rib surface temperature T_{rib} on friction ratio when the V_{air} is varied from 1.3157m/s to 3.29m/s at constant V_{water}. The effect of increasing T_{rib} from 50°C to 60°C to 70°C on f/f_o is analyzed. The f/f_o values increased with increasing T_{rib}, because it is led to increase the pressure drop so as to kinetic energy is increased and created more losses. Also, the increasing V_{air} is led to decrease the friction ratio because the increase velocity is created more losses and more friction ratio.

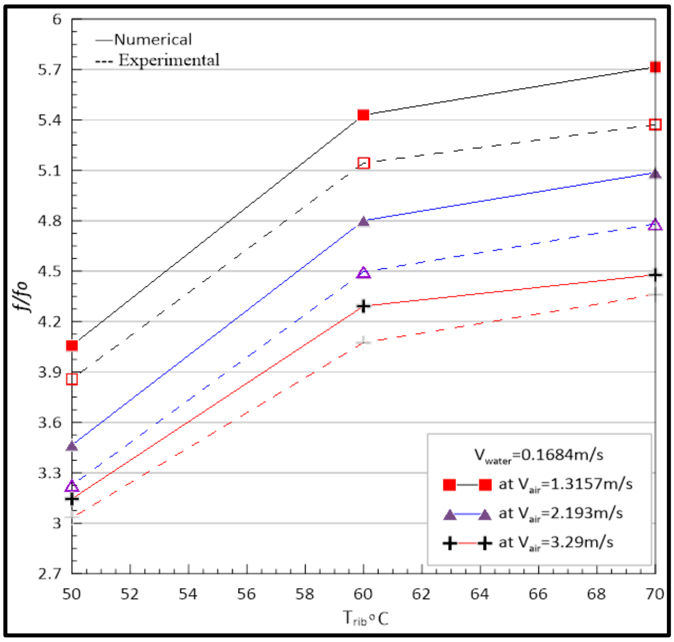

Figure (5.28): Variation friction ratio with rib surface temperature T_{rib}.

Figure (5.29) shows the effect of increasing rib surface temperature T_{rib} on friction ratio when the V_{water} is varied from 0.0842m/s to 0.2526m/s at constant V_{air}. The f/f_o values are increased with increasing T_{rib}, because it is led to increase the pressure drop so as to kinetic energy is increased and created more losses. Also, the increasing V_{water} is led to decrease the friction ratio because the increase velocity is created more losses and more friction ratio. The friction ratios of increasing V_{water} is lower than friction ratios of increasing V_{air} because the V_{air} three times V_{water} . The increasing percentages of friction ratio at different T_{rib} , V_{air} and V_{water} is calculated in APPENDIX B.

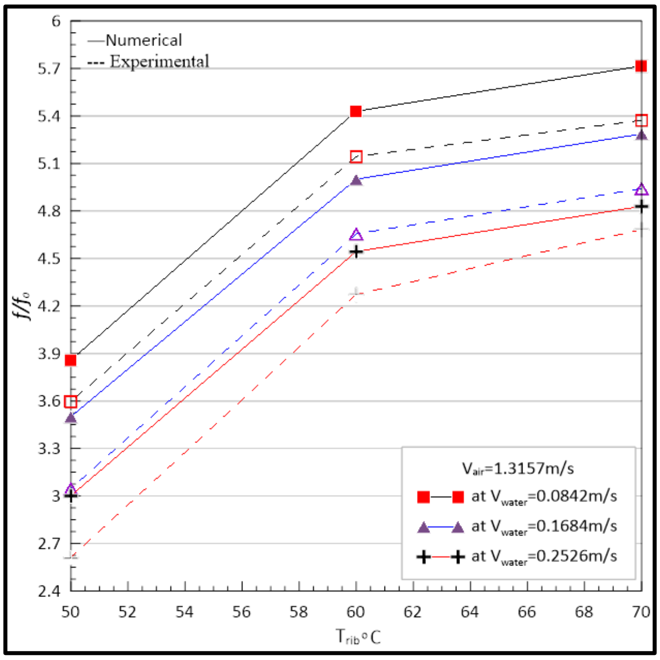

Figure (5.29): Variation friction ratio with rib surface temperature T_{rib}.

5.4.5 Effect of changing velocities of air and water on Thermal-Performance Criteria Evaluation (PCE) for different rib surface temperatures T_{rib} .

To balance the heat transfer enhancement quantity (Nu/Nu_o) to pressure losses (f/f_o) represented by (PCE).Figure (5.30) shows the effect of increasing rib surface temperature T_{rib} on (PCE) when the V_{air} is varied from 1.3157m/s to 3.29m/s at constant V_{water}. The effect of increasing T_{rib} is represented by increasing (PCE) with increase of T_{rib} because of more heat rate and more heat transfer enhancement than friction ratio. The PCE decreases with increasing V_{air} because the (f/f_o) is increased because of low f and f_o lower lead to low over lower get value of f/f_o higher than enhance in heat transfer (Nu/Nu_o).Figure (5.31) shows the effect of increasing rib surface temperature T_{rib} on PCE when the V_{water} is varied from 0.0842m/s to 0.2526m/s at constant V_{air}.It observed that the PCE increased with increasing T_{rib} because it is led to more heat rate and more turbulence so as to more heat transfer enhancement than friction ratio.

Also, the increasing V_{water} is led to decrease the PCE because the ratio (f/f_o) is increased because of low f and f_o lower lead to low over lower get value of f/f_o higher than enhancement ratio of heat transfer (Nu/Nu_o). The increasing percentages of friction ratio at different T_{rib} , V_{air} and V_{water} is calculated in APPENDIX B.

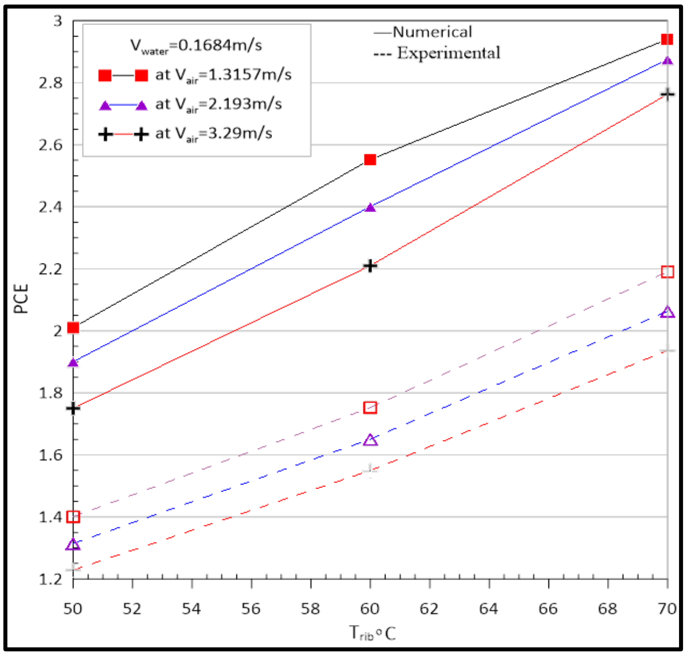

Figure (5.30): Variation friction ratio with rib surface temperature T_{rib}.

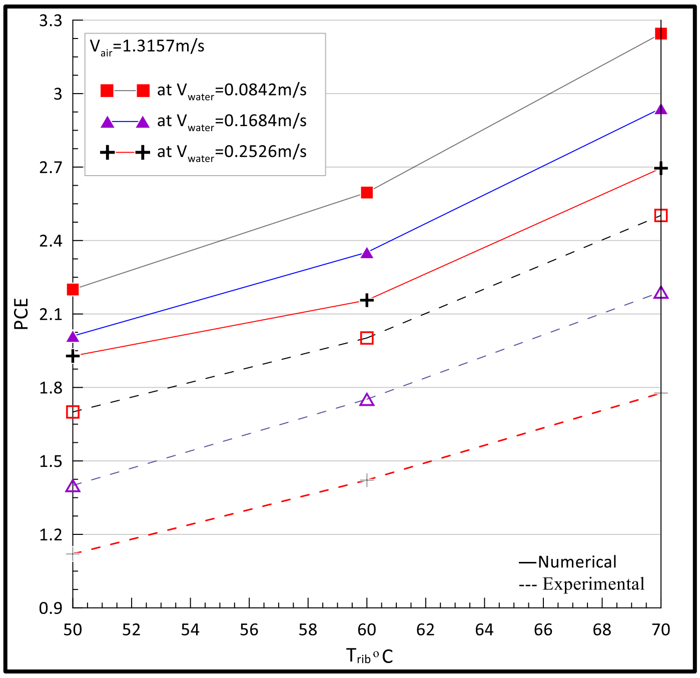

Figure (5.31): Variation friction ratio with rib surface temperature T_{rib}.

5.4.6 Distribution of Air-Water in channel

The presence of ribs has led to best distribution and breaking the boundary layer thereby creating interference between phases so high turbulence led to enhances heat transfer. The interference between water and air depended on volume fraction means the volume of fluid to total fluids volume. The conditions of this experiment are at water and air velocities (0.1684m/s and 2.193m/s) respectively, at T_{rib} equal 60°C. Figure (5.32) represents the air distribution regions and concentration in the ribbed and bend part between values (1.2429×10^{-9}~9.6×10^{-1}) of the channel. It observed that improvement the interference between phases in ribbed regions because breaking the boundary layer but the large areas (high volume fraction) of air concerned in bend region because air has velocity about three times water velocity. The red regions represent the air phase with high volume fraction values while blue regions represent the water phase, other colors represent the interference air-water with several values of volume fraction. Figure (5.32) shows the water distribution regions and concentration affected by the rib's presence in the channel. The red regions represent the water phase with high volume fraction while blue region for air phase. It observed that the good interference in ribbed regions because of presence rib break boundary layer. In bend region, water concentrated less than air because water heavy than air of high velocity. In comparison the two distributions, it observed in ribbed parts good interference between phases with volume fraction values (0.435~0.68) while in bend region air volume fraction is been higher than water because water presence is less and heavy than air of higher velocity.

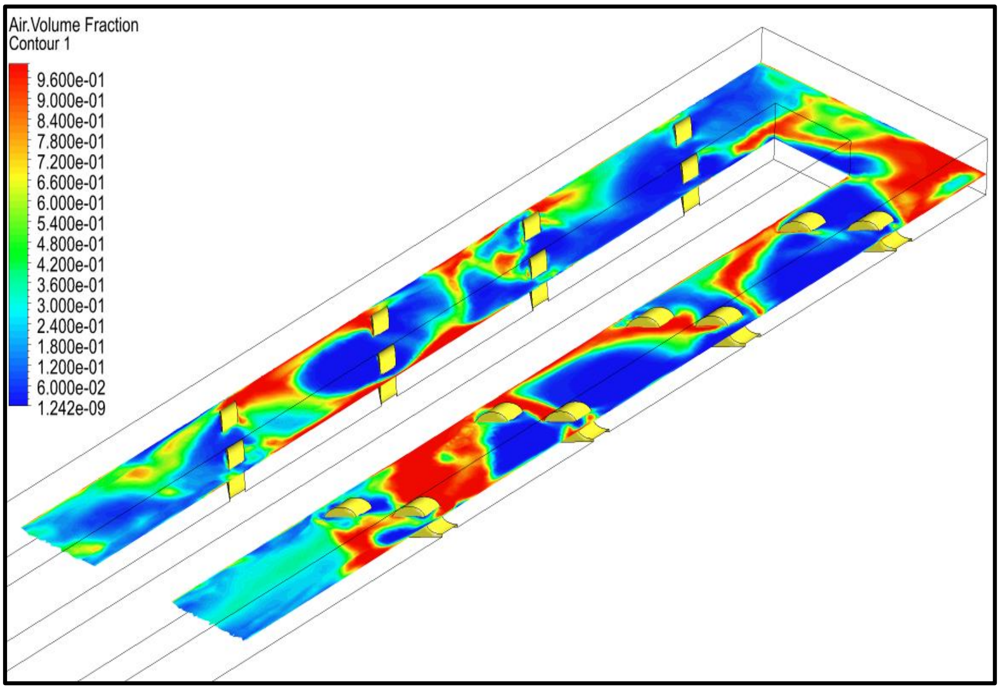

Figure (5.31): Air-distribution regions along ribbed channels.

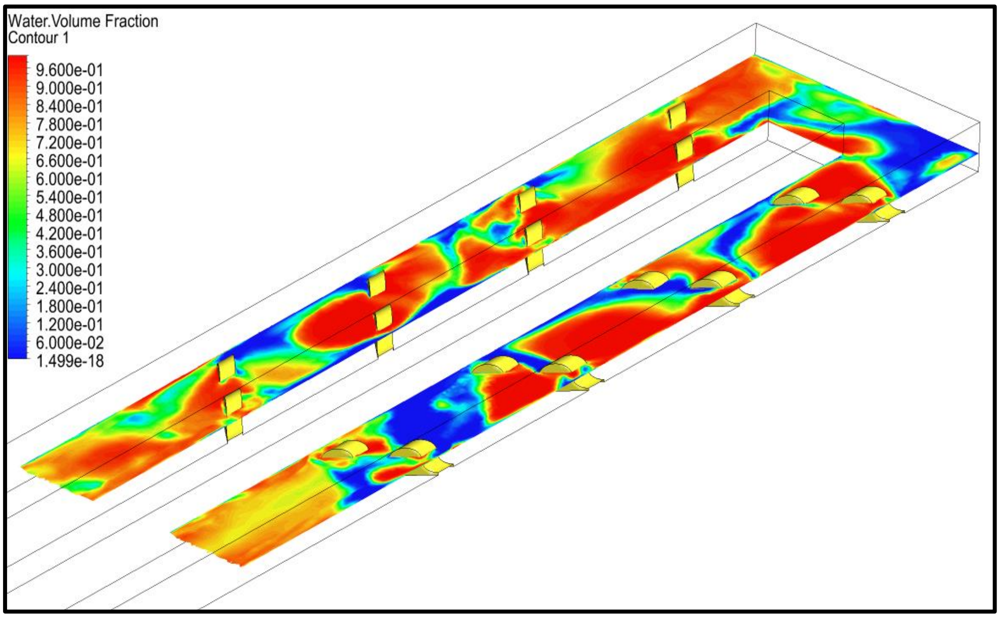

Figure (5.32): Water-distribution regions along ribbed channels.

5.4.7 Velocity distribution of Two-phase

Figure (5.33) show the effect of increasing V_{air} and V_{water} on the velocity distribution at constant T_{rib} about 50˚C when V_{water} are 0.0842m/s to 0.2526 and different V_{air} are 1.3157m/s to 3.29m/s .It observed that the areas of increasing velocity start gradually from the ribbed regions so as to break boundary layer create more turbulence ,where it notices the appearance of a greenish-yellow color until the greatest value of the mixture velocity of red orange color appeared reaches the bend region as a result of the presence of centrifugal force. In addition, it observed that the velocity of mixture increases with increasing V_{air} ,V_{water} because of increase flow rates of mixture lead to more turbulence.

Figure (5.34) show the effect of increasing V_{air} and V_{water} on the velocity distribution at constant T_{rib} about 60˚C where V_{water} are 0.0842m/s to 0.2526 and different V_{air} are 1.3157m/s to 3.29m/s. It observed that the increasing V_{air} and V_{water} lead to appear greenish-yellow color as more light than previous case because of increase flow rates of air and water. In bend region, the region of the red orange color of high velocity appeared because of centrifugal force. In addition, the velocity of mixture increased from previous case with increasing T_{rib} because of increasing kinetic energy of the mixture. Figure (5.35) shows the effect of increasing V_{air} and V_{water} on the velocity distribution at constant T_{rib} about 70˚C a V_{water} are 0.0842m/s to 0.2526 and different V_{air} are 1.3157m/s to 3.29m/s. The observation shows that the increase in V_{air} and V_{water} lead to increase mixture velocity and appear color as more light than previous case because of increased flow rates of air and water. Also, the areas of the red regions of high velocity in bend because the centrifugal force. the velocity of mixture increased with increasing T_{rib} because the kinetic energy of the particles of the mixture increases.

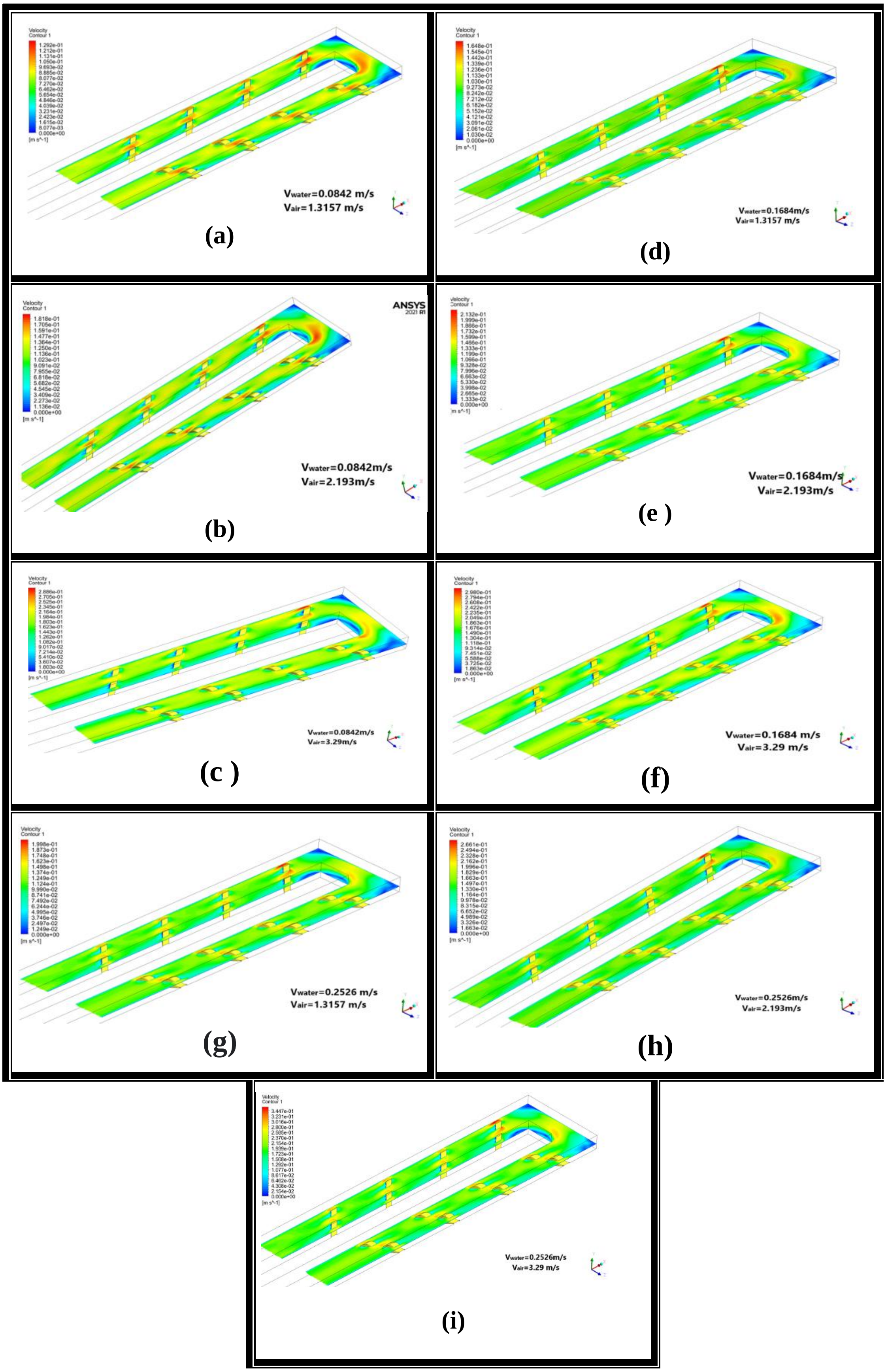

Figure (5.33). Velocity-distribution at T_{rib} =50 ˚C .

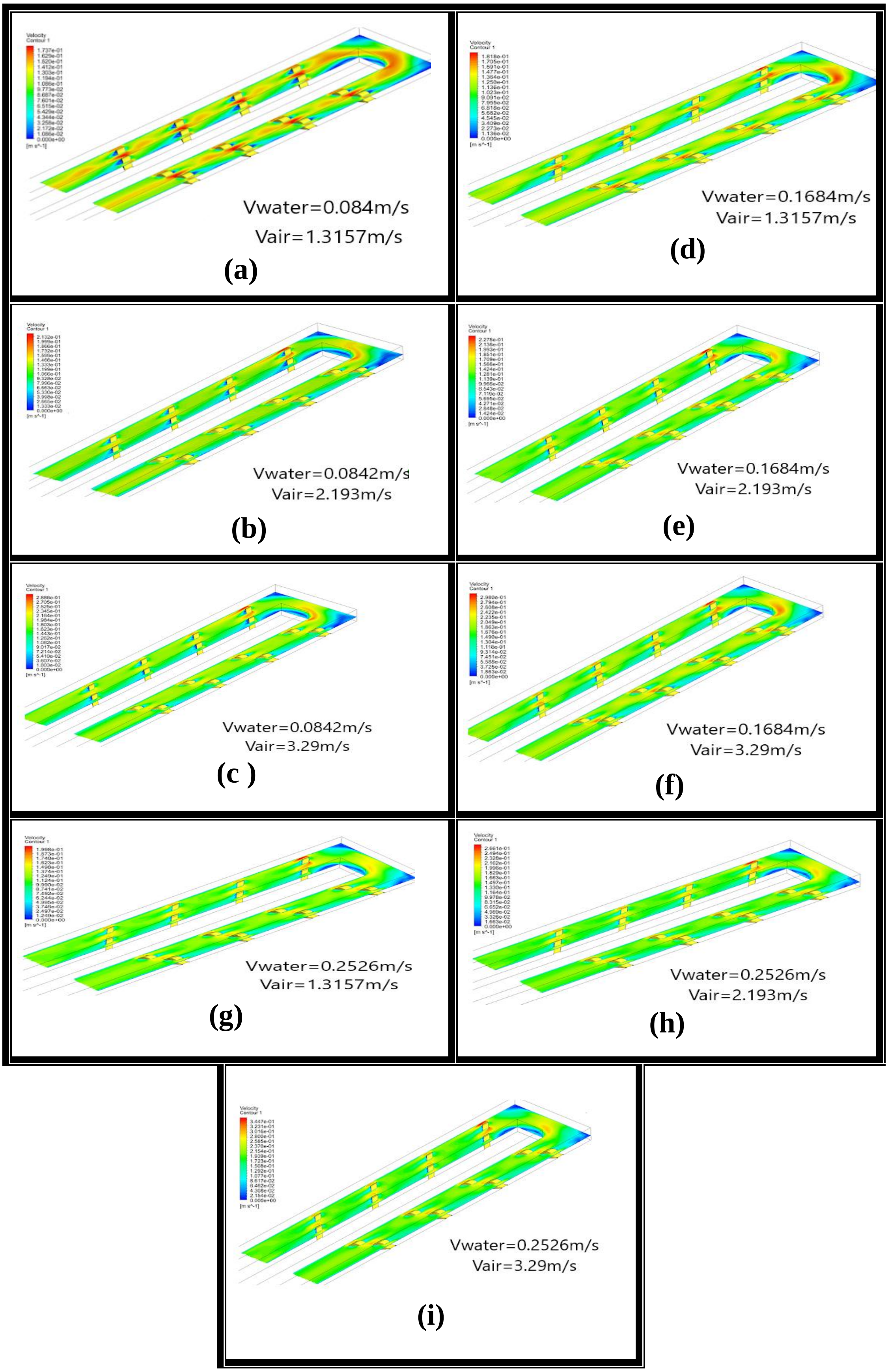

Figure (5.34). Velocity-distribution at T_{rib} =60°C.

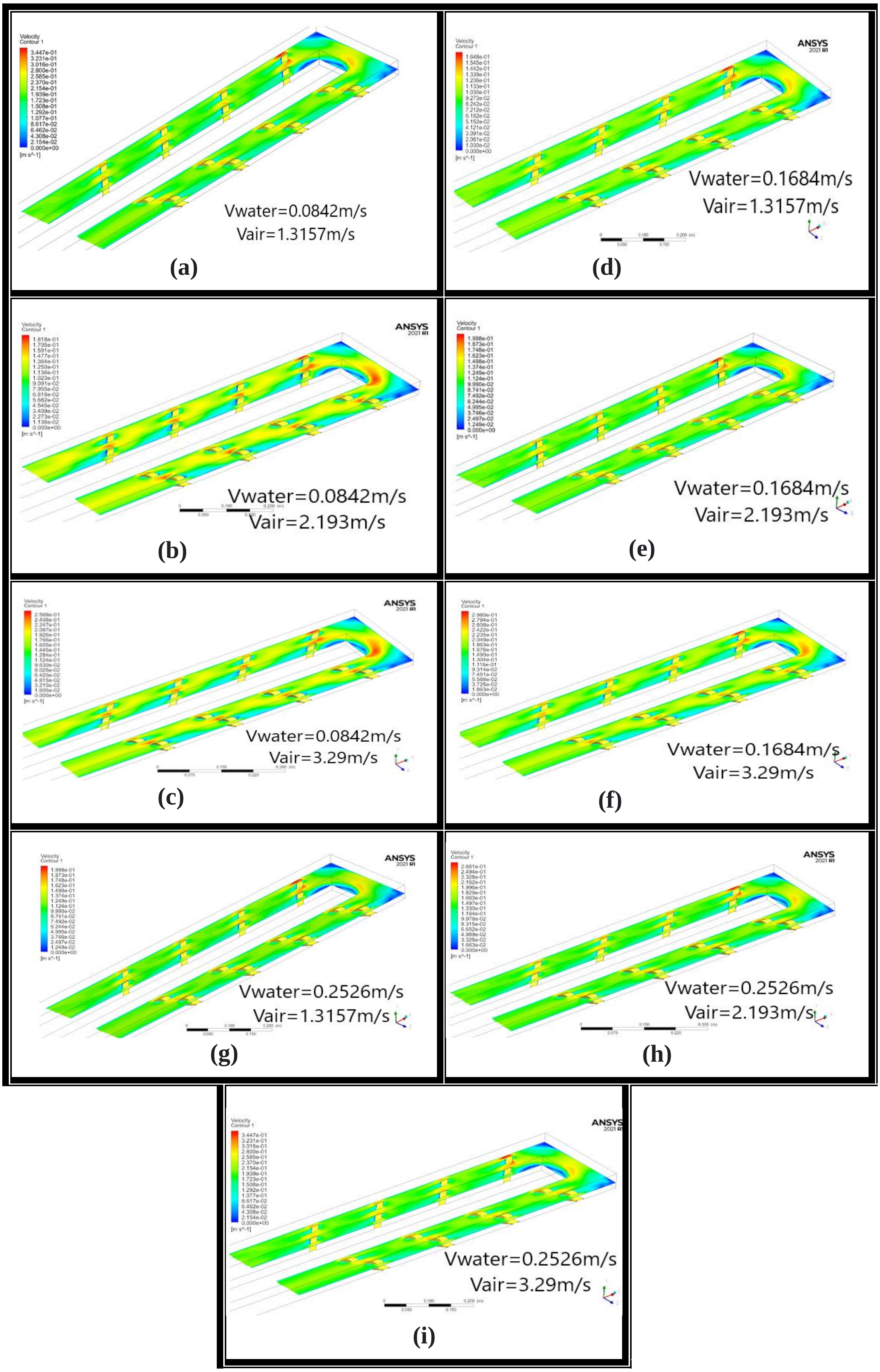

Figure (5.35): Velocity-distribution at T_{rib} =70 ^{o}C

5.4.8 Pressure Distribution.

Figure (5.36) shows the effect of increasing V_{air} and V_{water} on the pressure distribution at constant T_{rib} about 50˚C a V_{water} are 0.0842m/s to 0.2526 and different V_{air} are 1.3157m/s to 3.29m/s. It observed that the pressure decreased gradually with increasing V_{air} and V_{water} according Bernoulli's principle until reach minimum in bend region because the mixture velocity reached maximum values.

Figure (5.37) show the effect of increasing V_{air} and V_{water} on the pressure distribution at constant T_{rib} about 60˚C a V_{water} are 0.0842m/s to 0.2526 and different V_{air} are 1.3157m/s to 3.29m/s. It observed that the pressure decreased with increasing V_{air} and V_{water} according Bernoulli's principle until reach minimum in bend region because the mixture velocity reached maximum values. Also, the areas of the red regions retraction of pressure because the increasing T_{rib}. The retraction in cases of increasing V_{air} are higher than cases of increasing V_{water} because the air flow rates have values higher than water flow rates lead to increase mixture velocity .Figure (5.38) shows the effect of increasing V_{air} and V_{water} on the pressure distribution at constant T_{rib} about 70˚C a V_{water} are 0.0842m/s to 0.2526 and different V_{air} are 1.3157m/s to 3.29m/s with same behavior of above cases . It observed that the pressure decreased with increasing V_{air} and V_{water} according Bernoulli's principle until reach minimum in bend region because the mixture velocity reached maximum values. It observed that the red region of pressure decreased with increasing T_{rib} because of increase kinetic energy.

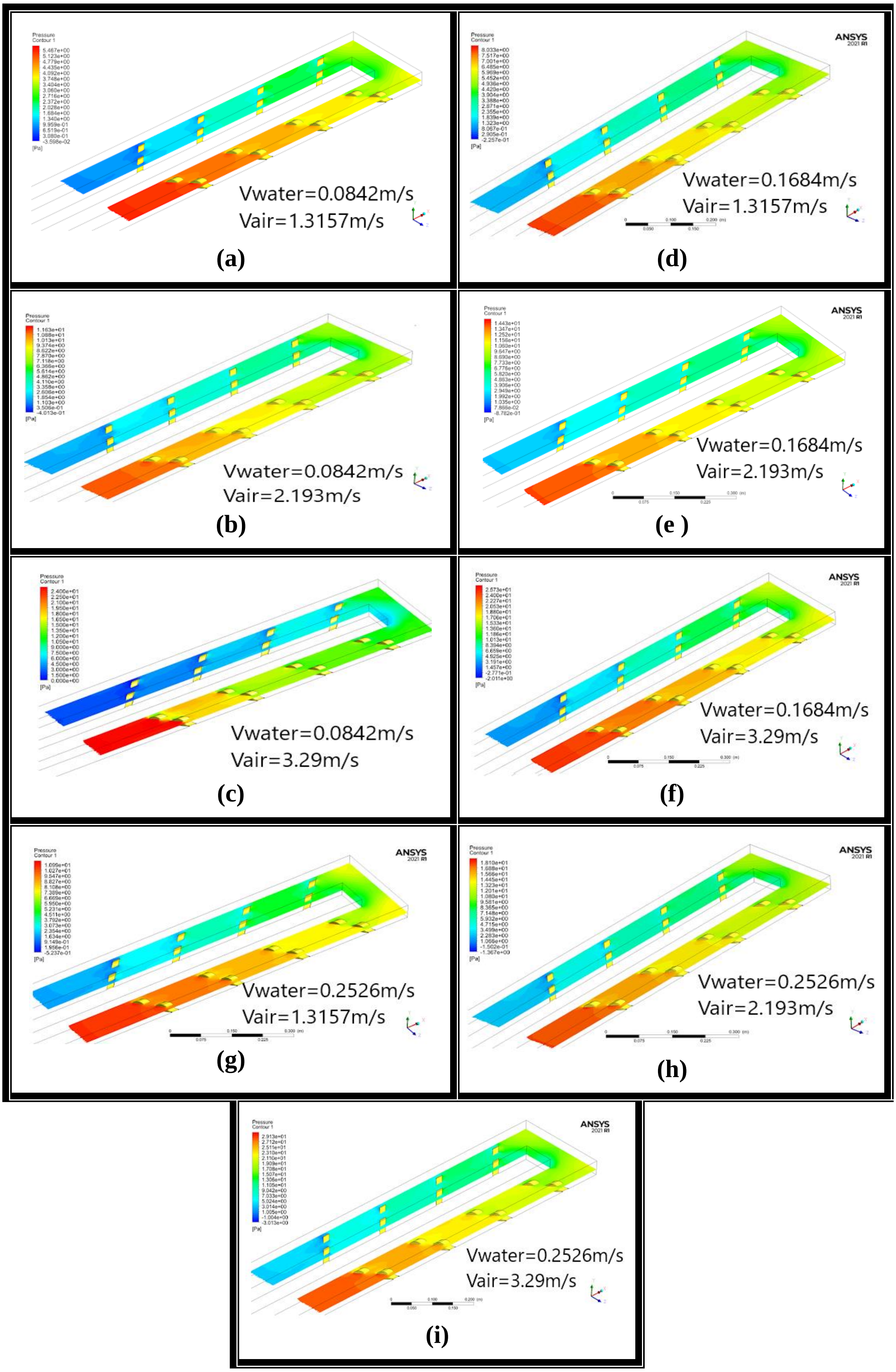

Figure (5.36). Pressure-distribution at T $_{rib}$ =50°C

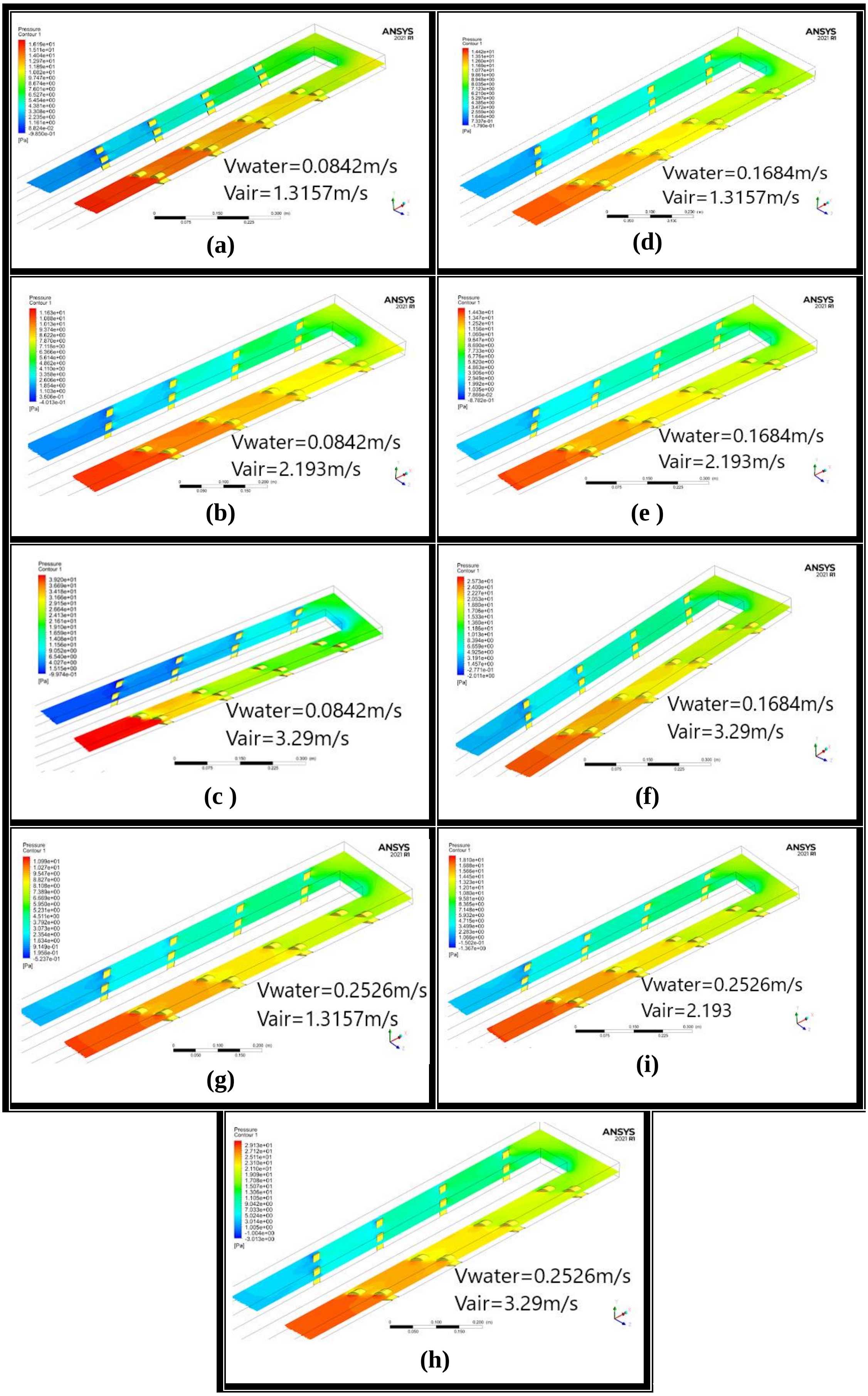

Figure (5.37). Pressure-distribution at T_{rib} =60°C.

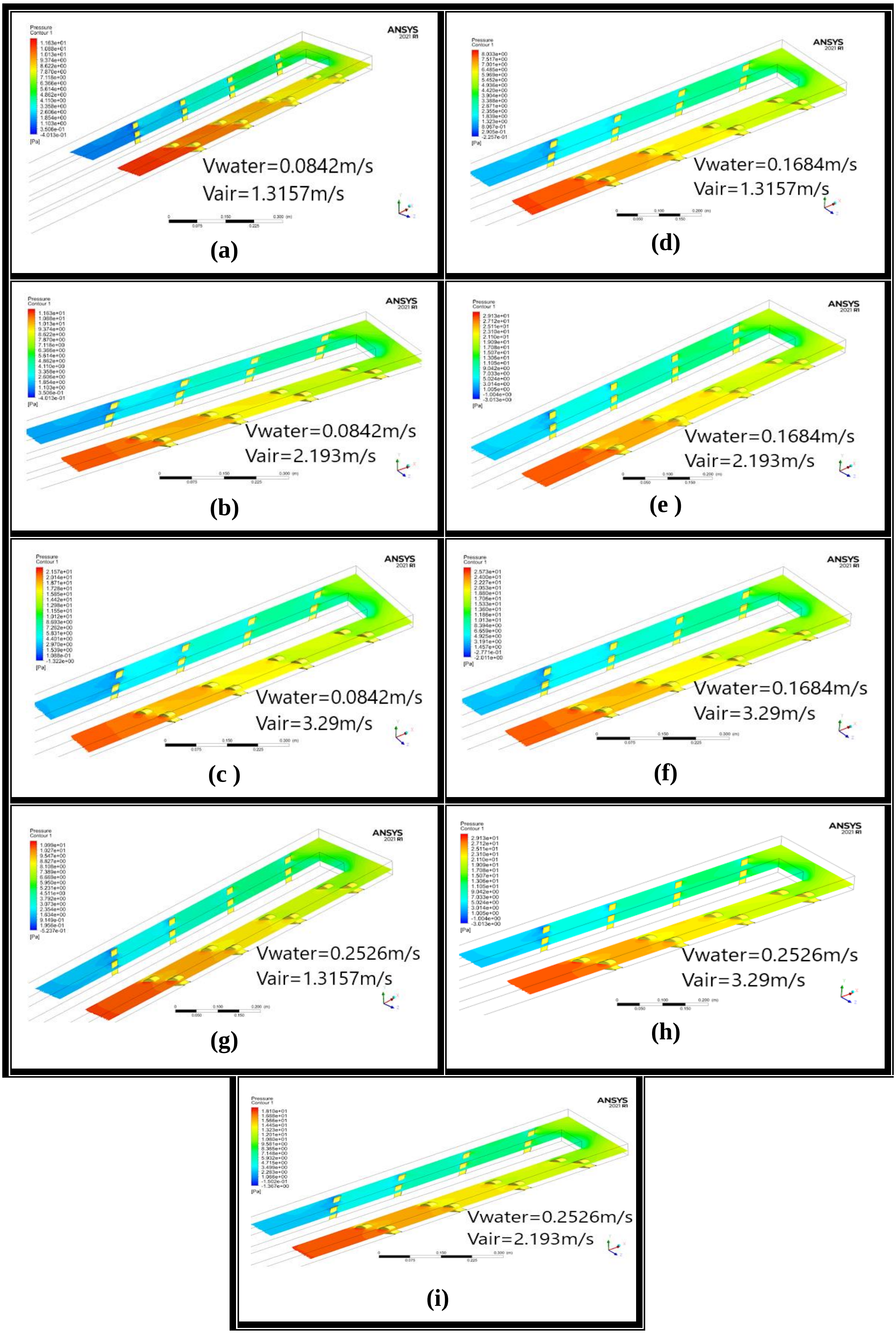

Figure (5.38): Pressure-distribution at T $_{rib}$ =70°C.

5.4.9 Flow pattern of two-phase flow behavior

Physically, the pattern of air-water flow mixture is described by depending on velocities. The best-known and most widely used flow regime map is that of Baker (1954). To utilizing this map, it must calculate the mass flux of phases and physical property parameters as APPENDIX D. This flow regime is a water flow with elongated air bubbles flowing along the top of the channel. The hydraulic diameter of the elongated bubbles is smaller than the channel such that the water phase is continuous. Experimentally, the pattern of air-water flow mixture is described by visual observation.

Figures (5.39) shows the effect of V_{air} and V_{water} on flow pattern of the mixture when increasing velocities at varies water velocities are 0.0842m/s to 0.2526 m/s and air velocities varied from 1.3157 m/s to 3.29 m/s for each velocity of water at constant T_{rib} equal 50˚C. It observed the increasing air velocity led to increase the volume of bubbles, and the flow pattern is "Plug pattern" Also the mass flux values was increased as APPENDIX D. Because the ranges of mass flux and physical property parameters determined in Plug region on map. Figures (5.40) shows the flow pattern of the mixture when using increasing the T_{rib} equal 60˚C at same previous group of T_{rib} equal 60˚C. It observed the same behavior above when increasing air velocity led to increase the volume of bubbles, and the flow pattern is "Plug pattern" because the water layers separate the air bubbles from the wall. Also, the mass flux values were increased as APPENDIX D. Because the ranges of mass flux and physical property parameters determined in Plug region on map. Figure (5.41) shows the flow pattern of the mixture when increasing velocities at the T_{rib} equal 70˚C. It observed the increasing air velocity led to increase the volume of bubbles, and the flow pattern is "Plug pattern" because the water layers separate the air bubbles from the wall. Also, the mass flux values were increased as

APPENDIX D. Because the ranges of mass flux and physical property parameters determined in Plug region on map.All figures compared together to explain the effect of increasing T_{rib} at different temperatures. From observation that the volume of bubbles increased when increasing T_{rib} and values of mass flux increased because of increasing mixture velocity and kinetic energy. The regimes in of all experiments observed the ranges of mass flux of air phase ($G_{air} \leq 2$) and for water phase ($2100 \geq G_{water} \geq 300$) determined in Plug region on map .

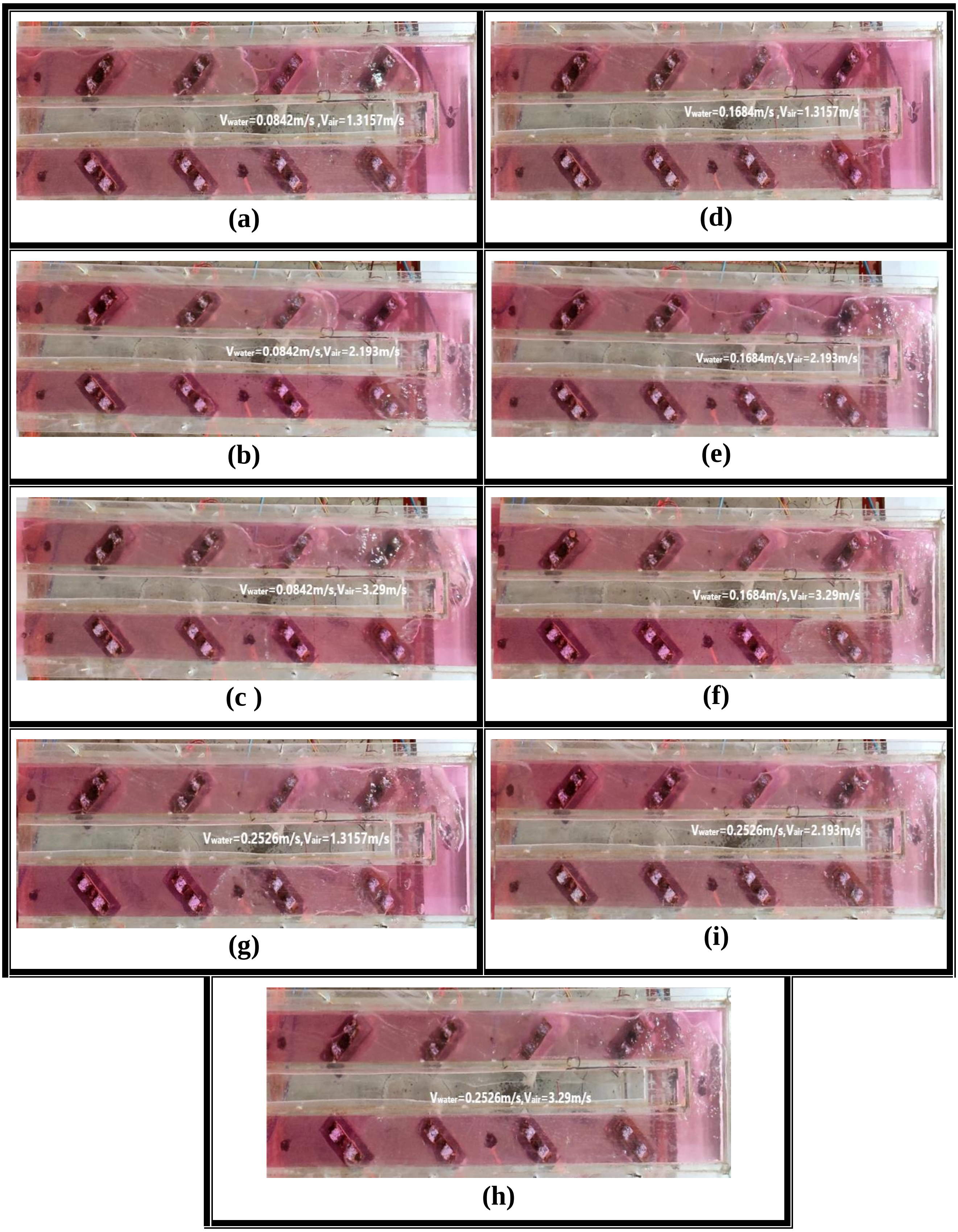

Figure (5.39): Flow pattern in V_{water} , V_{air} at T_{rib} =50°C.

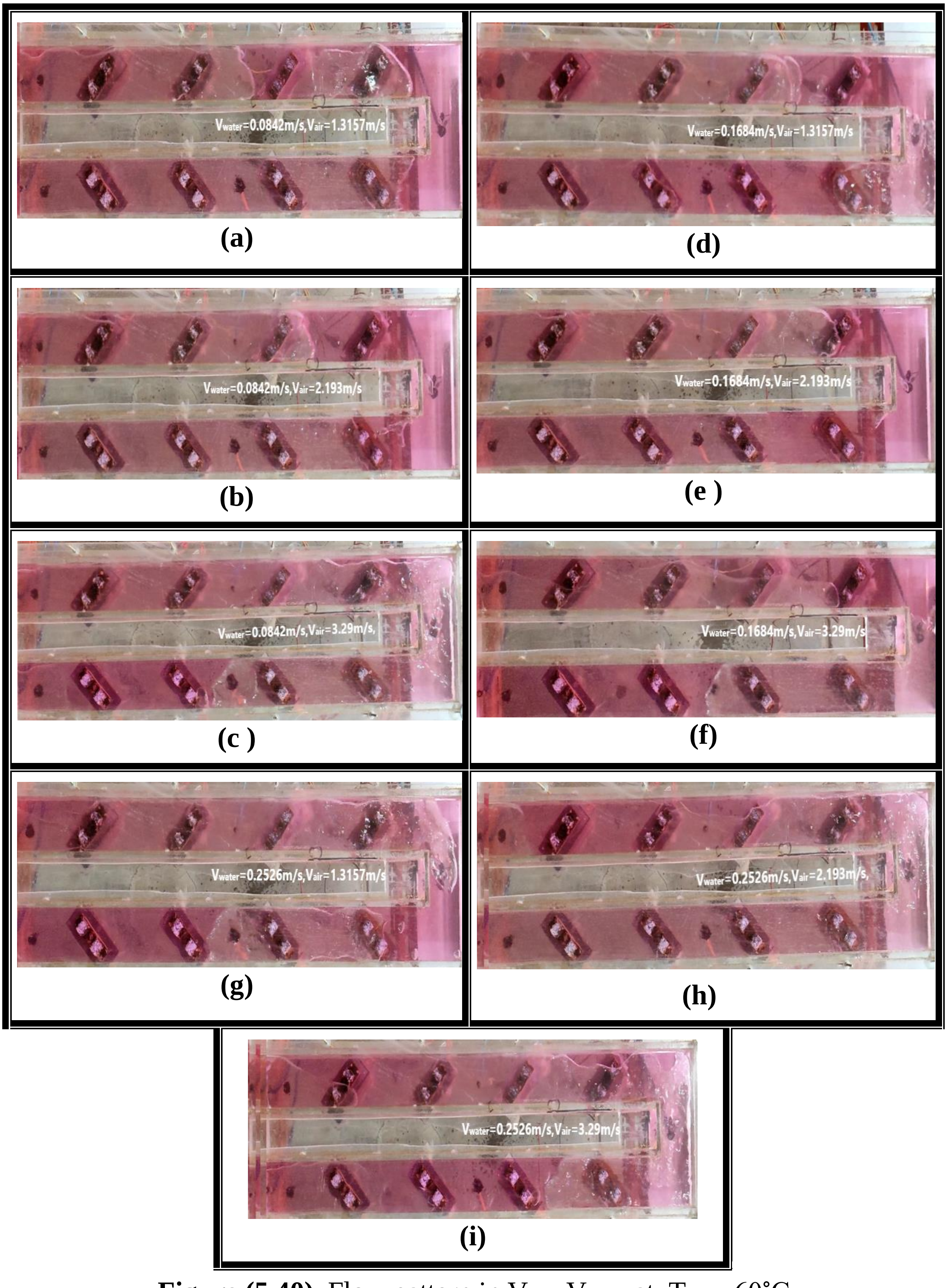

Figure (5.40). Flow pattern in V_{air} ,V_{water} at T_{rib} =60˚C

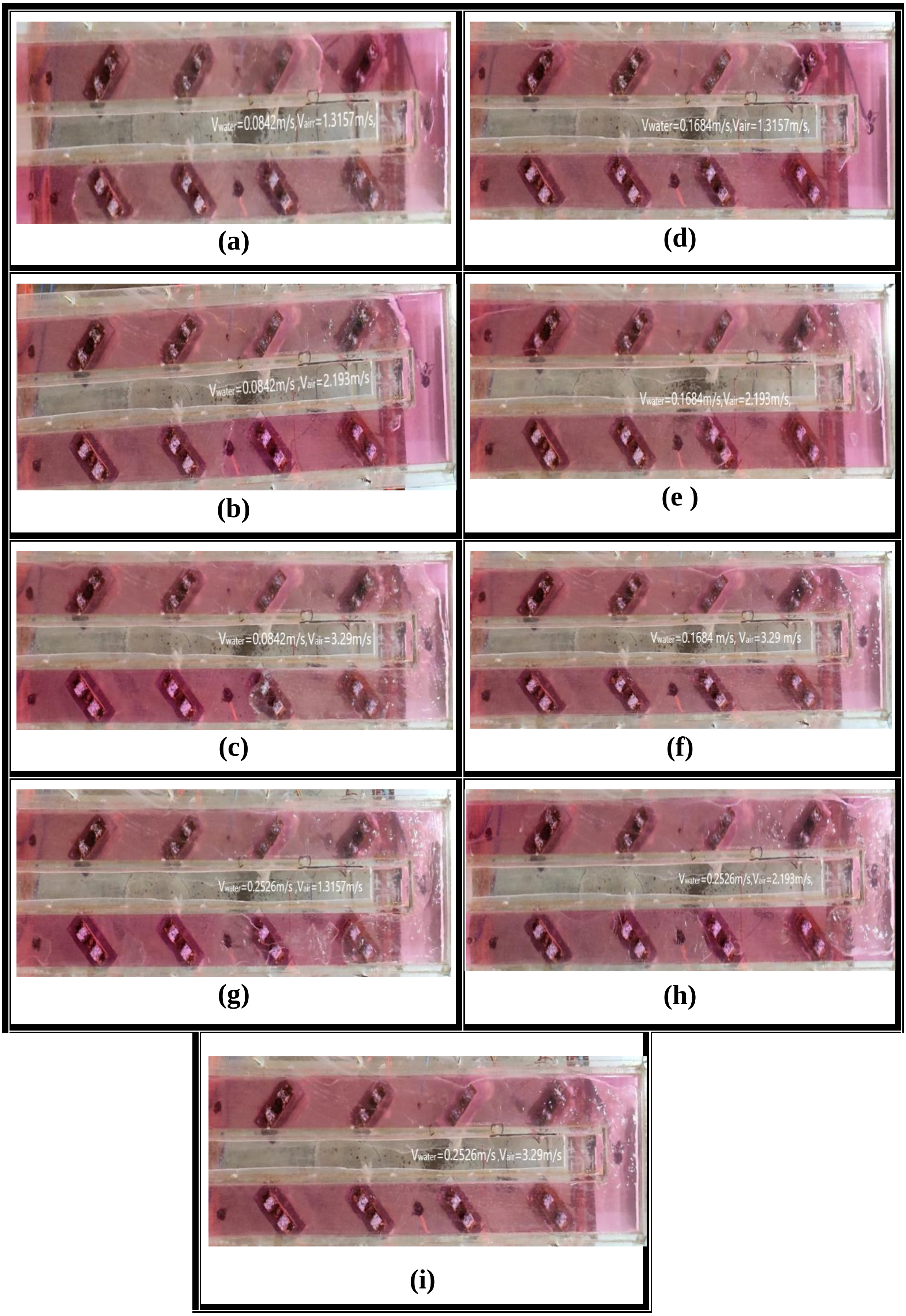

Figure (5.41): Flow pattern in V_{air} ,V_{water} at T_{rib} =70˚C.

5.5 Third Part: Three-phase flow internal Optimum channel.

5.5.1 Distribution of local Nusselt Number (Nu).

Similar to the behavior of Nu in two-phase flow, it observed that all the curves are contained from seven regions with the same reasons above.

Figures (5.42) to (5.44) show the effect of increasing V_{gasoil} from 0.042 to 0.0842m/s when T_{rib} varied for three degrees 50˚C, 60˚C and 70˚C at constant V_{air} and V_{water} equal to 1.3157 m/s and 0.0842 m/s, respectively. It observed the behavior of Nu in ribbed region described as fluctuant and it increased when increasing V_{gasoil} because increasing mixture velocity led to more turbulence. Also, it observed the effect of increasing T_{Rib} lead to enhance heat transfer because the heat transfer rate increased.

Figures (5.45) to (5.47) show the effect of increasing V_{gasoil} on Nu when T_{Rib} varied for three degrees 50˚C , 60˚C and 70˚C at constant V_{air} and V_{water} equal to 2.193 m/s and 0.0842 m/s ,respectively .It observed that increase V_{air} lead to increase Nu because so as to increase turbulence . Also, it observed the increasing in T_{rib} and V_{gasoil} lead to enhance Nu with same above reasons. The percentages of enhancing according as APPENDIX B.

Figures (5.48) to (5.50) show the effect of increasing V_{gasoil} on Nu when T_{Rib} varied for three degrees 50˚C , 60˚C and 70˚C at constant V_{air} and V_{water} equal to 3.29 m/s and 0.0842 m/s ,respectively . It observed that increase V_{air} led to increase Nu because so as to increase turbulence. Also, it observed the increasing in T_{rib} and V_{gasoil} lead to enhance Nu with same above reasons. The percentages of enhancing according as APPENDIX B.

Figures (5.51) to (5.53) show the effect of increasing V_{gasoil} on Nu when T_{rib} varied for three degrees 50˚C , 60˚C and 70˚C at constant V_{air} and V_{water} equal to 1.3157 m/s and 0.1684 m/s ,respectively .It observed that increasing in T_{rib} and V_{gasoil} lead to increase Nu because of more turbulence .Also ,it observed that increasing in V_{air} lead to increase Nu because of more turbulence . The percentages of enhancing according as APPENDIX B. Figures (5.54) to (5.56) show the effect of increasing V_{gasoil} on Nu when T_{Rib} varied for three degrees 50˚C, 60˚C and 70˚C at constant V_{air} and V_{water} equal to 2.193m/s and 0.1684 m/s, respectively. It observed that increasing in T_{rib} and V_{gasoil} lead to increase Nu because of more turbulence. Also, it observed that increasing in V_{air} from above cases lead to increase Nu because of more turbulence. The percentages of enhancing according as APPENDIX B.

Figures (5.57) to (5.59) show the effect of increasing V_{gasoil} when T_{Rib} varied for three degrees 50˚C, 60˚C and 70˚C at constant V_{air} and V_{water} equal to 3.29m/s and 0.1684 m/s, respectively. It observed that increasing in T_{rib} and V_{gasoil} lead to increase Nu because of more turbulence. Also, it observed that increasing in V_{air} from above cases lead to increase Nu because of more turbulence.

In comparison, Figures (5.42) to (5.50) and Figures (5.51) to (5.59) show the effect of increasing V_{water} is 0.0842m/s to 0.1684 m/s lead to increase Nu because of more turbulence so to increase of mixture velocity. The percentages of enhancing according as APPENDIX B.

Figures (5.60) to (5.62) show the effect of increasing V_{gasoil} on Nu when T_{Rib} varied for three degrees 50˚C, 60˚C and 70˚C at constant V_{air} and V_{water} equal to 1.3157 m/s and 0.2526 m/s ,respectively . It observed that increasing in T_{rib} and V_{gasoil} lead to increase Nu because of more turbulence. Also, it observed that increasing in V_{air} lead to increase Nu because of more turbulence. The percentages of enhancing according as APPENDIX B.

Figures (5.63) to (5.65) show the effect of increasing V_{gasoil} on Nu when T_{Rib} varied for three degrees 50˚C , 60˚C and 70˚C at constant V_{air} and V_{water} equal to 2.193m/s and 0.2526 m/s ,respectively It observed that increasing in T_{rib} and V_{gasoil} lead to increase Nu because of more turbulence

Also ,it observed that increasing in V_{air} from above cases lead to increase Nu because of more turbulence . The percentages of enhancing according as APPENDIX B.

Figures (5.66) to (5.68) show the effect of increasing V_{gasoil} on Nu when T_{Rib} varied for three degrees 50˚C, 60˚C and 70˚C at constant V_{air} and V_{water} equal to 3.29 m/s and 0.2526 m/s, respectively. It observed that increasing in T_{rib} and V_{gasoil} led to increase Nu because of more turbulence .Also ,it observed that increasing in V_{air} from above cases lead to increase Nu because of more turbulence . The percentages of enhancing according as APPENDIX B.

In comparison, Figures (5.51) to (5.59) and Figures (5.60) to (5.68) show the effect of increasing V_{water} is 0.1684m/s to 0.2526 m/s led to increase Nu because of more turbulence so to increase of mixture velocity. The percentages of an increasing Nu due to increasing T_{Rib} ,V_{gasoil} , V_{air} and V_{water} are tabled in APPENDIX B .

V_{water}=0.0842 m/s	V_{water}=0.0842 m/s
V_{air}=1.3157m/s	V_{air}=2.193m/s

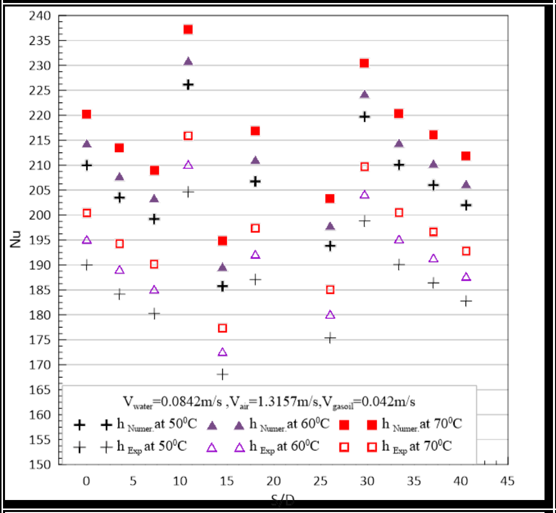

Figure (5.42). Nu at V_{gasoil}=0.042m/s

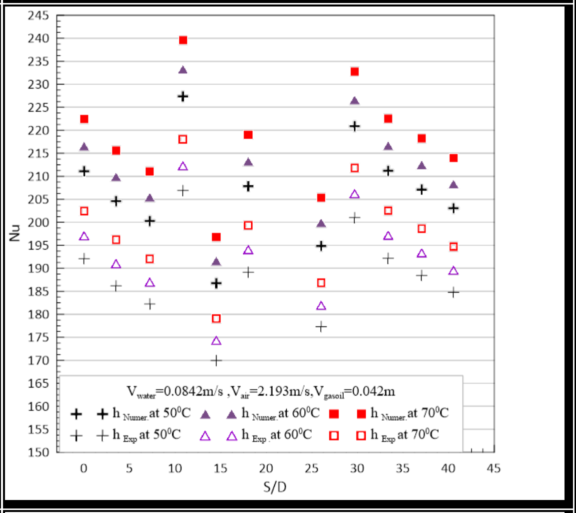

Figure (5.45). Nu at V_{gasoil}=0.042m/s

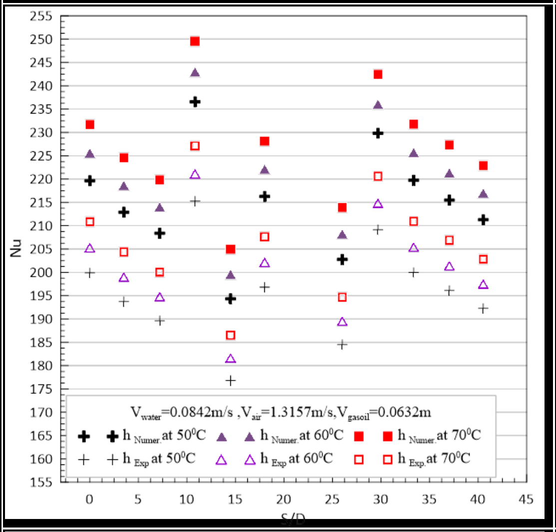

Figure (5.43). Nu at V_{gasoil}=0.0632m/s

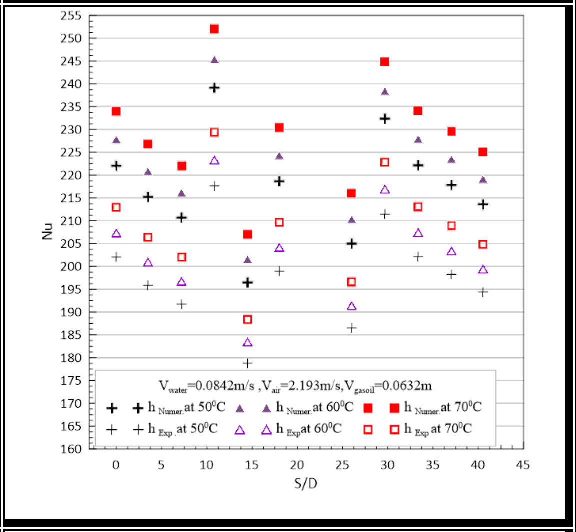

Figure (5.46). Nu at V_{gasoil}=0.0632m/s

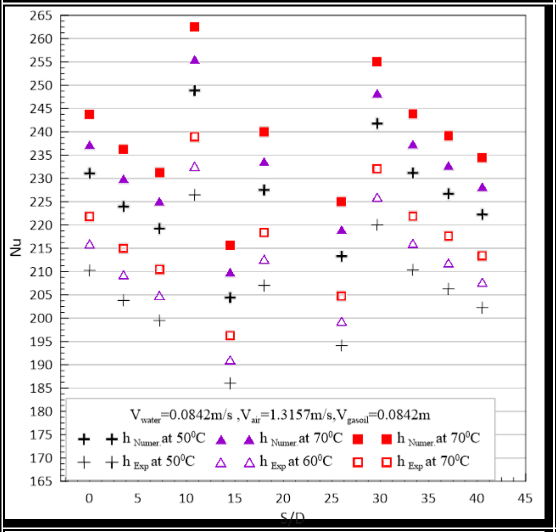

Figure (5.44). Nu at V_{gasoil}=0.0842m/s

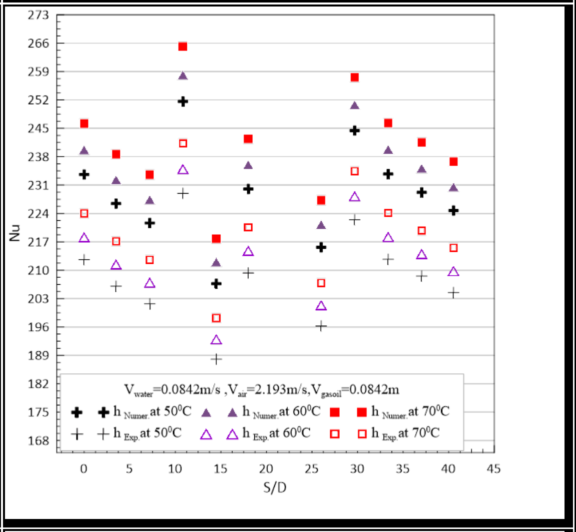

Figure (5.47). Nu at V_{gasoil}=0.0842m/s

V_{water}=0.0842 m/s	V_{water}= 0.1684 m/s
V_{air}=3.29m/s	V_{air}=1.3157m/s
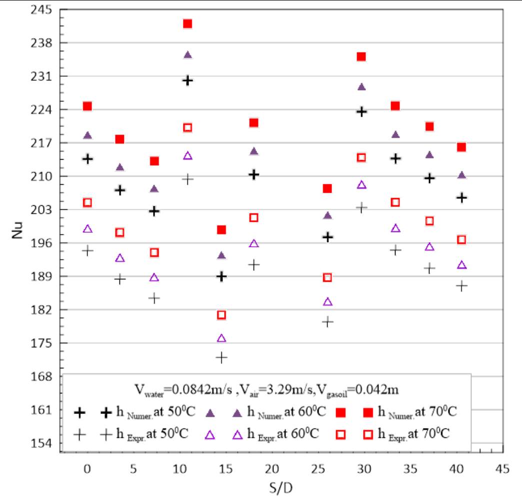	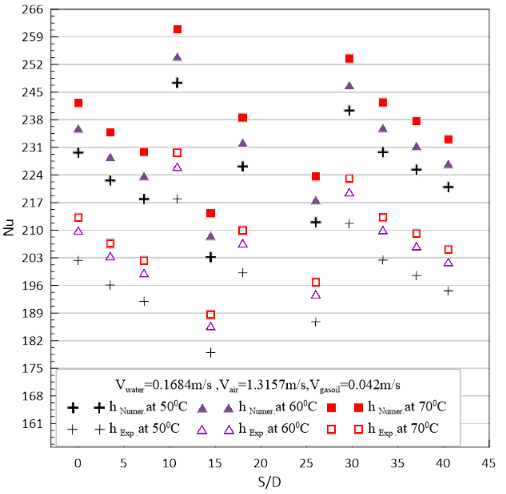
Figure (5.48). Nu at V_{gasoil}=0.042m/s	**Figure (5.51).**Nu at V_{gasoil}=0.042m/s
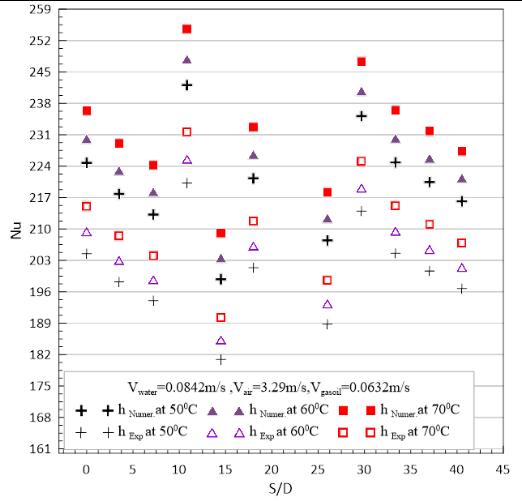	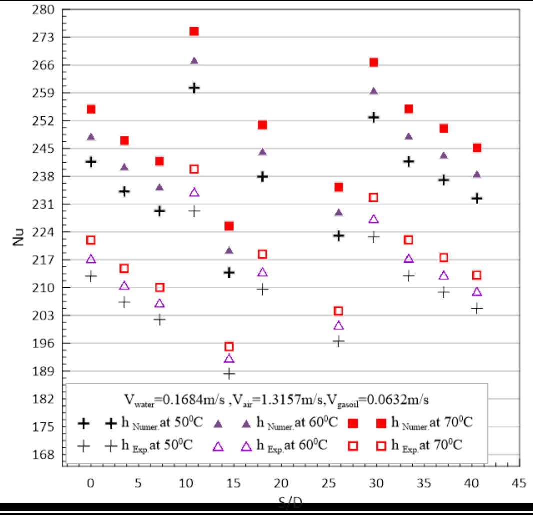
Figure (5.49). Nu at V_{gasoil}=0.0632m/s	**Figure (5.52).**Nu at V_{gasoil}=0.0632m/s
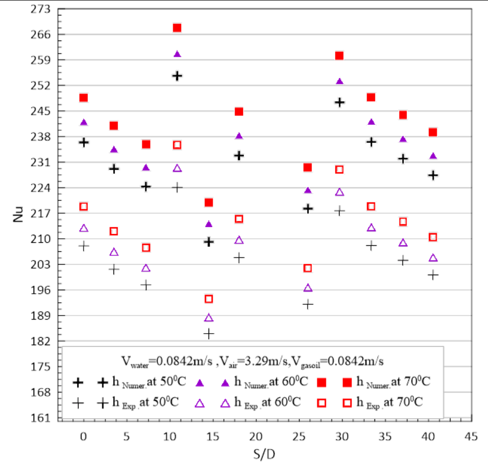	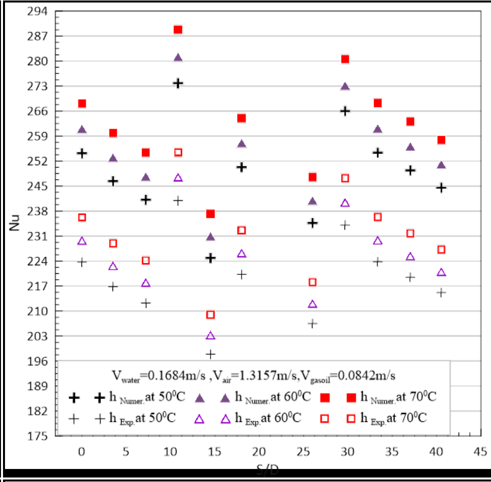
Figure (5.50). Nu at V_{gasoil}=0.084m/s	**Figure (5.53).**Nu at V_{gasoil}=0.084m/s

V_{water}= 0.1684 m/s

V_{air}=2.193m/s | V_{air}=3.29m/s

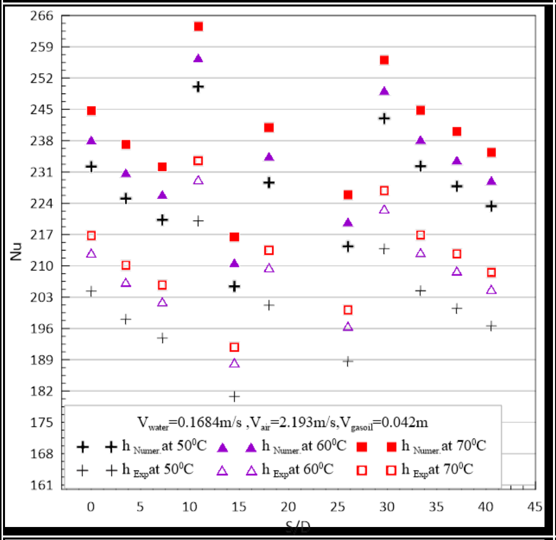

Figure (5.54). Nu at V_{gasoil}=0.04m/s

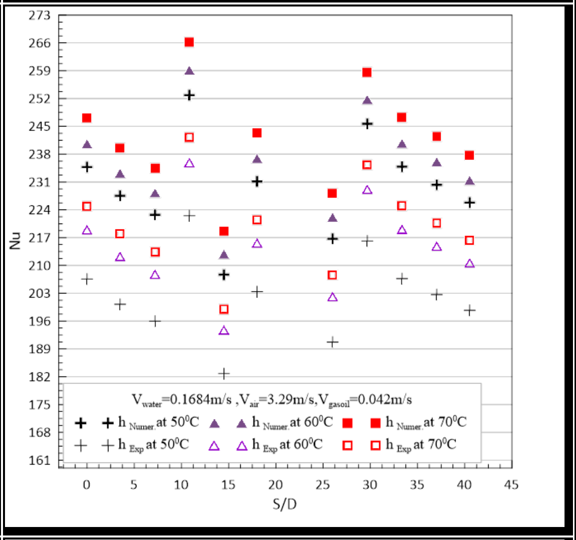

Figure (5.57). Nu at V_{gasoil}=0.04m/s

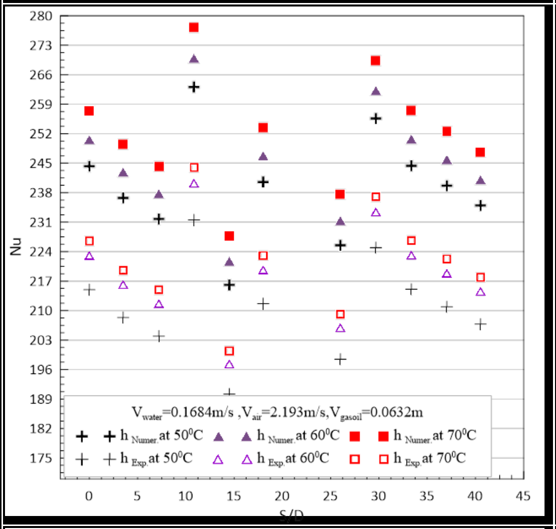

Figure (5.55). Nu at V_{gasoil}=0.0632m/s

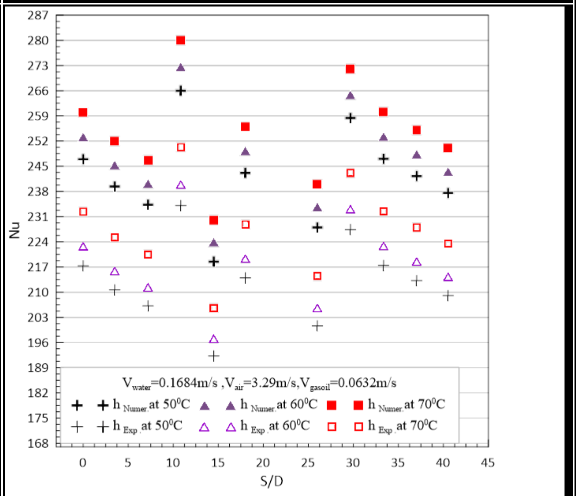

Figure (5.58). Nu at V_{gasoil}=0.0632m/s

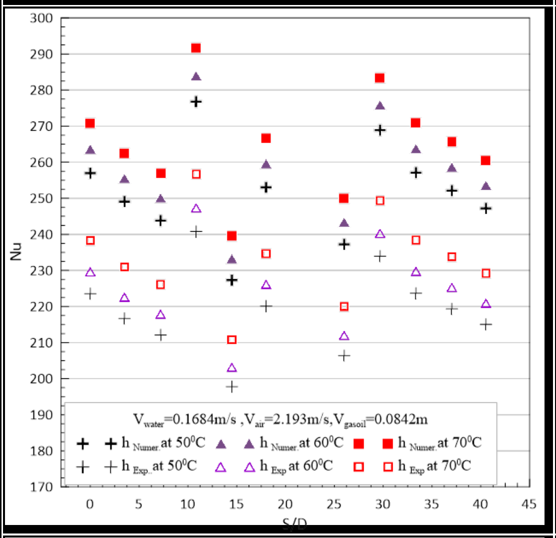

Figure (5.56). Nu at V_{gasoil}=0.084m/s

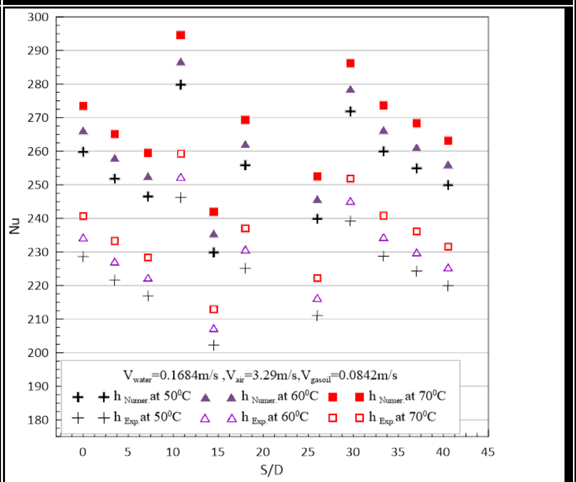

Figure (5.59).h at V_{gasoil}=0.084m/s

V_{water}= 0.2526 m/s

V_{air}= 1.3157m/s

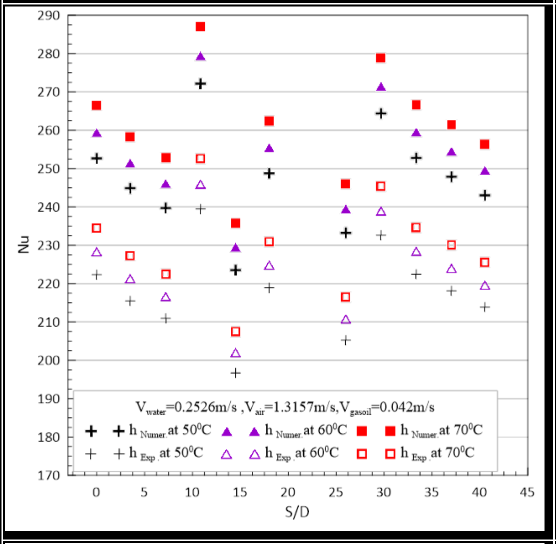

Figure (5.60). Nu at V_{gasoil}=0.042m/s

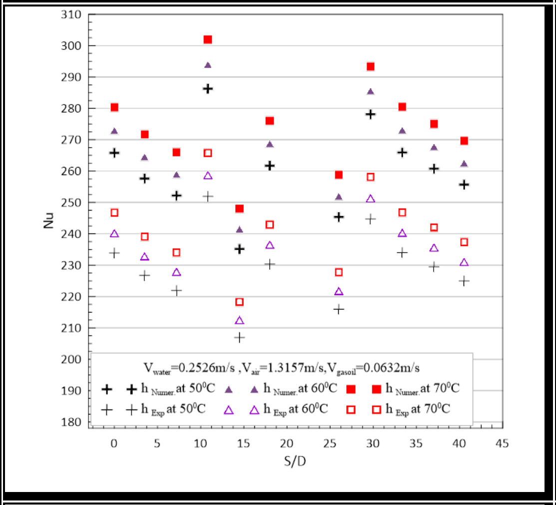

Figure (5.61). Nu at V_{gasoil}=0.0632m/s

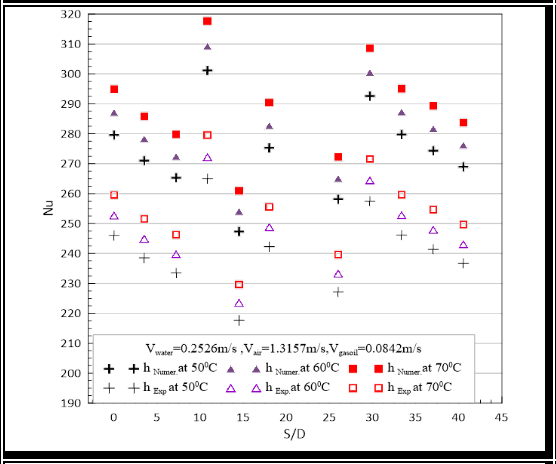

Figure (5.62). Nu at V_{gasoil}=0.0842m/s

V_{air}=2.193m/s

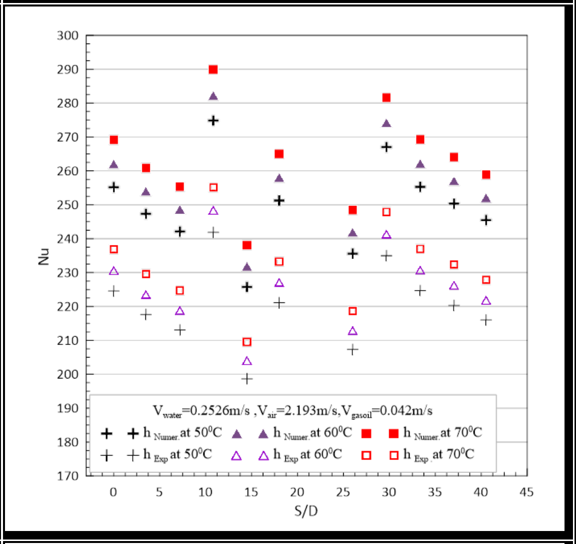

Figure (5.63). Nu at V_{gasoil}=0.042m/s

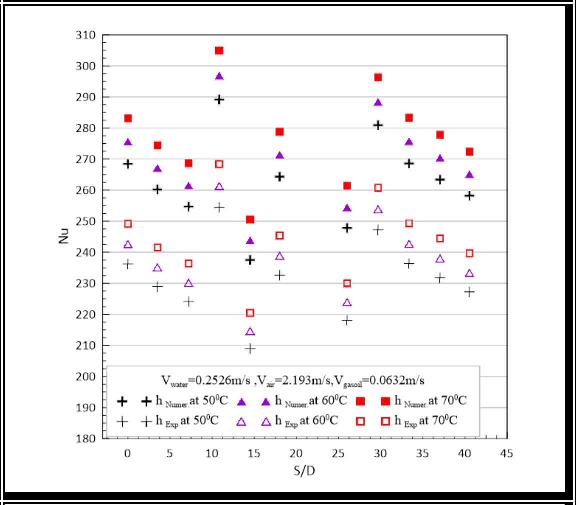

Figure (5.64). Nu at V_{gasoil}=0.0632m/s

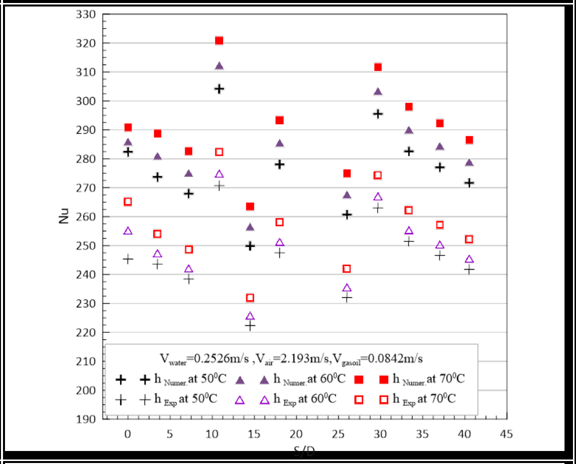

Figure (5.65). Nu at V_{gasoil}=0.0842m/s

V_{water}= 0.2526 m/s

V_{air}= 3.29 m/s

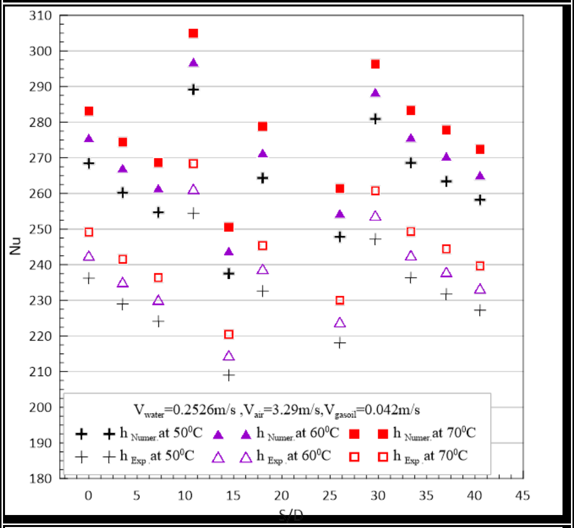

Figure (5.66). Nu at V_{gasoil}=0.042m/s

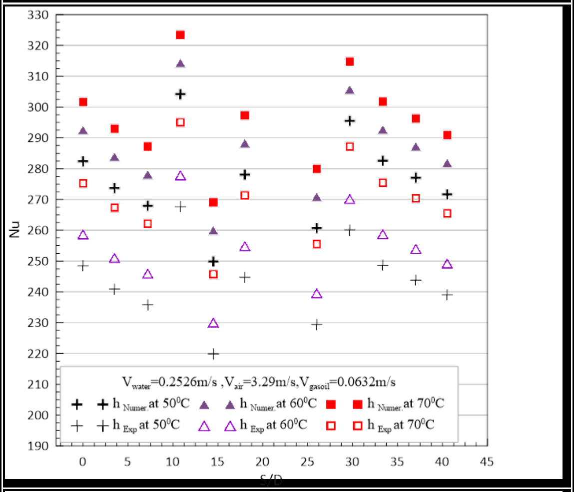

Figure (5.67). Nu at V_{gasoil}=0.0632m/s

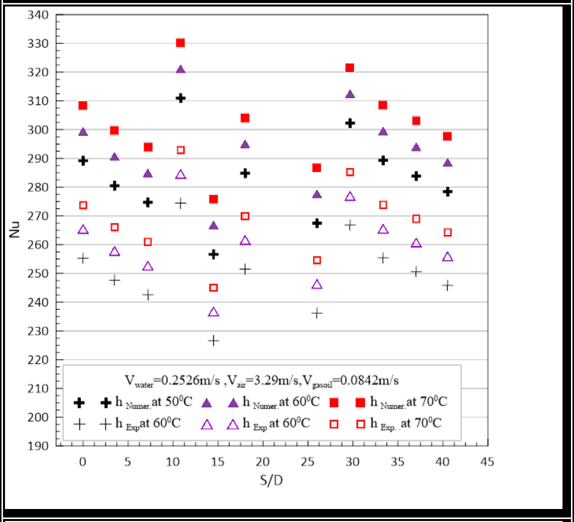

Figure (5.68). Nu at V_{gasoil}=0.0842m/s

5.5.2 Effect of changing velocities of air and water on average Nusselt number (Nu_{avg}) for different rib surface temperatures T_{rib} .

In general, to investigate the effect of increasing V_{water} ,V_{air} and T_{rib} on the Nu_{avg} for all regions along the ribbed part and bend region is performed by calculating the Nu_{avg} for all experiments . Figure (5.69) to (5.71) show the effect of increasing V_{gasoil} and V_{air} on Nu_{avg} at T_{rib} equal to 50ºC .The observation show that Nu_{avg} increased with increasing V_{gasoil} and V_{air} because of more turbulence with increasing velocities. Also, it observed that the increase in V_{gasoil} more than V_{air} because that the gasoil more efficient in heat transfer than air.

Also, it presents the effect of increase V_{water} from (0.082 ,0.1684 and 0.2526) m/s, it observed that Nu_{avg} increased with increasing V_{water}. Because increase V_{water} lead to more turbulence in mixture flow.The enhancing percentages so as to increase water velocities higher than enhancing due to increase T_{rib} and air velocities. The percentages of enhancing according as APPENDIX B.

Figure (5.72) to (5.74) show the effect of increasing V_{gasoil} and V_{air} on Nu_{avg} at T_{rib} equal to 60 ºC..The observation shows that Nu_{avg} increased with increasing V_{gasoil} and V_{air} with same previous reasons. Also, it observed that Nu_{avg} increased with increasing V_{water} with the same previous reasons.
Figure (5.105) to (5.107) show the effect of increasing V_{gasoil} and V_{air} on Nu_{avg} at T_{rib} equal to 70 ºC.. The observation shows that Nu_{avg} increased with increasing V_{gasoil} and V_{air} with same previous reasons. Also, it observed that Nu_{avg} increased with increasing V_{water} with the same previous reasons.

In comparison, Figures (5.69) to (5.71), Figures (5.72) to (5.74) and Figure (5.75) to (5.77) are investigated that Nu_{avg} increased with increasing T_{rib} . Because the increased heat rate leads to increase Nu_{avg} and enhancing heat transfer.

T_{rib} =50ºC	T_{rib} =60ºC

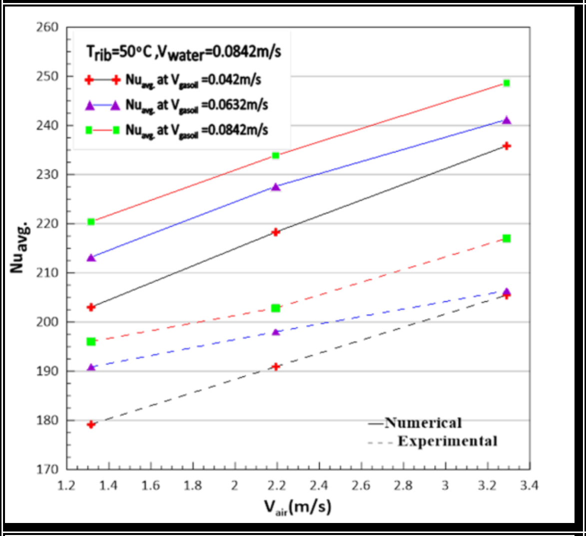

Figure (5.69). Nu_{avg} at. V_{water}=0.0842m/s

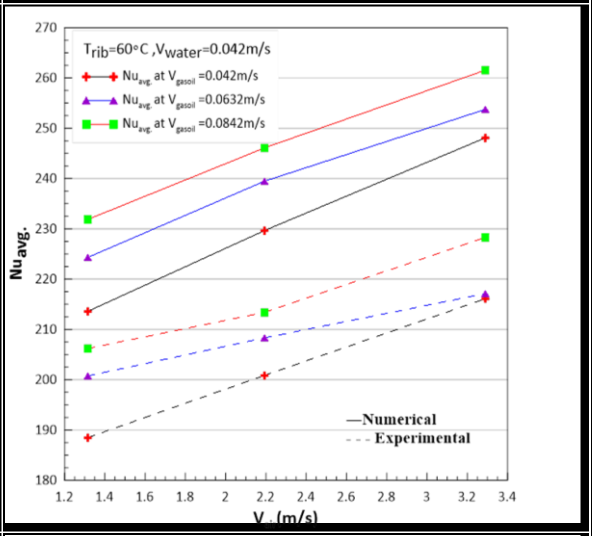

Figure (5.72) .Nu_{avg} at. V_{water}= 0.0842m/s

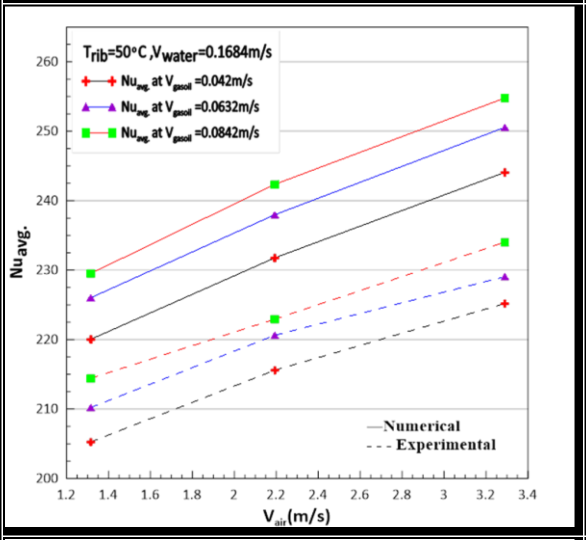

Figure (5.70) .Nu_{avg} at. V_{water}=0.1684m/s

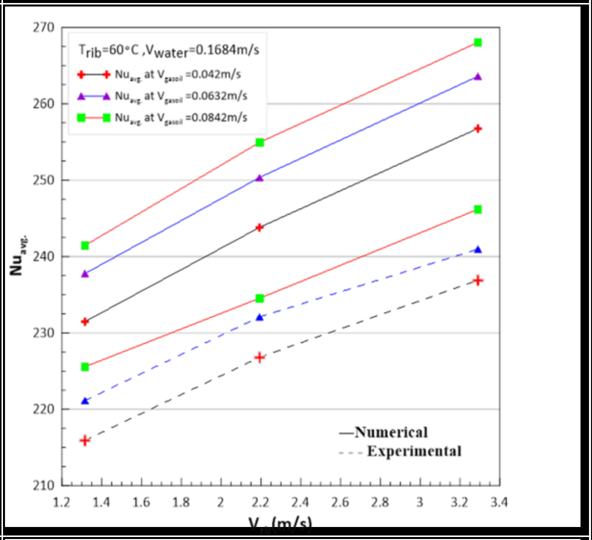

Figure (5.73). Nu_{avg} at. V_{water}= 0.1684m/s

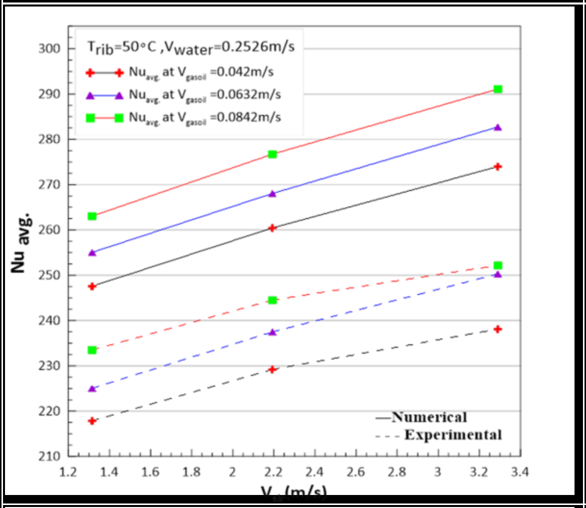

Figure (5.71) .Nu_{avg} at. V_{water}=0.2526m/s

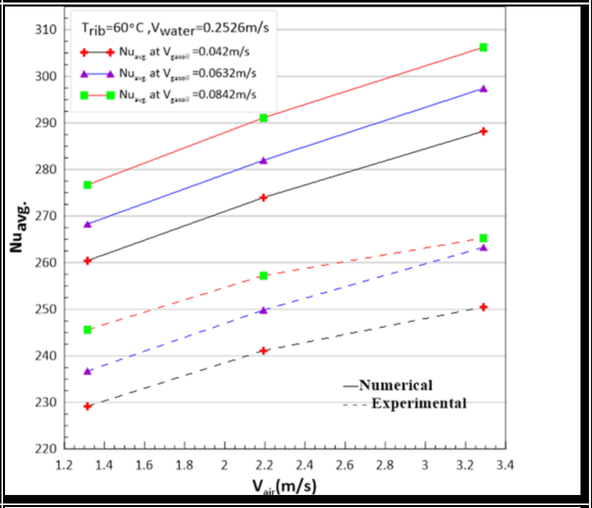

Figure (5.74) .Nu_{avg} at. V_{water}=0.2526m/s

T_{rib} =70°C

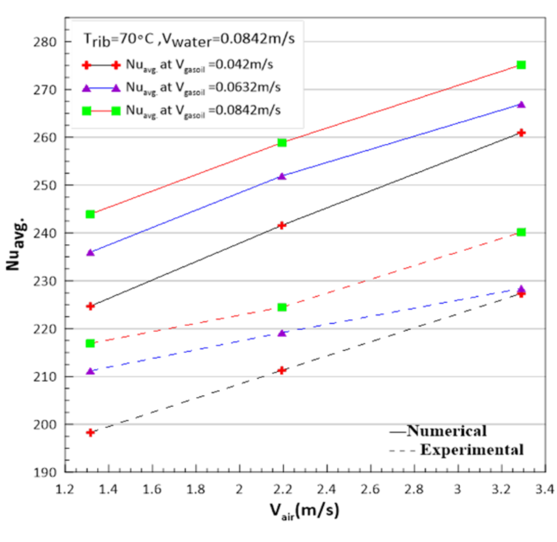

Figure (5.75) .Nu$_{avg}$ at. V$_{water}$=0.084m/s

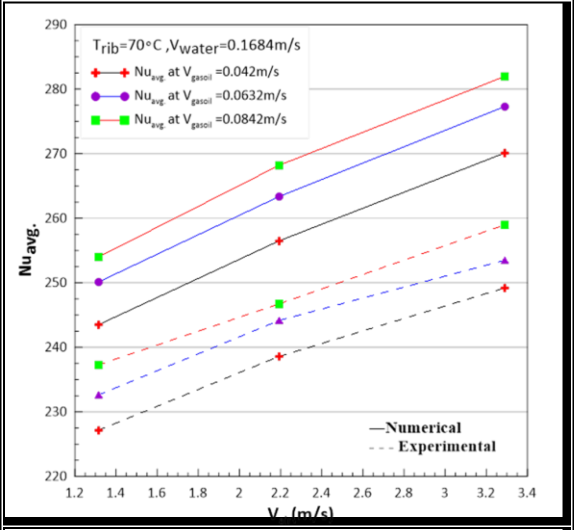

Figure (5.76).Nu$_{avg}$ at. V$_{water}$=0.1684m/s

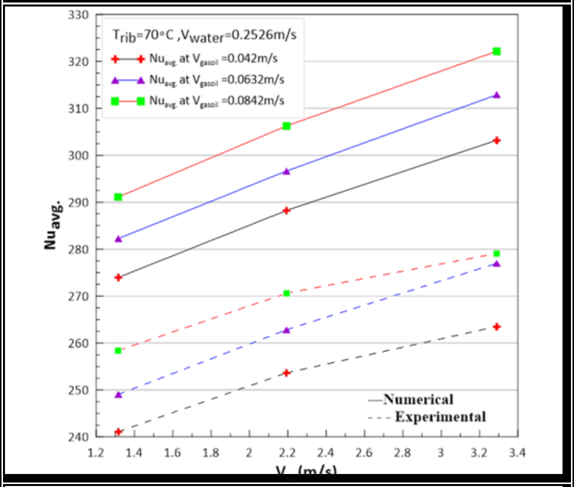

Figure (5.77).Nu$_{avg}$at. V$_{water}$=0.2526m/s

5.5.3 Effect of changing velocities of air and water on enhancement ratio Nu/Nu_o for different rib surface temperatures T_{rib} .

To investigate the heat transfer enhancement due to various velocities and different T_{Rib} ,the average Nusselt number ratio (Nu/Nu_o)is calculated for all regions along the ribbed part and bend region .Figure (5.78) to (5.80) show the effect of increasing V_{gasoil} and V_{air} on (Nu/Nu_o) at T_{rib} equal to 50°C.The observation show that (Nu/Nu_o) value enhanced with increasing V_{gasoil} and V_{air} because of more turbulence with increasing velocities. Also, it presents the effect of increase V_{water} from (0.082 ,0.1684 and 0.2526) m/s, it observed that (Nu/Nu_o) enhanced with increasing V_{water}. Because increase V_{water} lead to more turbulence in mixture flow as APPENDIX B.

Figure (5.81) to (5.83) show the effect of increasing V_{gasoil} and V_{air} on (Nu/Nu_o) at T_{rib} equal to 60°C.The observation shows that (Nu/Nu_o) enhanced with increasing V_{gasoil} and V_{air} with same previous reasons. Also, it observed that (Nu/Nu_o) enhanced with increasing V_{water} with the same previous reasons as APPENDIX B.

Figure (5.84) to (5.86) show the effect of increasing V_{gasoil} and V_{air} on (Nu/Nu_o) at T_{rib} equal to 70°C.The observation shows that (Nu/Nu_o) enhanced with increasing V_{gasoil} and V_{air} with same previous reasons. Also, it observed that (Nu/Nu_o) enhanced with increasing V_{water} with the same previous reasons as APPENDIX B.

In comparison, Figures (5.78) to (5.80) , Figures (5.81) to (5.83) and Figure (5.84) to (5.86) are investigated and (Nu/Nu_o) enhanced with increasing T_{rib}. Because the increased heat rate leads to enhanced (Nu/Nu_o). The enhanced in Nu/Nu_o due to increase in V_{water} have more than in V_{air} because the water is able to absorb more heat than air so it has higher heat capacity than air as APPENDIX B .

$T_{rib}=50^oC$

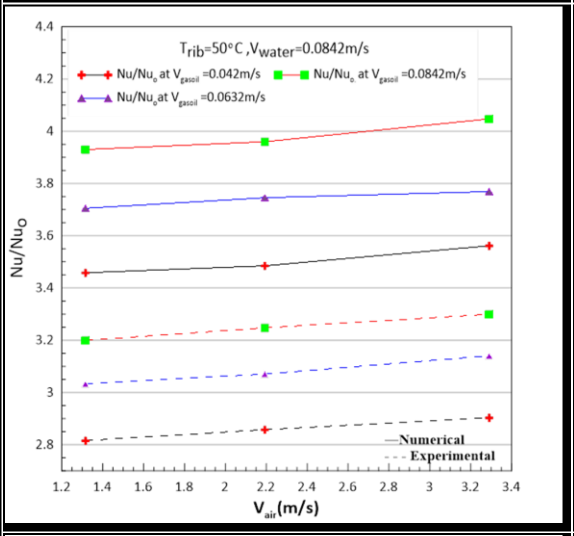

Figure (5.78) .Nu/Nu$_o$at. V$_{water}$=0.042m/s

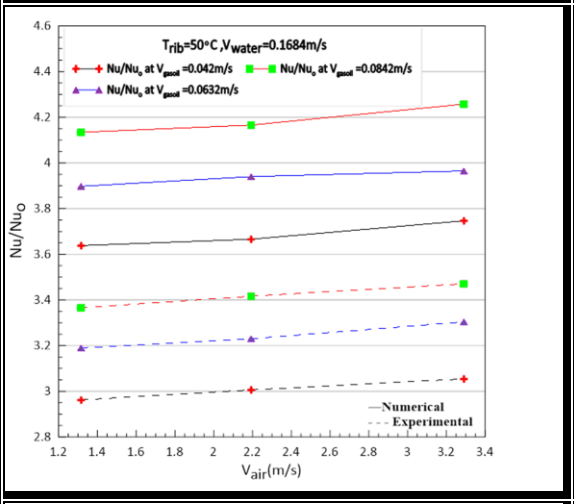

Figure (5.79)..Nu/Nu$_o$ at. V$_{water}$=0.0632m/s

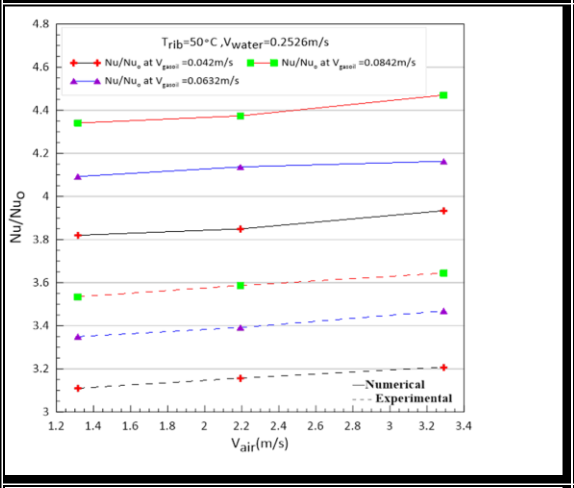

Figure (5.80).Nu/Nu$_o$ at. V$_{water}$=0.2526m/s

$T_{rib}=60^oC$

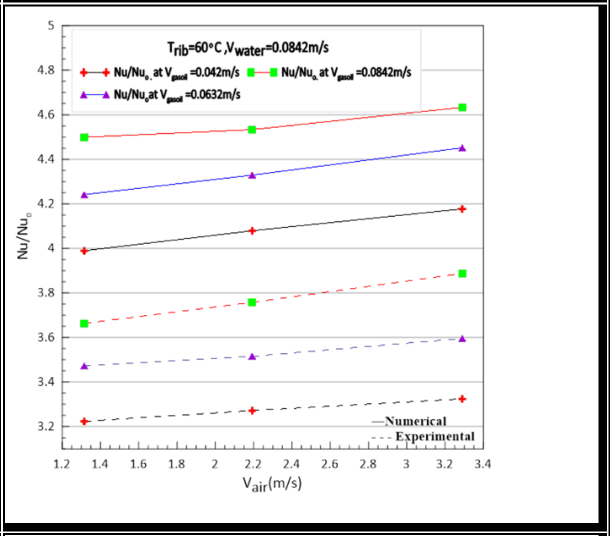

Figure (5.81) Nu/Nu at. V$_{water}$=0.0842m/s

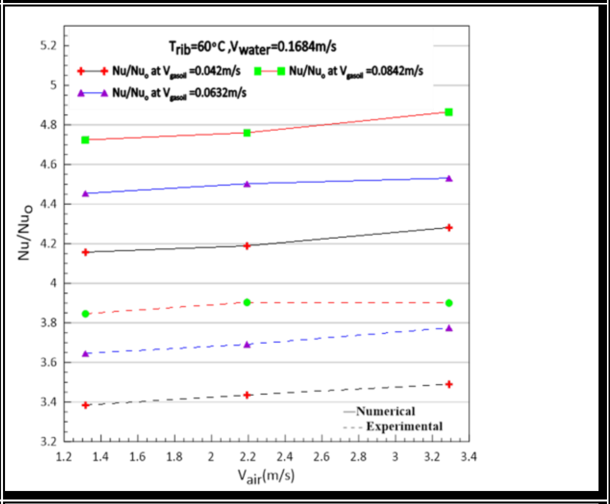

Figure (5.82).Nu/Nu at. V$_{water}$=0.1684m/s

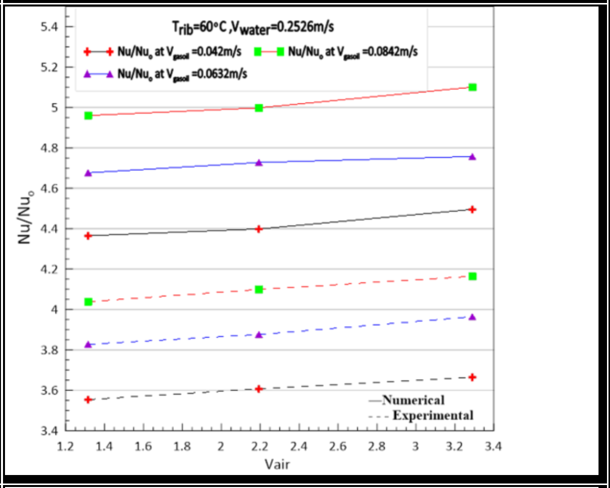

Figure(5.83). Nu/Nu$_o$at.V$_{water}$=0.2526m/s

T_{rib} =70°C

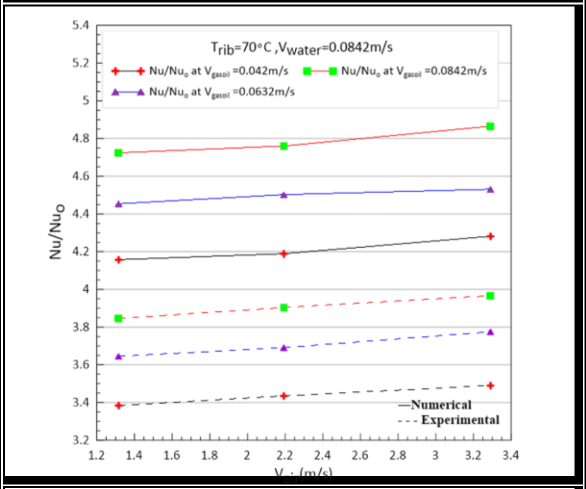

Figure (5.84). Nu/Nuoat. V_{water}=0.0842m/s

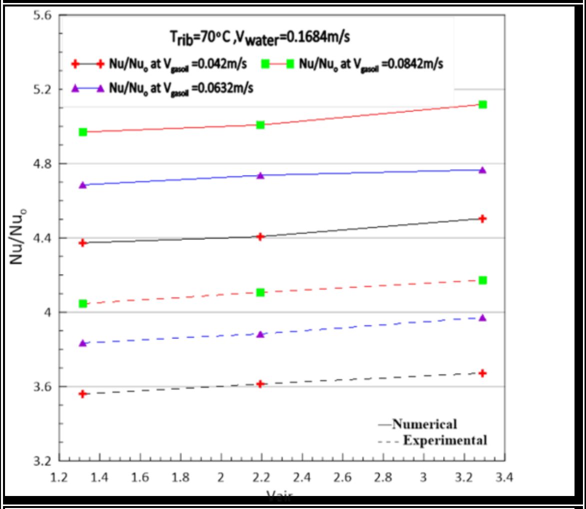

Figure (5.85). Nu/Nuo at. V_{water}=0.0632m/s

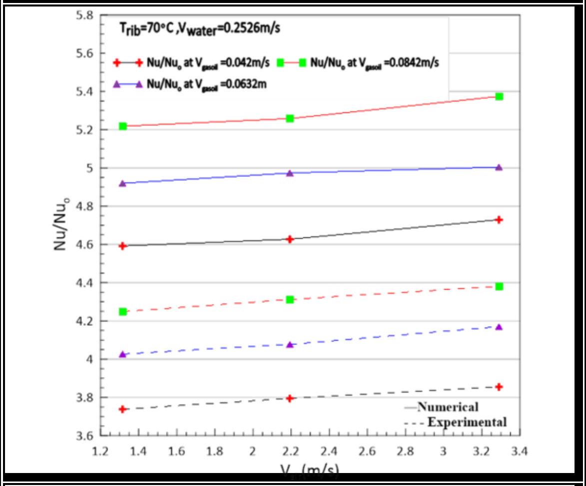

Figure (5.86). Nu/Nuoat. V_{water}=0.2526m/s

5.5.4 Effect of changing velocities of air and water on pressure drop (ΔP) for different rib surface temperatures T_{rib} .

The difference in total pressure between two points results from the friction caused by mixture against the channel walls and components. Figure (5.87) to (5.89) show the effect of increasing V_{gasoil} and V_{air} on (ΔP) at T_{rib} equal to 50°C .It observed that the (ΔP) increased with increasing velocities V_{gasoil} and V_{air} .Because the kinetic energy increased lead to increase friction due to increase (ΔP). The increase V_{water} from 0.0842m/s to 0.2526m/s lead to increase (ΔP) because of increasing friction.

Figure (5.90) to (5.92) show the effect of increasing V_{gasoil} and V_{air} on (ΔP) at T_{rib} equal to 60°C . It observed that the (ΔP) increased with increasing velocities V_{gasoil} and V_{air} because the kinetic energy increased lead to increase friction due to increase (ΔP). The increase V_{water} from 0.0842m/s to 0.2526m/s lead to increase (ΔP) because of increasing friction.

Figure (5.93) to (5.95) show the effect of increasing V_{gasoil} and V_{air} on (ΔP) at T_{rib} equal to 70°C.The observation shows that the (ΔP) increased with increasing velocities V_{gasoil} and V_{air} because the kinetic energy increased lead to increase friction due to increase (ΔP). The increase V_{water} from 0.0842m/s to 0.2526m/s lead to increase (ΔP) because of increasing friction.

In comparison the three above groups of (50°C, 60°C, 70°C), these observed that the effect of increasing T_{rib} led to increase(ΔP) because of increase velocity so as to increase kinetic energy caused more friction.

T_{rib} =50°C	T_{rib} =60°C

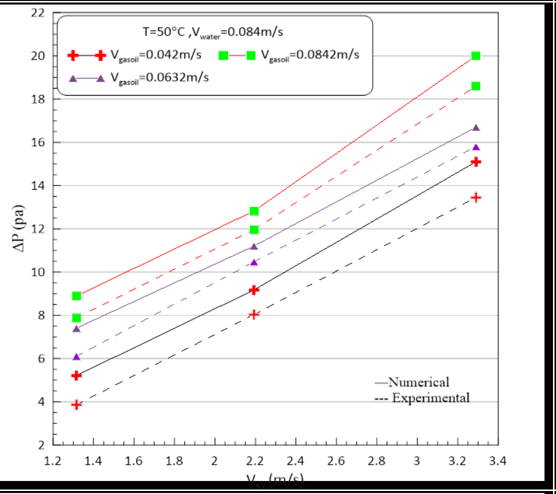

Figure (5.87).ΔP at. V_{water}=0.0842m/s

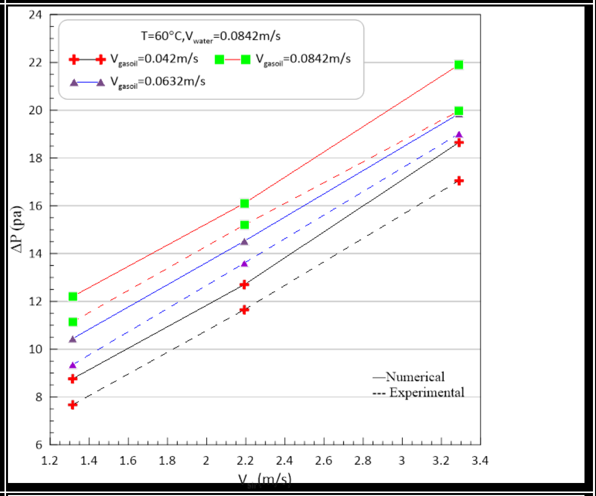

Figure (5.90) ΔP at . V_{water}=0.0842m/s

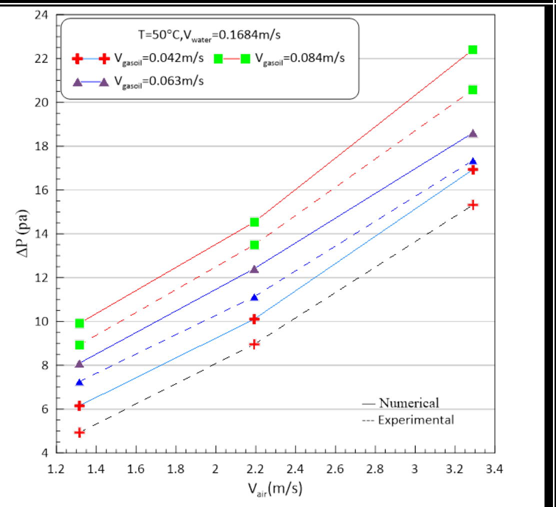

Figure (5.88). ΔP at. V_{water}=0.1684m/s

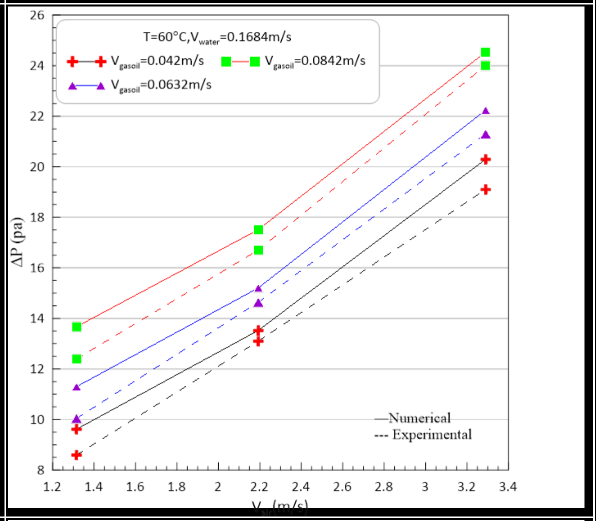

Figure (5.91). ΔP at. V_{water}=0.0632m/s

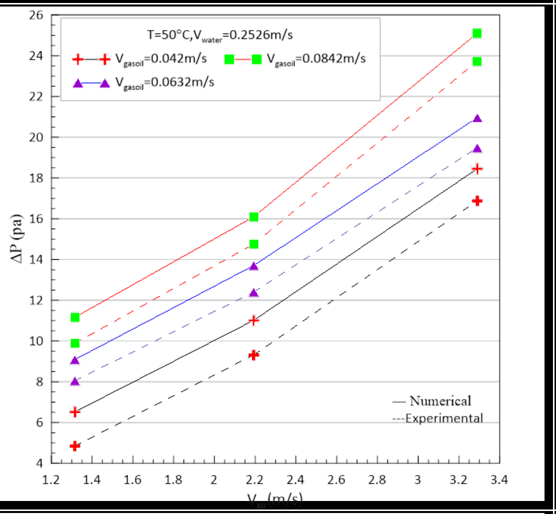

Figure (5.89). ΔP at.V_{water}=0.2526m/s

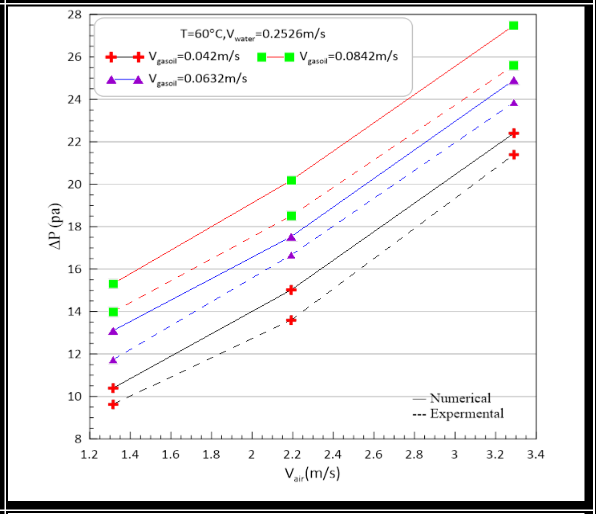

Figure (5.92). ΔP at . V_{water}=0.2526m/s

T_{rib} =70°C

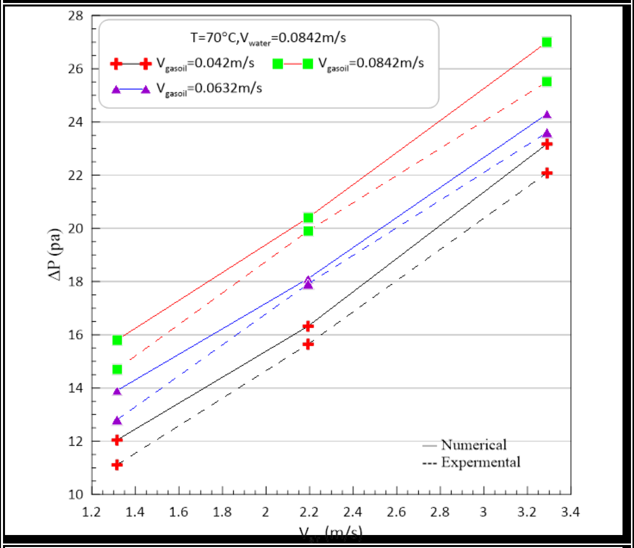

Figure (5.93) ΔP at. V_{water}=0.0842m/s

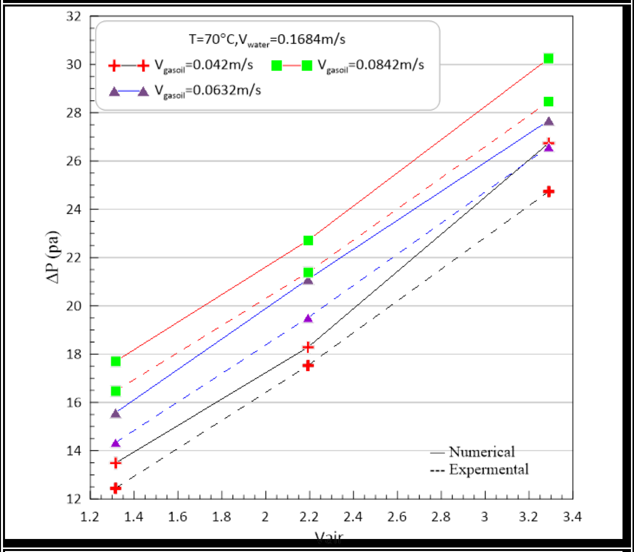

Figure (5.94). ΔP at. V_{water}=0.1684m/s

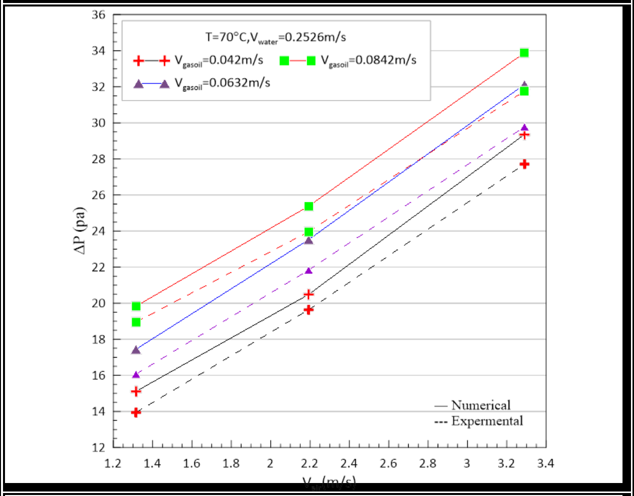

Figure (5.95). ΔP at.V_{water}=0.2526m/s

5.5.5 Effect of changing velocities of air and water on friction ratio (f/f_o) for different rib surface temperatures T_{rib} .

To investigate the friction factor ratio (f/f_o) is ratio between friction factor with exiting the ribs to its value without ribs, and depending on pressure drop and mixture velocity along the ribbed part and bend through the channel. Figure (5.96) to (5.98) show the effect of increasing V_{gasoil} and V_{air} on (f/f_o) at T_{rib} equal to 50°C .The observation shows that(f/f_o)value decreases with increasing V_{gasoil} and V_{air} because of more kinetic energy and low friction. Also, it presents the effect of increase V_{water} from (0.082 ,0.1684 and 0.2526) m/s, it observed that (f/f_o) decreased with increasing V_{water} because of low friction so as to high velocity. Figure (5.99) to (5.101) show the effect of increasing V_{gasoil} and V_{air} on (f/f_o) at T_{rib} equal to 60°C .The observation shows that (f/f_o) value decreases with increasing V_{gasoil} and V_{air} because of increase kinetic energy led to low friction . Also, it presents the effect of increase V_{water} from (0.082 ,0.1684 and 0.2526) m/s, it observed that (f/f_o) decreased with increasing V_{water} because it does not allow a high friction when velocity of mixture increased.

Figure (5.102) to (5.104) show the effect of increasing V_{gasoil} and V_{air} on (f/f_o) at T_{rib} equal to 70°C . The observation shows that (f/f_o) value decreases with increasing V_{gasoil} and V_{air} because of increase kinetic energy led to low friction . Also, it presents the effect of increase V_{water} from (0.082 ,0.1684 and 0.2526) m/s, it observed that (f/f_o) decreased with increasing V_{water} because of increasing velocity of mixture.

These observations for Figures (5.96) to (5.98), Figures (5.99) to (5.101) and Figures (5.102) to (5.104) show that increasing T_{rib} leads to increase the (f/f_o) as percentages in APPENDIX B because the pressure drop increased lead to high friction losses.

T_{rib} =50°C	T_{rib} =60°C

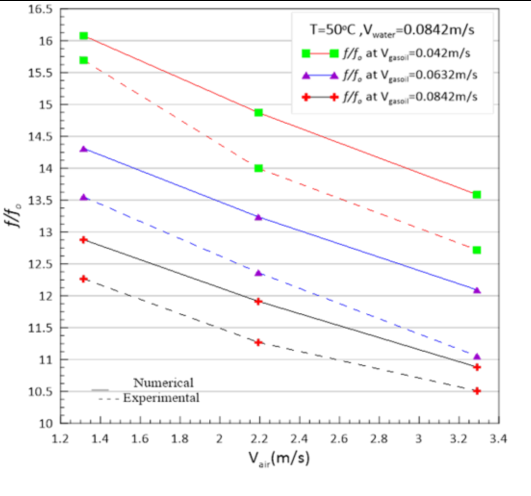

Figure (5.96).f/f_o.at. V_{water}=0.0842m/s.

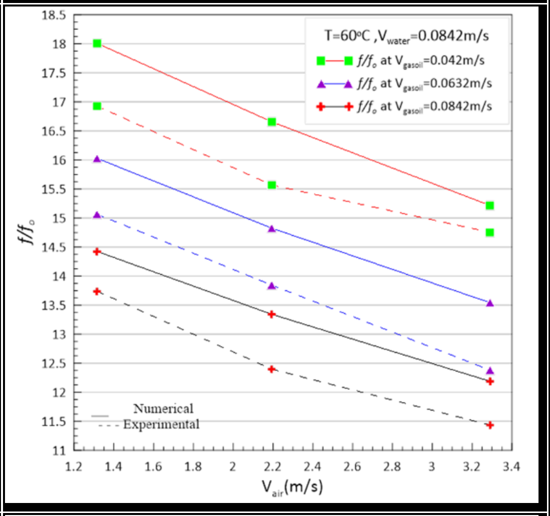

Figure (5.99) f/f_oat. V_{water}=0.0842m/s.

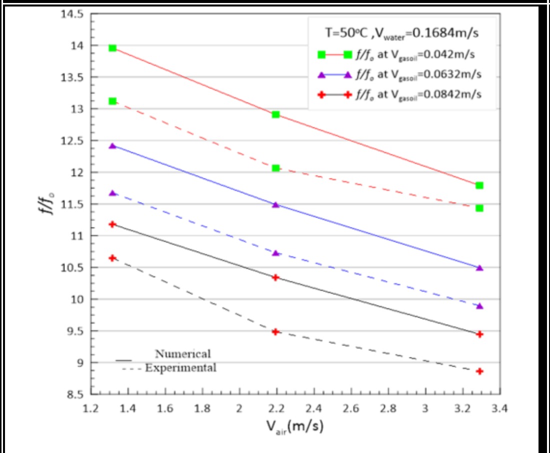

Figure (5.97).f/f_o at. V_{water}= 0.0632m/s

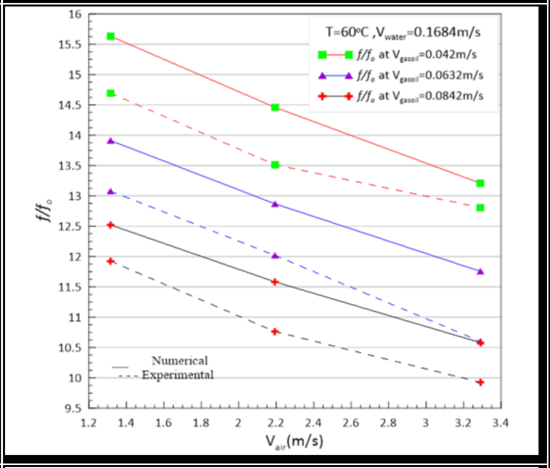

Figure(5.100).f/f_o at. V_{water}= 0.1684m/s.

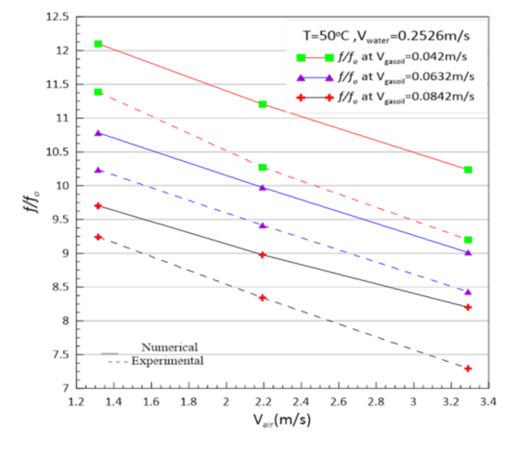

Figure (5.98)..f/f_o at. V_{water}=0.2526m/s

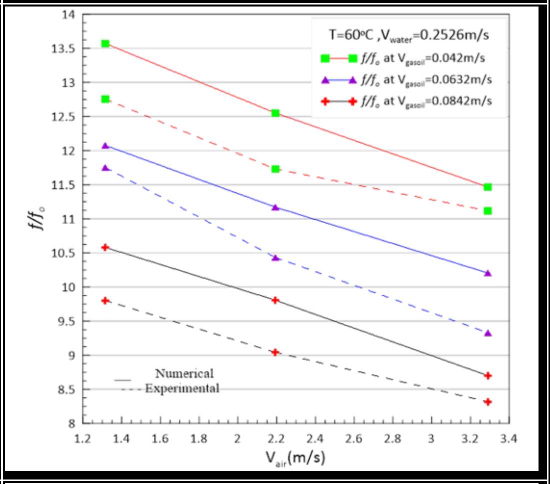

Figure (5.101) .f/f_oat. V_{water}=0.2526m/s

T_{rib} =70°C

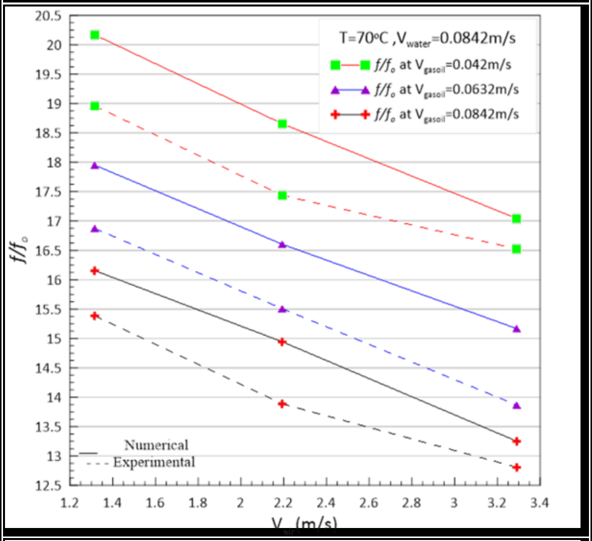

Figure (5.102). f/f_o.at. V_{water}=0.0842m/s.

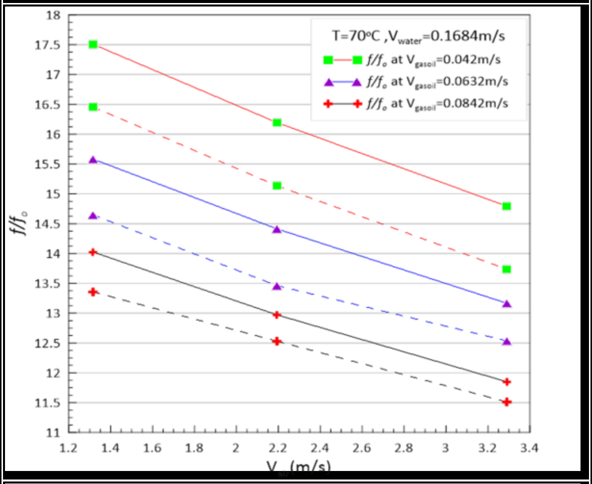

Figure (5.103). f/f_o at. V_{water}= 0.0632m/s

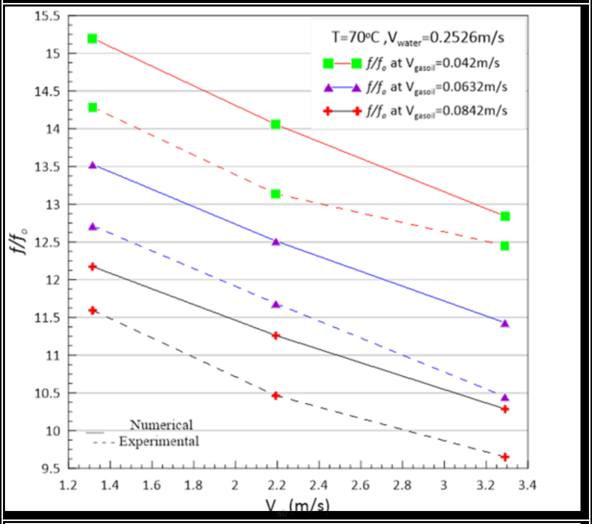

Figure (5.104). f/f_o at. V_{water}=0.2526m/s.

5.5.6 Effect of changing velocities of air and water on Thermal-Performance Criteria Evaluation (PCE) for different rib surface temperatures T_{rib} .

The ratio of the enhanced heat transfer to the increased friction represented by (PCE). Figure (5.105) to (5.107) present the effect of increasing V_{gasoil} and V_{air} on (PCE) at T_{rib} equal to 50ºC .The (PCE)value decreases with increasing V_{gasoil} and V_{air} with percentages as APPENDIX B for air and water respectively. Because (PCE) is the ratio of *(f/f_o)* is increased because of low *f* and f_o lower with increase velocities lead to low over lower get value of f/f_o higher than enhance in heat transfer (Nu/Nu_o). mixture. Also, it presents the effect of increase V_{water} from (0.082 ,0.1684 and 0.2526) m/s, it observed that (PCE) decreased with increasing V_{water} .The reasons of decreases relating to the value of *(f/f_o)* is more than enhance in heat transfer (Nu/Nu_o) .

Figure (5.108) to (5.110) show the effect of increasing V_{gasoil} and V_{air} on (PCE) at T_{rib} equal to 60ºC. The (PCE)value decreases with increasing V_{gasoil} and V_{air} with percentages as APPENDIX B for air and water respectively. Because (PCE) is the ratio of *(f/f_o)* is increased because of low *f* and f_o lower with increase velocities lead to low over lower get value of f/f_o higher than enhance in heat transfer (Nu/Nu_o). mixture. Also, it presents the effect of increase V_{water} from (0.082 ,0.1684 and 0.2526) m/s, it observed that (PCE) decreased with increasing V_{water}. The reasons of decreases relating to the value of *(f/f_o)* is more than enhance in heat transfer (Nu/Nu_o) .

Figure (5.111) to (5.113) show the effect of increasing V_{gasoil} and V_{air} on (PCE) at T_{rib} equal to 70ºC . The (PCE)value decreases with increasing V_{gasoil} and V_{air} with percentages as APPENDIX B for air and water respectively. Because (PCE) is the ratio *(f/f_o)* is increased because of low *f* and f_o lower with increase velocities lead to low over lower get value of ratio f/f_o higher than enhance in heat transfer (Nu/Nu_o) in mixture. Also, it presents the effect of increase V_{water} from (0.082 ,0.1684 and 0.2526) m/s, it observed that (PCE) decreased with increasing V_{water}.The reasons of decreases relating to the value of ratio (f/f_o) is more than enhance in heat transfer (Nu/Nu_o) .

These observations for Figures (5.105) to (5.107), Figures (5.108) to (5.110) and Figure (5.111) to (5.113) show that increasing T_{rib} leads to increase (PCE) because increase T_{Rib} leads to more heat rate and more enhancement in heat transfer more than friction ratio.

T_{rib} =50ºC	T_{rib} =60ºC
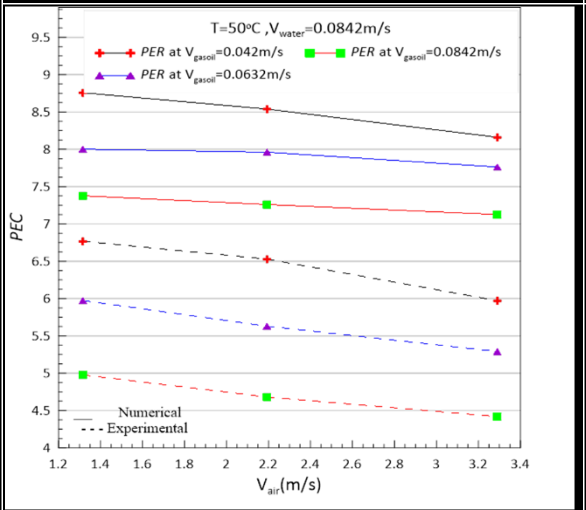	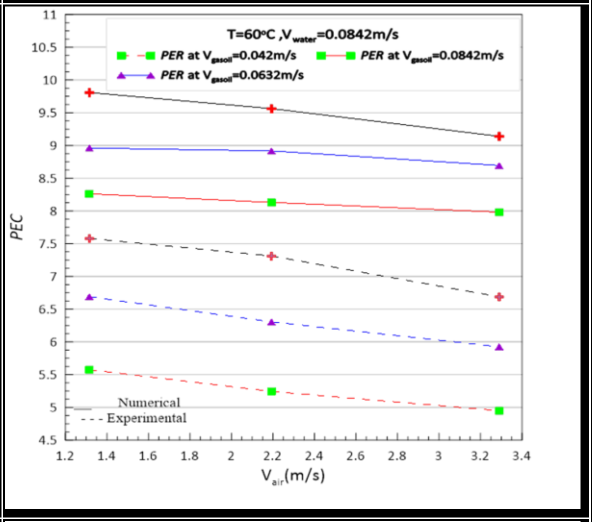
Figure (5.105) *PCE* at. V_{water}=0.0842m/s	**Figure (5.108).***PCE*.at. V_{water}=0.0842m/s
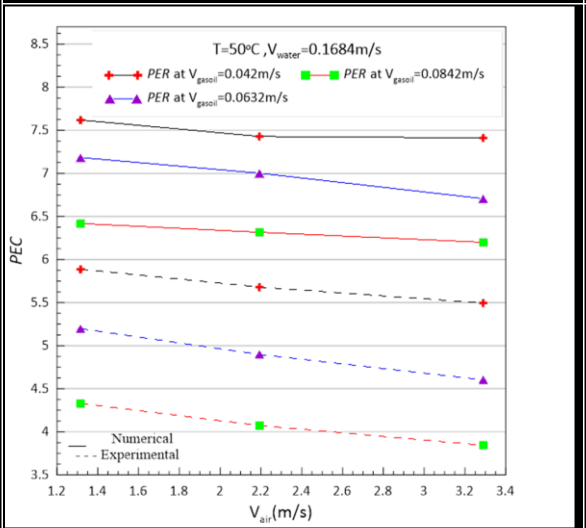	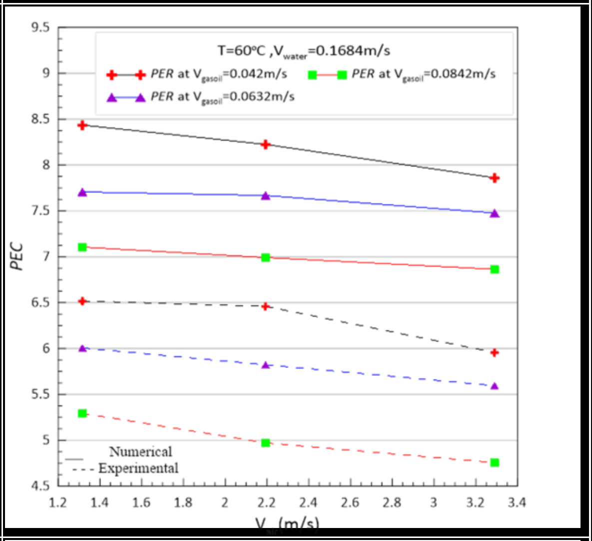
Figure (5.106). PCE at. V_{water}= 0.1684m/s	**Figure (5.109).** PCE at. V_{water}= 0.0632m/s

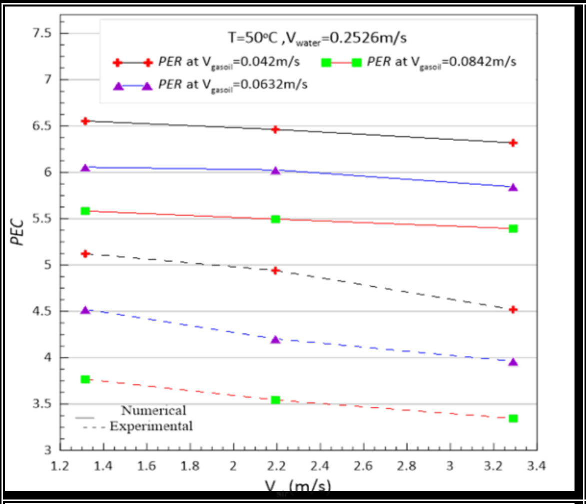

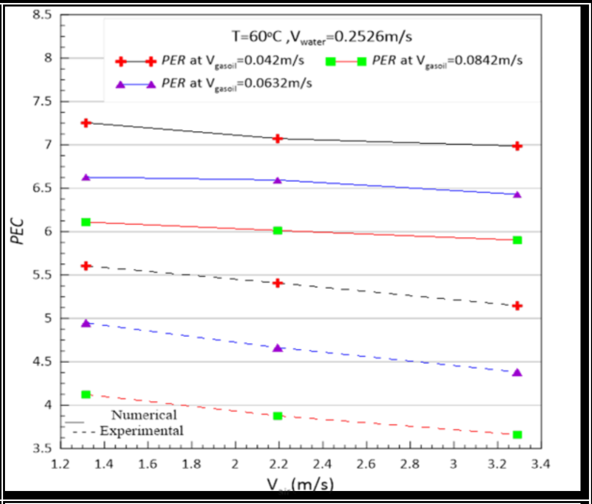

Figure (5.107). PCE at. V$_{water}$=0.2526m/s **Figure (5.110). PCE at. V$_{water}$=0.2526m/s**

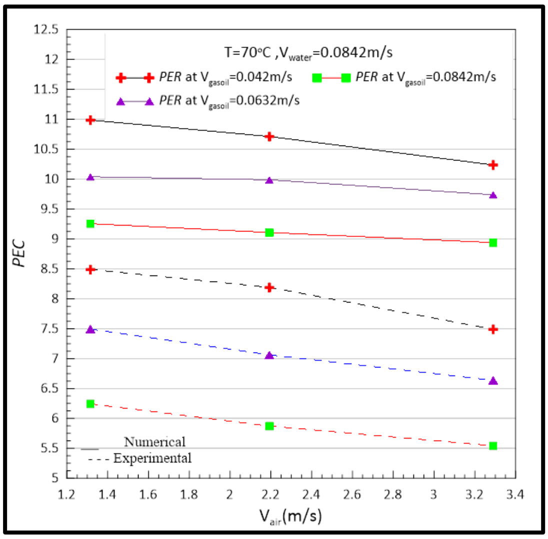

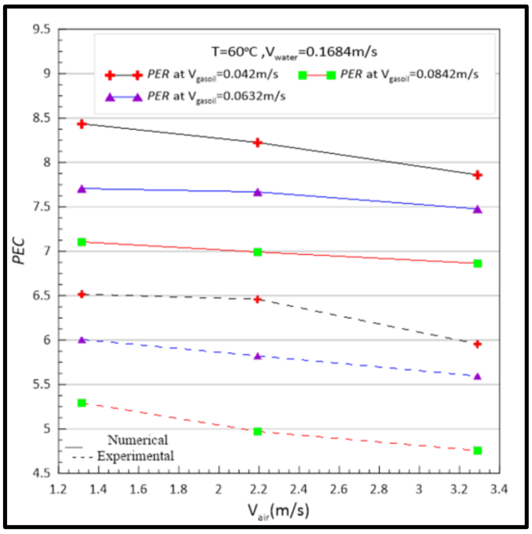

Figure (5.111). PCE. at. V$_{water}$=0.0842m/s **Figure (5.112).** PCE at. V$_{water}$= 0.0632m/s

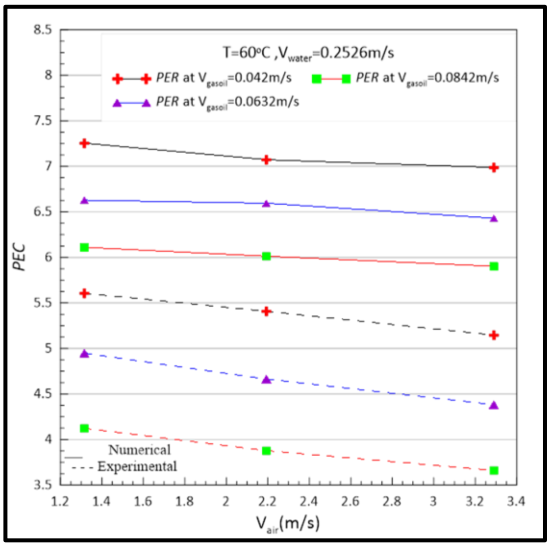

Figure (5.113). PCE at. V$_{water}$=0.2526m/s

5.5.7 Velocity distribution of Three-phase

Figure (5.112) shows the effect of increasing V_{gasoil} and V_{air} are 0.042m/s to 0.0842m/s and 1.3157m/s to 3.29m/s, respectively, when V_{water} is 0.0842m/s at T_{rib} constant 50˚C. It observed that the areas of increasing velocity start gradually from the ribbed regions so as to break boundary layer create more turbulence higher than two phase flow, where it notices the appearance of a greenish-yellow color until the greatest value of the mixture velocity of red orange color appeared reaches the bend region as a result of the presence of centrifugal force. The red region in cases of increasing V_{air} are higher than cases of increasing V_{gasoil}. The reason is that the air flow rate is higher than gasoil (high kinetic energy). Figure (5.113) shows the effect of increasing V_{gasoil} and V_{air} on the velocity distribution at constant V_{water}= 0.1684 m/s and varied air and gasoil as 1.3157m/s to 3.29m/s and 0.042m/s to 0.084m/s at T_{rib} about 50˚C respectively. It observed that the mixture velocity increases with increasing V_{air} and V_{gasoil} because of increased flow rates. The areas of the orange regions enlarged because the increasing flow rate quantity leads to high kinetic energy.

In comparison, Figures (5.112) and (5.113) observe the effect of increasing V_{water} from 0.0842 to 0.1684m/s at constant T_{rib} about 50˚C. It observed that the mixture velocity increases with increasing V_{water} because of more turbulence. Also, the orange region enlarged because of more kinetic energy. Figure (5.114) shows the effect of increasing V_{gasoil} and V_{air} are 0.042m/s to 0.0842m/s and 1.3157m/s to 3.29m/s ,respectively ,when V_{water} is 0.0842m/s at T_{rib} constant 60˚C .It observed that the velocity of mixture increases with increasing V_{gasoil} and V_{air} because of increased kinetic energy .Also, the areas of the orange regions enlarged because the increasing flow rates quantity lead to more kinetic energy and more turbulence .The orange region in cases of increasing V_{air} are higher than cases of increasing V_{gasoil} .The reason is that the air flow rate is higher than gasoil (high kinetic energy).

Figure (5.115) shows the effect of increasing V_{gasoil} and V_{air} on the velocity profile at constant T_{rib} about 60˚C a V_{water} is 0.1684 m/s and different V_{air} are 1.3157m/s to 3.29m/s .It observed that the velocity of mixture increases with increasing V_{air} and V_{gasoil} because of increased flow rates. The areas of the orange regions enlarged because the increasing flow rate quantity leads to high kinetic energy.

In comparison, Figures (5.114) and (5.115) observe the effect of increasing V_{water} from 0.0842 to 0.1684m/s at constant T_{rib} about 60˚C .It observed that the observed that the mixture velocity increases because of increased water flow rates .Also ,the orange region enlarged because of more kinetic energy.

Figure (5.116) shows the effect of increasing V_{gasoil} and V_{air} are 0.042m/s to 0.0842m/s and 1.3157m/s to 3.29m/s ,respectively ,when V_{water} is 0.0842m/s at T_{rib} constant 70˚C .It observed that the mixture velocity increases with increasing V_{gasoil} and V_{air} because of increased kinetic energy .Also, the areas of the orange regions enlarged because the increasing flow rates quantity lead to more kinetic energy and more turbulence .The orange region in cases of increasing V_{air} are higher than cases of increasing V_{gasoil} .The reason is that the air flow rate is higher than gasoil (high kinetic energy).

Figure (5.117) shows the effect of increasing V_{gasoil} (0.042m/s to 0.0842m/s) and V_{air} (1.3157m/s to 3.29m/s) on the velocity distribution at V_{water} is 0.1684 m/s at constant T_{rib} about 70˚C.It observed that the velocity of mixture increases with increasing V_{air} and V_{gasoil} because of increased flow rates. The areas of the orange regions enlarged because the increasing flow rate quantity leads to high kinetic energy.

In comparison, Figures (5.116) and (5.117) observe the effect of increasing V_{water} from 0.0842 to 0.1684m/s at constant T_{rib} about 70˚C .It observed that the increasing V_{water} lead to increase mixture velocity because of increasing flow rates. Also, the orange region enlarged because of more kinetic energy.

In comparison groups (5.112) to (5.117) represent the effect of increasing T_{rib} on mixture velocity distribution, it observed that the mixture velocity value increased with increasing T_{rib} because the kinetic energy increased so as to increase of temperature.

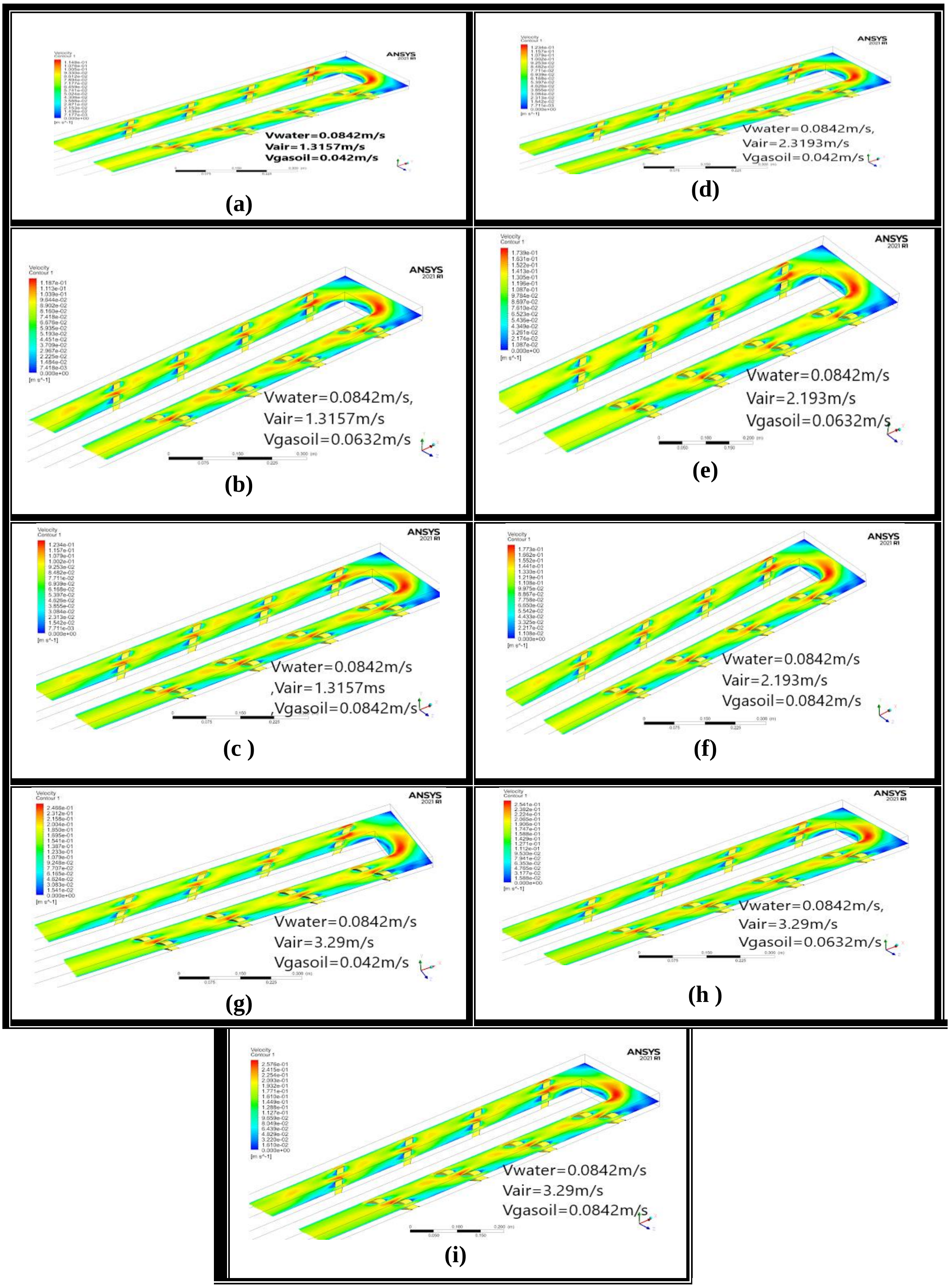

Figure (5.112): Velocity-distribution at V_{water}=0.0842m/s, T_{rib}=50^{o}C.

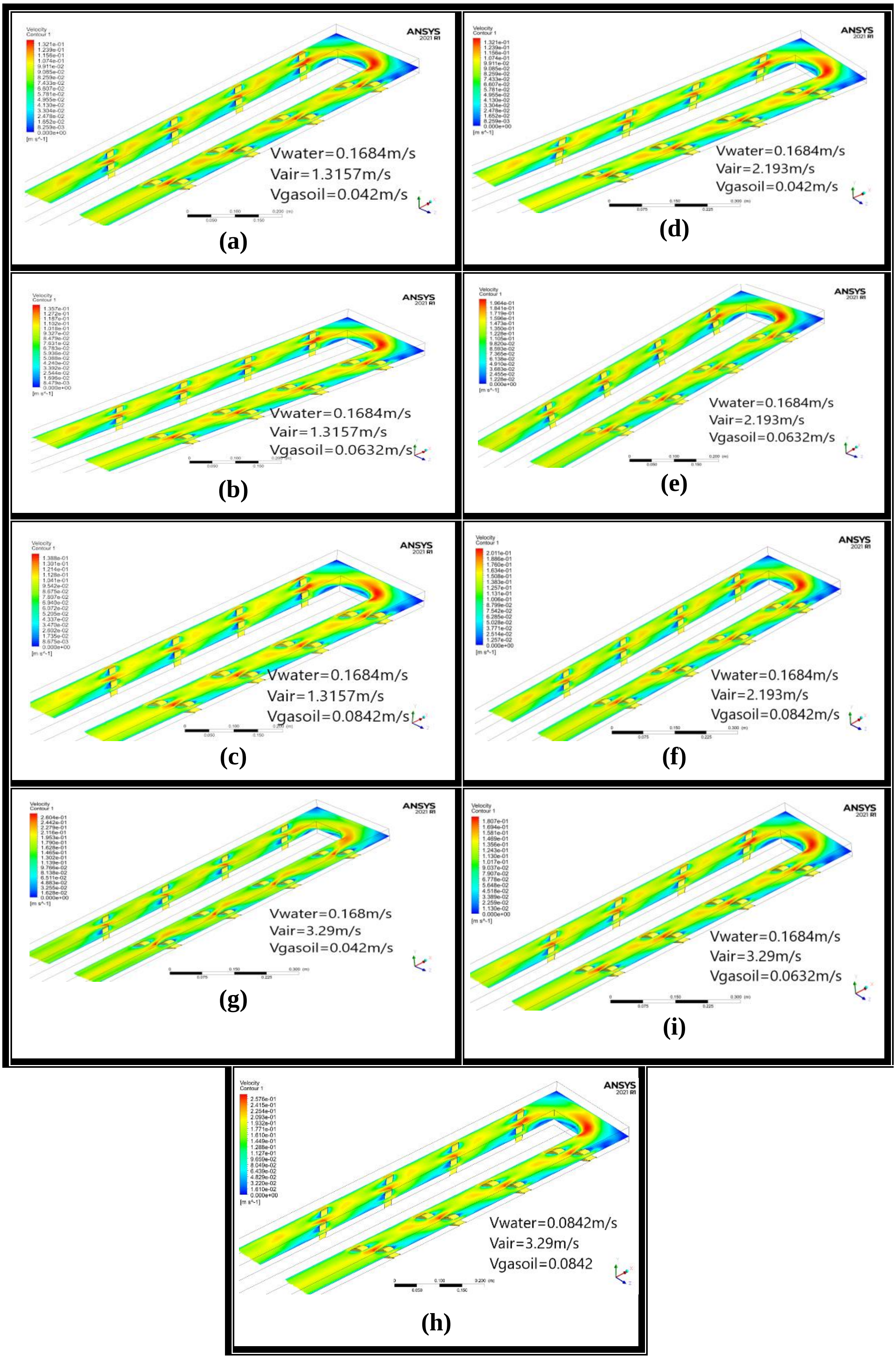

Figure (5.113): Velocity-distribution at V_{water}= 0.1684 m/s and T_{rib} =50°C.

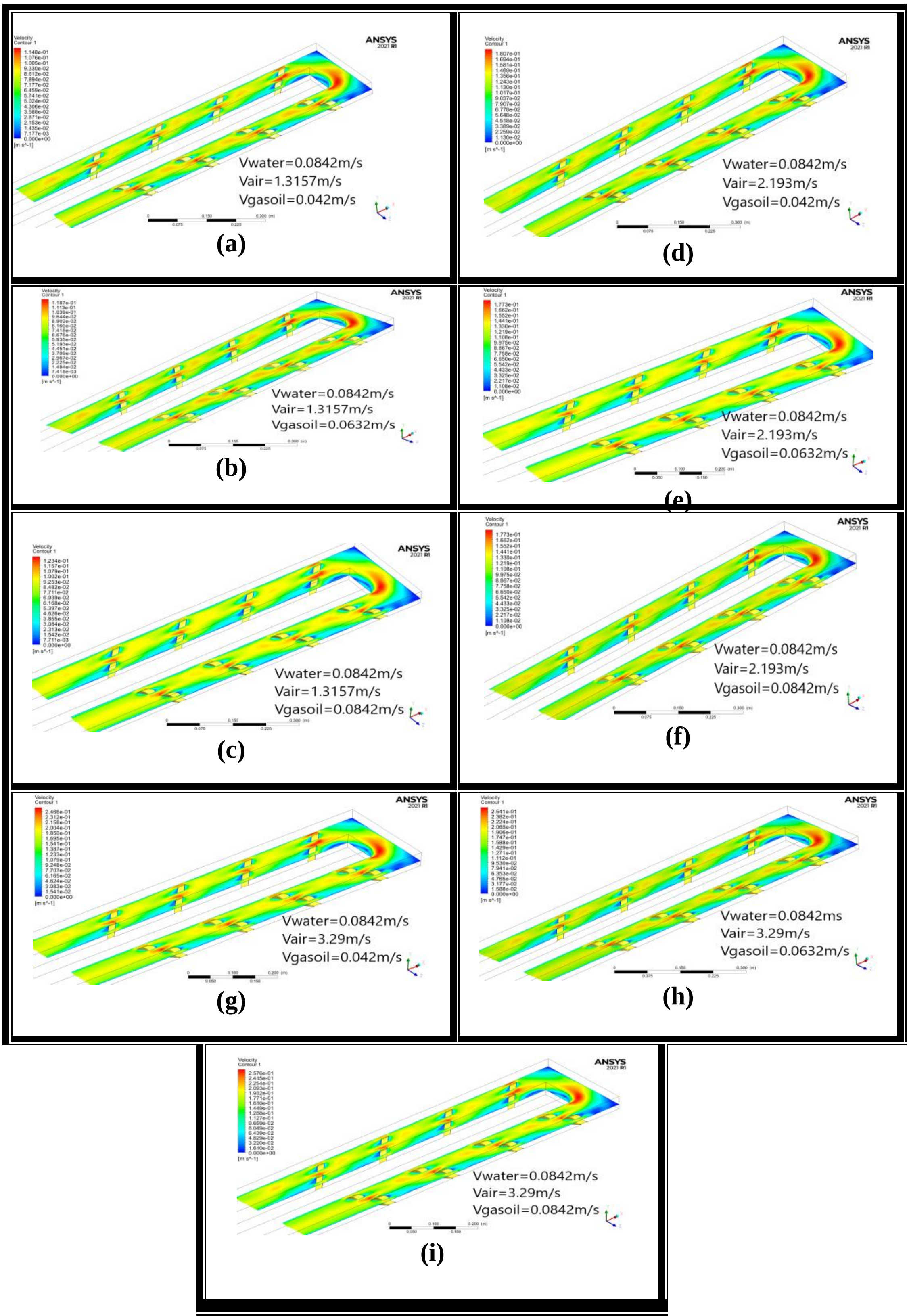

Figure (5.114). Velocity-distribution at V_{water}= 0.0842 m/s and T_{rib}=60^{o}C.

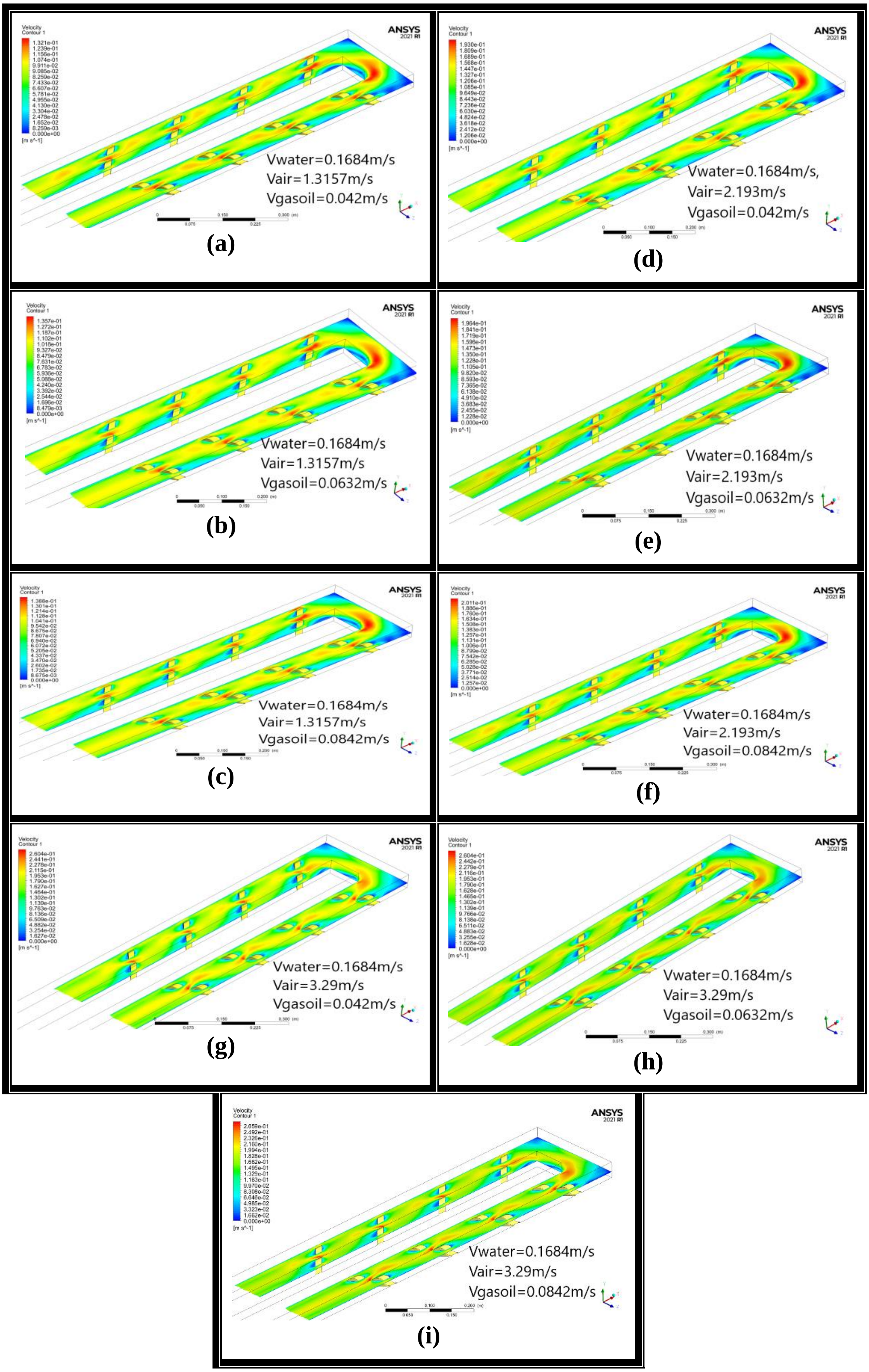

Figure (5.115): Velocity-distribution at V_{water}= 0.1684 m/s and T_{rib} =60°C

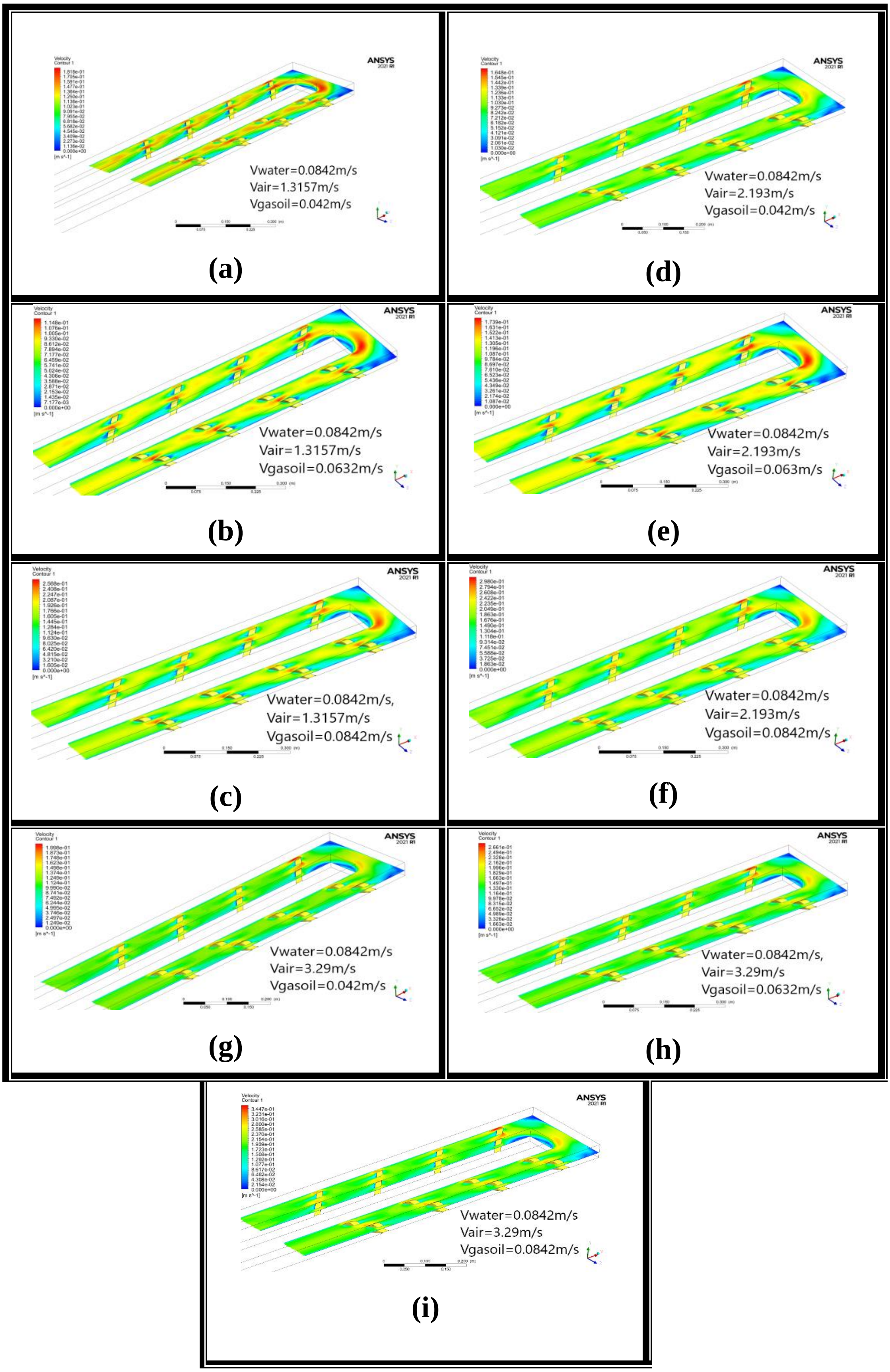

Figure (5.116). Velocity-distribution at V_{water}= 0.0842 m/s and T_{rib} =70°C.

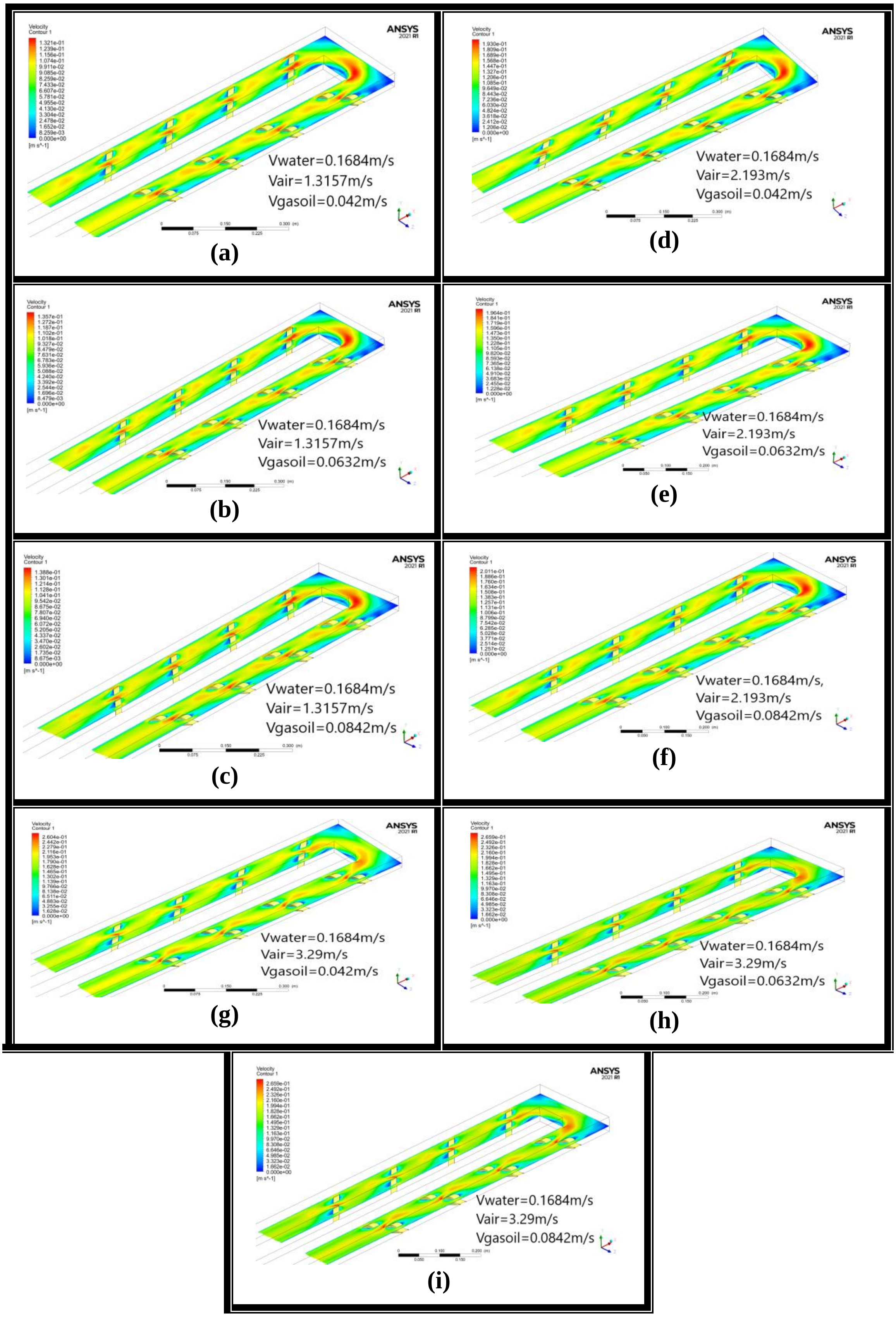

Figure (5.117). Velocity-distribution at V_{water}= 0.1684 m/s and T_{rib}

5.5.8 Pressure-distribution of Three-phase

Figure (5.118) shows the effect of increasing V_{gasoil} and V_{air} on pressure distribution and varying as 0.042m/s to 0.0842m/s and 1.3157m/s to 3.29m/s, respectively, when V_{water} is 0.0842m/s at T_{rib} constant 50˚C.It observed that the pressure decreased gradually with increasing V_{gasoil} and V_{air} according Bernoulli's principle until reach minimum in bend region because the mixture velocity reached maximum values.

Figure (5.119) shows the effect of increasing V_{gasoil} and V_{air} on pressure distribution and varying as 0.042m/s to 0.0842m/s and 1.3157m/s to 3.29m/s, respectively, when V_{water} is 0.1684 m/s at T_{rib} constant 50˚C.It observed that the pressure decreased gradually with increasing V_{gasoil} and V_{air} according Bernoulli's principle until reach minimum in bend region because the mixture velocity reached maximum values.

Figure (5.120) shows the effect of increasing V_{gasoil} and V_{air} on pressure distribution and varying as 0.042m/s to 0.0842m/s and 1.3157m/s to 3.29m/s, respectively, when V_{water} is 0.2526 m/s at T_{rib} constant 50˚C.It observed that the pressure decreased gradually with increasing V_{gasoil} and V_{air} according Bernoulli's principle until reach minimum in bend region because the mixture velocity reached maximum values.

Figure (5.121) shows the effect of increasing V_{gasoil} and V_{air} on pressure distribution and varying as 0.042m/s to 0.0842m/s and 1.3157m/s to 3.29m/s, respectively, when V_{water} is 0.0842m/s at T_{rib} constant 60˚C.It observed that the pressure decreased gradually with increasing V_{gasoil} and V_{air} according Bernoulli's principle until reach minimum in bend region because the mixture velocity reached maximum values.

Figure (5.122) shows the effect of increasing V_{gasoil} and V_{air} on pressure distribution and varying as 0.042m/s to 0.0842m/s and 1.3157m/s to 3.29m/s, respectively, when V_{water} is 0.1684m/s at T_{rib} constant 60˚C.It observed that the pressure decreased gradually with increasing V_{gasoil} and V_{air} according Bernoulli's principle until reach minimum in bend region because the mixture velocity reached maximum values.

Figure (5.123) shows the effect of increasing V_{gasoil} and V_{air} on pressure distribution and varying as 0.042m/s to 0.0842m/s and 1.3157m/s to 3.29m/s, respectively, when V_{water} is 0.2526m/s at T_{rib} constant 60˚C.It observed that the pressure decreased gradually with increasing V_{gasoil} and V_{air} according Bernoulli's principle until reach minimum in bend region because the mixture velocity reached maximum values.

In comparison the Figures (5.118) to (5.120), (5.121) to (5.123) and (5.124), these observed that increase in T_{rib} from 50˚C, 60˚C to 70˚C lead to increase pressure values of flow in channel because increase in kinetic energy of mixture and distances between particles.

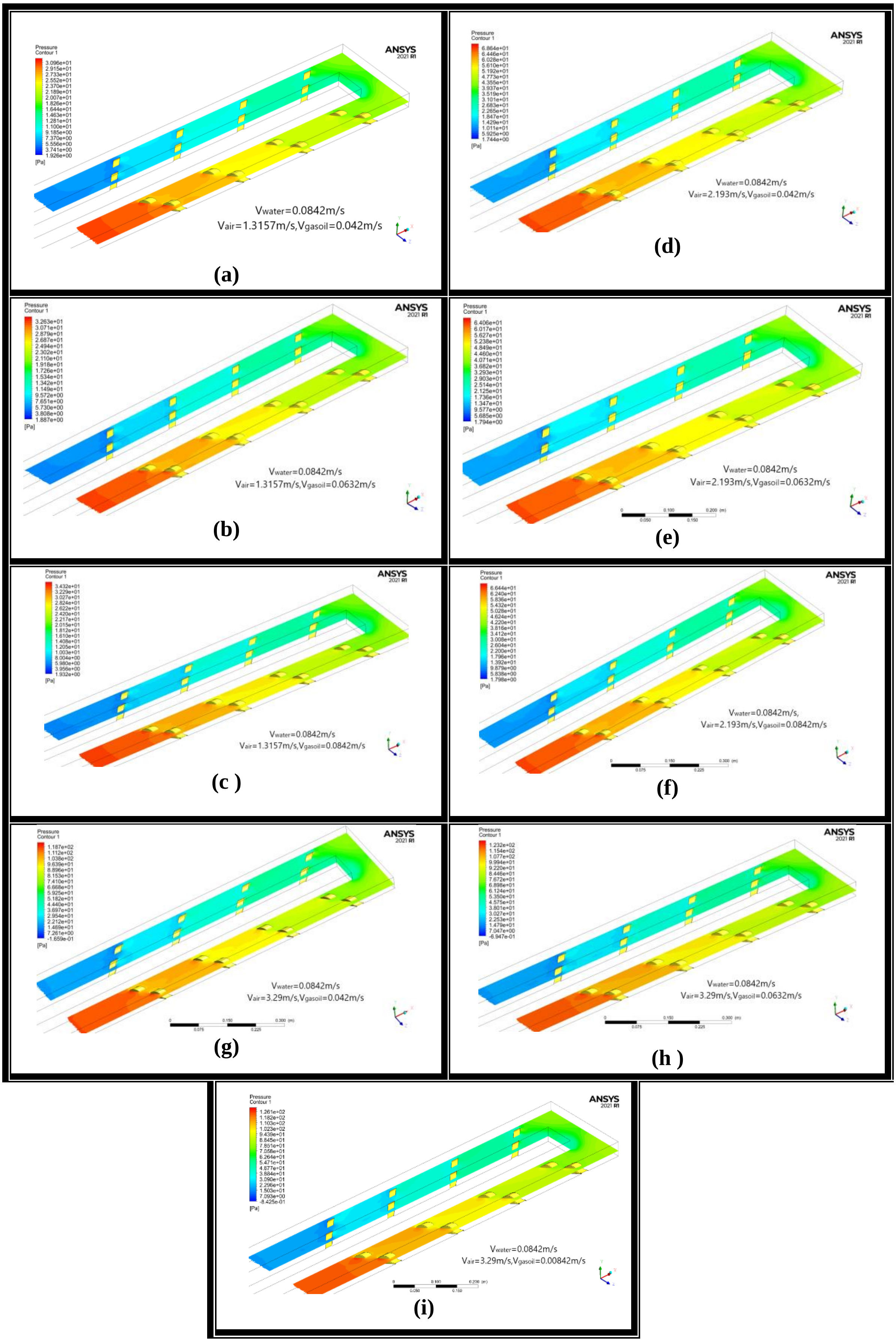

Figure (5.118): Pressure-distribution at V_{water}=0.0842m/s, T_{rib}=50^{o}C .

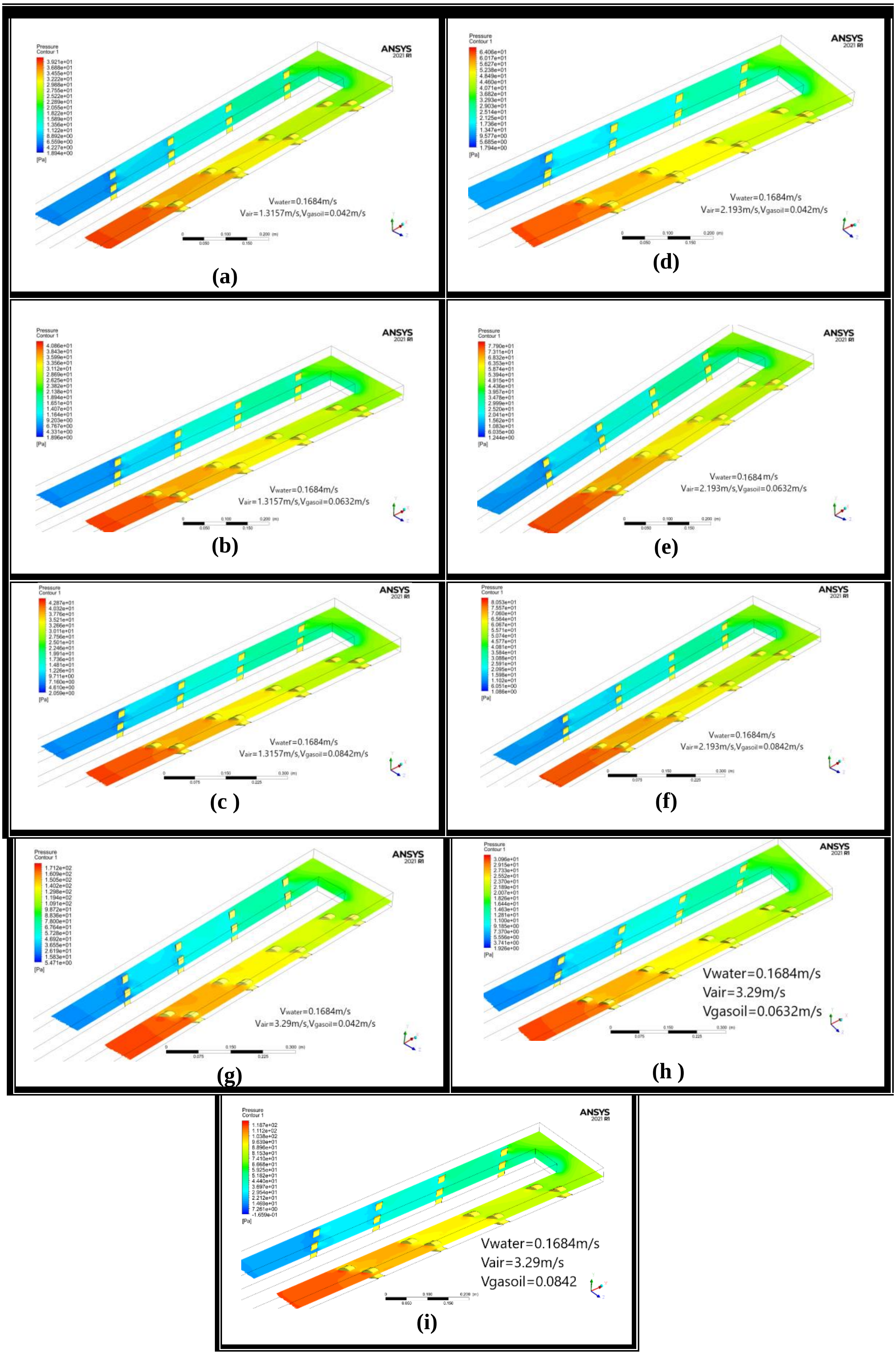

Figure (5.119): Pressure-distribution at V_{water}=0.1684m/s, T_{rib}=50°C .

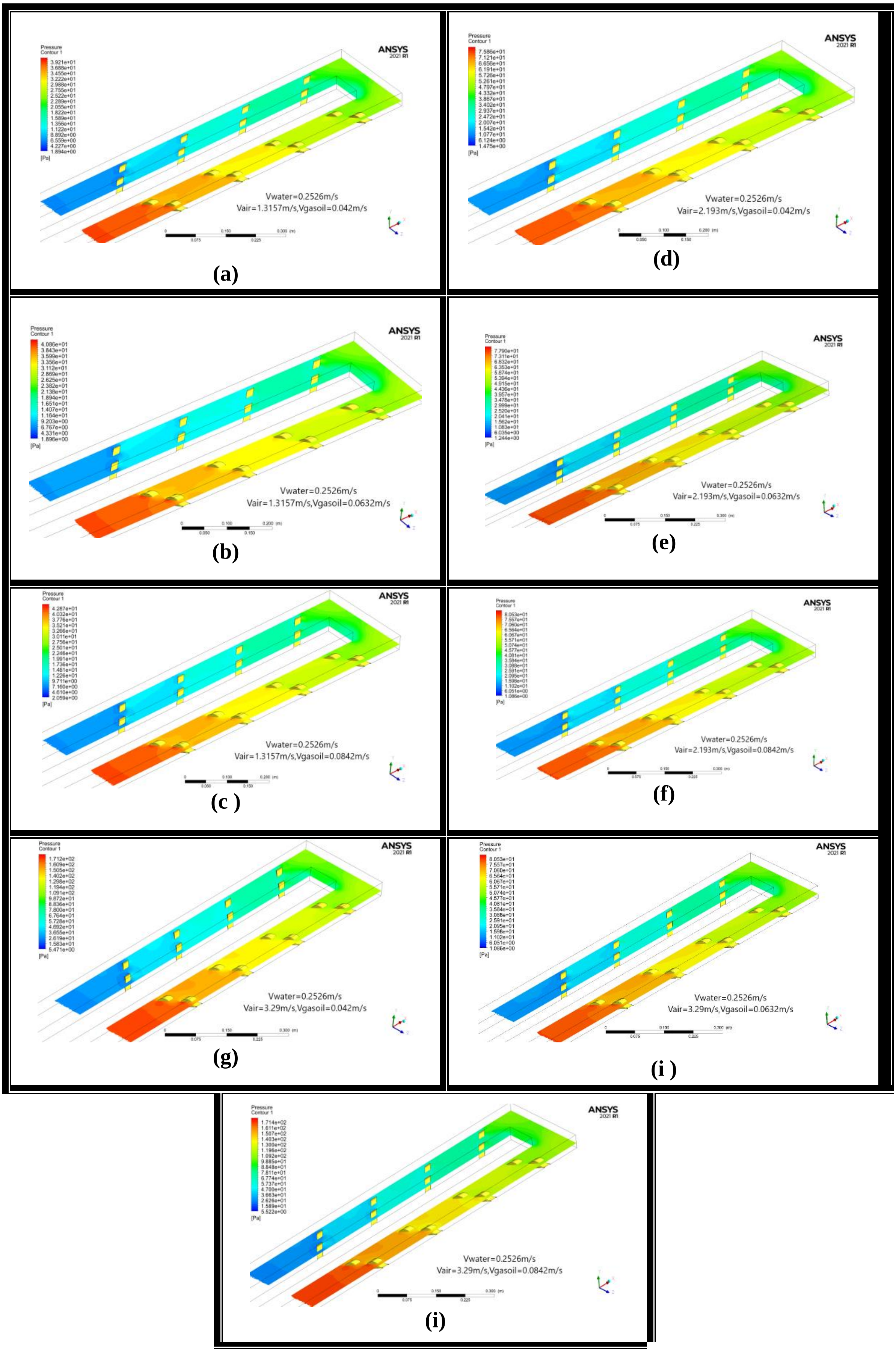

Figure (5. 120): Pressure-distribution at V_{water}=0.2526 m/s, T_{rib}=50°C .

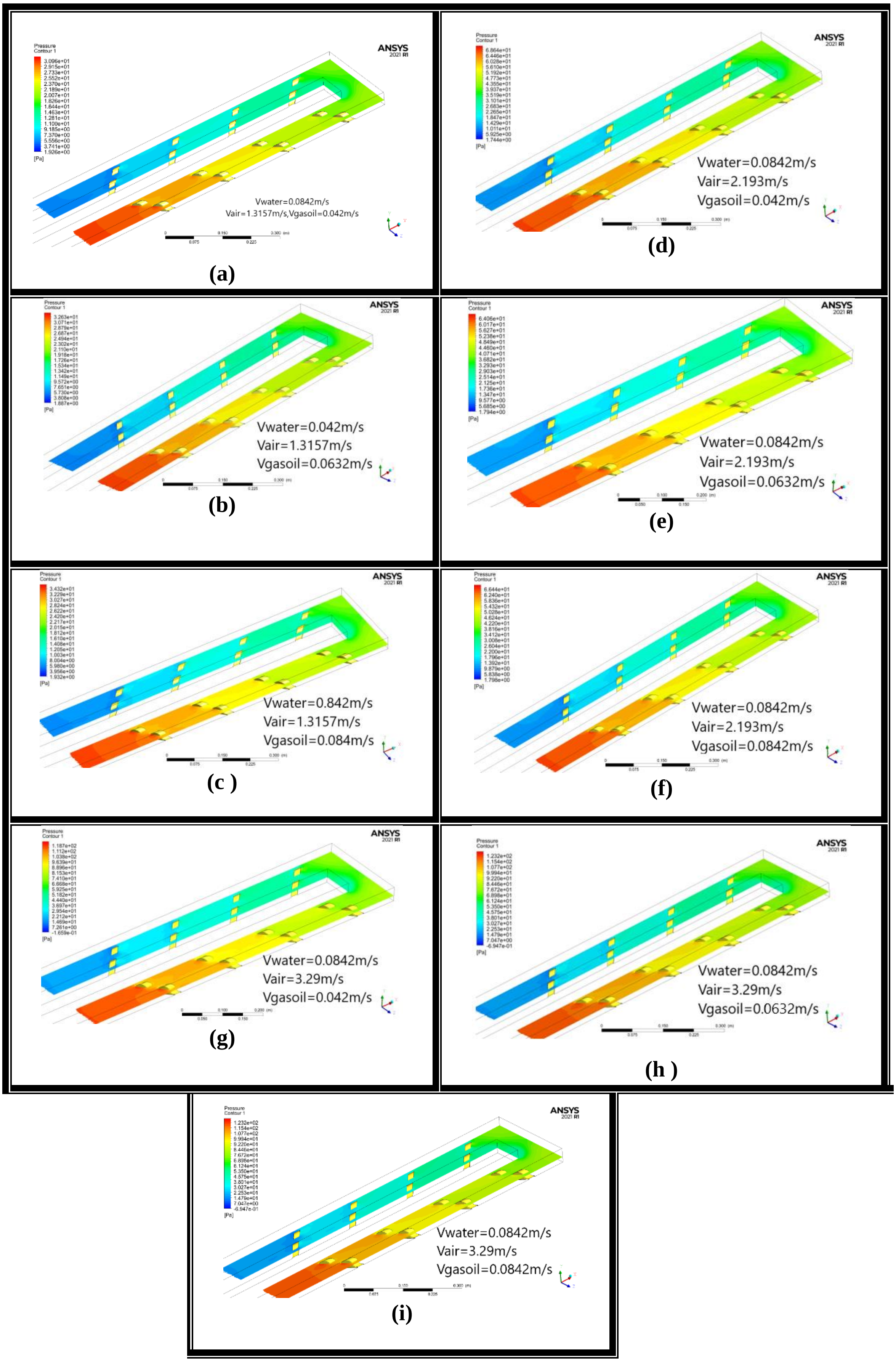

Figure (5.121): Pressure-distribution at V_{water}=0.0842m/s, T_{rib}=60^{o}C .

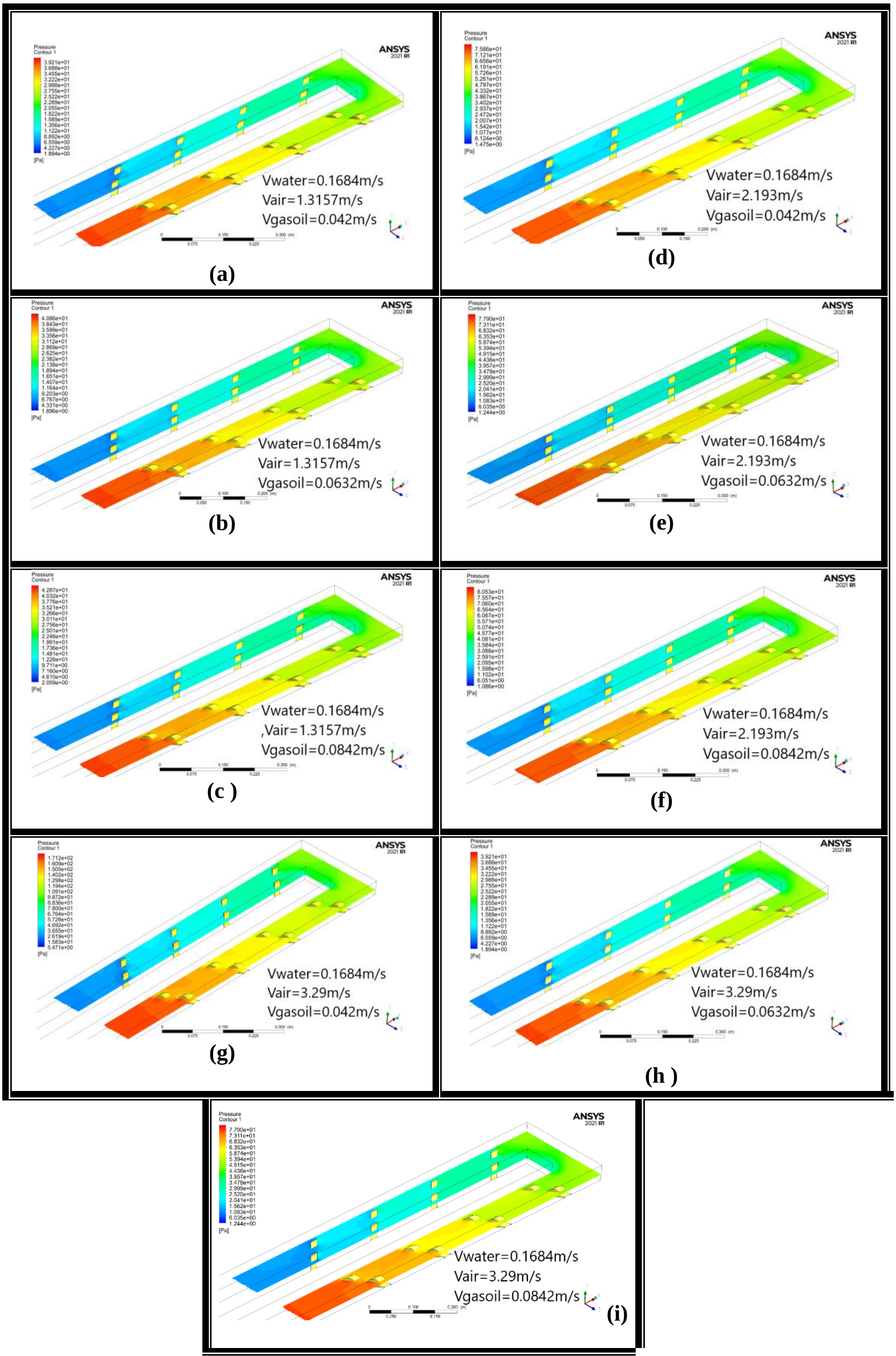

Figure (5. 122): Pressure-distribution at V_{water}=0.1684m/s, T_{rib}=60^{o}C .

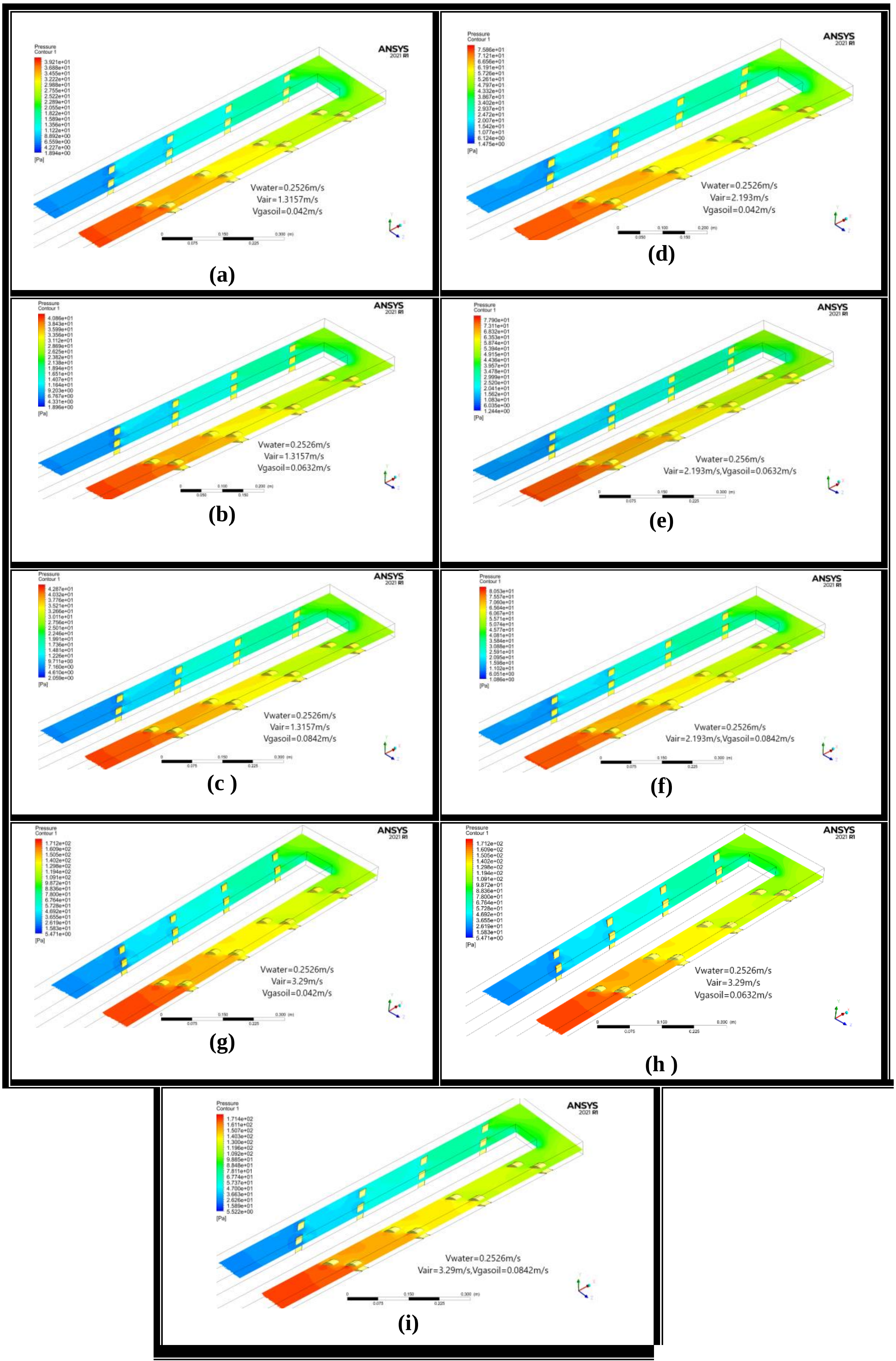

Figure (5. 123): Pressure-distribution at V_{water}=0.2526m/s, T_{rib}=60^{o}C.

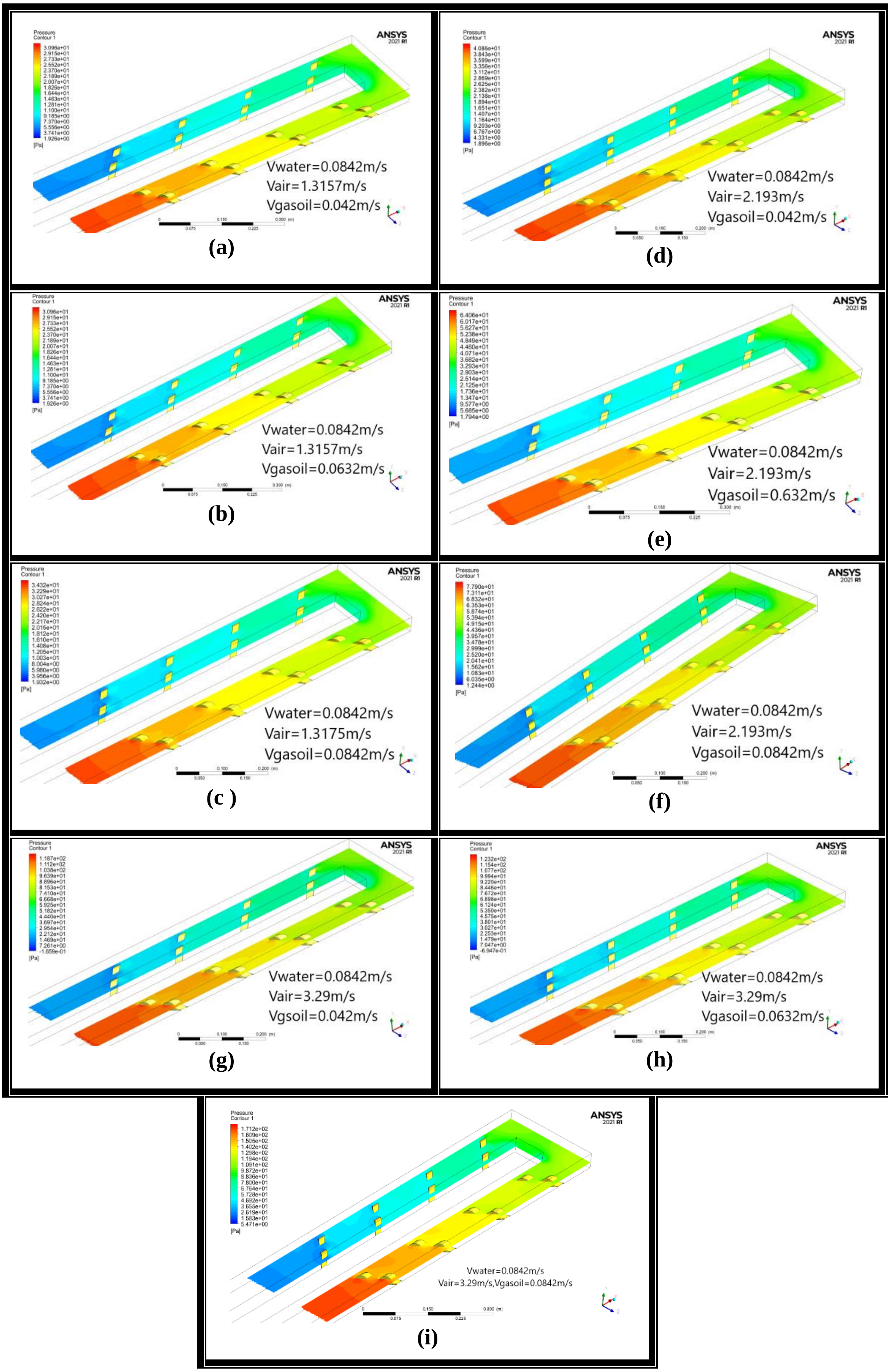

Figure (5.124): Pressure-distribution at V_{water}=0.0842/s, T_{rib}=70^{o}C .

5.5.9 Volume Fraction of Three-phase flow

It is one of the most important parameters used to characterize three-phase flow in channel and identify the volume of phase to another phases.

Figure (5.125) presents the distribution of three-phases in ribbed part and bend region at conditions V_{air} =2.193m/s and V_{gasoil}=0.0632m/s when at V_{water} equal 0.1684m/s and T_{rib} =60˚C.

Figure (5.125) (a) shows the air volume fraction and distribution along ribbed and bend part of channel. It observed that the distribution of phase more homogenous distribution than two-phase flow and air spaces are too small or vanishing because the turbulence made to efficient distribution.

Figure (5.125) (b) shows the gasoil volume fraction and distribution along ribbed and bend part of channel. It observed that the distribution of phase more homogenous because the turbulence made to efficient distribution. Figure (5.125) (c) shows the water volume fraction and distribution of air. It observed that the distribution of phase more homogenous distribution than two-phase flow and air spaces are too small or vanishing because the turbulence made to efficient distribution.

Also, the effect of increasing velocities by increase flow rates or by increase T_{rib} ,it works to increase turbulence and excellent mixing of the three phases inside the channel and the disappearance of the spaces for each phase that were clear in the case of two-phase flow.

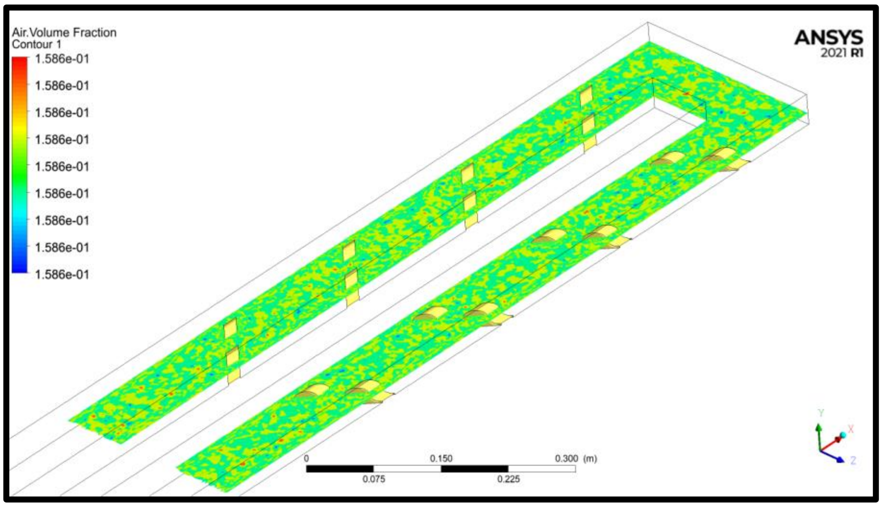

a) Air volume fraction.

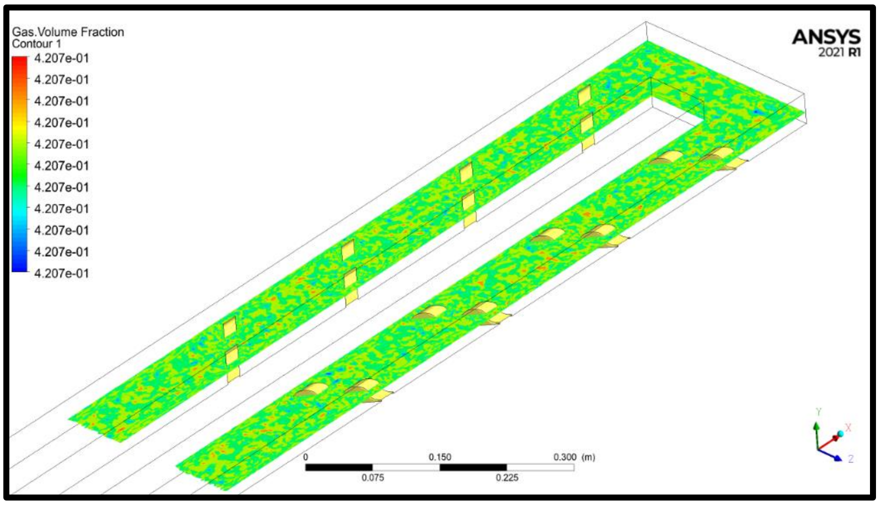

b) Gasoil volume fraction.

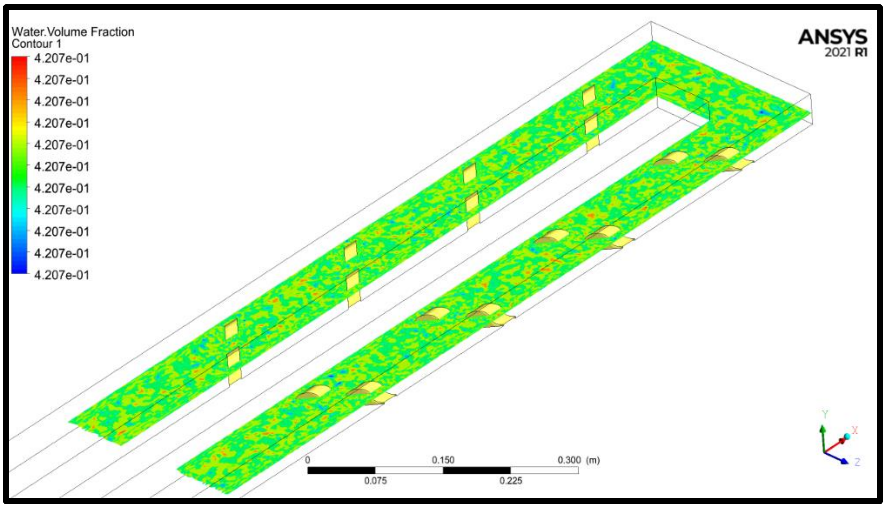

c) Water volume fraction.

Figure (5.125). Volume fraction of three phases.

5.5.10 Flow pattern of Three-phase flow behavior

To identify the flow pattern of three-phase flow is described by depending on velocities, characteristics of fluids and geometry. Through mixture flow, air and gasoil tend to separate up and water down so as to the gravity. Figure (5.126) (a) ,(b) and (c) shows the effect of increasing V_{gasoil} at constant V_{water}=0.0842m/s, V_{air}=1.3157m/s and T_{rib} equal to 50ºC .It observed that the mixture velocity increase with increasing V_{gasoil} from (0.042 to 0.0842)m/s because of gasoil flow rate increased . Also, the flow pattern is “Plug flow “because the values of mass flux for water and gasoil phases (liquid phase) determined on map as Plug pattern region in ranges 2100 $\geq G_{water+gasoil} \geq$ 300 and $G_{air} \leq$ 2 as APPENDIX D.

Figure (5.127) (a), (b) and (c) presents the effect of increasing V_{gasoil} (0.042 to 0.0842) m/s when V_{air} increased on the previous experiment to 2.193m/s at same above conditions. Also, the flow pattern is “Plug flow “because the values of mass flux for water and gasoil phases (liquid phase) determined on map as Plug pattern region in ranges 2100 $\geq G_{water+gasoil} \geq$ 300 and $G_{air} \leq$ 2 as APPENDIX D. The observation shows that volume of bubbles increases with increasing V_{air}.

Figure (5.128) (a), (b) and (c) presents the effect of increasing V_{gasoil} when V_{air} increased on the previous experiments to 3.29 m/s at same above conditions. The observation shows that volume of bubbles increases with increasing V_{air}. Also, the flow pattern is “Plug flow “because the values of mass flux for water and gasoil phases (liquid phase) determined on map as Plug pattern region in ranges 2100 $\geq G_{water+gasoil} \geq$ 300 and $G_{air} \leq$ 2 as APPENDIX D.

In comparison Figure (5.126), Figure (5.127) and Figure (5.128) at same T_{rib} and V_{water} grow up the size of the bubbles with more air flow rates.

Figure (5.129) (a) ,(b) and (c) shows the effect of increasing V_{gasoil} at constant V_{water}=0.1684m/s, V_{air}=1.3157m/s and T_{rib} equal to 50ºC .It observed that the mixture velocity increase with increasing V_{gasoil} from (0.042 to 0.0842)m/s because of gasoil flow rate increased . Also, the flow pattern is “Plug flow “because the values of mass flux for water and gasoil phases (liquid phase) determined on map as Plug pattern region in ranges 2100 $\geq G_{water+gasoil} \geq$ 300 and $G_{air} \leq 2$ as APPENDIX D.

Figure (5.130) (a), (b) and (c) presents the effect of increasing V_{gasoil} (0.042 to 0.0842) m/s when V_{air} increased on the previous experiment to 2.193m/s at same above conditions. Also, the flow pattern is “Plug flow “because the values of mass flux for water and gasoil phases (liquid phase) determined on map as Plug pattern region in ranges 2100 $\geq G_{water+gasoil} \geq$ 300 and $G_{air} \leq$ 2 as APPENDIX D.

The observation shows that volume of bubbles increases with increasing V_{air}. Figure (5.131) (a), (b) and (c) presents the effect of increasing V_{gasoil} when V_{air} increased on the previous experiments to 3.29 m/s at same above conditions. The observation shows that volume of bubbles increases with increasing V_{air}. Also, the flow pattern is “Plug flow “because the values of mass flux for water and gasoil phases (liquid phase) determined on map as Plug pattern region in ranges 2100 $\geq G_{water+gasoil} \geq$ 300 and $G_{air} \leq 2$ as APPENDIX D.

In comparison Figure (5.129), Figure (5.130) and Figure (5.131) at same T_{rib} and V_{water} grow up the size of the bubbles with more air flow rates.

Figure (5.132) (a) ,(b) and (c) shows the effect of increasing V_{gasoil} at constant V_{water}=0. 2526m/s, V_{air}=1.3157m/s and T_{rib} equal to 50°C. It observed that the mixture velocity increase with increasing V_{gasoil} from (0.042 to 0.0842) m/s because of gasoil flow rate increased. Also, the flow pattern is “Plug flow “because the values of mass flux for water and gasoil phases (liquid phase) determined on map as Plug pattern region in ranges 2100 $\geq G_{water+gasoil} \geq$ 300 and $G_{air} \leq 2$ as APPENDIX D.

Figure (5.133) (a), (b) and (c) presents the effect of increasing V_{gasoil} (0.042 to 0.0842) m/s when V_{air} increased on the previous experiment to 2.193m/s at same above conditions. Also, the flow pattern is “Plug flow “because the values of mass flux for water and gasoil phases (liquid phase) determined on map as Plug pattern region in ranges $2100 \geq G_{water+gasoil} \geq 300$ and $G_{air} \leq 2$ as APPENDIX D. The observation shows that volume of bubbles increases with increasing V_{air}. Figure (5.134) (a), (b) and (c) presents the effect of increasing V_{gasoil} when V_{air} increased on the previous experiments to 3.29 m/s at same above conditions. The observation shows that volume of bubbles increases with increasing V_{air}. Also, the flow pattern is “Plug flow “because the values of mass flux for water and gasoil phases (liquid phase) determined on map as Plug pattern region in ranges $2100 \geq G_{water+gasoil} \geq 300$ and $G_{air} \leq 2$ as APPENDIX D.

In comparison Figure (5.132), Figure (5.133) and Figure (5.134) at same T_{rib} and V_{water} grow up the size of the bubbles with more air flow rates.

Figure (5.135) (a) ,(b) and (c) shows the effect of increasing V_{gasoil} at constant V_{water}=0.0842m/s, V_{air}=1.3157m/s and T_{rib} equal to 60°C .It observed that the mixture velocity increase with increasing V_{gasoil} from (0.042 to 0.0842)m/s because of gasoil flow rate increased . Also, the flow pattern is “Plug flow “because the values of mass flux for water and gasoil phases (liquid phase) determined on map as Plug pattern region in ranges $2100 \geq G_{water+gasoil} \geq 300$ and $G_{air} \leq 2$ as APPENDIX D .

Figure (5.136) (a), (b) and (c) presents the effect of increasing V_{gasoil} (0.042 to 0.0842) m/s when V_{air} increased on the previous experiment to 2.193m/s at same above conditions. Also, the flow pattern is “Plug flow “because the values of mass flux for water and gasoil phases (liquid phase) determined on map as Plug pattern region in ranges $2100 \geq G_{water+gasoil} \geq 300$ and $G_{air} \leq 2$ as APPENDIX D.The observation shows that volume of bubbles increases with increasing V_{air}. Figure (5.137) (a), (b) and (c) presents the effect of increasing V_{gasoil} when V_{air} increased on the previous experiments to 3.29 m/s at same above conditions. The observation shows that volume of bubbles increases with increasing V_{air}. Also, the flow pattern is “Plug flow “ because the values of mass flux for water and gasoil phases (liquid phase) determined on map as Plug pattern region in ranges 2100 $\geq G_{water+gasoil} \geq 300$ and $G_{air} \leq 2$ as APPENDIX D .In comparison Figure (5.135), Figure (5.136) and Figure (5.137) at same T_{rib} and V_{water} grow up the size of the bubbles with more air flow rates. Figure (5.138) (a) ,(b) and (c) shows the effect of increasing V_{gasoil} at constant V_{water}=0.1684m/s, V_{air}=1.3157m/s and T_{rib} equal to 60^{o}C .It observed that the mixture velocity increase with increasing V_{gasoil} from (0.042 to 0.0842)m/s because of gasoil flow rate increased . Also, the flow pattern is “Plug flow “ because the values of mass flux for water and gasoil phases (liquid phase) determined on map as Plug pattern region in ranges 2100 $\geq G_{water+gasoil} \geq 300$ and $G_{air} \leq 2$ as APPENDIX D .Figure (5.139) (a), (b) and (c) presents the effect of increasing V_{gasoil} (0.042 to 0.0842) m/s when V_{air} increased on the previous experiment to 2.193m/s at same above conditions. Also, the flow pattern is “Plug flow “because the values of mass flux for water and gasoil phases (liquid phase) determined on map as Plug pattern region in ranges 2100 $\geq G_{water+gasoil} \geq 300$ and $G_{air} \leq 2$ as APPENDIX D. The observation shows that volume of bubbles increases with increasing V_{air}. Figure (5.140) (a), (b) and (c) presents the effect of increasing V_{gasoil} when V_{air} increased on the previous experiments to 3.29 m/s at same above conditions. The observation shows that volume of bubbles increases with increasing V_{air}. Also, the flow pattern is “Plug flow “ because the values of mass flux for water and gasoil phases (liquid phase) determined on map as Plug pattern region in ranges 2100 $\geq G_{water+gasoil} \geq 300$ and $G_{air} \leq 2$ as APPENDIX D.

In comparison Figure (5.138), Figure (5.139) and Figure (5.140) at same T_{rib} and V_{water} grow up the size of the bubbles with more air flow rates.

Figure (5.141) (a) ,(b) and (c) shows the effect of increasing V_{gasoil} at constant V_{water}=0. 2526m/s, V_{air}=1.3157m/s and T_{rib} equal to 60°C .It observed that the mixture velocity increase with increasing V_{gasoil} from (0.042 to 0.0842)m/s because of gasoil flow rate increased . Also, the flow pattern is "Plug flow " because the values of mass flux for water and gasoil phases (liquid phase) determined on map as Plug pattern region in ranges 2100 $\geq G_{water+gasoil} \geq$ 300 and $G_{air} \leq 2$ as APPENDIX D .
Figure (5.142) (a), (b) and (c) presents the effect of increasing V_{gasoil} (0.042 to 0.0842) m/s when V_{air} increased on the previous experiment to 2.193m/s at same above conditions. Also, the flow pattern is "Plug flow " because the values of mass flux for water and gasoil phases (liquid phase) determined on map as Plug pattern region in ranges 2100 $\geq G_{water+gasoil} \geq$ 300 and $G_{air} \leq 2$ as APPENDIX D .The observation shows that volume of bubbles increases with increasing V_{air}. Figure (5.143) (a), (b) and (c) presents the effect of increasing V_{gasoil} when V_{air} increased on the previous experiments to 3.29 m/s at same above conditions. The observation shows that volume of bubbles increases with increasing V_{air}. Also, the flow pattern is "Plug flow " because the values of mass flux for water and gasoil phases (liquid phase) determined on map as Plug pattern region in ranges 2100 $\geq G_{water+gasoil} \geq$ 300 and $G_{air} \leq 2$ as APPENDIX D.In comparison Figure (5.141), Figure (5.142) and Figure (5.143) at same T_{rib} and V_{water} grow up the size of the bubbles with more air flow rates.Figure (5.144) (a) ,(b) and (c) shows the effect of increasing V_{gasoil} at constant V_{water}=0.084m/s, V_{air}=1.3157m/s and T_{rib} equal to 70°C .It observed that the mixture velocity increase with increasing V_{gasoil} from (0.042 to 0.0842)m/s because of gasoil flow rate increased . Also, the flow pattern is "Plug flow "because the values of mass flux for water and gasoil phases (liquid phase) determined on map as Plug pattern region in ranges 2100 $\geq G_{water+gasoil} \geq$ 300 and $G_{air} \leq$ 2 as APPENDIX D.

Figure (5.145) (a), (b) and (c) presents the effect of increasing V_{gasoil} (0.042 to 0.0842) m/s when V_{air} increased on the previous experiment to 2.193m/s at same above conditions. Also, the flow pattern is "Plug flow "because the values of mass flux for water and gasoil phases (liquid phase) determined on map as Plug pattern region in ranges 2100 $\geq G_{water+gasoil} \geq$ 300 and $G_{air} \leq$ 2 as APPENDIX D.

The observation shows that volume of bubbles increases with increasing V_{air}. Figure (5.146) (a), (b) and (c) presents the effect of increasing V_{gasoil} when V_{air} increased on the previous experiments to 3.29 m/s at same above conditions. The observation shows that volume of bubbles increases with increasing V_{air}. Also, the flow pattern is "Plug flow " because the values of mass flux for water and gasoil phases (liquid phase) determined on map as Plug pattern region in ranges 2100 $\geq G_{water+gasoil} \geq$ 300 and $G_{air} \leq$ 2 as APPENDIX D.In comparison Figure (5.144), Figure (5.145) and Figure (5.146) at same T_{rib} and V_{water} grow up the size of the bubbles with more air flow rates .Figure (5.147) (a) ,(b) and (c) shows the effect of increasing V_{gasoil} at constant V_{water}=0.1684m/s, V_{air}=1.3157m/s and T_{rib} equal to 70°C .It observed that the mixture velocity increase with increasing V_{gasoil} from (0.042 to 0.0842)m/s because of gasoil flow rate increased . Also, the flow pattern is "Plug flow "because the values of mass flux for water and gasoil phases (liquid phase) determined on map as Plug pattern region in ranges 2100 $\geq G_{water+gasoil} \geq$ 300 and $G_{air} \leq$ 2 as APPENDIX D.

Figure (5.148) (a), (b) and (c) presents the effect of increasing V_{gasoil} (0.042 to 0.0842) m/s when V_{air} increased on the previous experiment to 2.193m/s at same above conditions. Also, the flow pattern is "Plug flow " because the values of mass flux for water and gasoil phases (liquid phase) determined on map as Plug pattern region in ranges 2100 $\geq G_{water+gasoil} \geq$ 300 and $G_{air} \leq$ 2 as APPENDIX D.The observation shows that volume of bubbles increases with increasing V_{air}. Figure (5.149) (a), (b) and (c) presents the effect of increasing V_{gasoil} when V_{air} increased on the previous experiments to 3.29 m/s at same above conditions. The observation shows that volume of bubbles increases with increasing V_{air}. Also, the flow pattern is “Plug flow “ because the values of mass flux for water and gasoil phases (liquid phase) determined on map as Plug pattern region in ranges $2100 \geq G_{water+gasoil} \geq 300$ and $G_{air} \leq 2$ as APPENDIX D .In comparison Figure (5.147), Figure (5.148) and Figure (5.149) at same T_{rib} and V_{water} grow up the size of the bubbles with more air flow rates.Figure (5.150) (a) ,(b) and (c) shows the effect of increasing V_{gasoil} at constant V_{water}=0. 2526m/s, V_{air}=1.3157m/s and T_{rib} equal to 70ºC. It observed that the mixture velocity increase with increasing V_{gasoil} from (0.042 to 0.0842) m/s because of gasoil flow rate increased. Also, the flow pattern is “Plug flow “ because the values of mass flux for water and gasoil phases (liquid phase) determined on map as Plug pattern region in ranges $2100 \geq G_{water+gasoil} \geq 300$ and $G_{air} \leq 2$ as APPENDIX D.Figure (5.151) (a), (b) and (c) presents the effect of increasing V_{gasoil} (0.042 to 0.0842) m/s when V_{air} increased on the previous experiment to 2.193m/s at same above conditions Also, the flow pattern is “Plug flow “ because the values of mass flux for water and gasoil phases (liquid phase) determined on map as Plug pattern region in ranges $2100 \geq G_{water+gasoil} \geq 300$ and $G_{air} \leq 2$ as APPENDIX D.The observation shows that volume of bubbles increases with increasing V_{air}. Figure (5.152) (a), (b) and (c) presents the effect of increasing V_{gasoil} when V_{air} increased on the previous experiments to 3.29 m/s at same above conditions. The observation shows that volume of bubbles increases with increasing V_{air}. Also, the flow pattern is “Plug flow “because the values of mass flux for water and gasoil phases (liquid phase) determined on map as Plug pattern region in ranges $2100 \geq G_{water+gasoil} \geq 300$ and $G_{air} \leq 2$ as APPENDIX D.In comparison Figure (5.149), Figure (5.151) and Figure (5.152) at same T_{rib} and V_{water} grow up the size of the bubbles with more air flow rates.

<table>
<tr><td colspan="2">T_{rib} =50ºC</td></tr>
<tr><td colspan="2">V_{water} =0.0842m/s</td></tr>
<tr><td>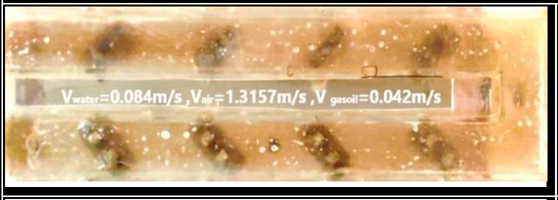</td><td>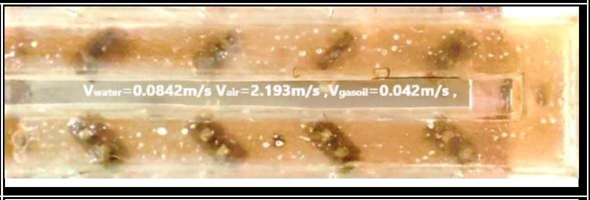</td></tr>
<tr><td>-a-</td><td>-a-</td></tr>
<tr><td>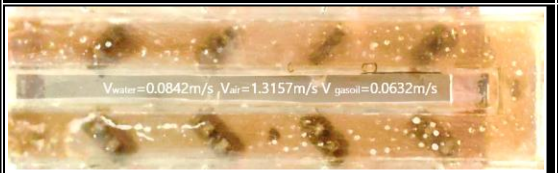</td><td>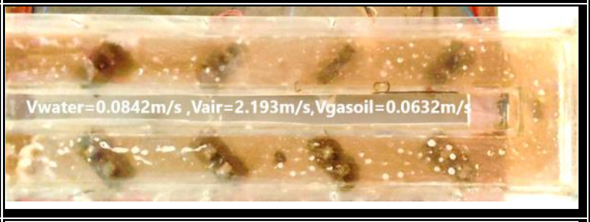</td></tr>
<tr><td>-b-</td><td>-b-</td></tr>
<tr><td>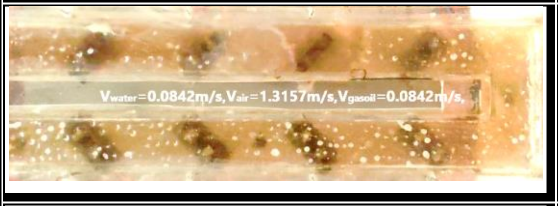</td><td>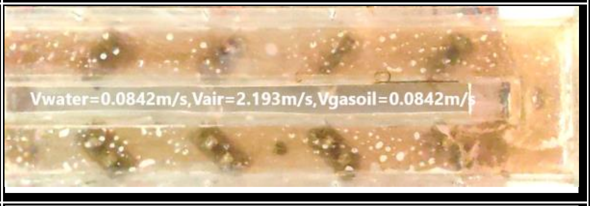</td></tr>
<tr><td>-c-</td><td>-c-</td></tr>
</table>

Figure (5.126). Pattern V_{air} =1.3157m/s **Figure(5.127).**Pattern V_{air} =2.193m/s

<table>
<tr><td colspan="2">T_{rib} =50ºC</td></tr>
<tr><td>V_{water} =0.0842m/s</td><td>V_{water} =0.1684m/s</td></tr>
<tr><td>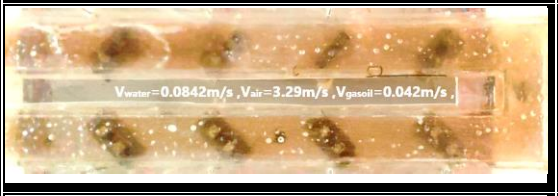</td><td>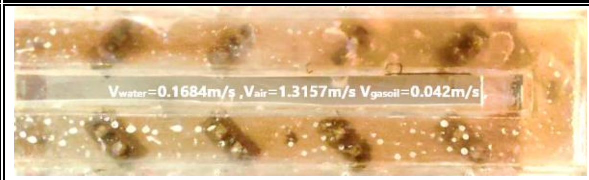</td></tr>
<tr><td>-g-</td><td>-a-</td></tr>
<tr><td>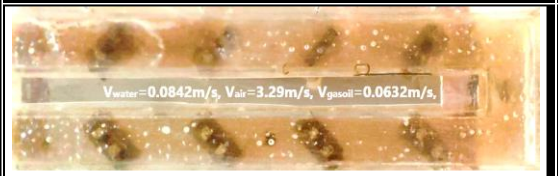</td><td>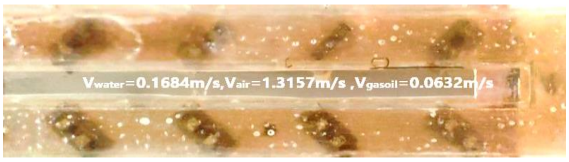</td></tr>
<tr><td>-h-</td><td>-b-</td></tr>
<tr><td>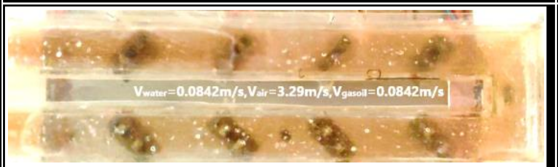</td><td>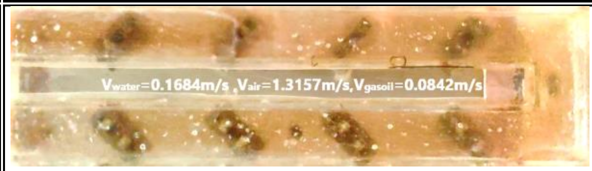</td></tr>
<tr><td>-i-</td><td>-c-</td></tr>
</table>

Figure (5.128). PatternV_{air} =3.29m/s **Figure(5.129).**Pattern V_{air} =1.3157m/s

T_{rib} =50°C

V_{water} =0.1684m/s

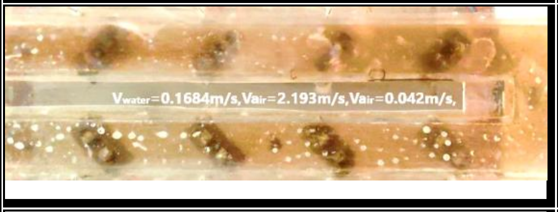

-d-

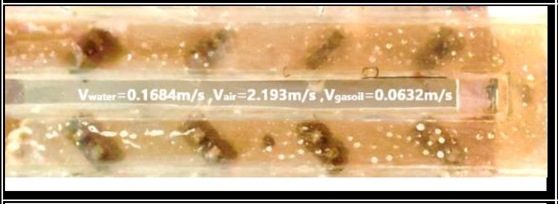

-e-

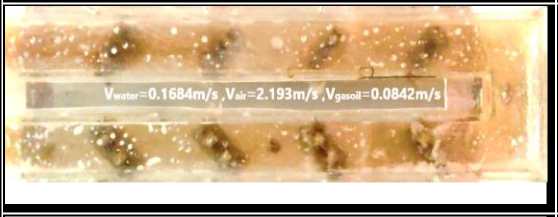

-f-

Figure (5.130). Pattern V_{air} =2.193m/s

V_{water} =0.1684m/s

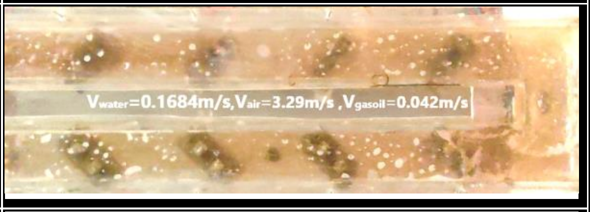

-g-

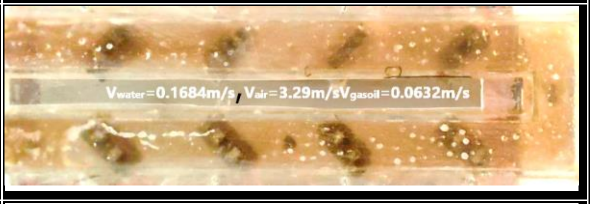

-h-

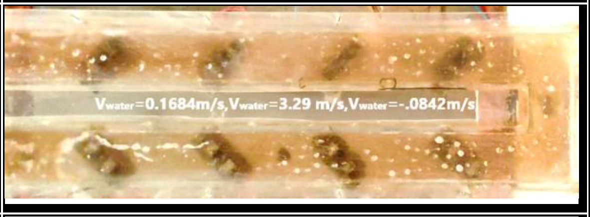

-i-

Figure(5.131). Pattern V_{air} =3.29m/s

T_{rib} =50°C

V_{water} =0.2526m/s

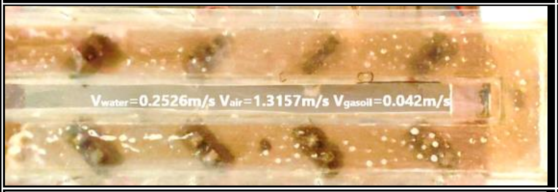

-a-

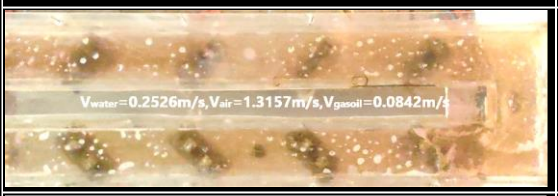

-b-

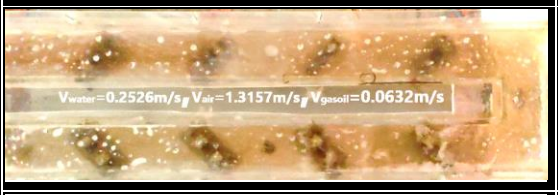

-c-

Figure (5.132). Pattern V_{air} =1.3157m/s

T_{rib} =50°C

V_{water} =0.2526m/s

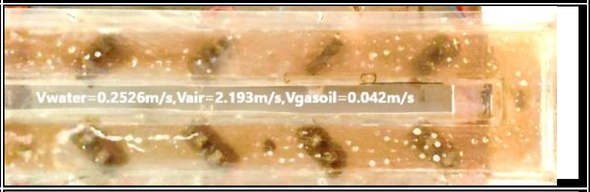

-d-

-e-

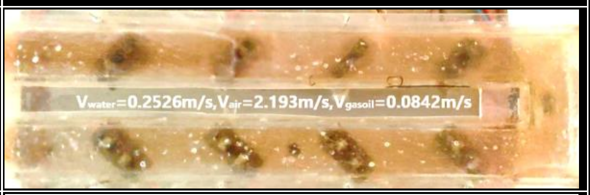

-f-

Figure(5.133). Pattern V_{air} =2.193m/s

T_{rib} =50°C

V_{water} =0.2526m/s

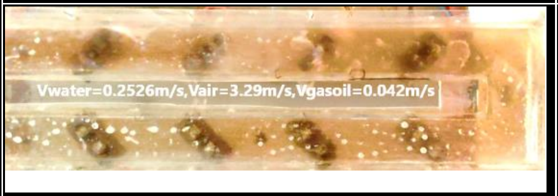

-g-

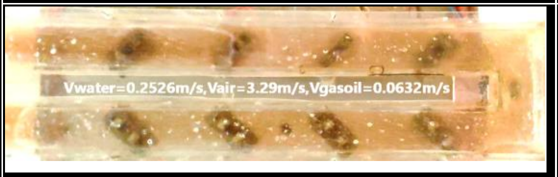

-h-

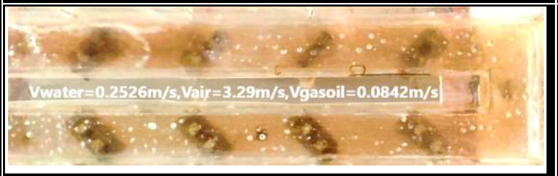

-i-

Figure(5.134). Pattern V_{air} =3.29m/**s**

T_{rib} =60°C

V_{water} =0.0842m/s

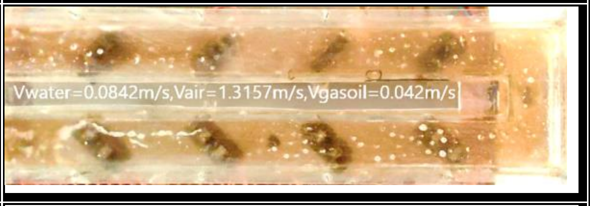

-a-

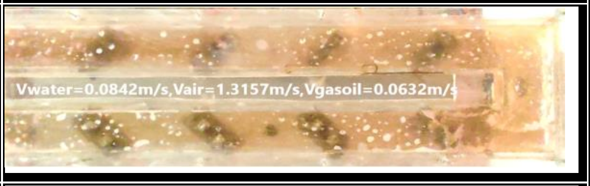

- -b-

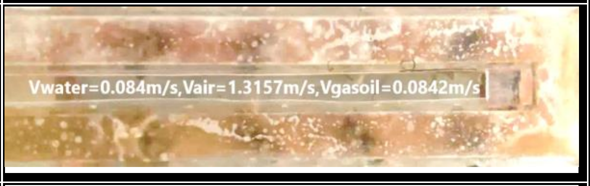

-c-

Figure(5.135). Pattern V_{air} =1.3157m/s

T_{rib} =60°C

V_{water} =0.0842m/s

-d-

-e-

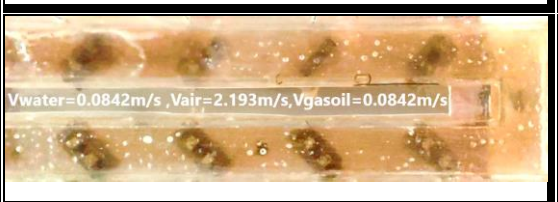

-f-

Figure (5.136). Pattern V_{air} =2.193m/s

T_{rib} =60°C

V_{water} =0.0842m/s

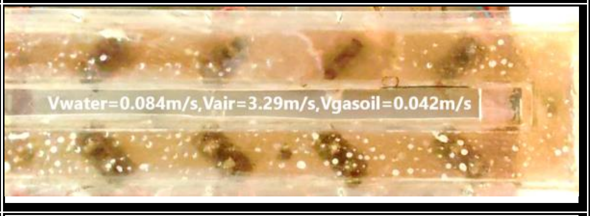

-g-

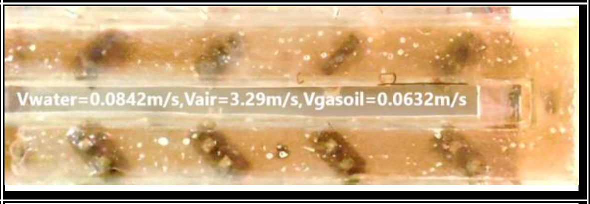

-h-

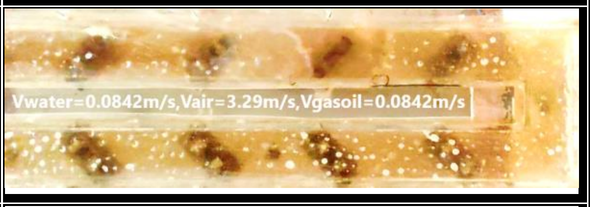

-i-

Figure (5.137). Pattern V_{air} =3.29m/s

T_{rib} =60°C

V_{water} =0.1684m/s

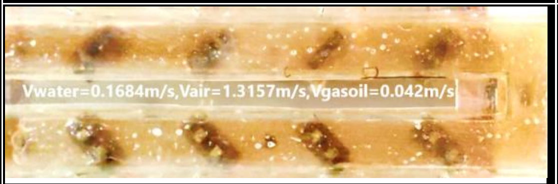

-a-

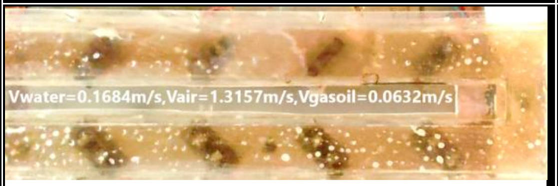

-b-

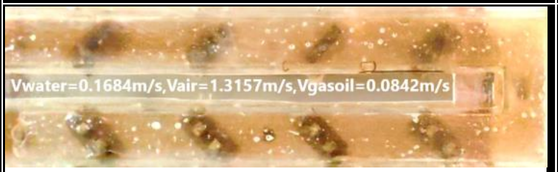

-c-

Figure (5.138). Pattern V_{air} =1.3157m/s

T_{rib} =60°C

V_{water} =0.1684m/s

-d-

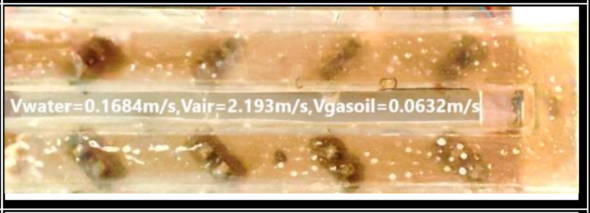

-e-

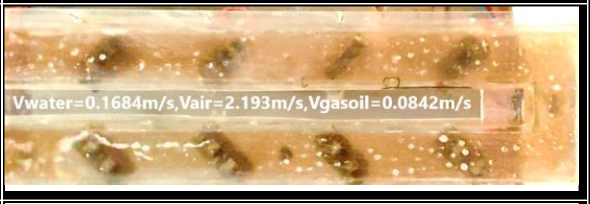

-f-

Figure(5.139). Pattern V_{air} =2.193m/s

T_{rib} =60°C

V_{water} =0.1684m/s

-g-

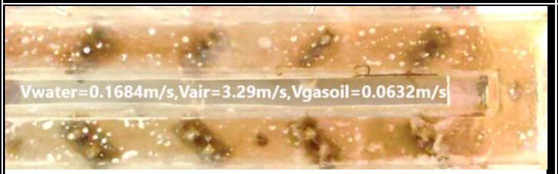

-h-

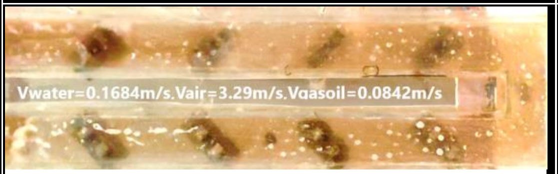

-i-

Figure (5.140). Pattern V_{air} =3.29m/s

T_{rib} =60°C

V_{water} =0.2526m/s

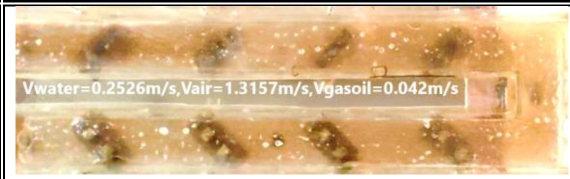

-a-

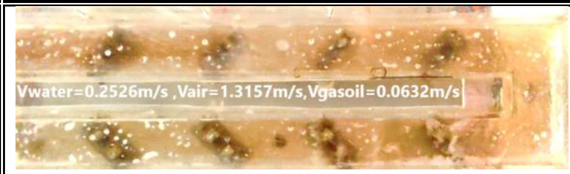

-b-

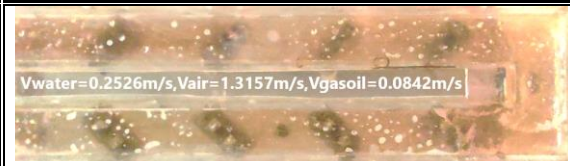

-c-

Figure(5.141). Pattern V_{air} =1.3157m/s

T_{rib} =60°C

V_{water} =0.2526m/s

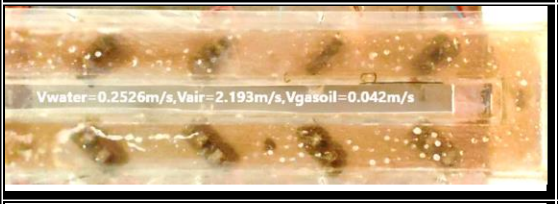

-d-

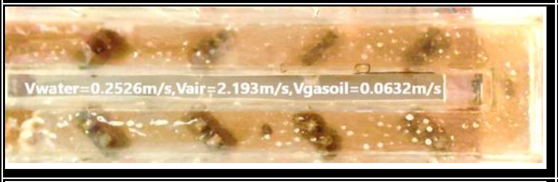

-e-

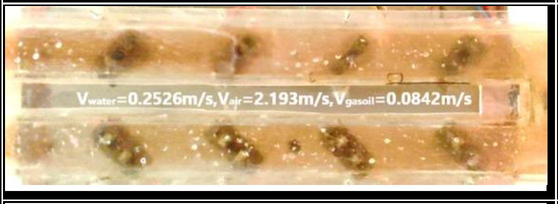

-f-

Figure(5.142). Pattern V_{air} =2.193m/s

T_{rib} =60°C

V_{water} =0.2526m/s

-g-

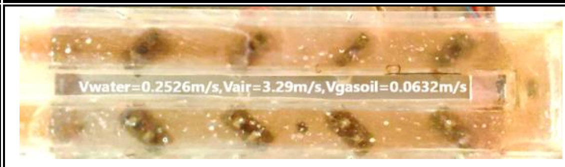

-h-

-i-

Figure(5.143). Pattern V_{air} =3.29m/s

T_{rib} =70°C

V_{water} =0.0842m/s

-a-

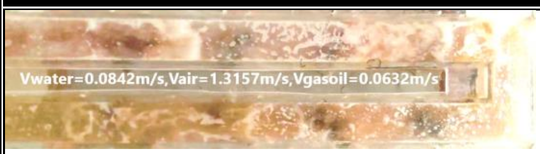

-b-

-c-

Figure (5.144). Pattern V_{air} =1.3157m/s

T_{rib} =70°C

V_{water} =0.0842m/s

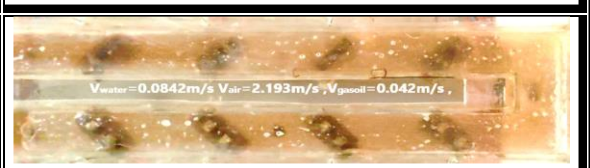

-d-

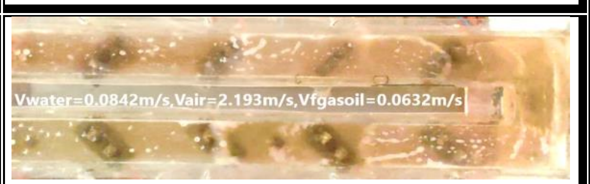

-e-

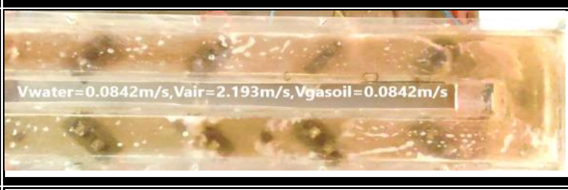

-f-

Figure(5.145). Pattern V_{air} =2.193m/s

T_{rib} =70ºC	T_{rib} =70ºC
V_{water} =0.0842m/s	**V_{water} =0.1684m/s**
	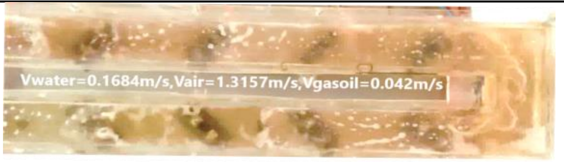
-g-	**-a-**
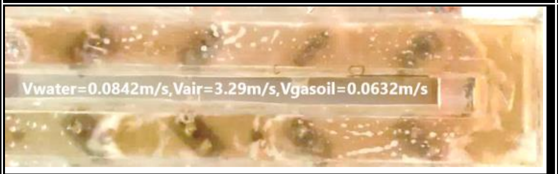	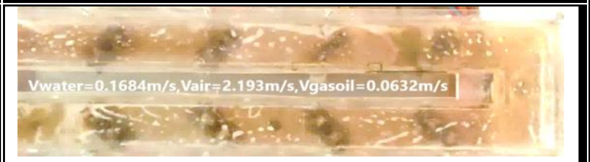
-h-	**-b-**
	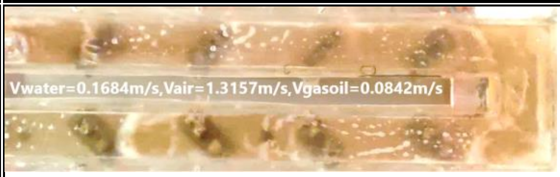
-i-	**-c-**

Figure (5.146). Pattern V_{air} =3.29m/s **Figure(5.147).**Pattern V_{air} =1.3157m/s

T_{rib} =70ºC	T_{rib} =70ºC
V_{water} =0.1684m/s	**V_{water} =0.1684m/s**
	
-a-	**-d-**
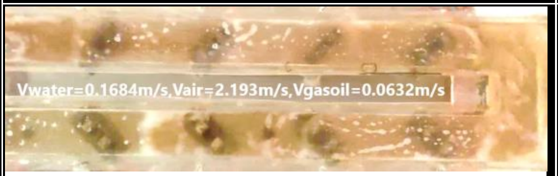	
-b-	**-e-**
	
-c-	**-f-**

Figure (5.148). Pattern V_{air} =2.193m/s **Figure(5.149).**Pattern V_{air} =3.29m/s

T_{rib} =70ºC

V_{water} =0.2526m/s

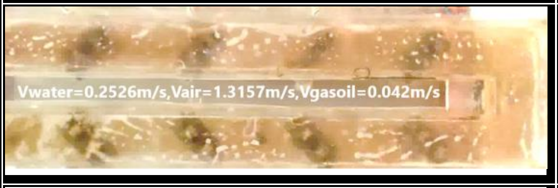

-a-

-b-

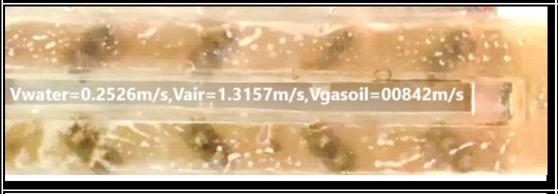

-c-

Figure (5.150). Pattern V_{air} =1.3157m/s

T_{rib} =70ºC

V_{water} =0.2526m/s

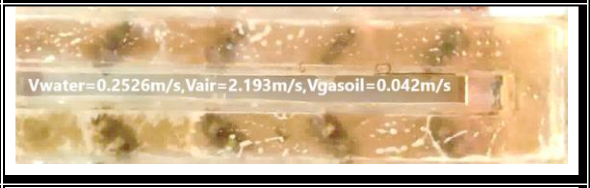

-d-

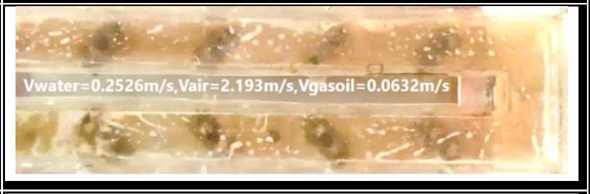

-e-

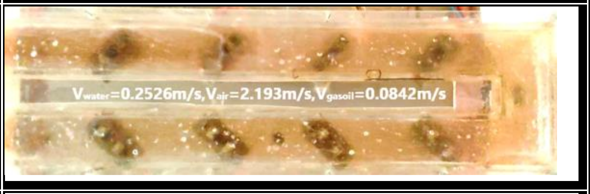

-f-

Figure(5.151). Pattern V_{air} =2.193m/s

T_{rib} =70ºC

V_{water} =0.2526m/s

-g-

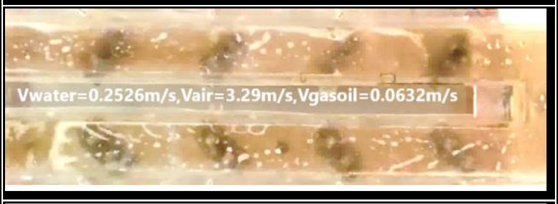

-h-

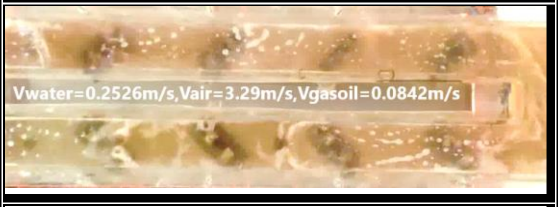

-i-

Figure (5.152). Pattern V_{air} =2.193m/s

5.6 Comparison between Numerical and Experimental.

To clarify the deviations between numerical results and experimental results, it is necessary to discuss and analysis these reasons. Figure (5.153) shows the deviation between numerical and experimental results for two phase flow at conditions V_{water}=0.1684m/s at constant T_{rib}=60°C.It observed that the deviations of Nu, temperature of fluid, ΔP, and f/f_o have about 9.5 % ,0.2 %,11.6 %, and 5.21 % respectively. Because numerical results assumed that the experiments performed at steady state conditions and neglected all influences from weather conditions, the state of device, accuracy of measuring devices and calibration, etc. Also, the uncertainties are neglected, but the experimental side, which takes all these influences. All above reasons lead to that the numerical results higher than experimental.

Figure (5.154) shows the deviation in coefficients of heat transfer for three phase flow at conditions V_{water}=0.1684m/s and V_{gasoil}=0.1684m/s at constant T_{rib}=60°C.It observed that the deviations of Nu, temperature of fluid, ΔP and f/f_o have about 9.02 % ,0.5 %,12.7 %,and 6.23 % respectively.

The reasons of deviations that the numerical results assumed that the experiments performed at steady state conditions and neglected all influences from weather conditions, the state of device, accuracy and errors of measuring devices, calibration and neglected the uncertainties. While the experimental side performed at real conditions, which takes all these influences. All above reasons lead to that the numerical results higher than experimental.

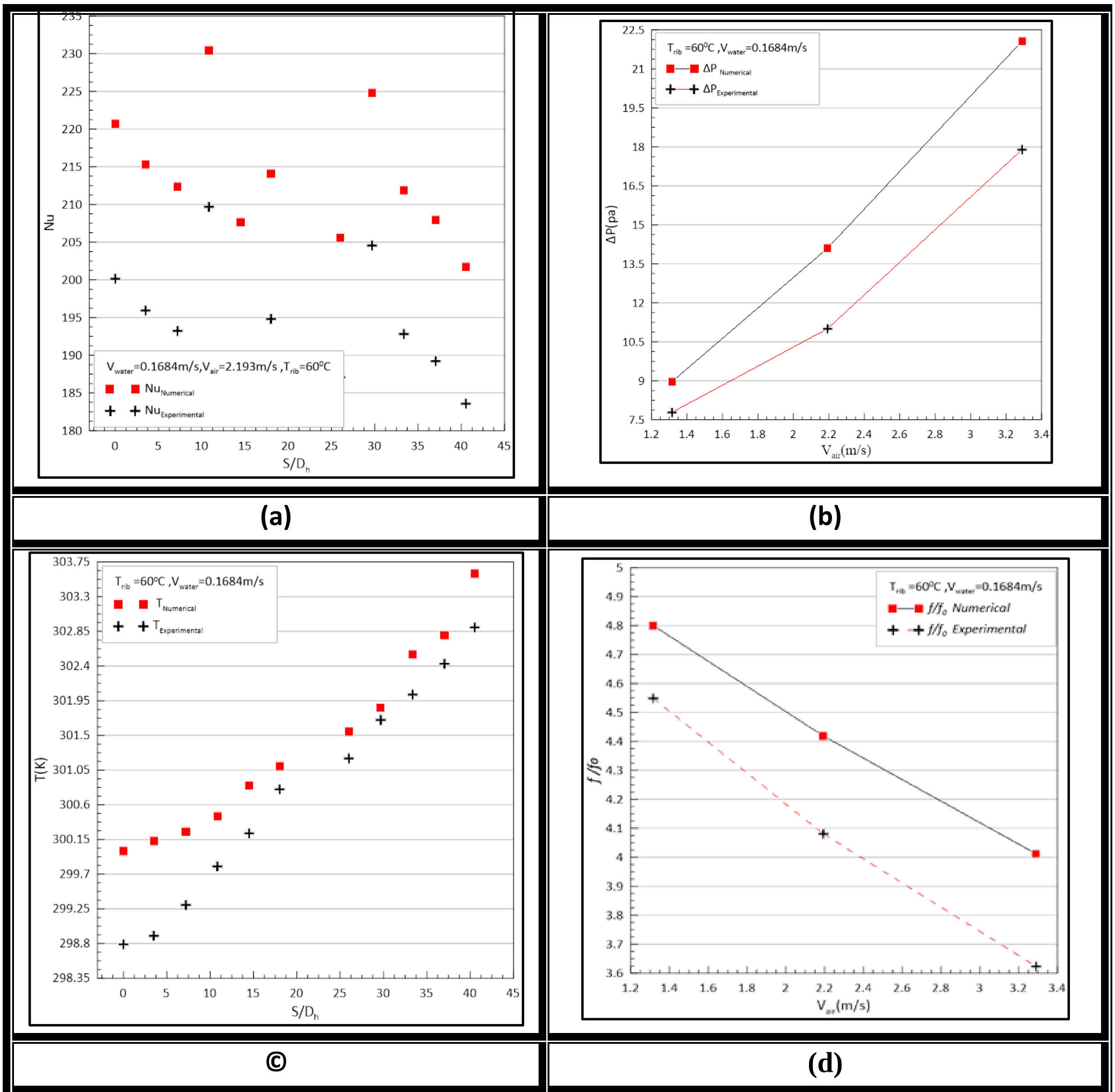

Figure (5.153). Comparison of Numerical and Experimental for Two-Phase flow.

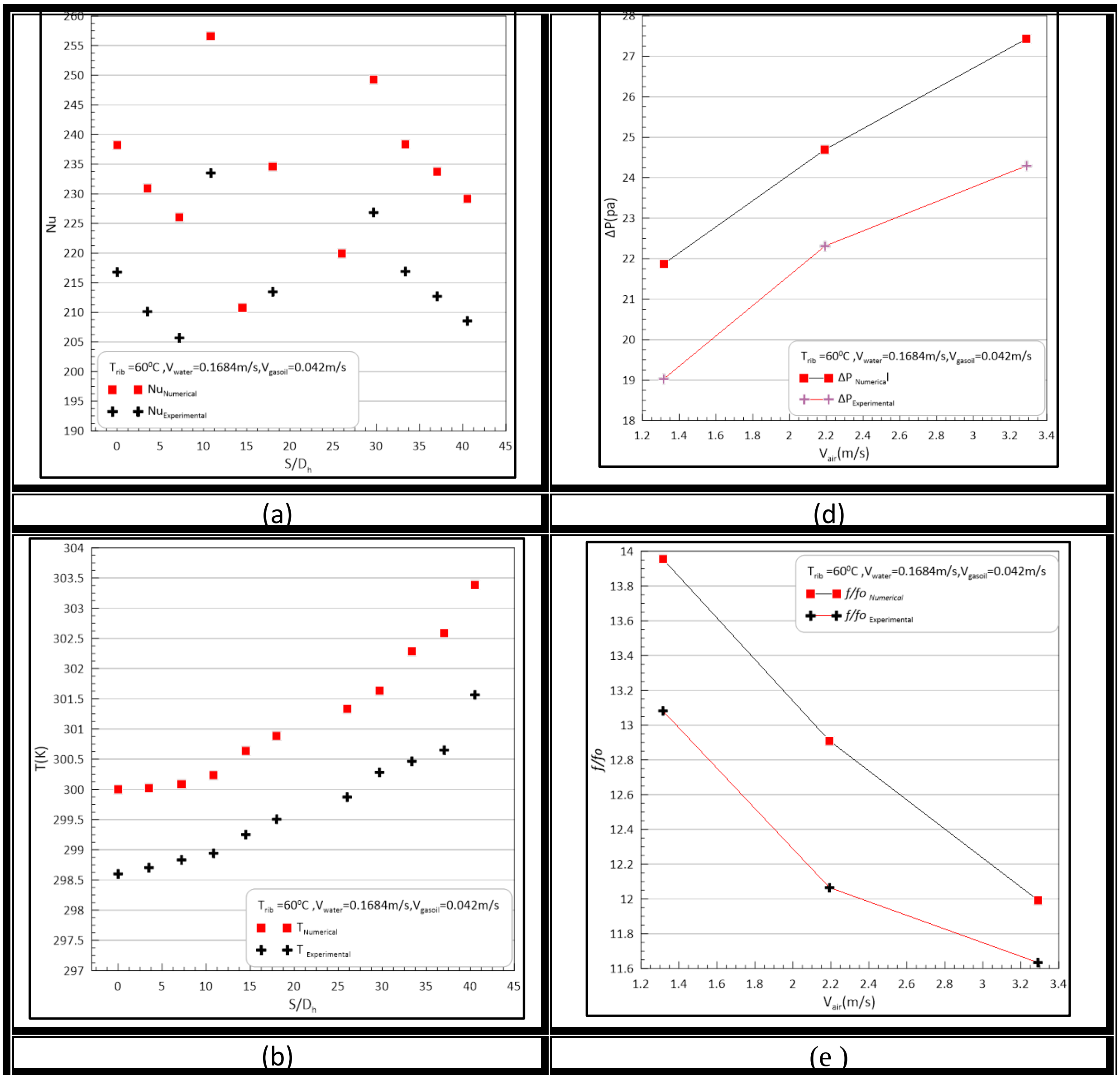

Figure (5.154). Comparison of Numerical and Experimental for Three-Phase flow.

CHAPTER SIX:

Conclusion and Suggestions

Chapter Six: Conclusion and Suggestions

6.1 Conclusion

Present work focused on building an optimum design for heat transfer enhancement and pressure drop for two-pass ribbed channel with investigations Internal flow with two cases: two-phase and three phase flow was done to come out with following conclusions:

6.1.1 Conclusions of Numerical and Experimental Results:

From the experimental results, the following are concluded: -

1. The Curved ribs enhanced heat transfer with percentages about 34.55% higher than V-shaped ribs. While the pressure drop for V-shaped ribs increased 60.01% higher than Curved.
2. The circle of ((3 mm)) represents the optimum area with percentages of enhancement are higher than ((6 and 9 mm)) about 15.4% and 21.25% respectively. Also, the increasing percentages of pressure drop for ((3 mm)) were higher than (6 and 9 mm) about (15.1% and 22.82%) respectively.
3. The circle shape of perforating is enhanced heat transfer higher than square and triangle perforating shape for same area about 7.47 % and 6.1% respectively, pressure drops in square area has maximum value, the percentages of increasing pressure drop for square were about (7.48% and 12.3%) triangle and circle areas, respectively.
4. The percentages of heat transfer enhancement for 45° are about 19.45% and 7.52% with respect to 30° and 60° respectively, while the percentages of

increasing pressure drop in 60° was about 43.98 % and 15.27 % with respect to 30° and 45° respectively.

5. The optimum design for the two-pass channel of sharp bend described as with curved ribs have circle perforating of (3mm) with rib angle 45° depending on the same condition.
6. The ratio of heat transfer enhancement (Nu/Nuo) increases with increasing velocities and rib temperature while the friction ratio decreases with increasing velocities and increase with increasing rib temperature.
7. The flow pattern is “Plug pattern” for two types of flow have mass flux for liquid phase and gas phase determining in ranges ($2100 \geq G_{liquid} \geq 300$ and $G_{gas} \leq 2$) .
8. The observation shows that (PCE) decreases with increasing V_{air} and V_{water} for two-phase flow and V_{air} , V_{water} and V_{gasoil} for three-phase flow at constant T_{Rib} but it increases with increasing T_{rib} at constant velocities.

6.2 Suggestions for Future Scope

To enhancement heat transfer and increased turbulence.

1. Study the effect of varying bend shape of channel of two-pass.
2. Adding another bend at outlet of first channel.
3. Studying a channel with circular cross section with internal annular ribs.
4. Studying different design and shapes of rib.
5. Adding a bleed hole in the walls of channel.
6. Adding a set of ribs in top of channel.
7. Add a nanoparticle to water base to increase PCE.

REFERENCES

References

[1] Abdulmajeed A. Ramadhan • Yaser T. Al Anii •Amer J. Shareef" **Groove geometry effects on turbulent heat transfer and fluid flow**" ,Heat Mass Transfer (2013) 49:185–195

DOI10.1007/s00231-012-1076-9.

[2] in ch. 1 & **[37]** in ch. 2 Al-Shamani, Ali Najah, K. Sopian, and H. A. Mohammed. "Sohif Mat, Mohd Hafidz Ruslan, Azher M. *Abed"* **Enhancement heat transfer characteristics in the channel with Trapezoidal rib–groove using nanofluids***", Case Stud. Therm. Eng* 5 (2015):48-58.

https://doi.org/10.1016/j.csite.2014.12.003

[3] Mohammed, H. A., Azher M. Abed, and M. A. Wahid. **"The effects of geometrical parameters of a corrugated channel with in out-of-phase arrangement."** International Communications in Heat and Mass Transfer 40 (2013):47-57.

https://doi.org/10.1016/j.icheatmasstransfer.2012.10.022

[4] Bergles A. E. (1998). Techniques to augment heat transfer. In "**Hand book of Heat Transfer**" (W. M. Bohsenow, J. P. Hartnett , and Y.I. Cho, Eds.), 3rd ed., Ch. 11. Mc Graw-Hill, New York.

[5] Adrian B. and Allan K. D. **"Heat transfer enhancement"** In Heat Transfer Handbook, Chapter 14, pg.1033, -1101, Wiley-2003.

[6] Khaled A. R., Abdulhafiz N. I., and Boukhary A. Y., **"Recent Advances in Heat Transfer Enhancements"**, Hindawi Publishing Corporation International Journal of Chemical Engineering Volume 2010, Article ID 106461.

[7] Liu S., M. Sakr, 2013, **"A comprehensive Review on Passive Heat Transfer Enhancements in Pipe exchangers"**, Renewable and Sustainable Energy Reviews, Vol. 19 ,pp. 64–81.

[8] Mohammed A. Al-Yaari* and Basel F. Abu-Sharkh **"CFD Prediction of Oil-Water Phase flow in 180° Bend"** Asian Transactions on Engineering (ATE ISSN: 2221-4267) Volume 01 Issue 05.

[9] Rabia Abrahim Saikoshad **"CFD Simulation of Heat Transfer in Vertical Ribbed Tube"** University Tun Hussein Onn Malaysia - Mechanical Engineering Department. M.Sc., thesis, MAY ,2011.

[10] Webb RL, Kim NH (2005) **Principles of enhanced heat transfer**. Taylor & Francis, New York.

[11] Mozafari M, Akhavan-Behabadi MA, Qobadi-Arfaee H **"Experimental study on condensation flow patterns inside inclined U-bend tubes"** ,Exp Therm Fluid Sci 68:276–287,2015.

[12] Shyy Woei Chang, Tong Miin Liou, Kuo-Ching Yu, Sung-Sen Huang "**Thermal-hydraulic performance of longitudinal wavy rib along wavy two-pass Channel**" Applied Thermal Engineering, Vol.133,224-236,(2018).

https://doi.org/10.1016/j.applthermaleng.2018.01.007

[13] Longfei Wang ,Songtao Wang,Xun Zhou,FengboWen and Zhongqi Wang **"Numerical prediction of 45° angled ribs effects on U-shaped channels heat transfer and flow under Multi-conditions'** J Turbo Jet Eng. ,(2017).

DOI 10.1515/tjj-2017-0008

[14] in ch. 1 but**[68]** in ch 2] Hao QIAN, Tao GUO, Xing-si HAN, Jun-kui MAO (2021) "**Very-large eddy simulation of the rotational effects on turbulent flow in a ribbed channel"** Journal of Zhejiang University-SCIENCE A (Applied Physics & Engineering) & Eng) 22(7):564-584,2021.

https://doi.org/10.1631/jzus.A2000175

[15] Kamali, R., and Binesh, A.R., **"Heat Transfer and Friction Characteristics Optimization with Compound Turbulators in Roughened Ducts"** Journal of Mechanics, Vol.25, pp. 271-278 ,2009.

[16] Z. Ghorbani-Tari, L. Wang, and B. Sunden."**Heat Transfer Characteristics of an Obstacle Controlled by the Presence of Ribs**" ,Manuscript submitted for Journal publication, 2014.

[17] Guangwen Jiang, Jianmin Gao, Xiaojun Shi,Wang Zhao, Yunlong Lia **"Flow and Heat Transfer of mist/steam two-phase flow in two-pass rectangular channels with paralleled and V-shaped rib turbulators "**,International Mechanical Engineering Congress and Exposition, November 9-15, Pittsburgh, PA, USA ,2018.

DOI: 10.1115/IMECE2018-88532.

[18] Tieyu Gao, Junxiong Zeng, Jiangnan Zhu, Jun Li and Jianying Gong" **Effects of rib angle and rib orientation on flow and heat transfer in two-pass ribbed channels"**, Journal of Mechanical Science and Technology, 32 (1) ,513~526 , (2018).

DOI 10.1007/s12206-017-1253-3

[19] Manca, Oronzio, Sergio Nardini, and Daniele Ricci. **"Numerical study of air forced convection in a channel provided with inclined ribs."** Frontiers in Heat and Mass Transfer (FHMT) 2, no. 1 ,2011.

https://doi.org/10.5098/hmt.v2.1.3007

[20] A.E. Bergles, “**Recent developments in convective heat transfer augmentation”** Applied Mechanics Reviews 26 , 675–682,1973.

[21] R.L. Webb, **"Principles of Enhanced Heat Transfer"** , John Wiley Sons, Chichester,1994.

[22] F.P. Incropera, **"Convection heat transfer in electronic equipment cooling"**, Journal of Heat Transfer 110 (1988) 1097–1111.

[23] Oliwie S. and Al.Turaihi R.”**The effect of ribs height in twophase flow(air-water)on heat transfer coeffiecient in vertical ribbed duct.”**Ain Shams Engineering Journal ,10,P.p 801-810. ,2019.

https://doi.org/10.1016/j.asej.2019.1.002

[24] Al-Turaihi R., Fadhli D. Abed A. **“Effect of semi-circle rib on heat transfer coeffiecient in rectangular channel”** Frontiner in Heatand Mass Transfer(FHMT),13,29 ,(2019).

DOI:10.5098/hmt.13.29.

[25] Sujoy Kumar Saha ,Manvendra Tiwari , Bengt Sundén et al (2016) **Advances in Heat Transfer Enhancement** Springer Nature, India.

DOI 10.1007/978-3-319-29480-3

[26] Wu Z, Sundén B (2015a)” **Frictional pressure drop correlations for single-phase flow, condensation, and evaporation in micro fin tubes**” ,ASME J Heat Transf 138(2):022901.

[27] Su Guoguang , Hamn-Ching Chen , Je-Chin Han , James D. Heidmann **“Computation of flow and heat transfer in rotating two-pass rectangular channels (AR = 1:1, 1:2, and 1:4) with smooth walls by a**

Reynolds stress turbulence model", International Journal of Heat and Mass Transfer , 47,5665–5683 ,2004.
doi:10.1016/j.ijheatmasstransfer.2004.07.019

[28] Kamali, R., and Binesh, A.R., **"Heat Transfer and Friction Characteristics Optimization with Compound Turbulators in Roughened Ducts"** International Communications in Heat and Mass Transfer 35 ,1032–104 0,2008.

[29] Dhanasekaran T. S. and Ting Wang **" Mist/air Cooling in a Two-Pass Rectangular Rotating Channel with 45-deg Angled Rib Turbulators "** Proceedings of ASME Turbo Expo 2011 Canada, GT2011-45954 ,2011.

[30] Wei Wang, Gao Jianmin, Xu Liang,Shi Xiaojun **"Flow and Heat Transfer Characteristics in Rotating Two-pass Channels Cooled by Superheated Steam"** ,Chinese Journal of Aeronautics ,25 , 524-532 ,2012.

doi: 10.1016/S1000-9361(11)60416-0

[31] Siddique Waseem, Igor V. Shevchuk, Lamyaa El-Gabry ,Narmin B. Hushmandi, Torsten H. Fransson **"On flow structure, heat transfer and pressure drop in varying aspect ratio two-pass rectangular channel with ribs at 45 degree"** ,Heat Mass Transfer ,49:679–694,2013.
DOI 10.1007/s00231-013-1111-5

[32] Shen Zhongyang, Huancheng Qu, Di Zhang, Yonghui Xie **" Effect of bleed hole on flow and heat transfer performance of U-shaped channel with dimple structure "** , International Journal of Heat and Mass Transfer Vol. 66, ,p.p 10-22 , 2013.
http://dx.doi.org/10.1016/j.ijheatmasstransfer.2013.07.008

[33] in ch.2 ,**[1]** in ch. 1, Abdulmajeed A. Ramadhan • Yaser T. Al Anii •Amer J. Shareef **" Groove geometry effects on turbulent heat transfer and fluid flow"** ,Heat Mass Transfer , 49:185–195 ,2013.

[34] Saha Krishnendu, Sumanta Acharya **"Effect of Bend Geometry on Heat Transfer and Pressure Drop in a Two-Pass Coolant Square Channel "** Journal of Turbomachinery , , Vol. 135 ,021035-1 ,2013. DOI: 10.1115/1.4006665.

[35] Balasubramanian Sudharsan Annur, Vesselina Roussinova, Ram Balachandar, Ronald Barron **" CFD Simulations of Flow and Heat Transfer in a Two-Pass Channel "** Conference: 22nd Annual Conference of the CFD Society of Canada , at Toronto, Ontario, Canada , 2014.

[36] Zhu Jiangnan , Tieyu Gao, Jun Li , Guojun Li,Jianying Gong" **NUMERICAL INVESTIGATION OF SECONDARY FLOW VORTEX CORE STRUCTURE IN THE TWO-PASS RECTANGULAR CHANNEL WITH 45° RIBS ",** Proceedings of ASME Turbo Expo 2015: Turbine Technical Conference and Exposition GT2015, June 15 – 19, 2015.

[37] in ch. 2 & **[2]** in ch. 1 Al-Shamani, Ali Najah, K. Sopian, and H. A. Mohammed. "Sohif Mat, Mohd Hafidz Ruslan, Azher M." Abed, **"Enhancement heat transfer characteristics in the channel with Trapezoidal rib–groove using nanofluids" Case** Stud. Therm. Eng 5 (2015): 48-58.

[38] Andreozzi Assunta, Oronzio Manca , Sergio Nardini, Daniele Ricci **"Forced convection enhancement in channels with transversal ribs and nanofluids"** ,Applied Thermal Engineering, ATE 7558 ,2015. http://dx.doi.org/doi: 10.1016/j.applthermaleng.2015.12.140

[39] Zheng Nianben, Peng Liu, Feng Shan, Zhichun Liu,Wei Liu **“Effects of rib arrangements on the flow pattern and heat transfer in an internally ribbed heat exchanger tube “** ,International Journal of Thermal Sciences 101 , 93-10 5 ,2016 .
http://dx.doi.org/10.1016/j.ijthermalsci.2015.10.035

[40] Gao Tieyu , Jiangnan Zhu, Changwei Liu and Jiamin Xu **“Numerical study of conjugate heat transfer of steam and air in high aspect ratio rectangular ribbed cooling channel”** ,Journal of Mechanical Science and Technology 30 (3) , 1431~1442,2016 .
DOI 10.1007/s12206-016-0251-1

[41] Kim Dae Hyun ,Byung Ju Lee , Jung Shin Park ,Jae Su Kwak , Jin Taek Chung **“Effects of inlet velocity profile on flow and heat transfer in the entrance region of a ribbed channel”** International Journal of Heat and Mass Transfer ,Volume 92 ,Pages 838-849 , , January 2016.
https://doi.org/10.1016/j.ijheatmasstransfer.2015.05.077

[42] Riyadh S. Al-Turaihi , Sarah Hasan Oleiwi**” HEAT TRANSFER OF TWO PHASES (WATER – AIR) IN HORIZONTAL SMOOTH AND RIBBED DUCTS”** International Journal of Energy Applications and Technologies ,Vol. 3, Issue 2, pp. 21 – 29, 2016.
www.academicpaper.org

[43] Pourfattaha F.,Mahdi Motamedian,Ghanbarali Sheikhzadeh ,Davood Toghraie Omid Akbarid **“The numerical investigation of angle of attack of inclined rectangular rib on the turbulent heat transfer of Water-Al2O3 nanofluid in a tube”,** International Journal of Mechanical Sciences, Volumes 131–132, Pages 1106-1116 , October 2017.
https://doi.org/10.1016/j.ijmecsci.2017.07.049

[44] in ch.2 & **[13]** in ch. 1 Wang Longfei ,Songtao Wang,Xun Zhou, Feng Wen and Zhongqi Wang **"Numerical prediction of 45° angled ribs effects on U-shaped channels heat transfer and flow under Multi-conditions'** J Turbo Jet Eng. ,(2017).

DOI 10.1515/tjj-2017-0008

[45] Ravi Bharath Viswanath ,Prashant Singh,Srinath V.Ekkad " **Numerical investigation of turbulent flow and heat transfer in two-pass ribbed channels** "International Journal of Thermal Sciences Volume 112 ,Pages 31-43 , February 2017.

https://doi.org/10.1016/j.ijthermalsci.2016.09.034

[46] Xie Gongnan, Xueting Liu , Hongbin Yan , Jiang Qin **" Turbulent flow characteristics and heat transfer enhancement in a square channel with various crescent ribs on one wall"** , International Journal of Heat and Mass Transfer ,Volume 115, Part A, Pages 283-295 , December 2017.

http://dx.doi.org/10.1016/j.ijheatmasstransfer.2017.07.012

[47] Rasool Arjumand , Adnan Qayoum **"Numerical analysis of heat transfer and friction factor in two-pass channels with variable rib shapes"** International Journal of Heat and Technology,Vol.36, No.1 ,pp. 40-48 , , March, 2018 .

https://doi.org/10.18280/ijht.360106

[48] Rasool Arjumand , Adnan Qayoum **"Numerical Investigation of Fluid Flow and heat transfer in a Two-Pass Channels with Perforated rib"** PERTANIKA SCIENCE& TECHNOLOGY,Vol.26, No.4,pp. 2009-2029 , 2018 .

https://wwwreserachgate.net/publication /328867800.

[49]in ch.2 & **[18]** in ch. 1 Tieyu Gao, Junxiong Zeng, Jiangnan Zhu, Jun Li and Jianying Gong **"Effects of rib angle and rib orientation on flow and heat transfer in two-pass ribbed channels "** Journal of Mechanical Science and Technology 32 (1) ,513~526 , (2018) .
DOI 10.1007/s12206-017-1253-3

[50] Guangwen Jiang,Jianmin Gao ,Xiaojun Shia,, Wang Zhaoa,, Yunlong Lia **,"Flow And Heat Transfer Of Mist/Steam Two-Phase Flow In Two-Pass Rectangular Channels With Paralleled And V-Shaped Rib Turbulators"**, Proceedings of the ASME 2018 ,International Mechanical Engineering Congress and Exposition IMECE2018 .,November 9-15, 2018
http://www.asme.org/about-asme/terms-of-use

[51] Göhring Michael , Tobias Krille, Julian Feile, Jens Wolfers**."Heat Transfer Predictions in Smooth and Ribbed Two-Pass Cooling Channels under Stationary and Rotating Conditions "** , International Symposium on Transport Phenomena and Dynamics of Rotating Machinery Hawaii, Honolulu April 10-15 , 30 Sep 2018 .
https://hal.archives-ouvertes.fr/hal-01884254

[52] Jiang Guangwen, Jianmin Gao, Xiaojun Shi,Wang Zhao, Yunlong Lia **"Flow and Heat Transfer Characteristics of mist/steam two-phase flow in the U-shaped cooling passage with 60 deg. Ribs** ",International communication in Heat and mass transfer 105 ,73-83,2019 .

https://doi.org/10.1016.2019.02.023.

[53] Mondol Sonkar , Md. Ismail Hossain , and Md. Tajul Islam , **" Numerical Study of Water Flow through U-Bend Pipe"** IOSR Journal of Mathematics (IOSR-JM ,e-ISSN: 2278-5728, p-ISSN: 2319-765X. Volume 15, Issue 4 Ser. I ,PP 48-57 ,2019.

DOI: 10.9790/5728-1504014857

[54] Gao Tieyu,Jiangnan Zhu,Jun Li ,Jianying Gong , Jianmin Gao **"Flow and Heat Transfer Characteristics of mist/steam two-phase flow in the U-shaped cooling passage with 60 deg. Ribs "**, International communication in Heat and mass transfer 103 ,43-53,2019 .

[55] Luan Yigang, Lianfeng Yang a, Shi Bu a, Tao Sun a,⇑, Haiou Sun a, Pietro Zunino "Effect of connecting holes on flow and heat transfer in a two-pass channel with and without rib turbulators" , International Journal of Heat and Mass Transfer ,Volume 133, Pages 80-95 , April 2019.
https://doi.org/10.1016/j.ijheatmasstransfer.2018.12.043

[56] He Ping, Charles , Mader , Joaquim R.R.A. Martins ,Kevin J. Maki " **Aerothermal optimization of a ribbed U-bend cooling channel using the adjoint method "** International Journal of Heat and Mass Transfer ,Volume 140, Pages 152-172 , September 2019 .
https://doi.org/10.1016/j.ijheatmasstransfer.2019.05.075

[57] Han Yan,Lei Luo , Wei Du , Songtao Wang , Bengt Sunden , **"Flow structure and heat transfer characteristics in a ribbed two-pass channel with varying divider inclination angle "**, International Journal of Thermal Sciences , Volume 166, 106969 , August 2021 .
https://doi.org/10.1016/j.ijthermalsci.2021.106969

[58] Al-Hadhrami Luai ,Je-Chin Han **"Effect of rotation on heat transfer in two-pass square channels with five different orientations of 45 angled rib turbulators "** , International Journal of Heat and Mass Transfer 46 , 653–669 ,2003 .
PII: S 0 0 1 7 - 9 3 1 0 (0 2) 0 0 3 2 5 – 3

[59] Liu Yao-Hsien, Lesley M. Wright, Wen-Lung Fu, and Je-Chin Han " **Rib Spacing Effect on Heat Transfer and Pressure Loss in a Rotating**

Two-Pass Rectangular Channel (AR=1:2) with 45-Degree Angled Ribs" May 8-11, Barcelona, Spain ,GT2006-90368 , 2006, .

[60] Salameh Tareq and Bengt Sunden **"An Experimental Study of Heat Transfer and Pressure Drop on the Bend Surface of a U-duct"** , dings of ASME Turbo Expo 2010: Power for Land, Sea and Air Proceedings of ASME Turbo Expo 2010.

[61] Elfert, M .,Schroll, M .,Förster, W **."PIV-Measurement Of Secondary Flow In A Rotating Two-Pass Cooling System With An Improved Sequencer Technique "**Institute of Propulsion Technology, D-51170 Cologne, Germany Proceedings of ASME Turbo Expo 2010: Power for Land, Sea and Air Proceedings of ASME TURBO EXPO 2010GT2010 June 14-18, 2010,GT-2010-23510 ,2010.

[62] Wang Lei ,Zahra Ghorbani-Tari, Chenglong Wang ,Zan Wu **"endwall heat transfer at the turn section in a two-pass square channel with and without ribs"**Journal of Enhanceced heat transfer ,20(40) :321-332 ,2013.

[63] Pietrzak Marcin ,Stanislaw Witczak **" Flow pattern and void fraction of phase during gas-liquid two-phase and gas-liquid -liquid three phase flow in U-bends "**International Journal of Heat and fluid flow 44,700-410,2013 .

[64] Oliveira Pedro, Eduardo Strle, Jader R. Barbosa Jr. **"Developing air–water flow downstream of a vertical 180 return bend "** International Journal of Multiphase Flow, Volume 67, Supplement, Pages 32-41 , December 2014.

https://doi.org/10.1016/j.ijmultiphaseflow.2014.05.006

[65] Liou Tong-Miin, Shyy Woei Chang , Shu-Po Chan , Yu-Shuai Liu **"Effect of Rib Angle Orientation on Flow Field in a Two-Pass Parallelogram Channel with 180-Deg Sharp Turn"** , Proceedings of

ASME Turbo Expo 2015: Turbine Technical Conference and Exposition GT2015 , Montréal, Canada , June 15 – 19, 2015 .

[66] Singh Prashant ,Srinath Ekkad **"Experimental study of heat transfer augmentation in a two-pass channel featuring V-shaped ribs and cylindrical dimples** ",Applied Thermal Engineering 116 ,205–216, 2017 .
http://dx.doi.org/10.1016/j.applthermaleng.2017.01.098

[67] T. M. Liou1 , S. W. Chang , Y. A. Lan **"Heat Transfer and Flow Characteristics of Two-Pass Parallelogram Channels With Attached and Detached Transverse Ribs ",**Journal of Heat Transfer Vol. 139 /042001-1 , APRIL 2017 .
DOI: 10.1115/1.4035279

[68] Weihua Yang ,Shulin Xue ,Yihong He ,Wei Li **"Experimental study on the heat transfer characteristics of high blockage rib channel "** ,Experimental thermal and Fluid science ,83,248-259 ,2017 .
http://dx.doi.org/10 .1016/j.expthermflusci

[69] Adnan Qayoum ,Pradipta Panigrahi **"Experimental Investigation of heat transfer enhancement in a two-pass Square Duct by permeable ribs** "Heat transfer Engineering ,P.p 1521-0537, 2018 .
DOI:10.1080/01457632.2018.1436649.

[70] in ch. 2 &**[12]** in ch .1 Chang Shyy Woei , Tong Miin Liou, Kuo-Ching Yu, Sung-Sen Huang"**Thermal-hydraulic performance of longitudinal wavy rib along wavy two-pass channel "** Applied Thermal Engineering ,ATE 11661,January 2018 .
https://doi.org/10.1016/j.applthermaleng.2018.01.007

[71] Hayashia Kosuke,,, Junichiro Kazia,b, Naoyuki Yoshidaa, Akio Tomiyama **"Pressure drops of air-water two-phase flows in horizontal**

U-bends ",International Journal of Multiphase Flow , Volume 131, 103403 , October 2020 .
https://doi.org/10.1016/j.ijmultiphaseflow.2020.103403

[72] Kore Sandeep S, Sunil V. Dingare2, Satish Chinchanikar , Pravin Hujare , and Ashok Mache1," **Experimental Analysis of different shaped ribs on heat transfer and fluid flow characteristics "**, E3S Web of Conferences 170, 01019,2020.
https://doi.org/10.1051/e3sconf/202017001019

[73] Sriromreun Parkpoom ,Chinaruk Thianpong,Pongjet Promvonge **"Experimental and numerical study on heat transfer enhancement in a channel with Z-shaped baffles ",**International Communications in Heat and Mass Transfer ,Volume 39, Issue 7, Pages 945-952 , August 2012.

[74] Shian Li,Zahra Ghorbani-Tari ,Gongnan Xie and Bengt Sundén "**An Experimental and Numerical Study of Flow and Heat Transfer in Ribbed Channels with Large Rib Pitch-to-Height Ratios "** , Proceedings of ASME International Mechanical Engineering Congress and Exposition 2013 ,IMECE2013-64328 , November 15-21, 2013 .

[75] Erelli, Ramesh , Arun K. Saha, P.K. Panigrahi" **Influence of turn geometry on turbulent fluid flow and heat transfer in a stationary two-pass square duct "** , International Journal of Heat and Mass Transfer ,Volume 89, October 2015, Pages 667-684 .
http://dx.doi.org/10.1016/j.ijheatmasstransfer.2015.05.081

[76] Singh Prashant, Bharath Viswanath Ravi, Srinath V. Ekkad **"Experimental and numerical study of heat transfer due to developing flow in a two-pass rib roughened square duct "** International Journal of Heat and Mass Transfer Volume 102, , Pages 1245-1256 , November 2016 .

[77] Kaewchoothong Natthaporn, Kittinan Maliwan ,Kenichiro Takeishi , Chayut Nuntadusit ,**“ Effect of inclined ribs on heat transfer coefficient in stationary square channel “** ,Theoretical and Applied Mechanics Letters Volume 7, Issue 6, Pages 344-350 , November 2017.
https://doi.org/10.1016/j.taml.2017.09.013

[78] Al-Jibory Mohammed W. **“Heat Transfer Enhancement for Rectangular Channels by Using Triangular-Shaped Ribs at High Reynold Numbers “** Journal University of Kerbala , Vol. 16 No.1 Scientific . 2018 .

[79] Kumait Aadel A. R , Thamir K. Ibrahim ,Maysoon A. Abdullah **“Experimental and numerical study of forced convection heat transfer in different internally ribbed tubes configuration using TiO2 nanofluid “** ,Heat Transfer—Asian Res., 1-27.6 January 2019
DOI: 10.1002/htj.21457

[80]. Abed Azher M , Doaa Fadhil Kareem,Hasan Sh Majdi, Ammar Abdulkadhim “Experimental and CFD Analysis of Two-Phase Forced Convection Flow in Channels of Various Rib Shapes “ , Journal of Advanced Research in Fluid Mechanics and Thermal Sciences 77, Issue 1 36-50 , 2021 .
https://doi.org/10.37934/arfmts.77.1.3650

[81] Rebay S., **"Efficient Unstructured Mesh Generation by Means of Delainay Triangulation and Bowyer–Watson Algorithm"**, Journal of Computational Physics, Vol.106, pp.125-138, 1993.

[82] FLUENT Incorporated, FLUENT 5 User’s Guide, Fluent Incorporated Lebanon, NH-USA, 1998.

[83] ANSYS FLUENT 2021 Documentation, 2021 R1.

[84] Fluent User Services Center, www. Fluent users .com .

[85] Dr.James P.Brill ,Dr. H.Dale Beggs **“Two-phase flow in Pipes** ”Six edition ,Third Printing,1991 .

[86] Fu, W.W.,Wright,LM. Han J.C., **“Rotational Buoyancy Effects on Heat transfer in Five Different Wall and 45 degree Ribbed Walls “**ASME J.Heat transfer ,Vol.128, PP.1130-1141,2006.

[87] Operation Manual ISO-9001, CE, IEC1010, "**Specification .7000 mbar Manometer, differential input, Model: PM-9107",**2013.

[88] G. F. HEWITT & N. S. HALL-TAYLOR **“Annular Two-Phase Flow”** Oxford · New York · Toronto 1970.

[89] Catalog specification ISO-9001, CE, IEC1010, "**Specification .12 channel Temp. Recorder. Model: BTM-4208SD",**2008

[90] Hameed K. H.. **"Experimental and numerical investigation of turbulent for CFD convection in a circular pipe with induced viberation"** . D.ph dissertation, University of Babylon,2016.

[91] Holman, J. P. (Jack Philip) **“Experimental methods for engineers “8**th Edition. (McGraw-Hill series in mechanical engineering), New York, 2011.

[92] Ghorbani-Tari, Zahra. **"Experimental investigations of heat transfer in a channel with ribs and obstacle."** PhD diss., Lund University (2014).